



# VCU

Virginia Commonwealth University  
VCU Scholars Compass

---

Theses and Dissertations

Graduate School


---

2022

## DEVELOPMENT AND OPTIMIZATION OF A LOW VOLUME AIR-JET DRY POWDER INHALER (DPI) PLATFORM FOR THE DELIVERY OF HIGH DOSE AEROSOLIZED POWDER TO INFANTS

Connor Howe  
*Virginia Commonwealth University*

Follow this and additional works at: <https://scholarscompass.vcu.edu/etd>

 Part of the [Computer-Aided Engineering and Design Commons](#), [Other Mechanical Engineering Commons](#), and the [Other Pharmacy and Pharmaceutical Sciences Commons](#)

© Connor Matthew Howe

---

Downloaded from

<https://scholarscompass.vcu.edu/etd/7142>

This Dissertation is brought to you for free and open access by the Graduate School at VCU Scholars Compass. It has been accepted for inclusion in Theses and Dissertations by an authorized administrator of VCU Scholars Compass. For more information, please contact [libcompass@vcu.edu](mailto:libcompass@vcu.edu).

© Connor M. Howe 2022

All Rights Reserved

**DEVELOPMENT AND OPTIMIZATION OF A LOW VOLUME AIR-JET DRY POWDER  
INHALER (DPI) PLATFORM FOR THE DELIVERY OF HIGH DOSE AEROSOLIZED  
POWDER TO INFANTS**

A dissertation submitted in partial fulfillment of the requirements for the degree  
of Doctor of Philosophy at Virginia Commonwealth University

By

CONNOR MATTHEW HOWE

Bachelor of Science, Longwood University, USA, 2005

Director: Dr. P. WORTH LONGEST

Professor, Department of Mechanical and Nuclear Engineering and Department of  
Pharmaceutics

Virginia Commonwealth University

Richmond, Virginia

December, 2022

## **Acknowledgement**

Completing my doctorate has been one of the most challenging, but rewarding experiences in my life, and it would not have been possible without support from my family and friends. I would like to thank my advisor Dr. P. Worth Longest for taking me in while changing directions in my program and starting a new research area while still making progress on my degree, and especially for his guidance and support over the years. I would also like to thank Dr. Michael Hindle for use of his lab and the extensive collaboration with the Department of Pharmaceutics. I would like to thank my committee members; Dr. Laleh Golshahi, Dr. Michael Hindle, Dr. Rebecca Heise, and Dr. Sheng-Chieh Chen, for their help in making this possible. I am also grateful for my colleagues in the Mechanical & Nuclear Engineering Department and the Department of Pharmaceutics at VCU; your comradery, support, and willingness to help have been wonderful.

I would also like to acknowledge funding from the National Institutes of Health, which facilitated the completion of this work.

Finally, my wife, Dr. Maria Higgins, your love, support, and patience made this possible, and I am eternally grateful to have you by my side.

# Table of Contents

<b>ACKNOWLEDGEMENT</b> .....	<b>II</b>
<b>TABLE OF CONTENTS</b> .....	<b>III</b>
<b>LIST OF FIGURES</b> .....	<b>VII</b>
<b>LIST OF TABLES</b> .....	<b>XIII</b>
<b>ABBREVIATIONS</b> .....	<b>XVI</b>
<b>ABSTRACT</b> .....	<b>XVII</b>
<b>CHAPTER 1 - SPECIFIC AIMS</b> .....	<b>1</b>
1.1 OBJECTIVE 1: DEVELOPMENT AND OPTIMIZATION OF AN AIR-JET DPI PLATFORM FOR AEROSOL DRUG DELIVERY TO INFANTS .....	3
1.2 OBJECTIVE 2: EXPANSION OF THE INFANT AIR-JET DPI PLATFORM TO INCLUDE CAPABILITIES FOR HIGH POWDER MASS LOADINGS WITH MINIMAL CHANGE AND POTENTIAL ENHANCEMENTS IN AEROSOLIZATION PERFORMANCE .....	5
<b>CHAPTER 2 - BACKGROUND AND MOTIVATION</b> .....	<b>7</b>
2.1 NEONATAL RESPIRATORY DISTRESS SYNDROME (RDS) .....	7
2.2 SURFACTANT REPLACEMENT THERAPY .....	7
2.3 ALTERNATIVE TREATMENT APPROACHES.....	8
2.4 REVIEW OF CURRENT NEBULIZED SURFACTANT AEROSOL DELIVERY .....	9
2.5 HIGHLY EFFICIENT DRY POWDER THERAPY .....	13
2.6 EEG AND SPRAY DRIED AEROSOL FORMULATIONS .....	14
2.7 MOTIVATION FOR AIR-JET DPI AND OPERATING PRINCIPLES.....	15
2.8 POSITIVE PRESSURE DPIS .....	17
2.9 REVIEW OF VCU AIR-JET DPIS.....	19

2.10 MECHANICS OF POWDER DEAGGREGATION .....	21
2.11 REQUIREMENTS FOR AN INFANT AIR-JET DPI PLATFORM .....	23
2.12 REVIEW OF DPI DOSE LOADING STRATEGIES .....	24
2.13 DOSE LOADING STRATEGIES FOR THE AIR-JET DPI PLATFORM .....	26
<b>CHAPTER 3 - INITIAL DEVELOPMENT OF AN AIR-JET DRY POWDER INHALER FOR RAPID DELIVERY OF PHARMACEUTICAL AEROSOLS TO INFANTS .....</b>	<b>28</b>
3.1 INTRODUCTION .....	28
3.2 MATERIALS AND METHODS .....	33
3.3 RESULTS .....	44
3.4 DISCUSSION .....	49
3.5 CONCLUSIONS .....	53
<b>CHAPTER 4 - ADVANCEMENT OF THE INFANT AIR-JET DRY POWDER INHALER (DPI): EVALUATION OF DIFFERENT POSITIVE-PRESSURE AIR SOURCES AND FLOW RATES .....</b>	<b>70</b>
4.1 INTRODUCTION .....	70
4.2 MATERIALS AND METHODS .....	75
4.3 RESULTS .....	90
4.4 DISCUSSION .....	95
4.5 CONCLUSIONS .....	99
<b>CHAPTER 5 - <i>IN VITRO</i> ANALYSIS OF NASAL INTERFACE OPTIONS FOR HIGH EFFICIENCY AEROSOL ADMINISTRATION TO PRETERM INFANTS .....</b>	<b>118</b>
5.1 INTRODUCTION .....	118
5.2 MATERIALS AND METHODS .....	124

5.3 RESULTS.....	135
5.4 DISCUSSION.....	141
5.5 CONCLUSIONS.....	146
<b>CHAPTER 6 - DEVELOPMENT OF A HIGH-DOSE INFANT AIR-JET DRY POWDER INHALER (DPI) WITH PASSIVE CYCLIC LOADING OF THE FORMULATION.....</b>	<b>164</b>
6.1 INTRODUCTION.....	164
6.2 MATERIALS AND METHODS.....	168
6.3 RESULTS.....	182
6.4 DISCUSSION.....	186
6.5 CONCLUSIONS.....	190
<b>CHAPTER 7 - ADVANCEMENT OF THE INFANT AIR-JET DPI PLATFORM WITH PASSIVE CYCLIC LOADING AND PASSIVE METERING ELEMENTS FOR VARIOUS FORMULATIONS.....</b>	<b>204</b>
7.1 INTRODUCTION.....	204
7.2 MATERIALS AND METHODS.....	208
7.3 RESULTS.....	220
7.4 DISCUSSION.....	227
7.5 CONCLUSIONS.....	229
<b>CHAPTER 8 - CONCLUSIONS AND FUTURE WORK.....</b>	<b>245</b>
8.1 OBJECTIVE 1: DEVELOPMENT AND OPTIMIZATION OF AN AIR-JET DPI PLATFORM FOR AEROSOL DRUG DELIVERY TO INFANTS.....	245

8.2 OBJECTIVE 2: EXPANSION OF THE INFANT AIR-JET DPI PLATFORM TO INCLUDE CAPABILITIES FOR HIGH POWDER MASS LOADINGS WITH MINIMAL CHANGE AND POTENTIAL ENHANCEMENTS IN AEROSOLIZATION PERFORMANCE .....	249
8.3 SYNOPSIS AND FUTURE DIRECTIONS .....	253
<b>LIST OF REFERENCES .....</b>	<b>256</b>
<b>VITA .....</b>	<b>268</b>



## List of Figures

<b>Figure 2.1</b>	Illustrations of basic setup for different nebulizer types .....	10
<b>Figure 2.2</b>	Basic drawing air-jet DPI platform with three main components labeled (1. Air Source, 2. Air-jet DPI, 3. Nasal Interface) in connection to a full-term infant NT model.....	17
<b>Figure 2.3</b>	Axial cross section of assembled low-volume dry powder inhalers (LV-DPIs) for <b>(a)</b> initial device and <b>(b)</b> modified animal delivery device .....	21
<b>Figure 2.4</b>	Illustrations of the basic operating principles for the three main dose delivery strategies for <b>(a)</b> Single dose, <b>(b)</b> Multi-dose Unit, and <b>(c)</b> Multi-dose Reservoir ..	25
<b>Figure 3.1</b>	Schematic representation of infant air-jet DPI aerosol delivery system attached to an infant nose-throat (NT) airway model .....	54
<b>Figure 3.2</b>	Axial cross section of the infant air-jet DPI connected to a gradually expanding nasal interface illustrating internal flow passages.....	55
<b>Figure 3.3</b>	Internal airflow geometry of each device from air source inlet (left side of each image) to the device outlet (right side of each image).....	56
<b>Figure 3.4</b>	Connection of the nasal interface to the infant NT model illustrating <b>(a)</b> angle of the nasal interface and <b>(b)</b> position of the nasal interface and NT model .....	57
<b>Figure 3.5</b>	Overview of the infant NT airway model and regional sections.....	58
<b>Figure 3.6</b>	Experimental setup for device aerosolization performance as determined by Next Generation Impactor (NGI) with parts labeled .....	59
<b>Figure 3.7</b>	Experimental setup for aerosol delivery efficiency testing through the infant NT model with parts labeled .....	60
<b>Figure 3.8</b>	<b>(a)</b> Average cumulative primary particle size distribution [n=3] of the powder and <b>(b)</b> Pressure profile graphs of 30 mL AAVs using the hand operated syringe through devices D2, D5, and D6, measured at the air-jet DPI outlet [n=6] .....	61

<b>Figure 3.9</b>	Mean (SD) values of MMAD vs. ED based on device actuation into the NGI and AAVs of <b>(a)</b> 30 mL and <b>(b)</b> 10 mL using room-condition air .....	62
<b>Figure 3.10</b>	Mean (SD) values of MMAD vs. ED based on device actuation into the NGI for the three best performing devices actuated with 30 mL (open circles) or 10 mL (filled circles) of room-condition air .....	63
<b>Figure 3.11</b>	Experimentally determined mean (SD) drug deposition fraction (based on loaded dose) grouped by <b>(a)</b> region and <b>(b)</b> device .....	64
<b>Figure 4.1</b>	Schematic representation of infant air-jet DPI platform in experimental setup. <b>(a)</b> Next Generation Impactor (NGI) experimental setup and <b>(b)</b> Preterm nose-throat (NT) airway model setup .....	101
<b>Figure 4.2</b>	Images of air sources with main components labeled: <b>(a)</b> Timer air source, <b>(b)</b> Pneumatic air source, and <b>(c)</b> Spring air source.....	102
<b>Figure 4.3</b>	Plots of measured flow rate (L/min) for each air source and the corresponding flow rate waveform during actuation at a Q90 of 4 L/min .....	103
<b>Figure 4.4</b>	Internal airflow geometry of each device from air source inlet (left side of each image) to the device outlet (right side of each image) and side view of airflow geometry of D1-Single connected to the nasal interface .....	104
<b>Figure 4.5</b>	Schematic overview of the preterm infant NT airway model and regional sections. <b>(a)</b> Assembly with parts labeled and <b>(b)</b> Internal airway geometry of the infant NT model with regions labeled.....	105
<b>Figure 4.6</b>	Experimental setup for aerosol delivery efficiency testing through the infant NT model showing orientation and insertion of the platform .....	106
<b>Figure 4.7</b>	Experimental setup for aerosol delivery efficiency testing through the infant NT model with the pulmonary mechanics (PM) outlet condition.....	107
<b>Figure 4.8</b>	Mean (SD) values of mass median aerodynamic diameter (MMAD) vs. emitted dose (ED) of the I-leucine EEG formulation based on device actuation into the NGI for each combination of air source and air-jet DPI [n=3] .....	108

<b>Figure 4.9</b>	Plot of experimentally determined mean (SD) drug deposition fractions (based on loaded dose) of the l-leucine EEG formulation grouped by air source and operated at a Q90 of either 4 L/min (left) or 2 L/min (right) [n=3] .....	109
<b>Figure 4.10</b>	Experimentally determined mean (SD) drug deposition fraction (based on loaded dose) of the l-leucine EEG formulation for the Timer air source operated at varied Q90 flow rates, with total NT deposition [n=3] .....	110
<b>Figure 4.11</b>	Graph of experimentally determined mean (SD) drug deposition fraction (DF) of the l-leucine EEG formulation in the NT region compared to impaction parameter ( $d_p^2Q$ ) where $d_p$ and $Q$ are the MMAD at each Q90 and the Q90 for each tested value, respectively [n=3] .....	111
<b>Figure 4.12</b>	Experimentally determined mean (SD) drug deposition fraction of the l-leucine EEG formulation (based on loaded dose) in each NT region and filter deposition for the Timer air source operated at varied Q90 flow rates [n=3] .....	112
<b>Figure 4.13</b>	Plot of the measured internal infant airway pressure taken during PM outlet condition experimental testing for each actuation, including a 5 sec breath hold [n=5] .....	113
<b>Figure 5.1</b>	Overview of air-jet DPI and nasal interface connection with expanded internal view, illustrating attachment to the outlet of the air-jet DPI .....	148
<b>Figure 5.2</b>	Overview of the infant air-jet DPI aerosol delivery system connected to a preterm infant nose-throat (NT) airway model .....	149
<b>Figure 5.3</b>	Internal airflow geometries of each air-jet DPI from device inlet (left side of each image) to the device outlet(s) (right side of each image) and central aerosolization chamber.....	150
<b>Figure 5.4</b>	Overview of the infant NT airway model and regional sections.....	151
<b>Figure 5.5</b>	Interface Set 1: Nasal interface designs (internal surfaces) beginning with the air-jet DPI outlet capillary (left side), followed by different flow pathways and ending with the same flexible straight prong .....	152

<b>Figure 5.6</b>	Interface Set 2: Axial sectioned view of dual prong nasal interface designs from air-jet outlet capillary (left side of each image) to the straight flexible prongs (right side of each image) .....	153
<b>Figure 5.7</b>	Interface Sets 3 and 4: Internal airflow geometry of curved prong designs from air-jet outlet capillary (left side of each image) to the curved prong (right side of each image).....	154
<b>Figure 5.8</b>	Interface Set 5: Internal airflow geometry of combined flow pathway and curved prong designs from air-jet outlet capillary (left side of each image) to the curved prong (right side of each image) .....	155
<b>Figure 5.9</b>	Pictures of infant NT models during <i>in vitro</i> experimental setup for the <b>(a)</b> Scaled-6m model and <b>(b)</b> Preterm NT model .....	156
<b>Figure 5.10</b>	Experimentally determined mean drug deposition fractions (based on loaded dose) of the l-leucine formulation (Batch 3) using the D1-Single air-jet DPI and Rigid-3 nasal interface across different Q90 flow rates.....	157
<b>Figure 5.11</b>	Experimentally determined mean drug deposition fraction (based on loaded dose) using the D1-Single air-jet DPI and Rigid-3 nasal interface. Total nose-throat (NT) deposition represents sum of infant NT regional deposition fractions for each respective model.....	158
<b>Figure 6.1</b>	Graphical overview of the experimental setup including the infant air-jet DPI platform with passive cyclic loading .....	192
<b>Figure 6.2</b>	Internal airflow geometry of each infant air-jet DPI passive design (PD) from air source inlet (left side of each image) to the device outlet (right side of each image) .....	193
<b>Figure 6.3</b>	Overview of the single nasal interface used in this study illustrating the flow pathway and prong regions .....	194
<b>Figure 6.4</b>	Schematic overview of the preterm infant NT airway model and regional sections. <b>(a)</b> Assembly of infant NT model with connection to custom low-volume filter	

	housing and <b>(b)</b> Internal airway geometry of the infant NT model with assessed regions.....	195
<b>Figure 6.5</b>	Experimental setup for sensitivity analysis testing with the infant NT model connected to the infant pulmonary mechanics (PM) outlet condition and breathing simulator.....	196
<b>Figure 6.6</b>	Renderings of the two device configurations for the powder reservoir sensitivity analysis .....	197
<b>Figure 6.7</b>	Plot of experimentally determined mean (SD) drug deposition fractions (based on loaded dose) of the AS-EEG formulation compared with the Surfactant-EEG formulation.....	198
<b>Figure 6.8</b>	Experimentally determined mean (SD) drug deposition fractions (based on loaded dose) of the Surfactant-EEG formulation for different Q90 flow rates [n=3].....	199
<b>Figure 7.1</b>	Graphical rendering of the experimental setup including the infant air-jet DPI platform with passive cyclic loading in connection to a preterm infant model ...	231
<b>Figure 7.2</b>	Internal airflow geometry of the air-jet DPI.....	232
<b>Figure 7.3</b>	Overview of the single nasal interface used in this study.....	233
<b>Figure 7.4</b>	Graphical renderings of infant NT airway geometry with regional sections and model assembly connected to custom low-volume (LV) filter housing.....	234
<b>Figure 7.5</b>	Renderings of the two powder reservoir configurations. <b>(a)</b> PD-2 device with standard (0.55 mL volume) reservoir attached and <b>(b)</b> PD-2 device with adjustable powder reservoir (up to 1.5 mL volume) attached .....	235
<b>Figure 7.6</b>	Rendering of air-jet DPI connected to aerosol collection assembly for emitted dose (ED) per actuation experimental study .....	236
<b>Figure 7.7</b>	Image of experimental setup for device aerosolization performance as determined by Next Generation Impactor (NGI) with parts labeled .....	237

<b>Figure 7.8</b>	Plot of experimentally determined mean and $\pm 1$ SD error bars for emitted-dose (ED) per actuation and total ED (based on loaded dose) of the AS-EEG formulation, at a Q90 flow rate of 4 L/min [n=3].....	238
<b>Figure 7.9</b>	Experimentally determined mean aerodynamic particle size distribution (APSD – left Y-axis) and NGI pre-separator deposition fraction (right Y-axis) of each formulation (based on loaded dose) for the PD-2 device and 10 mg powder loading[n=3] .....	239
<b>Figure 8.1</b>	Axial cross section view of CFD simulated air flow velocity profile for a co-flow nasal interface design.....	248
<b>Figure 8.2</b>	Automatic venting schemes for the slider in the adjustable powder reservoir. <b>(a)</b> Push button and <b>(b)</b> Squeeze button configuration .....	251
<b>Figure 8.3</b>	Concept model renderings for adjustable passive metering elements. <b>(a)</b> Shows a 2-D cross-sectional cut while <b>(b)</b> shows an isometric view with full ring and shelf parts.....	254

## List of Tables

<b>Table 2.1</b>	Summary of select nebulized surfactant studies, grouped by study type ( <i>in vitro</i> , <i>in vivo</i> animal, or clinical).....	11
<b>Table 2.2</b>	List of dose per actuation and total delivery time for select total doses .....	27
<b>Table 3.1</b>	Air-jet dry powder inhaler (DPI) design parameters and configurations .....	65
<b>Table 3.2</b>	Aerosolization performance and measured flow rate with an air actuation volume (AAV) of 30 mL.....	66
<b>Table 3.3</b>	Aerosolization performance and measured flow rate with an AAV of 10 mL .....	67
<b>Table 3.4</b>	Comparison of best design aerosolization performance at 10 and 30 mL AAVs....	68
<b>Table 3.5</b>	Regional deposition fractions (based on loaded dose) for air-jet DPI designs in full-term nose-throat (NT) model and 30 mL AAV .....	69
<b>Table 4.1</b>	Air source flow rate properties compared at a target Q90 of 4 L/min and air actuation volume (AAV) of 10 mL, n=5 actuations .....	114
<b>Table 4.2</b>	Aerosolization performance of the I-leucine EEG formulation in the air-jet DPIs based on air source, in terms of air-jet DPI emitted dose (ED) and mass median aerodynamic diameter (MMAD) at 4 L/min (Q90).....	115
<b>Table 4.3</b>	Impaction Parameter details for D1-Single and Timer air source at selected Q90 flow rates using the I-leucine EEG formulation. MMAD from impaction testing and deposition fraction from preterm NT model testing .....	116
<b>Table 4.4</b>	Regional deposition fractions (based on loaded dose) of the trileucine EEG formulation for D1-Single with Timer air source at Q90 = 1.7 L/min for the filter only outlet condition and the pulmonary mechanics (PM) outlet condition .....	117
<b>Table 5.1</b>	Interface Set 1: Lung delivery efficiencies (estimated as Tracheal Filter %) and regional deposition fractions (based on loaded dose) for the I-leucine EEG formulation (Batch 1) and an initial round of nasal interface designs with differing	

	flow pathways and the same straight flexible prong with 3 mm internal diameter .....	159
<b>Table 5.2</b>	Interface Set 2: Lung delivery efficiencies (estimated as Tracheal Filter %) and regional deposition fractions (based on loaded dose) for the l-leucine EEG formulation (Batch 1) and Dual interface designs connected to the dual outlet version of the air-jet DPI, compared with initial GE-S results.....	160
<b>Table 5.3</b>	Interface Set 3: Lung delivery efficiencies (estimated as Tracheal Filter %) and regional deposition fractions (based on loaded dose) for the l-leucine EEG formulation (Batch 2) and comparison of curved prong nasal interface configurations with 3 or 4 mm internal diameter.....	161
<b>Table 5.4</b>	Interface Set 4: Lung delivery efficiencies (estimated as Tracheal Filter %) and regional deposition fractions (based on loaded dose) for trileucine EEG formulation and comparison of small versus large curvature prong .....	162
<b>Table 5.5</b>	Interface Set 5: Lung delivery efficiencies (estimated as Tracheal Filter %) and regional deposition fractions (based on loaded dose) for the l-leucine EEG formulation (Batch 3) and comparison of nasal interface design effect .....	163
<b>Table 6.1</b>	Lung delivery efficiencies (estimated as Tracheal Filter %) and regional deposition fractions (based on 10 mg loaded dose) for the AS-EEG formulation and an initial round of different device designs .....	200
<b>Table 6.2</b>	Lung delivery efficiencies (estimated as Tracheal Filter %) and regional deposition fractions (based on loaded dose) for the AS-EEG formulation and comparisons of 10 vs 30 mg loaded powder in lead devices .....	201
<b>Table 6.3</b>	Lung delivery efficiencies (estimated as Tracheal Filter %) and regional deposition fractions (based on loaded dose) of the AS-EEG formulation and 30 mg dose loadings with the PD-3 device and filter-only vs. pulmonary mechanics (PM) outlet conditions .....	202



<b>Table 6.4</b>	Lung delivery efficiencies (estimated as Tracheal Filter %) and regional deposition fractions (based on loaded dose) for the AS-EEG formulation and comparisons of standard (0.55 mL) vs extended (1.5 mL) powder reservoir volume with the PD-3 device .....	203
<b>Table 7.1</b>	Lung delivery efficiencies (estimated as Tracheal Filter %) and regional deposition fractions (based on 10 mg loaded dose) for the AS-EEG formulation and NGI determined particle size characteristics for PD-2 device.....	240
<b>Table 7.2</b>	Lung delivery efficiencies (estimated as Tracheal Filter %) and regional deposition fractions (based on loaded dose) for the AS-EEG formulation and comparisons of 0.55 mL (standard) vs 1.5 mL (adjustable) powder reservoir with PD-2 device...	241
<b>Table 7.3</b>	Powder properties for each formulation based on primary particle size (geometric) and approximate bulk density.....	242
<b>Table 7.4</b>	Lung delivery efficiencies (estimated as Tracheal Filter %) and regional deposition fractions (based on loaded dose) for each formulation with 10 mg powder loadings and relative best metering element configuration PD-2 device .....	243
<b>Table 7.5</b>	Aerosol characterization based on next generation impactor (NGI) testing for each formulation with 10 mg powder loadings and the best metering element configuration PD-2 device (aerosol at air-jet DPI device outlet) .....	244

## Abbreviations

AAV	Air actuation volume
AS	Albuterol sulfate
BPD	Bronchopulmonary dysplasia
CFD	Computational fluid dynamics
CPAP	Continuous positive airway pressure
DPI	Dry powder inhaler
DPPC	Dipalmitoylphosphatidylcholine
ED	Emitted dose
EEG	Excipient enhanced growth
EET	Endotracheal tube
FPF	Fine particle fraction
GA	Gestational age
GE	Gradual expansion
HFNC	High flow nasal cannula
HPLC	High performance liquid chromatography
LV	Low volume (considered as $\leq 30$ mL)
MDI	Metered dose inhaler
MM	Metal mesh
MMAD	Mass median aerodynamic diameter
MP	Middle passage
N2L	Nose-to-lung
nCPAP	Nasal continuous positive airway pressure
NGI	Next generation impactor
NIPPV	Nasal intermittent positive pressure ventilation
NIV	Non-invasive ventilation
NMT	Nose-mouth-throat
NT	Nose-throat
PD	Passive design
PL	Phospholipid
PM	Pulmonary mechanics
RDS	Respiratory distress syndrome
SD	Standard deviation
SDD	Surfactant deficiency disorder
SLA	Stereo-lithography
VEI	Ventilation efficiency index

## **Abstract**

DEVELOPMENT AND OPTIMIZATION OF A LOW VOLUME AIR-JET DRY POWDER INHALER (DPI) PLATFORM FOR THE DELIVERY OF HIGH DOSE AEROSOLIZED POWDER TO INFANTS

By Connor Matthew Howe

A dissertation submitted in partial fulfillment of the requirements for the degree of Doctor of Philosophy at Virginia Commonwealth University.

Virginia Commonwealth University, 2022

Director: Dr. P. Worth Longest

Professor, Department of Mechanical & Nuclear Engineering and Department of Pharmaceutics

The overall goal of this research project was the development of an infant air-jet dry powder inhaler (DPI) platform for high-efficiency nose-to-lung (N2L) aerosol administration to infants through optimization of individual system components followed by expansion of the system to higher doses using a new approach. Primary challenges associated with aerosol delivery to infants using the N2L route include the extremely narrow extrathoracic airways, short inspiratory times (~0.2 sec) and very low volumes of air (~10 mL) available to form the aerosol. The infant air-jet DPI system was comprised of three main components: an air source, a small volume turbulence-based aerosolization engine (comprised of an aerosolization chamber and inlet/outlet flow passages, referred to as the air-jet DPI), and nasal interface, which form the “Infant Air-Jet DPI Platform”. The platform efficiently aerosolized spray-dried powder formulations with conditions safe for infant inhalation and provided lung-targeted delivery of inhaled therapeutics. Design parameters for safe inhalation included total air actuation volumes (AAVs) in the range of 10-30 mL, air flow rates below 10 L/min, and outlet

pressures below 35 cm H<sub>2</sub>O. Therapeutic dry powder formulations utilized in this project used the excipient enhanced growth (EEG) approach, which has previously been developed at VCU.

Initial optimization of the platform focused on the air-jet DPI design, resulting in three lead devices that produced emitted doses (ED) >80% (based on loaded dose) and mass median aerodynamic diameters (MMAD) <1.8 μm. The three leading devices all delivered approximately 50% of the loaded dose through a full-term NT *in vitro* model using an AAV of 30 mL, and maintained similar EDs and MMADs when lowered to an AAV of 10 mL. The remaining studies focused on the more challenging NT geometry of a preterm (estimated 1600 g) infant. Development of the air source produced three devices that were highly tunable and consistent, and when matched by the Q90 value (90<sup>th</sup> percentile of measured flow rate values during an actuation), each device performed similarly. With the ability to control the flow rate, lung delivery efficiency was increased from ~33% to over 50% in the preterm *in vitro* model when lowering the Q90 value from 4 L/min to 1.7 L/min. Performance of the platform was found to be insensitive to downstream pulmonary mechanics (lung resistance and compliance) and operated in a safe pressure range. Modifications to the nasal interface, including a rigid curved prong, improved lung delivery by 5-10% (absolute difference) resulting in a ~57% lung delivery efficiency. The final portion of this project expanded the air-jet DPI platform to enable large dose powder loading without impacting performance, and identified air-jet DPI design parameters that enabled similar performance across different formulations. The final prototype consisted of a passive design (PD) that enabled passive cyclic loading of the powder and provided an estimated >60% lung delivery efficiency of a model spray-dried formulation. Modifications to the dose metering elements produced similar performance between the

model formulation and a surfactant-EEG formulation, and performance was expected to remain consistent across a range (10 – 90 mg) of dose loadings.

In conclusion, the results of this study have produced an infant air-jet DPI platform that can safely (based on presented metrics) and rapidly (full dose estimated in under 3 minutes) deliver a variable (estimated 10 – 90 mg) dry powder formulation with high efficiency (~45 – 60% of loaded dose) to preterm infants (1600 g in vitro model) with consistent performance across multiple formulations via passive metering element configurations, which has not been previously achieved.

# Chapter 1 - Specific Aims

## *Introduction and Overview of Medical Need*

Neonatal respiratory distress syndrome (RDS) is a lung disorder most commonly affecting infants born prematurely [1]. Neonatal RDS often results from insufficient surfactant production in the underdeveloped lungs, and of the approved treatment options for RDS, surfactant replacement therapy is one of the most effective [1]. This therapy delivers a liquid bolus of surfactant to the lungs through intubation, which is then followed by a period of mechanical ventilation [1-3]. While this method is effective for treating RDS, it is not without risks and drawbacks. Performing intubation itself is invasive, can cause injury or infection and is often unsuccessful [4-6]. The liquid surfactant therapy can also lead to hypoxia, hypotension, fluctuations in hemodynamics and cerebral perfusion, or increased risks of pulmonary and intracranial hemorrhage [2, 4, 5, 7, 8]. Other issues with using liquid surfactant include non-uniform distribution in the airways and multiple high dose requirements around 100 mg/kg of phospholipids, which can be as low as 1.25 mL/kg or as high as 5.8 mL/kg of instilled surfactant solution [9]. Considering intratracheal volumes < 2 mL for infants up to 2 years of age [10], a 4 kg infant with a 4 mL/kg surfactant dose would need 16 mL of solution, which is a distressing amount of liquid to force through the windpipe.

The desire for alternate therapies to avoid the complications that can arise from liquid instillation have been well documented [1-3], with a leading solution being the aerosol delivery of the surfactant, in the form of either a nebulized solution or dry powder product. When considering aerosol delivery to the lungs of infants, common problems include very low lung delivery efficiencies (typically < 1%) [11], high inter-subject dose variability [12], and long

administration times [13]. While dry powder inhalers delivered doses much quicker than nebulizers, current interfaces and aerosol size lead to major depositional loss before reaching the small airways of infant lungs, resulting in low delivery efficiencies. On the other hand, if aerosolized drug particles are small enough to reach the small airways, they also run the risk of loss through exhalation.

To overcome challenges of safely delivering inhaled therapeutics to small airways, including those of infants, researchers at VCU have proposed and developed an Excipient Enhanced Growth (EEG) method [14-16]. An EEG formulation will facilitate improved lung delivery efficiencies by allowing relatively small sized aerosol (e.g., 1  $\mu\text{m}$ ) to penetrate infant upper airways and then deposit in the lungs through hygroscopic growth [17, 18]. Combining this drug delivery strategy with a newly developed and optimized delivery platform will allow for rapid, high efficiency delivery of a therapeutic to infant lungs without the associated risks of liquid instillation or intubation. Challenges that must be overcome include forming an aerosol with a small air volume consistent with an infant, delivering a high dose aerosol, navigating the small infant upper airways to enable sufficient lung delivery, and fostering lung deposition of the aerosol with very limited air volume for administration.

#### *Overall goal of this project*

The overall goal for this work is to develop and optimize a platform to effectively aerosolize carrier-free EEG formulations and deliver the associated inhaled therapeutics to infant lungs. Based on the EEG approach, micrometer sized drug particles can be delivered to and retained in infant lungs through hygroscopic growth. The use of a dry powder aerosol will

avoid the negative side effects associated with intubation and instillation, and rapidly deliver therapeutics over a time frame of seconds, compared to hours with nebulization at high doses. Safety considerations for delivery will include a maximum extrathoracic pressure of 25 cm H<sub>2</sub>O [19, 20]. A highly efficient lung delivery dose will be considered as > 60% of the loaded dose delivered to the lungs (tracheal filter for *in vitro* testing based on a preterm model) with a model EEG formulation.

### **1.1 Objective 1: Development and optimization of an air-jet DPI platform for aerosol drug delivery to infants**

*Rationale:* DPIs offer the ability to administer large doses of inhaled medications very quickly. It is expected that rapid dose delivery is important when administering surfactant aerosols to infants. However, all current DPIs on the market are passive devices that are actuated by large inhaled volumes consistent with an adult (~2 L and above). To make the advantages of DPIs applicable to infants, designs are necessary that can be actuated with positive pressure and form an aerosol with multiple orders of magnitude less air volume (e.g., 10 mL) than used with adult devices.

*Methods:* Platform development and prototyping were conducted using 3D modeling software and an in-house 3D printer. Initial device design was inspired by previous and current air-jet DPI studies performed at VCU [21-25]. Infant nose-throat (NT) models were used for *in vitro* testing and 3D printed in-house or from an outside company. The *in vitro* model was based on a high-quality infant CT scan and scaled down to full-term and preterm geometries based on height scaling. Aerosolization performance of an EEG powder formulation was



determined through cascade impaction testing (Next Generation Impactor; NGI) and established High Performance Liquid Chromatography (HPLC) drug content analysis, in collaboration with VCU Department of Pharmaceutics (Dr. Michael Hindle).

**Task 1.1:** Initial development of an air-jet dry powder inhaler (DPI) platform for rapid delivery of pharmaceutical aerosols to infants.

*Status:* Completed and published [26]

**Task 1.2:** Advancement of the infant air-jet DPI platform; Evaluation of different positive-pressure air sources and flow rates, as well as downstream pulmonary mechanics.

*Status:* Completed and published [27]

**Task 1.3:** *In Vitro* Analysis of Nasal Interface Options for High-Efficiency Aerosol Administration to Preterm Infants

*Status:* Completed and published [28]

*Outcomes:* Outcomes of this objective are a fully functional prototype of a positive pressure air-jet DPI platform for high efficiency aerosol delivery to infants that avoids the risks associated with current surfactant replacement therapy. As opposed to most alternative non-invasive therapies such as nebulization, this platform allows for rapid (seconds to minutes) full dose delivery instead of estimated nebulization times of hours to days. Expected performance of the final prototype includes lung delivery efficiency >60% of loaded dose using a model EEG formulation, an automated air source to eliminate operator variability, and consistent lung

delivery efficiency, all while maintaining safe operating parameters (extrathoracic pressure  $\leq$  25 cm H<sub>2</sub>O).

## **1.2 Objective 2: Expansion of the infant air-jet DPI platform to include capabilities for high powder mass loadings with minimal change and potential enhancements in aerosolization performance**

*Rationale:* While the previous objective seeks to develop and optimize the air-jet DPI platform for surfactant replacement therapy, the infant air-jet DPI is viewed as a general aerosol delivery platform with multiple potential applications also including but not limited to inhaled antibiotic or antiviral therapy. For the widest range of applications, an easy-to-use platform should enable a wide range of dose selection (e.g., 10-100 mg of dry powder formulation) with a passive reloading strategy utilizing a single loading action, and consistent performance across the range of loaded doses. The platform should be able to effectively aerosolize and deliver a variety of powder formulations with different properties and densities.

*Methods:* Best performing platform components, as established in Objective 1, guided the expansion and design modifications to enable consistent performance across larger powder mass loadings and various formulations. Aerosolization characterization (MMAD, ED, as well as FPF) and performance (regional deposition fractions and estimated lung delivery efficiency) were determined by the same methods as with Objective 1. Studies utilized NGI characterization and *in vitro* NT deposition and transmission performance through an infant NT model.

**Task 2.1:** Develop and test multiple passive cyclical dose loading strategies, select a lead design, and explore potential enhancements in lung delivery efficiency.

*Status:* Completed and published [29]

**Task 2.2:** Investigate advancements for the Infant air-jet DPI platform with passive cyclic loading and passive metering elements for various powder formulations.

*Status:* Completed, pending publication

*Outcomes:* Outcomes of this objective was an infant air-jet DPI platform that utilizes passive cyclic loading, and building upon the previously developed platform, consistency and safety parameters were maintained. Expected performance of the final prototype included lung delivery efficiency ~50% of loaded dose using multiple EEG formulations and consistent performance across a range of loaded dose (e.g., 10-30 mg for initial testing) while enabling a large selectable range without expected performance loss.

## **Chapter 2 - Background and Motivation**

### **2.1 Neonatal respiratory distress syndrome (RDS)**

Neonatal respiratory distress syndrome (RDS), also known as surfactant deficiency disorder (SDD) or previously hyaline membrane disease, is a breathing disorder caused by insufficient surfactant production [1]. This occurs more commonly the more preterm an infant is born and it is estimated that worldwide, over 1 in 10 babies are born prematurely [30]. The pulmonary surfactant system does not typically develop until 29-32 weeks gestational age [31]. The role of pulmonary surfactant is to facilitate breathing and gas exchange by forming a surface-active layer and lowering surface tension in the alveolar region, making it easier for the lung to expand and contract. For underdeveloped lungs, this lack of surfactant and consequent increase in surface tension can lead to alveoli collapse (less surface area for gas exchange), reduced pulmonary compliance, and increased work of breathing, resulting in RDS [32, 33]. Of the treatment options for RDS (such as invasive and non-invasive ventilation) one of the most effective forms of treatment is surfactant replacement therapy [34, 35].

### **2.2 Surfactant replacement therapy**

Currently, the only FDA approved method for surfactant delivery to the infant lungs is in the form of a liquid bolus delivered through intubation, followed by mechanical ventilation [1-3, 36, 37]. While this method is effective for treating RDS, it can lead to significant secondary problems. Performing intubation itself is invasive, can cause injury or infection and is often unsuccessful [4-6]. Intubation efforts can lead to hypoxemia, bradycardia, increased cranial pressure and trauma [38]. Potential problems with liquid surfactant instillation include

endotracheal tube or airway blockage leading to hypoxia and hypotension [1], fluctuation in hemodynamics and cerebral perfusion [39-42], and also increases the risks of pulmonary and intracranial hemorrhage [8, 43]. Other issues with using liquid surfactant include non-uniform distribution in the airways and multiple high dose requirements around 100 mg/kg of phospholipids [9], while in theory, only 3 mg/kg is sufficient to coat the alveolar airways [44]. This therapy also typically requires mechanical ventilation after instillation which can cause inflammatory lung injury [45] and bronchopulmonary dysplasia (BPD) [5, 46, 47]. The long list of potential side effects has led to a high interest in seeking alternative, non-invasive methods of delivery for surfactant therapy [2, 3].

### **2.3 Alternative treatment approaches**

Newer methods such minimally invasive surfactant therapy (MIST) and less invasive surfactant administration (LISA) seek to lessen the trauma and side effects associated with traditional instillation by using a catheter or small tube. While further conformation is needed, initial studies indicate lower occurrences of BPD and hemorrhage; however, for many immature infants, intubation and mechanical ventilation is only delayed [48]. It has also been shown that surfactant instillation only delivers about 7% of the instilled volume of surfactant to the non-dependent alveolar regions [49]. While these methods are a step in the right direction, a non-invasive alternative form of treatment is still greatly needed.

Forms of non-invasive ventilation (NIV) that are available to infants include continuous positive airway pressure (CPAP), high flow nasal cannula (HFNC) therapy, variable pressure methods, and others [50]. In conjunction, new methods to deliver inhaled medications during

NIV have also been explored [1-3, 51, 52]. Unfortunately, these aerosol delivery methods during NIV have shown problems including very low lung delivery efficiencies, high inter-subject dose variability, and long administration times [53-57]. The poor delivery efficiencies of pharmaceuticals to infant lungs have been documented in both *in vitro* experiments [58-60] and *in vivo* studies [12, 52, 61, 62] with lung delivery efficiencies typically around 1% [58, 63]. Another significant concern as seen in an *in vivo* study of Fok et al. [12], using an MDI, is dose variability where the maximum lung dose (4.52  $\mu\text{g}$ ) to an individual was over 20-fold higher than the minimum (0.215  $\mu\text{g}$ ), with two actuations. Furthermore, with such low efficiencies, delivering a surfactant dose on the order of 10 mg or higher could take hours to days. Surfactant therapy within the first 2 hours of birth have been shown to reduce mortality as well as short- and long-term complications [9], making long delivery times unattractive.

#### **2.4 Review of current nebulized surfactant aerosol delivery**

Most investigations for alternative surfactant delivery methods have been in the form of nebulized therapy. Types of nebulizers include jet, vibrating mesh, and ultrasonic. Jet nebulizers use pressurized air flowing through a small orifice to aerosolize a solution, while a vibrating or ultrasonic nebulizer typically uses a piezoelectric mesh/membrane. While there are a number of different configurations, Figure 2.1 illustrates the basic setup of each nebulizer type. Nebulized aerosol has the benefit of being able to integrate into other forms of NIV support such as CPAP, HFNC, or nasal intermittent positive pressure ventilation (NIPPV) therapy.

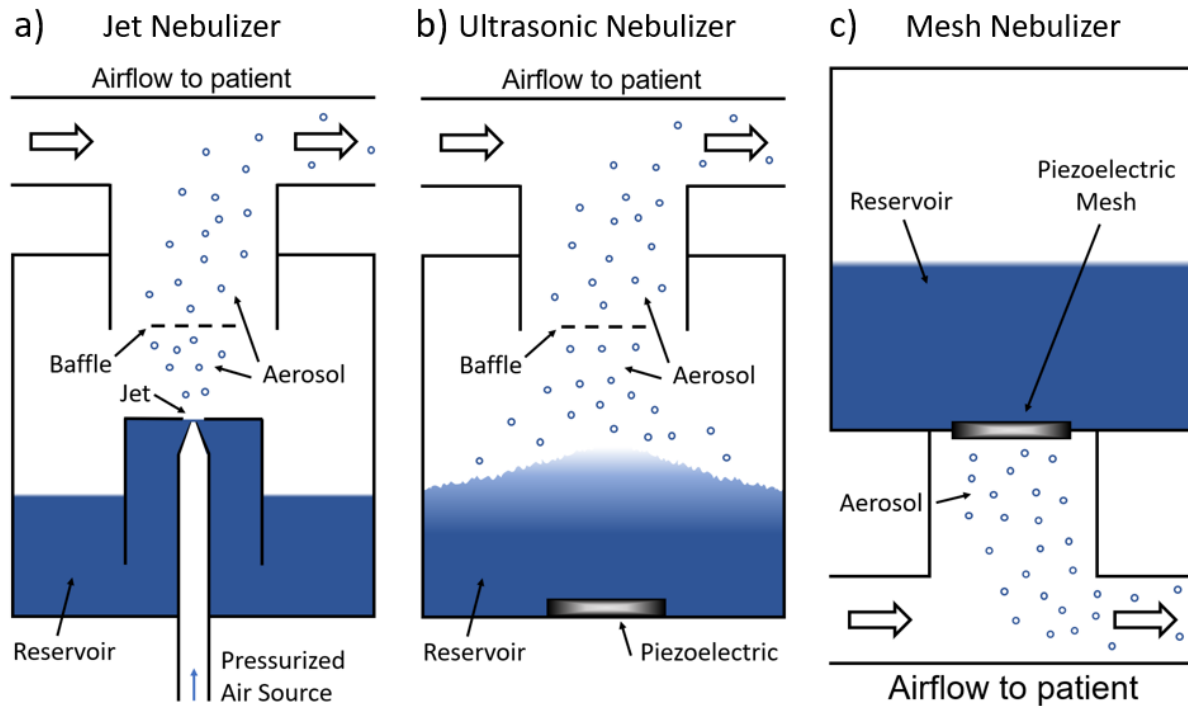


**Figure 2.1** Illustrations of basic setup for different nebulizer types. **(a)** Jet, **(b)** Ultrasonic, and **(c)** Mesh

Despite relative ease of interfacing with NIV support, nebulized surfactant therapy still has significant drawbacks, such as extremely low lung delivery efficiencies  $\sim 0\text{-}3\%$  [64, 65] or less than  $\sim 14\%$  with some of the most recent advancements [66], while inter-subject variability is another concern [49, 67], especially considering an *in vivo* study by Linner et al. [49] in which lung delivery efficiencies ranged from only 2% up to 40% across subjects while no significant difference in blood gasses was observed. Few studies show benefit from nebulized surfactant treatment while treatment times remain long (hours), indicating the most benefit from this treatment type may only be as a prophylactic therapy or for a small range of infants and conditions, while a wide range solution is still lacking. Table 2.1 lists a summary of studies (*in vitro*, *in vivo* animal, and clinical) utilizing nebulized surfactant treatment.

**Table 2.1** Summary of select nebulized surfactant studies, grouped by study type (*in vitro*, *in vivo* animal, or clinical)

Study	Subject	Nebulizer / Delivery Method	Delivery Dose of PL (mg/kg)	Lung Delivery Efficiency (%)	Delivery Time	Outcomes
Bianco 2019 <sup>[66]</sup>	1750 g Infant model (PrINT)	Mesh / Nasal prong via nCPAP	200, Poractant Alfa	13.7	18.9 minutes	<14% mean lung delivery efficiency
Lewis 1991 <sup>[64]</sup>	Preterm Lamb	VISAN / Ventilator	~40, Harvested natural surfactant or Survanta	1.9 (Natural) 2.7 (Survanta)	~3 hours	Improved VEI compared to control group
Fok 1998 <sup>[65]</sup>	Rabbit	Jet and Ultrasonic / Ventilator	~70, Exosurf ~125, Survanta	0-1	1 hour	Little to no improvement in blood gasses observed
Hutten 2015 <sup>[68]</sup>	Preterm Lamb	Mesh / Nasal prong via nCPAP	Average 229-978, Poractant Alfa	unknown	30-180 minutes	Improvement in large 3-hour treatment only
Linner 2015 <sup>[49]</sup>	Piglet	Mesh / Neonatal mask or prong via nCPAP	200, Poractant Alfa	3-16 (mask) 2-40 (prong)	16-92 minutes	No significant difference in blood gasses
Nord 2019 <sup>[67]</sup>	Piglet	Mesh / Custom nasal prong via nCPAP or NIPPV	200, Poractant Alfa	15.9 ± 11.9 (nCPAP) 21.6 ± 10.0 (NIPPV)	~15-25 minutes	Large deviations in lung delivery efficiency
Rey-Santano 2020 <sup>[69]</sup>	Surfactant-deficient Piglets	Mesh / Nasal prong via nCPAP	100/200/400/600, Poractant Alfa	unknown	~13-71 minutes	Improved pulmonary status for dose >100mg/kg, not as much as instillation



Berggren 2000 <sup>[70]</sup>	Infant with diagnosed RDS (28-34 weeks GA)	Jet / Nasal prong via nCPAP	~300, Curosurf	unknown	~3 hours	No significant difference compared with control group
Finer 2010 <sup>[71]</sup>	Infant at risk of RDS (28-32 weeks GA)	Mesh / Neonatal prong via nCPAP	~40-50, Aerosurf initial dose, up to 170-210	unknown	3-12 hours	Treatment tolerated; no control group used
Minocchieri 2019 <sup>[72]</sup>	Infant with evolving RDS (29-32 weeks GA)	Mesh / Mask via bubble nCPAP	200, Poractant Alfa	unknown	unknown	Reduced need for intubation with infants at least 32 weeks GA
Sood 2019 <sup>[73]</sup>	Infant with diagnosed RDS (24-36 weeks GA)	Jet / Nasal prong via nCPAP, NIPPV, or HFNC	100/200, Surfactant (1 or 2 total doses)	unknown	unknown	Treatment well tolerated for infants above 28 weeks GA, no control group used

GA, Gestational Age; PL, Phospholipid; RDS, Respiratory Distress Syndrome; VEI, Ventilation Efficiency Index

## 2.5 Highly efficient dry powder therapy

New aerosol delivery techniques have been developed that avoid invasive intubation and ventilation, yet high efficiency aerosol delivery is lacking. Nebulization rates and lung delivery efficiencies limit the effectiveness of these treatments in infants. While maintaining the non-invasive benefits, therapeutic drug in the form of a dry powder aerosol is an attractive approach as it has the potential to be rapidly administered in large doses. Dry powders also avoid dilution effects not having to be suspended in a liquid, and are typically more stable and less susceptible to environmental factors. However, the current limiting factors to dry powder lung delivery efficiency is the ability to deaggregate or aerosolize the powder affecting device retention and particle size.

Particle size of an aerosol is an important factor because it will determine the deposition mechanism. Deposition can occur through inertial impaction (larger and intermediate sizes), gravitational sedimentation (larger and intermediate sizes), or Brownian diffusion (smallest sizes), and the particles aerodynamic size should be considered as it takes into account both geometric size and density [74]. For infants, it is typically held that particles  $> 5 \mu\text{m}$  will deposit in the upper respiratory tract through impaction, intermediate sized particles ( $2\text{-}5 \mu\text{m}$ ) will deposit via impaction or settling in the central respiratory tract, and particles in the range of  $\sim <1$  to  $3 \mu\text{m}$  can deposit in the small airways through multiple mechanisms (impaction, sedimentation, and diffusion) if not lost through exhalation [53]. To overcome these challenges and requirements for dry powder delivery, the dynamic increasing particle size approach of Excipient Enhanced Growth (EEG) has been developed at VCU by Hindle and Longest [14-16].

## 2.6 EEG and spray dried aerosol formulations

For a dry powder formulation to be truly effective and have a high lung delivery efficiency, it needs to be highly dispersible under target operating conditions (infant delivery in this case) and have desired particle sizes. The EEG method is a potential solution to increasing lung deposition efficiencies through dynamic sizing. An EEG formulation includes a hygroscopic excipient that allows particles to grow in size through water absorption in the high humidity environment of the lungs. This approach allows for particles small enough in size to penetrate the extrathoracic and larger airways to then grow sufficiently to deposit in the small airways. For this approach to work, the dry powder formulation will need to be highly dispersible and have sufficiently small primary particles. As aerosols are typically polydisperse with a lognormal size distribution, the mass median aerodynamic diameter (MMAD) is a useful parameter for indicating how well a powder could penetrate the upper airways. For example, considering the infant respirable range of  $\sim < 2 \mu\text{m}$ , if the MMAD of the aerosolized powder is  $2 \mu\text{m}$ , it is likely that half of the drug mass will not reach the deep lungs, as half of the mass belongs to particles with sizes larger than  $2 \mu\text{m}$ . While the standard deviation of the size distribution can vary, the smaller the MMAD the higher penetration to small airways will be. It is expected that EEG aerosols with an MMAD between  $1\text{-}1.5 \mu\text{m}$  will be able to achieve high lung delivery efficiencies.

Preparations of dry powders are typically performed by micronizing and milling, or through spray drying. Micronizing involves the crystallization of a formulation followed by milling, and results in powders with high surface charge leading to a tendency to aggregate and having poor dispersibility [75]. Spray drying powders is a preferable approach as it is widely

used and scalable, and can produce particles of relatively uniform size in the respirable range [60]. The spray drying process involves feeding a formulation solution or suspension into a controlled drying chamber with an atomizer producing liquid droplets of a desired size, which are then dried and collected. The stock EEG formulation contains an excipient and dispersion agent as well as the therapeutic. Combining the EEG method and spray-drying technique, a highly dispersible dry powder formulation (using mannitol as the hygroscopic excipient and leucine as the dispersion enhancer) has been shown to have low upper airway depositional loss [76].

## **2.7 Motivation for air-jet DPI and operating principles**

As mentioned earlier, a desirable alternative to liquid instillation is the delivery of a therapeutic in aerosol form. Aerosol delivery is achieved by three main platforms; nebulizers, metered dose inhalers (MDIs), and dry powder inhalers (DPIs). Nebulizers convert a liquid solution or suspension formulation into an aerosol which can be produced through compressed air jets, ultrasonics, or a vibrating mesh. Nebulizers are predominately the most expensive method to produce aerosols and also the slowest. While this form of aerosolization can be easily incorporated into long term treatment such as CPAP or HFNC, some studies in humans have not shown that aerosolized surfactant delivered during this method to have a benefit [77], expectedly from the low lung delivery efficiencies and very slow aerosol delivery rate. Metered dose inhalers typically come in the form of a liquid propellant-drug formulation filled canister with a manually operated dosing actuator. Each actuation is designed to release a precise amount of aerosol, but this also requires a precise coordination and inhalation procedure

performed by the patient. Spaces and holding chambers have been developed to help aid the process, but even with good technique lung deposition is often poor [78]. MDIs also deliver very small quantities of inhalation aerosol ( $\sim 100 \mu\text{g}$ ), so cannot be considered for surfactant aerosol delivery ( $>10 \text{ mg}$ ). Lastly, dry powder inhalers can be active or passive, and can deliver high powder masses during inhalation. A passive DPI relies on patient inhalation to aerosolize the powder, which eliminates the need to coordinate between actuation and inhalation as with MDIs; however, the inhalation rates for passive DPIs are typically over 30 L/min, which is well beyond the capabilities of an infant. Lastly, there are active DPIs, which do not contain propellants but use an external energy source (pneumatic, mechanical, or electrical), to deaggregate and aerosolize the powder.

The aim of this work is in developing an active air-jet DPI style platform for the aerosolization and delivery of an inhaled therapeutic at high dose to an infant. The operating principle of an air-jet DPI uses a positive pressure air source directly upstream of an aerosolization chamber that contains a therapeutic formulation in dry powder form [23, 79-81]. Small diameter flow passages form an inlet and outlet to the aerosolization chamber. The turbulent energy generated by the air-jet aerosolizes the powder within the aerosolization chamber [82]. In contrast to a passive DPI that relies on the negative pressure generated by the patient's inhalation, a positive pressure source can facilitate a full inhalation for an infant who is unable to coordinate or control a specific breath profile. Delivering both the aerosol and inhalation breath to an infant requires that the infant air-jet DPI system is in airtight communication with the infant's airways. This platform will allow for controlled and repeatable delivery conditions, thereby eliminating one major source of inter- and intra-subject variability

in aerosol delivery. Initial development of the platform will be considered as three main components; the air source, the air-jet DPI, and the nasal interface. Initial development will utilize a manually operated syringe as the air source; however, a final platform prototype will use a highly controllable and consistent automated air source. Figure 2.2 depicts the general platform setup with initial hand operated air source, in connection with an *in vitro* infant nose-throat model. Labeled parts include (1.) the air source which provides the actuation volume and aerosolization energy, (2.) the air-jet DPI which contains the aerosolization chamber housing the powder, (3.) the nasal interface responsible for dissipating the turbulent jet of air exiting the DPI and delivering it to the infant, and others.

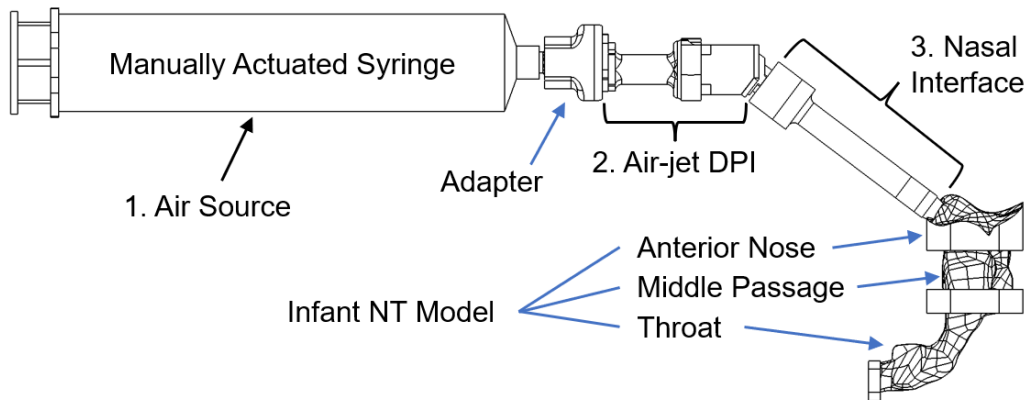


**Figure 2.2** Basic drawing air-jet DPI platform with three main components labeled (1. Air Source, 2. Air-jet DPI, 3. Nasal Interface) in connection to a full-term infant NT model

## 2.8 Positive pressure DPIs

While there are many commercially available passive DPIs, fewer options exist for active DPIs. Of the available active DPIs, fewer still use positive pressure or compressed air as the

energy source. One example is the Exubera system (Pfizer, New York, NY/Nektar Therapeutics, San Carlos, CA) which uses compressed air (through a hand actuated piston pump) to initially aerosolize an insulin therapy powder into a holding chamber before the patient inhales [83]. While this system uses a compressed air source, it would not allow for controlled delivery to an infant in its current form as it still requires the patient to actively inhale the therapeutic. Other devices such as the PuffHaler (Aktiv-Dry, LLC, Boulder, CO, USA) and Solovent (Becton, Dickinson and Company, Franklin Lakes, NJ, USA) use a bulb or syringe actuation to aerosolize a powder into a holding chamber in a similar manner as the Exubera system, and are made for adult or pediatric applications. While these devices require inhalation by the patient from the holding chamber or via mask interface, these two systems have also been used in a direct nasal actuation configuration through a prong or nare adapter in a dry powder measles vaccine study; however, the direct nasal route was shown to be less effective likely due to increased nasal deposition [84]. One device that meets infant delivery conditions is the Insufflator (DP-4M Dry Powder Insufflator, PennCentury), which is designed specifically for intra-tracheal delivery of dry powders during mouse testing [85]. While this device used positive pressure syringe actuation to deliver aerosols directly to the lungs, it is no longer commercially available, and nasal depositional losses are anticipated to remain high.

Other custom positive pressure active DPI devices have been developed as reviewed by Longest et al. [81], but most are designed for adults, operating at conditions not suitable for infant delivery. As there are no commercially available platforms for the desired infant air-jet DPI, initial work and investigation on this platform has been performed at VCU.

## 2.9 Review of VCU air-jet DPIs

Based on the EEG approach, initial development for a positive pressure DPI system has been performed at VCU. Devices using capsule based loading (size 0 capsule) of an EEG therapeutic followed by a 3D rod array were first investigated for alternatives to passive DPIs and were tested in conjunction with HFNC treatment [86]. Using a realistic adult nose-mouth-throat (NMT) model, *in vitro* testing of these devices produced upper airway depositions of < 10% and lung delivery efficiencies of approximately 60% [87]. For pediatric and infant conditions, low air volume (LV) DPI devices were developed that operate with air actuation volumes of 10 mL, and while several configurations were considered, the best performing device was able to produce an aerosol with 1.56  $\mu\text{m}$  MMAD and an emitted dose (ED) of 61.9% [23]. *In vitro* testing using a pediatric model was conducted for both nose and mouth inhalation, using a nose-throat (NT) or mouth-throat (MT) model and optimized LV-DPI devices [22], resulting in approximately 60% lung delivery efficiencies and < 10% upper airway depositional loss [88]. It should be noted that scaling down the target patient (from adult, to child, to infant) significantly increases the difficulty of efficient lung delivery. As the geometry of patient airways shrink, the lower the tidal volumes (amount of air in the normal breathing cycle), and the more restrictive the pulmonary mechanics (such as resistance, compliance, and safe pressure or flow rate limits), all lead to more restrictive delivery conditions, less energy available for aerosolization, and higher demands for aerosol properties and device efficiency.

Considering infant conditions, initial studies utilizing the previously developed LV-DPI and a surfactant EEG formulation have been performed [89, 90]. In these studies, several modifications were made with the goal of animal testing via oral tracheal intubation of rats. For



this type of delivery, the actuation volume was reduced to 3 mL, and an extended delivery tube was included. Other configurations tested included removing the capsule loading style and using a containment chamber approach, and well as modifications to the aerosolization chamber. Of the configurations tested, the best results were seen with a reduced size aerosolization chamber (0.21 mL volume opposed to the 0.68 mL of a size 0 capsule) with three inlet jets and a 90 mm extended delivery tube, with a 3 mg loading dose, leading to an ED of 92.4% and a Dv50 of 2.7  $\mu\text{m}$  (MMAD size not reported).

Figure 2.3 illustrates the axial cross sections of the assembled DPIs initially developed (Figure 2.3a) [23] and modified for animal testing (Figure 2.3b) [91]. The main components labeled include the DPI Inlet and Outlet, as well as the aerosolization chamber. For the initial DPI (Figure 2.3a) the aerosolization chamber consisted of a size 0 capsule which is loaded with powder and then pierced by the capillaries upon device assembly. The aerosolization chamber for the modified DPI (Figure 2.3b) utilized a chamber that was directly loaded with powder before device assembly.

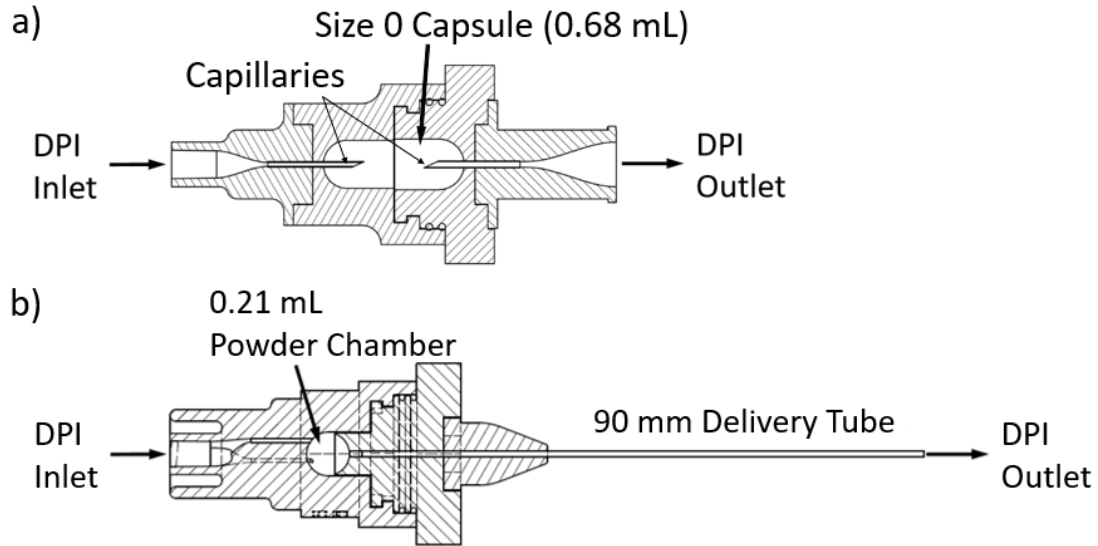


**Figure 2.3** Axial cross section of assembled low-volume dry powder inhalers (LV-DPIs) for **(a)** initial device and **(b)** modified animal delivery device

## 2.10 Mechanics of powder deaggregation

Generally, pharmaceutical powder deaggregation is most affected by turbulence and impaction [82]. Turbulence is chaotic swirling eddies of air flow, which can separate particles through shear forces as well as causing impactions. The turbulent based shear forces can be quantified as shear stress as described by Xu et al. [92]. Multiple studies have shown a strong correlation between turbulence and deaggregation using entrainment tubes or DPIs [92-97]. The presence of turbulent flow can be determined through the calculation of Reynolds number for a specific scenario, where Reynolds number ( $Re$ ) depends on the density ( $\rho$ ) and viscosity ( $\mu$ ) of a fluid, its velocity ( $v$ ), and the diameter ( $D$ ) of the pipe or capillary it is flowing through as described by equation 1.

$$Re = \frac{\rho v D}{\mu} \quad (1)$$

A Reynolds number value greater than 4000 is accepted as fully turbulent, with a transitional range down to 2300 where flow becomes laminar. Initial designs of the air-jet DPI utilize an inlet diameter of 0.6 mm, and flow rates around 3 L/min, resulting in a jet velocity around 175 m/s. Using the properties of NTP room air, it can be calculated that the air-jet entering the aerosolization chamber is fully turbulent with a Reynolds number of nearly 7000. Using this dimension for the inlet, flow rates as low as 1.75 L/min will also be fully turbulent, with a Reynolds number slightly over 4000.

Deaggregation from impaction occurs when clusters of particles collide with an object, causing separation of individual particles. Impaction can be controlled by directing an aerosol stream into an object such as a wall or baffle, or through a mesh screen. In a study by Voss and Finlay, [98] both turbulence and impaction-based breakup was investigated, utilizing entrainment tubes with and without mesh screens. To determine if particles impact on the mesh screen or not, Stokes number can be calculated for a particle or cluster size, flowing around an obstruction (bars of the mesh). If a particle has a Stokes number  $\ll 1$  it will not likely detach from the air stream thereby avoiding impaction, whereas a value  $\gg 1$  or  $>10$  will impact on a bar of the mesh. Calculating the particles Stokes number ( $Stk$ ) can be performed using equation 2, where ( $U$ ) is the velocity of the particle, ( $\rho$ ) is the density of the particle, ( $d$ ) is the diameter of the particle, ( $\mu$ ) is the viscosity of air, and ( $D$ ) is the diameter of the mesh bars.

$$Stk = \frac{U\rho d^2}{18\mu D} \quad (2)$$

In the study, the meshes were found to produce Stokes numbers  $\gg 1$ , indicating impaction occurred for the carrier particles. However, the addition of the mesh was found to have little effect on additional deaggregation for the setup used.

While turbulence may be the strongest deaggregation method, both factors will be investigated using various aerosolization chamber designs as well as the inclusion of rods or meshes in the nasal interface, as impaction based deaggregation may be more significant for different air-jet DPI configurations.

### **2.11 Requirements for an infant air-jet DPI platform**

In order to address problems with aerosol delivery without the use of intubation, and to avoid interface issues with the wide array of existing NIV systems, a stand-alone air-jet DPI platform for nose-to-lung (N2L) aerosol delivery is desired. This platform will allow for the rapid and efficient delivery of high dose therapeutics to infant lungs and can be used as either a prophylactic or rescue treatment. For a rapid surfactant replacement therapy such as this to be safe and effective, multiple issues must be considered. Control over the extrathoracic pressure generated by the platform is important as excessive pressure can cause lung damage as well as other complications [99, 100]. Studies have shown pressures in the range of 20-25 and as high as 35 cm H<sub>2</sub>O to be safe for full-term and preterm neonates [19, 20, 101, 102]. Another consideration is the amount of air being delivered to the lungs. Tidal volumes (standard breathing volumes) for infants are generally accepted to be between 5-10 mL/kg [39, 40, 99, 103] and for this work, a tidal volume of 7.5 mL/kg will be used. During ventilation or resuscitation, inspiratory times range from 0.25 to 0.5 seconds for infants, and are typically around 0.5 seconds [20, 99, 101, 103]. Using these tidal volumes and inspiratory times, an acceptable range for flow rate in this work will be considered as 1 to 5 L/min.

Two initial design parameters will be used for infants; a preterm condition representing a 1600 g neonate and a full-term condition representing a 3550 g neonate. For valid *in vitro* testing, downstream pulmonary mechanics will also be considered in terms of compliance and resistance. Expected pulmonary resistance for an infant with RDS is between 100-200 cm H<sub>2</sub>O/l/s [104-107]. While compliance can vary, especially during the first hour after birth [108], reasonable values are expected between 0.3-0.5 mL/cm H<sub>2</sub>O kg [104, 109]. With the above parameters, a highly efficient air-jet DPI platform will be developed to provide safe and rapid surfactant treatment to an infant to replace intubation and invasive ventilation.

## **2.12 Review of DPI dose loading strategies**

There are three main strategies when it comes to delivering doses with a DPI, which can be categorized as single dose, multi-dose unit, or multi-dose reservoir. A single dose DPI can be either disposable (one-time use) or need to be reloaded (typically with a preloaded capsule or blister) between treatments. Examples of commercial single dose DPIs include the Rotohaler<sup>®</sup>, Aerolizer<sup>®</sup>, and Handihaler<sup>®</sup> which require active inhalation for aerosolization and strong patient compliance for efficacy, while other examples include the Puffhaler, Solovent, and Exubera as previously described. A multi-dose unit DPI works similarly to a single dose DPI however, multiple doses can be loaded at a time in the form of a pre-filled cartridge, blister pack, or blister strip. Once a dose has been administered, advancement to the next dose can be performed automatically or manually for subsequent treatments. Examples of commercial multi-dose unit DPIs include the Diskhaler<sup>®</sup>, Diskus<sup>®</sup>, and Elipta<sup>®</sup>. The multi-dose reservoir strategy utilizes a large (relative to dose) reservoir of powder that can be metered into single

doses. The metering action is typically performed volumetrically by the patient twisting or pushing a metering cup or slot, which brings a single dose from the reservoir to an aerosolization area. Examples of commercial multi-dose reservoir DPIs include the Easyhaler<sup>®</sup>, Taifun<sup>®</sup>, and Turbuhaler<sup>®</sup>. For all the multi-dose DPIs mentioned, active inhalation and patient compliance are required to aerosolize the dose once it has been exposed or metered into the aerosolization area. Figure 2.4 illustrates the basic operating principles for each type of dose loading strategy.

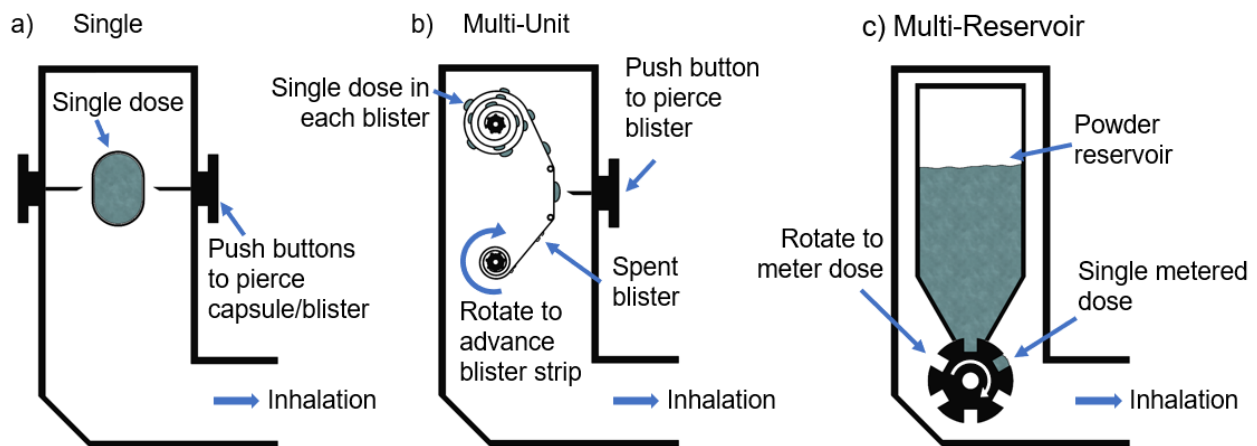


**Figure 2.4** Illustrations of the basic operating principles for the three main dose delivery strategies for **(a)** Single dose, **(b)** Multi-dose Unit, and **(c)** Multi-dose Reservoir

A benefit of a multi-dose system is that it allows for a period of continued treatment without the significant interruption of a reloading action. For neonates with RDS, different doses based on birth weight and the time sensitivity of treatment could be important driving factors for the need of a multi-dose system for a positive pressure infant device. One reservoir style multi-dose system has been developed by Pohlmann et al. [110] which is meant to continuously produce aerosol over a period of time, delivering treatment in conjunction with

nasal CPAP for example. This system uses a powder container above and feeding into a small dispersion chamber and capillary tube through which pulses of air continuously aerosolize small amounts of powder at a time. Another approach that could be adapted is the use of a dry powder nebulizer as described by Fleming et al. [111] which is meant to be used with spontaneously breathing patients. A dry powder nebulizer of this design incorporates a preloaded blister pack (like similar multi-dose unit systems) with a piezo vibrating element to aid in powder aerosolization once the blister has been pierced. The piezo element (nebulizer) can be triggered to only vibrate at the beginning of an inhalation cycle to improve efficiency.

### **2.13 Dose loading strategies for the air-jet DPI platform**

The final prototype for the air-jet DPI platform will need to enable selectable dose loadings in the estimated range of 10-90 mg of powder with bulk densities as low as  $0.03 \text{ g/cm}^3$ , and with minimal to no impact on performance or operating procedures. The bulk of the powder dose should be protected from repeated actuation air cycles, which could form aggregates and expose the powder to water vapor content (i.e., a large aerosolization chamber housing the full dose). Another consideration is the mass and rate of dry powder delivery. In a pilot study by Pohlmann et al. [110], mechanically ventilated pigs received  $\sim 1000 \text{ mg}$  of dry or humidified surfactant aerosol delivered through a thin catheter in an endotracheal tube, in which the dry surfactant aerosol formed a soft aggregate clot in the lower trachea. While the delivery rate was not reported, and the dose delivered was an estimated 1-2 orders of magnitude larger than expected for the air-jet DPI platform, the ability to control the dose delivery rate is needed to avoid overly rapid dose delivery. Balancing good lung delivery

efficiency and fast delivery times is a significant design challenge. Table 2.2 highlights different delivery time ranges with different drug mass delivered per actuation, and assumes a 5 second breath hold and estimated 6 second actuation cycle. For rapid treatment (emergency and rescue), a max delivery time of 2-3 minutes is a design goal.

**Table 2.2** List of dose per actuation and total delivery time for select total doses

Dry powder dose (mg)	Dose per actuation (mg)	Total actuations	Total time (s)
10	1	10	60
	3	4	24
	5	2	12
30	1	30	180
	3	10	60
	5	6	36
90	1	90	540
	3	30	180
	5	18	108

To address the challenges for dose delivery in the infant air-jet DPI platform, a *passive cyclic loading* strategy will be investigated which employs a separate powder reservoir, connected to the aerosolization chamber via a metering element. Utilizing a passive approach, a selectable dose can be loaded and administered with no additional steps required by the user. Passive loading for each dose per actuation will be performed by gravity and/or hydrodynamic forces during operation. The final platform prototype will consist of a single device able to accommodate a variable range of powder doses with consistent dose per actuations and overall performance.



## Chapter 3 - Initial Development of an Air-Jet Dry Powder Inhaler for Rapid Delivery of Pharmaceutical Aerosols to Infants

Task 1.1 – Published: *Journal of Aerosol Medicine and Pulmonary Drug Delivery*

### 3.1 Introduction

Aerosol delivery to infants is known to have a number of problems including poor lung delivery efficiency, high inter-subject dose variability and long administration times.[53-57] These issues occur for infants receiving aerosols during spontaneous respiration, non-invasive ventilation (NIV) and mechanical ventilation with an endotracheal tube (ETT).[54, 56, 112, 113] Poor delivery efficiency of pharmaceutical aerosols to infant lungs has been documented with both *in vitro* experiments[58-60] and *in vivo* studies[12, 52, 61, 62] employing commercial delivery systems and patient interfaces. Considering *in vitro* studies employing preterm or full-term newborn infant conditions and nasal or nasal-oral interfaces (i.e., nose-to-lung aerosol administration), lung delivery efficiencies are typically <1% and often 0% of the nebulized or nominal dose.[58, 59] One exception is the *in vitro* study of Sunbul et al.,[58] which achieved a maximum 1.3% lung delivery efficiency with a preterm model through selection of the best performing mode of NIV for aerosol administration (high-flow nasal cannula) and optimization of the nebulizer position in the flow circuit. *In vivo* studies employing jet nebulizers or metered dose inhalers (MDIs) report similar lung delivery efficiencies with values <1% for preterm infants[12] and increasing to <1.5% for infants up to one year old.[114-116]

It is often held that modern mesh nebulizers will substantially increase aerosol lung delivery efficiency to infants. However, Reminiac et al.[61] considered the delivery of a mesh nebulized radiolabeled aerosol to a macaque model of a full-term infant using a nasal cannula

interface. Lung delivery efficiency of the aerosol remained <1% of the nebulized dose, was highly dependent on ventilation gas flow rate, and was not improved with the use of a mask interface.[61] The recent *in vivo* human subject study of Corcoran et al.[117] implemented a vibrating mesh nebulizer with nasal cannula interface applied to newborn infants and reported ~1% lung delivery efficiency of loaded dose over a 2 minute period. Using a mesh nebulizer system specifically designed for infants on nasal continuous positive airway pressure (CPAP) that positions the nebulizer directly beside the nasal interface, lung delivery efficiencies in the range of 10-20% have been reported.[66, 118-121] However, it is not clear how much of this dose is first deposited in the interface and is then blown into the airways resulting in much higher doses in the lower (dependent) lung of side lying animals.[49, 119]

Perhaps more significant than the poor delivery efficiency associated with administering aerosolized medications to infants is the very high inter-subject variability. For example, in the *in vivo* study of Fok et al.,[12] one patient population included spontaneously breathing infants that received an MDI aerosol administered with a valved holding chamber and facemask. While mean lung dose was 1.35 µg with two actuations, minimum and maximum lung doses were 0.215 and 4.52 µg, respectively. As a result, when using this common approach for respiratory drug delivery to an infant, a physician does not know if the expected dose is delivered to the lungs or if the dose delivered is approximately 5-fold lower or 3-fold higher than expected.

Poor delivery efficiency and current aerosol delivery systems for infants (including jet and mesh nebulizers and MDIs) result in relatively slow lung delivery rates. While delivery times may be acceptable for low dose medications such as bronchodilators and corticosteroids, they are likely unacceptably long for high dose medications. For example, medications like inhaled

surfactants, antibiotics or antivirals with drug masses on the order of 10 mg would require delivery times in the range of hours to days. These extended delivery times may render many inhaled medications ineffective, or may allow significant patient deterioration before the medication can act. Taken together, the issues of poor lung delivery efficiency, high inter-subject variability, and long delivery times (as well as poor penetration of the aerosol to the deep lung) are expected to contribute to poor clinical results of any inhaled medication delivered to an infant beyond low dose bronchodilators for asthma exacerbations.

One potential approach to improve the delivery efficiency of pharmaceutical aerosol to infants is to reduce the size of the particles or droplets. Multiple studies have previously suggested this approach;[53, 79, 113, 114, 122-125] however, it has seldom been implemented for improving the delivery efficiency of pharmaceutical aerosols to infants. A recent study by Tavernini et al.[126] evaluated the deposition fraction of ambient aerosols (inhaled without jet or spray momentum commonly associated with inhalers[127]) in a series of *in vitro* nasal geometries that were reproduced from CT scans of infants in the age range of 0 to 3 months. As with similar studies,[128, 129] Tavernini et al.[126] reported nasal deposition efficiency as a function of the particle impaction parameter (aerodynamic particle diameter squared times gas flow rate;  $d_a^2Q$ ) and as a combination of non-dimensional variables that collapsed the deposition data to a single curve. Considering the impaction parameter data, the delivery of a conventional 5  $\mu\text{m}$  aerosol from a mesh nebulizer[130] with an inhalation flow rate of 6 L/min results in a nasal deposition range of 15-80%.[126] In contrast, reducing the aerosol size to 1  $\mu\text{m}$  reduces the nasal depositional loss range to approximately 1-12%.[126] As a result, the use

of a relatively small particle aerosol, delivered without significant jet momentum forces,[127] will reduce nasal deposition losses and inter-subject variability of lung delivered doses.

Using a nebulizer system, the previous study of Bass et al.[79] recently demonstrated high efficiency lung delivery of a pharmaceutical aerosol in an infant airway model using a mesh nebulizer, custom mixer-heater,[131] and excipient enhanced growth (EEG)[16] aerosol formulation. The mixer-heater device was used to heat the gas stream to a temperature that remained safe for direct inhalation and reduced the aerosol mass median aerodynamic diameter (MMAD) to approximately 1.5  $\mu\text{m}$ . A streamlined nasal cannula interface was used to further reduce device system and nasal airway depositional loss.[132] *In vitro* experiments and corresponding computational fluid dynamics (CFD) simulations demonstrated >90% delivery efficiency of the nebulized dose to a tracheal filter.[79] In order to achieve the correct temperature, relative humidity and aerosol size combination, the output rate of the nebulizer was reduced. A study by Dhapare et al.[133] synchronized aerosol generation in the mixer-heater system with infant inhalation thereby maintaining high delivery efficiency during cyclic respiration.

Previous studies have not demonstrated high lung delivery efficiency in an infant model using a small particle dry powder aerosol. It is typically expected that small particle aerosols cannot be formed from dry powder formulations with the low air volumes and flow rates associated with infant respiration. Considering conventional DPs, Laube et al.[134] evaluated the penetration efficiency of a dry powder aerosol generated with the inline positive pressure Solovent (BD Technologies) device through an infant (9-month-old) nose-throat (NT) model. With this system, <4% of the loaded dose reached the tracheal filter, which required 200 mL of

actuation air. Pohlmann et al.[110] developed a powder delivery system for administering high doses of spray dried surfactant to infants. Delivery efficiency to the end of a delivery tube was approximately 50% of the loaded powder dose; however, a patient interface and extrathoracic airway model was not included.

Our group has recently developed a series of low volume air-jet DPIs using a combination of CFD simulations, rapid prototyping and *in vitro* experiments.[21-23, 25, 135] The air-jet DPI consists of an aerosolization chamber with small diameter air inlet and outlet flow passages. A positive pressure gas flows through the inlet to form an inlet air jet, which initially fluidizes and then deaggregates powder in the aerosolization chamber. The exit flow passage then serves as a filter to size select the particles that are sufficiently deaggregated. These devices have been designed to efficiently aerosolize highly dispersible small and large masses of spray dried powder formulations.[21-23, 25, 135] With 10 mL air bursts supplied from a hand operated syringe, and flow rates of only 3 L/min, excellent dispersion (MMAD = 1.8  $\mu$ m) and emptying (emitted dose, ED = 85%) have been achieved.

The objective of this study is to initially develop the air-jet DPI for high efficiency aerosol delivery to newborn infants using the nose-to-lung route (N2L). The air-jet DPI[23] should provide both a full infant inhalation simultaneously with the generation of a small particle aerosol. For initial device development, a spray dried EEG formulation is used with albuterol sulfate as a readily quantifiable model drug. Different styles of the aerosolization chamber and inlet/outlet capillary configurations (air-jet DPI) are assessed in terms of device emptying and aerosol formation at air actuation volumes (AAVs) of 30 mL and 10 mL. Initial device performance goals include an aerosol MMAD <1.8  $\mu$ m and device ED >80%. For the best devices

considered, delivery through a realistic NT model of a full-term newborn is evaluated with a targeted delivery efficiency value of  $\geq 50\%$  of the loaded dose reaching a tracheal filter.

### **3.2 Materials and Methods**

#### *Powder Materials and Formulation*

Albuterol sulfate (AS) USP was purchased from Spectrum Chemicals (Gardena, CA). Pearlitol® PF-Mannitol was donated from Roquette Pharma (Lestrem, France) and Poloxamer 188 (Leutrol F68) was donated from BASF Corporation (Florham Park, NJ). L-leucine and all other reagents were purchased from Sigma Chemical Co. (St. Louis, MO).

A batch of albuterol sulfate enhanced excipient growth (AS-EEG) powder was spray-dried using a Büchi Nano Spray Dryer B-90 HP (Büchi Laboratory-Techniques, Flawil, Switzerland) based on the optimized method described by Son et al.[76] The AS-EEG powder formulation contained a 30:48:20:2% w/w ratio of AS, mannitol, L-leucine, and Poloxamer 188, respectively. The solution was cooled and maintained at a temperature between 2-10° C during the spray drying process.

#### *Air-Jet DPI System and Experimental Overview*

An overview of the infant air-jet DPI system is illustrated in Figure 3.1. At the center of the system is the air-jet DPI, which consists of air inlet and outlet small diameter flow pathways and an aerosolization chamber. The device is actuated with a positive pressure gas source, which in this preliminary study is a hand-actuated syringe. An important aspect of the infant air-jet DPI system is that the nasal interface is used to form an airtight seal with one or both of the

infant's nostrils. Airtight communication with the infant's lungs is important such that with a single-prong interface the other nostril is held closed. The infant's mouth is also required to be held closed, either manually or with a chin strap as commonly used during infant respiratory support with nasal interfaces. The infant air-jet DPI delivers both the aerosol and a full inhalation breath to the infant in a short amount of time (typically < 1 sec for inhalation) and can be used to maintain a short breath hold. The use of positive pressure to deliver the aerosol and inhalation breath is expected to better expand the flexible upper airways and may enable deeper than tidal volume inhalation and improved lung penetration of the aerosol. As with manual ventilation with a bag and mask interface, this approach may also help to open closed or obstructed lung regions, further increasing the reach of the inhaled aerosol. For typical tidal volumes in the range of 7-8 mL/kg,[39, 40, 103] targeted inhalation volumes for full term (3550 g) and preterm (1600 g) infants are 30 mL and 10 mL, respectively, but can be higher for a limited number of breaths to improve lung recruitment.

As shown in Figure 3.2, once the aerosol is generated in the air-jet DPI, it enters a gradually expanding nasal interface. In this study, a single-prong nasal interface was employed to minimize changes to the aerosolization characteristics of the air-jet DPI, but future studies may consider a dual-prong design as well. The exterior distal end of the nostril interface has an expanded (conical) cross-section, which forms an airtight seal with the nostril when inserted approximately 5 mm. The other nostril was held closed in the experiments and the NT airway model was based on an infant with a closed oral airway.

Performance of the air-jet DPI approach was considered in two stages. In a first stage, aerosolization performance of the air-jet DPI through the end of the outlet flow passage

(excluding the nasal interface) was evaluated for multiple internal flow pathway designs. To determine expected aerosolization performance for full-term and preterm infant conditions, aerosolization performance was assessed for AAVs of 30 mL and 10 mL, respectively. After evaluation of aerosolization performance, a second stage of assessment was conducted to determine the penetration of the aerosol through an infant NT *in vitro* model. Best performing devices from the first stage experiments were connected to a gradually expanding nasal interface which was then inserted (~5 mm) into a single nostril of a full-term infant NT model ending with a tracheal filter. For evaluation with the full-term NT model, air-jet DPIs were actuated with 30 mL of air. Aerosol deposition on the tracheal filter was taken as an approximation of lung delivery. In this preliminary study, aerosol delivery through a preterm NT model was not assessed due to the limited amount of actuation air (10 mL) in comparison to the size of the tracheal filter housing (35 mL). Future assessment of preterm aerosol delivery will require the development of a very small volume high efficiency filter setup.

It is noted that *in vitro* assessment of lung aerosol delivery frequently includes cyclic respiration of the model subject over an extended period of time. This aspect of the experimental setup is not realistic in evaluation of the air-jet DPI, because the subject's breath is delivered by the positive pressure actuation of the device, much as it would be when using a manual ventilation bag. The device is actuated rapidly, with actuation times <1 sec, and leaving the device in place for a brief period is used to facilitate a breath hold. Furthermore, because the device is operated with a manual syringe filled with air, exhalation into the aerosolization chamber of the device (which could degrade powder performance) is not possible.



### *Air-Jet DPI Designs*

Basic elements of the air-jet DPI are illustrated in Figure 3.2 and include the small diameter inlet air flow passage, aerosolization chamber, and outlet flow passage. The design of the infant air-jet DPI was based on the studies of Farkas et al., [23, 135] which implemented sharpened capillaries to pierce a size zero capsule forming the inner flow pathway. In this study, the aerosolization chamber retains the size zero capsule volume of 0.68 mL; however, the capsule is not included as the device will be pre-loaded or implement a different loading mechanism. Approximate optimal inlet and outlet flow passage diameters from the studies of Farkas et al. [23, 135] are retained with values of 0.6 mm and 0.9 mm, respectively, in most designs.

As illustrated in Figure 3.3, six air-jet configurations are evaluated based on different inlet/outlet air flow pathways and aerosolization chamber geometries. Four of the devices implement a horizontal cylindrical chamber (HC), one is vertical (VC), and one is spherical (S). Inlet and outlet conditions for each air-jet DPI included the options of rounded (R), flush (F), protruding within the aerosolization chamber (P), and multiple inlets (M). Details of the air-jet designs considered, i.e., designs D1-D6, are provided in Table 3.1. Figure 3.2 illustrates the D2 design including an outlet to form a 37° bend and attached to the infant nasal interface.

When the infant air-jet DPI is in use, the inlet flow passage is to be held in the horizontal position with respect to gravity and with the infant lying in the supine position. This orientation forms a bed of un-aerosolized powder on the floor of the aerosolization chamber prior to actuation. The complete internal flow passage of the air-jet DPI is required to curve through an angle of approximately 37° for the nasal interface to correctly fit and seal with the infant's

nostrils. Figure 3.3 illustrates how the different air-jet DPIs achieve this change in flow direction. Connection between the gradually expanding nasal interface and infant nasal anatomy is illustrated in Figure 3.4. Determination of the angle was based on the best fit after inserting the gradually expanding nasal interface into a flexible 3-D printed infant nose model and achieving an airtight seal. More details on the infant nose model can be found in the *Full-Term Infant Nose-Throat (NT) Model* subsection.

The air-jet DPI designs were constructed using 3D printed parts with a division through the aerosolization chamber to allow for loading powder into the device. After powder loading, the inlet and outlet components were sealed together using a twist-lock design and intermediate O-ring. In most cases, the inlet flow passage was created as part of the 3D printed model, except with designs D2 and D6 where a custom cut stainless steel (SAE 304) hollow capillary tube was used to form the protruding inlet. Inlet diameters were 0.6 mm in all cases except for D5, where three diverging inlets were used of diameters of 0.5 mm, and D6, where three inlets ( $d=0.5$  mm) were again used but in a bundled configuration. All outlets included custom cut stainless steel capillaries with an internal diameter of 0.9 mm. Previous results have illustrated that very little spray dried powder is lost on the stainless-steel surface under the operating conditions of the infant air-jet DPI. The  $37^\circ$  angle was formed by bending the capillary against a fixed curve for all designs except for D1, which includes the angle as part of the aerosolization chamber design. All parts, including the nasal interface in the next subsection were designed in SolidWorks (Dassault Systèmes, Paris, France), and exported as .STL files. The parts were then 3D printed at  $32\ \mu\text{m}$  resolution on a Stratasys Objet24 3D Printer (Stratasys

Ltd., Eden Prairie, MN) using VeroWhitePlus resin. The parts were cleaned in a Stratasys waterjet cleaning station and allowed to dry before assembly.

### *Nasal Interface Design*

After initial aerosolization experiments, the lead air-jet DPIs were connected to an initial nasal interface design for aerosol delivery testing through the infant NT geometry. The nasal interface consisted of a straight gradually expanding circular cross-section. The design of the nasal interface with a length of 63 mm was based on computational fluid dynamics predictions that indicated a gradual expansion geometry could effectively slow the high-speed jet leaving the DPI with minimal aerosol loss and achieve the target outlet diameter of 4 mm for aerosol delivery to the infant nose. Dimensions of the nasal interface outlet section were based on a Hudson RCI Size No. 4 nasal CPAP cannula (Teleflex Medical, Research Triangle Park, NC) for a full-term infant. Resulting nasal interface inner and outer diameters at the outlet tip were 4 and 5.5 mm, respectively. A gradual exterior taper was included at the outlet of the nasal prong to help form an airtight seal with the infant's nostril. During aerosol delivery through the NT model, the single-prong nasal interface was inserted approximately 5 mm into one nostril and the other nostril was held closed.

### *Full-Term Infant Nose-Throat (NT) Model*

To test aerosol delivery efficiency to the lungs, administration was considered through a full-term NT airway model beginning at the nostrils and passing through the pharynx, larynx, and ending with a filter (Pulmoguard II, SDI Diagnostics, Easton, MA) at the start of the trachea.

In this initial study, the full-term NT model and delivery conditions were selected for a newborn infant with weight and height of 3550 g and 49.5 cm, respectively. As described by Tavernini et al.,[136] high quality airway CT scans of the NT region in the 0-3 month age range are rare. To address this issue, Tavernini et al.[136] presented key points on scaling nasal airways for different ages. Two methods that produced average age-appropriate depositions were achieved by scaling based on subject height or the  $D_{V/A_s}$  parameter. The  $D_{V/A_s}$  parameter is defined as the airway's volume divided by its surface area. However, since  $D_{V/A_s}$  is not known beyond the two points reported, scaling based on infant height is a reasonable approach. Average age-appropriate height data is readily available from growth charts and can be used for a scaling parameter. A number of studies have shown that subject height can be used as a parameter for scaling airway dimensions.[137-141] Our group recently developed a high-quality NT geometry of a 6-month-old infant that provided nasal airway deposition consistent with mean values.[79] Based on infant body length (height) the appropriate geometric scaling factor to reduce this model to that of a new-born infant was 0.73.[142] The resulting full-term newborn NT model employed in this study is displayed in Figure 3.5, and has a volume of 3.6 mL and a nasal  $D_{V/A_s}$  of 0.94 mm.

The resulting  $D_{V/A_s}$  value of the height scaled full-term NT model used in this study compares well with similar age-appropriate NT models in the literature. Tavernini et al.[126, 136] reported nasal anatomical data for 3 neonates under 10 days old. Their  $D_{V/A_s}$  values were 1.06 mm, 0.93 mm, and 1.0 mm with an average  $D_{V/A_s}$  of 0.99 mm. Xi J et al.[143] provided the nasal anatomical data for a 10 day old female with a  $D_{V/A_s}$  of 0.92 mm. Similarly, the nasal replica of a 10 day old neonate provided by Yue Zhou et al.[144] has a  $D_{V/A_s}$  of 0.92 mm. As

shown by Tavernini et al.[126], the characteristic length scale for collapsing impaction data to a single curve was  $D_{V/A_s}$  i.e., the  $D_{V/A_s}$  parameter is a good indicator for predicting age-appropriate nasal deposition. Since the full-term NT model employed in this study with a  $D_{V/A_s}$  of 0.94 mm has similar  $D_{V/A_s}$  values as other neonate models at the same age, we consider our scaled NT model to be a reasonable representative nasal geometry for this age.

In order to provide a smooth and accurate internal airway surface, the middle passage and throat sections of the infant NT model were built using stereo-lithography (SLA) with Accura ClearVue resin through 3D Systems On Demand Manufacturing, resulting in a rigid model. To facilitate nasal interface prong insertion and the formation of an airtight seal, the anterior nose was constructed in flexible Agilus Translucent 30-A material, also using SLA from 3D Systems. During experimental testing, the separate regions were securely connected with a paraffin film lining and a small amount of lubrication on the interface surfaces to ensure an airtight seal.

#### *Evaluation of Flow Rate and Actuation*

For each device, differences in air-jet design geometry led to different resistances that in turn alter the flow rate during actuation. Actuation was performed by hand after filling the 60 mL syringe to the desired AAV (either 10 mL or 30 mL) with room air and connecting to the device with a luer lock adapter. Quantification of the average flow rate for each device was performed using a pressure sensor (SSCDLNN040MBGSA5, Honeywell, Sensing and Control, Golden Valley, MN) affixed perpendicular to the outlet flow channel before the nasal interface. Pressure recordings (Sensor Evaluation Kit, Honeywell, Honeywell Sensing and Internet of

Things, Fort Mill, SC) were taken at 500 samples/second. The pressure profile of the actuation was used to calculate average flow rate based on the fixed AAV and elapsed time. Elapsed time was determined by the number of samples with a pressure reading over a set threshold recorded during actuation, where the threshold was set to double the baseline pressure value.

#### *Evaluation of Air-Jet DPI Aerosolization Performance*

Consistent with previous studies by our group, experiments used 10 mg of AS-EEG powder formulation (manually weighed) and a Next Generation Impactor (NGI; MSP, TSI Incorporated, Shoreview, MN) for aerosol particle size analysis. After weighing, the powder mass was poured into the inlet half of the air-jet DPI, which was then assembled and sealed with a twisting motion. To assess the aerosol size distribution, the air-jet DPI (without the nasal interface) was attached to the pre-separator inlet of the NGI using a custom adapter, as seen in Figure 3.6. This adapter positioned the outlet of the air-jet DPI one cm away, perpendicular from the center of the pre-separator inlet with open space allowing for co-flow room air to enter the NGI, which was operated at a flow rate of 45 L/min using a downstream vacuum pump. Room temperature and relative humidity were recorded for every run and found to be between 21-24°C and 20-40%, respectively. The NGI was positioned 53° off horizontal to allow the device to remain level during use and maintain an inline flow path from the device outlet to the NGI inlet (shown in Figure 3.6) as would be during administration to a supine infant. Each stage of the NGI was coated with MOLYKOTE® 316 silicone spray (Dow Corning, Midland, MI) to minimize particle bounce and re-entrainment. The NGI flow rate of 45 L/min was chosen to ensure collection of the aerosol, minimize any effects of settling, and provide appropriate stage

cutoff diameters for evaluating small aerosol sizes. Before each set of experimental runs, the flow rate was confirmed using a flow sensor (Sensirion SFM3000, Sensirion AG, Stafa, Switzerland) connected to the NGI inlet.

Each device was actuated into the NGI via the 60 mL hand syringe at 30 mL or 10 mL AAV to compare aerosolization at full-term or preterm infant conditions. Three replicate runs for each device at each condition were performed in a randomized order. Analysis metrics included emitted dose (ED) and mass median aerodynamic diameter (MMAD). ED was calculated as the mass of AS in the loaded dose minus the mass of AS remaining in the device divided by the initial loaded mass of AS. Aerosolization calculations were based on the mass of AS recovered in the NGI. MMAD/ED was also used as a general parameter to indicate overall performance (lower values being preferable). Drug masses were determined using HPLC analysis, as described below.

#### *Evaluation of Lung Delivery in the Full-Term NT Model*

Based on device assessment, the second stage of this study used the three best performing designs for full-term NT *in vitro* model testing at an AAV of 30 mL. The experimental setup was the same as for device assessment in terms of device actuation, powder loading, and randomization. However, instead of the device connecting to the NGI adapter, it was connected to the gradually expanding nasal interface, as seen in Figure 3.7, which was inserted approximately 5 mm into the left nostril of the infant NT model (the right nostril was manually held closed during actuation). A small amount of lubrication was applied to the exterior of the prong to ensure an airtight seal. All NT model segments were internally coated with silicon

spray to minimize particle bounce similar to airway surface liquid. At the end of the NT model, a respiratory filter (Pulmoguard II, SDI Diagnostics, Easton, MA) collected powder passing through the extrathoracic regions and represented the amount of drug delivered to the lung. After aerosol delivery, the nose was held closed and the syringe was not disconnected for 10 seconds to help aid in the capture of all particles. In practice, a breath-hold such as this would help prevent drug loss during expiration as the EEG particles significantly increase in size through hygroscopic growth.[145] Calculations for ED and regional deposition, including the nasal interface and in the NT model and tracheal filter (amount deliver to lung) were expressed as a percentage of the loaded dose of AS.

#### *Drug Mass Characterization Methods*

After actuation and aerosolization, drug masses retained or collected in the air-jet DPI and NGI or nasal interface, NT model, and filter were recovered by dissolving in an appropriate volume of deionized water followed by high performance liquid chromatography (HPLC) analysis. The loaded drug mass was determined through content uniformity analysis of the AS-EEG formulation; where known masses of AS-EEG were dissolved in water and the AS content ( $\mu\text{g}/\text{mg}$  of formulation) was determined. AS quantification was performed for each deposition site and for the drug mass used to calculate the drug recovery. Drug recovery percentage was expressed as the amount of AS recovered on all deposition sites divided by the loaded AS dose for each experiment.

Based on an airflow rate of 45 L/min, the NGI stage cut-off diameters were determined using the formula specified in USP 35 (Chapter 601, Apparatus 5). The MMAD was calculated



through linear interpolation between appropriate stages using a plot of cumulative percentage drug mass vs. cut-off diameter.

#### *Powder Formulation Characterization Method*

In preliminary experiments prior to device testing with the NGI and infant NT model, primary particle size of the AS-EEG powder formulation was determined by laser diffraction using the Sympatec HELOS (submicron R1 lens with 20 mm focal length) with RODOS/M disperser at 4 bar, and ASPIROS sample feeder set to 60 mm/sec (Sympatec GmbH, Clausthal-Zellerfeld, Germany). Three consecutive samples were tested on the same day. Testing at the high pressure of 4 bar is intended to show maximum particle dispersion. This primary particle size then serves as a benchmark to evaluate the aerosolization efficiency of the air-jet DPI, which is operated with 1000x – 10,000x less pressure.

#### *Statistical Analysis*

Statistical analysis for comparing aerosolization performance across all devices and comparison of device performance at different AAVs was performed using JMP Pro 15 (SAS Institute Inc., Cary, NC). Comparison of device performance utilized one-way ANOVA followed by post hoc Tukey. Comparison of preterm vs. full-term AAVs for each device were performed with the Student's *t*-test. All statistical tests used a significance limit of  $P=0.05$ .

### **3.3 Results**

#### *Powder and Air Flow Rate*

The AS-EEG formulation was characterized as having a mean (SD) geometric diameter of 0.99 (0.0)  $\mu\text{m}$ . In order to compare laser diffraction primary particle size to the air-jet DPI performance, the geometric size (measured with laser diffraction) was converted to an aerodynamic diameter using a theoretical solid particle density of 1.393  $\text{g}/\text{cm}^3$  (based on weighted particle densities of the formulation components).[146] Figure 3.8a shows the mean cumulative aerodynamic diameter size distribution of the AS-EEG powder formulation, resulting in a mean MMAD of 1.17  $\mu\text{m}$ . This size is expected to be near full dispersion based on the high pressure used with the laboratory scale dispersion unit.

Time-averaged air flow rates were determined for each device actuated by hand six times, with the mean (SD) results reported in Table 3.2 for an AAV of 30 mL. Figure 3.8b shows the pressure profile during actuation for D2, D5, and D6, which characterize pressure profiles for all devices tested. A fixed volume of 30 mL and the average total time for each device were used to calculate the time-averaged flow rate. D2 was found to have the lowest time-averaged flow rate of 1.9 L/min while D5 and D6 had the highest of 2.7 L/min. In the same manner, the time-average flow rates for each device were calculated with an AAV of 10 mL, with the results provided in Table 3.3. There was no statistically significant change in average flow rate between the two AAVs, with the exception of D6, which was slightly, but significantly lower at 10 mL ( $t$  test,  $P=0.007$ ). All devices have acceptable time-averaged flow rates within the target 1-5 L/min for infant aerosol delivery.

#### *Performance of Air-Jet DPIs*

Aerosolization metrics in terms of ED and MMAD for full-term and preterm AAVs of 30 mL and 10 mL are presented in Table 3.2 and Table 3.3, respectively. Surprisingly, all devices tested produced an aerosol MMAD below 2  $\mu\text{m}$  at both AAVs. ED values were also relatively high with multiple devices emptying over 85% of the loaded dose. The highest ED values were from designs D5 (94.1%) and D1 (88.1%) actuated with 30 mL of air. Choosing best device performance based only on aerosolization metrics is difficult as increasing ED is often associated with increasing MMAD, which may have a net negative effect on aerosol delivery to the trachea and lungs. A potentially useful metric is MMAD/ED, where lower values are desirable and expected to improve aerosol delivery to the lungs. For both AAVs, the lowest three values of MMAD/ED were provided by designs D5, D6, and D2 (using full-term AAV conditions the MMAD/ED values were 0.0198, 0.0200, and 0.0210, respectively). Examining Table 3.2 for the 30 mL AAV, it was observed that there were statistically significant differences among the different device designs for each aerosolization performance parameters. For the MMAD/ED metric, D4 design with the highest value MMAD/ED was observed to be significantly different to both designs D5 and D6, with the two lowest MMAD/ED values (post hoc Tukey:  $P=0.003$  and  $0.006$ , respectively).

To assess overall DPI performance, it is useful to graph MMAD vs. ED, as shown in Figure 3.9a and Figure 3.9b for the two AAVs considered (30 mL and 10 mL, respectively). In these figures, at each AAV, two distinct sets of DPI performance are observed, which fall along linear best-fit lines of MMAD vs. ED. If the linear performance curve formed by D1, D3, and D4 is considered as a reference, then improved performance is achieved by devices that fall in the space below and to the right of this line. As a result, devices D2, D5, and D6 are shown to have

overall improved performance compared with D1, D3, and D4. Viewed another way, if an ED of 85% is set as a performance target, both D1 and D6 are acceptable, but D6 reduces the MMAD at the same ED by approximately 0.1-0.3  $\mu\text{m}$ . Fortunately, the group of D2, D5, and D6 perform better than the other designs at both AAVs. Comparing performance between AAVs of 30 mL and 10 mL, D5 shows an increase in MMAD variability, which is not present with D2 or D6. Figure 3.10 provides a comparison of the three best performing (based on ranking of MMAD/ED and linear best-fit lines seen in Figure 3.9) DPI designs D2, D5, and D6 actuated at 30 mL and 10 mL. It is observed that reducing the AAV by a factor of 3-fold has little influence on device performance, based on similarity in the data points for each device along the best-fit curve. Table 3.4 reorganizes the data from Table 3.2 and Table 3.3 to show a side-by-side comparison of the best performing devices operated at each AAV. Statistical analysis (*t* test) was performed for each device comparing performance at the two AAVs. While it can be seen that the lower AAV (10 mL) corresponds with a slightly but statistically significant lower ED, there was no statistical difference for MMAD or the MMAD/ED parameter. Based on results from Table 3.4 and similarity in the data plot locations (Figure 3.10), it is observed that device D5 was least influenced by the 3-fold reduction in AAV.

#### *Nose-to-Lung (N2L) Aerosol Delivery*

Best performing devices D2, D5, and D6 were connected to the gradually expanding nasal interface and tested for aerosol delivery through the full-term NT model at an AAV of 30 mL. Deposition fractions in each region of the delivery system and NT model are displayed in Figure 3.11. Considering drug mass retained in the device, connecting to the nasal interface and

NT model moderately increased retention in device D2 to about 29%, while the drug retention for devices D5 and D6 slightly decreased to about 5% and 15%, respectively. All delivery systems lost approximately 7-10% in the gradually expanding nasal interface, which is significantly better than 30-40% loss in preliminary rapidly expanding nasal interfaces. In the nose, highest deposition was seen in the middle passage (MP) and throat regions. Surprisingly, results showed that depositional losses in different regions tend to provide similar total values leading to a narrow range of 48-53% lung delivery efficiency. Reasons for similar lung delivery efficiencies across the three devices tested can be further explored in Figure 3.11b and Table 3.5. These results present aerosol deposition (or retention) fractions grouped for each device and subdivided for the nasal interface, complete NT regions, and tracheal filter (lung delivery). Despite statistically significant differences between designs in all deposition regions leading up to the tracheal filter, there was no significant difference in filter deposition (lung delivery). Interestingly, it is observed that the D2 device generating the smallest aerosol ( $1.55 \mu\text{m}$ ), produced only 8.0% NT depositional loss, while increasing aerosol size to  $1.85 \mu\text{m}$  with D5 dramatically increased nasal depositional loss to 36.1%. With D2, the low nasal depositional loss is offset by approximately 29% device retention, resulting in a tracheal filter deposition fraction of 52.2%. Device D5 reduces DPI retention to about only 5%, but then dramatically increased NT deposition leading to a similar 48.5% lung delivery efficiency. Average total AS recovery percentages for the best performing designs were between 95-98% ensuring mass balance and validity of the experiments.

### 3.4 Discussion

A primary outcome of this study was the development of new infant air-jet DPI prototypes that achieved the performance metrics of >80% ED, MMAD <1.8  $\mu\text{m}$ , and a lung delivery efficiency of approximately 50% of device loaded dose. In assessing the air-jet DPI designs, two distinct sets of devices were identified based on aerosolization performance. Designs D2, D5, and D6 were found to produce a superior combination of MMAD and ED (based on MMAD/ED and linear best-fit lines) than the remaining three devices. Common design features of the three best performing air-jet designs were a cylindrical and horizontal aerosolization chamber together with a flush or protruding outlet. Designs that also included multiple inlets (D5 and D6) achieved the best aerosolization metrics of approximately >80% ED and MMAD <1.8 $\mu\text{m}$ , whereas D2 with a single air inlet did not. Nevertheless, when tested in conjunction with a gradually expanding nasal interface design and infant NT model, all three lead designs achieved approximately 50% drug delivery to the lungs, which compared to a previous positive pressure infant DPI[134] evaluated in a 9-month old infant model represents over a 12-fold improvement.

Several previous studies have considered air-jet DPIs operated with an AAV of 10 mL.[21-23, 25, 135] These studies have typically focused on single inlet aerosolization chamber designs with inlets and outlets protruding at least 2 mm as well as loading drug with a capsule. Best case performance with those previous devices has typically been an ED of about 85% and MMAD in the range of 1.7-1.8  $\mu\text{m}$  for a 10 mg powder fill mass. One exception is the previous study of Boc et al.,[89] in which multiple air inlets were employed with a much smaller aerosolization chamber volume. In the current study, D6 performance was the most consistent

with previous devices. In comparison, the D5 design appears to perform better than previous devices with an ED of 94% and small aerosol size increase to 1.85  $\mu\text{m}$ . As a result, this study indicates that air-jet performance was enhanced through the development of an aerosolization chamber with multiple inlets and a flush or protruding outlet.

Despite significant variation in the best performing devices (D2, D5, and D6 with an ED range of 75.6-94.1%), *in vitro* lung delivery efficiency was consistently around 50% using the full-term NT geometry. As described, the D2 design provided excellent NT penetration with only 8.0% depositional loss, but relatively poor emptying with ED of 75.6% (71.6% when connected to the infant NT model). Increasing the device emptying also increased the MMAD, which led to a significant depositional loss in the NT model. An ideal device for infant N2L aerosol delivery therefore appears to be one that can achieve an MMAD of 1.6  $\mu\text{m}$  and ED near 95%. However, as illustrated by persistent occurrence of aerosolization performance data points on a straight line of MMAD vs. ED, it is expected that new device design ideas will be required to achieve this level of performance.

Intended uses of the infant air-jet DPI include the rapid administration of high dose inhaled medications such as aerosolized antibiotics and surfactants. For either of these applications, total doses higher than the 10 mg loaded dose employed in this study will likely be needed. The aerosolization chamber in the current study has a total volume of 0.68 mL, which if approximately half full can accommodate 40-50 mg of powder based on typical EEG powder density. However, Longest et al.[21, 82] have previously found that forming the aerosol too quickly within the air-jet device increases measured MMAD. Further testing is therefore needed to determine which devices can best accommodate higher dose loading without affecting

performance. An alternative to accommodate higher total dose loading may be an auto-loading system for the air-jet DPI such that each actuation delivers a 10 mg dose of powder formulation.

As demonstrated in this initial study, the infant air-jet DPI is expected to provide a number of advantages for aerosol delivery to infants of all ages. First, device actuations of 10 mL and 30 mL require time periods between 0.2 and 1.0 s. The devices tested performed very similar at both AAVs in terms of aerosolization performance. Therefore, the only reason to implement the higher AAV for the older full-term infant is to provide a full inhalation breath. This air volume can be reduced to accommodate stiff or non-compliant lungs as needed. Further device testing will be required to reduce the AAV below 10 mL, as with 3 mL used in the previous study of Boc et al.[89] By operating the delivery system with positive pressure, it is expected that the highly flexible infant upper airways will be expanded, enabling better deep lung penetration of the aerosol. In the current study an enforced breath hold of 10 s was implemented; however, this length of time is not needed for aerosol retention as EEG aerosols approach their fully hydrated droplet size within approximately 0.5 to 1 s under infant airway conditions.[123] Nevertheless, under resuscitation conditions, te Pas and Walther[102] demonstrated that infant lung inflation followed by a 10 s breath hold improved lung mechanics and patient outcomes compared with standard rapid ventilation with a bag and mask. With a single-prong design, infant exhalation can be accomplished by releasing the nostril without the nasal interface. For a dual-prong design, an exhalation port will be included in the nasal interface close to the patient. Ideally, opening of the exhalation port can be automated with a single button on the device that also controls actuation of the air source.



The *in vitro* NT model employed in the current study has several differences from *in vivo* conditions that should be considered. As described previously, the air-jet DPI delivers both the aerosol and a full inhalation breath such that cyclic breathing of the model is not required. However, more realistic airway delivery conditions need to include the downstream resistance and compliance of the lungs. The effect of this resistance and compliance on aerosol generation is expected to be small considering the relatively low ventilation volumes (7-8 mL/kg) that are employed. Furthermore, the airway walls were not warmed and humidified to physiologic conditions. It is known that some size increase of hygroscopic aerosols occurs in the nose.[147, 148] However, this aerosol size increase in the extrathoracic region was previously reported to be small with an associated negligible increase in NT deposition (<5% relative difference) for adult airway conditions.[17] As described previously, the air-jet DPI forms a closed system with the airways such that subject exhalation into the aerosolization chamber containing the powder is not possible.

Additional study limitations include the use of a hand-operated air syringe as an air source, consideration of a limited number of designs, use of one nasal interface design and delivery testing through a single NT airway model. Variations in airflow delivery associated with hand-operation of the gas source are observed in Figure 3.8b. However, despite these variations, performance of the air-jet DPI was relatively consistent with acceptable standard deviation values. Although, it is expected that operation of the hand syringe will vary significantly across different operators. Therefore, a consistent push-button operated air source is needed for future device actuation. Considering all possible design choices provided by the air-jet DPI, the six designs explored in this study form a relatively small set of options. Still, a set

of improved designs with unique features were identified. The nasal interface is an important source of potential aerosol loss and also influences loss in the NT model. The single gradual expansion nasal interface used in this study was the result of preliminary design work that improved upon nasal interface losses as high as 40% of the loaded dose. While 10% nasal interface depositional loss is acceptable, it is expected that this deposition can be further reduced. Finally, this preliminary study considered only one NT model under full-term neonate conditions. Aerosol deposition in the NT region is known to be highly variable and where the tested model falls within this spectrum is currently not known. Future studies with additional aerosol delivery system optimizations will consider NT models based on even younger subjects with smaller AAVs (e.g., 6-9 mL).

### **3.5 Conclusions**

In conclusion, this study has developed an air-jet aerosol delivery system to administer high doses of spray-dried powder formulations to infants. The patient interface is a simple gradually expanding flow passage that produced low depositional loss and device actuation times are in a range between 0.2 and 1.0 s. Delivery efficiency of drug to the lungs was approximately 50% of the loaded dose across the three best performing devices. Advantageous design options in the air-jet DPI were identified as a horizontal and cylindrical aerosolization chamber, flush or protruding outlet, and multiple inlets. With continuing advances in device improvement, delivery will be tested and optimized in even younger airway models across multiple subjects with smaller administered volumes of air.

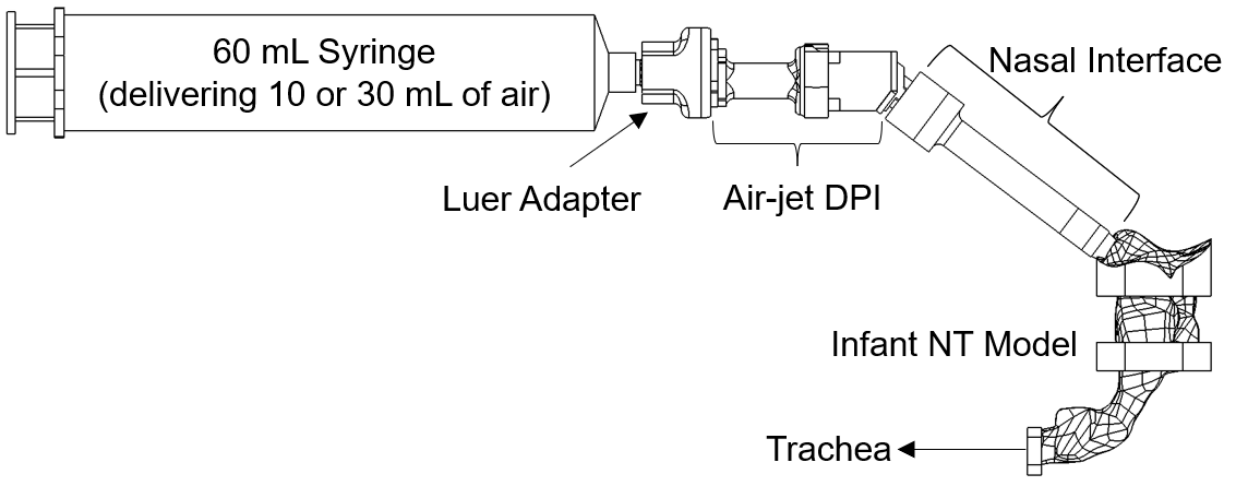


**Figure 3.1** Schematic representation of infant air-jet DPI aerosol delivery system attached to an infant nose-throat (NT) airway model

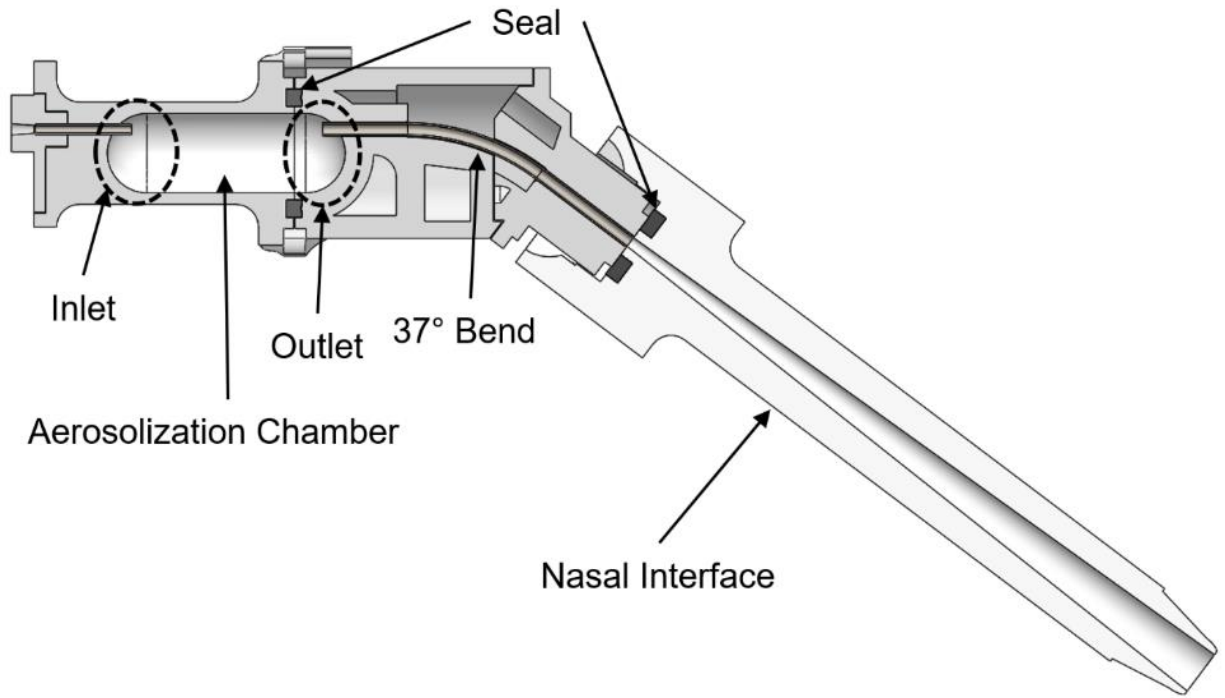


**Figure 3.2** Axial cross section of the infant air-jet DPI connected to a gradually expanding nasal interface illustrating internal flow passages. The infant air-jet DPI consists of the inlet flow passage, aerosolization chamber, and outlet flow passage up to the point of nasal interface attachment

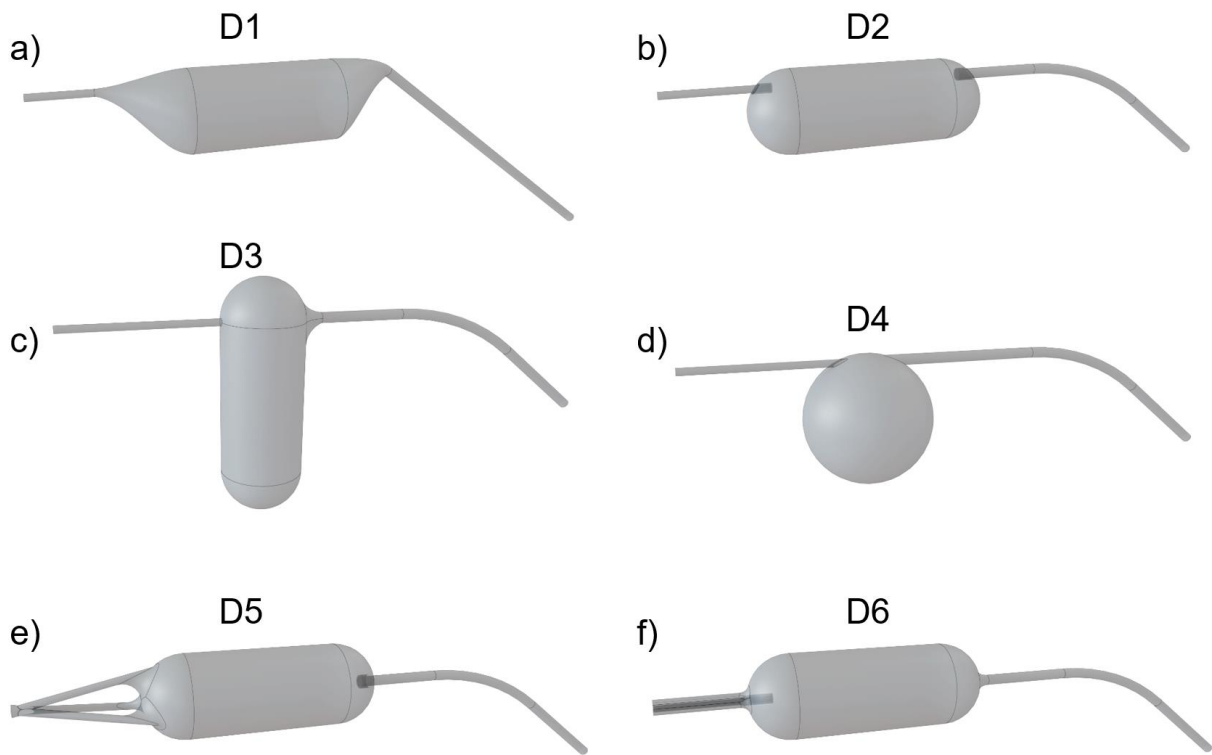
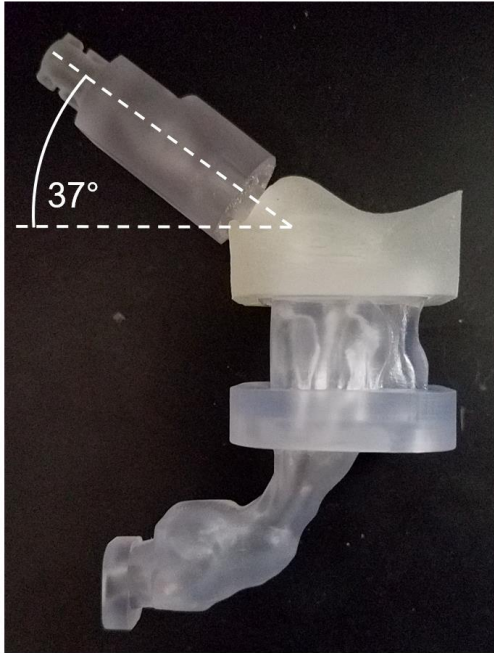


**Figure 3.3** Internal airflow geometry of each device from air source inlet (left side of each image) to the device outlet (right side of each image). **(a)-(f)** corresponds to D1-D6, respectively

a)



b)

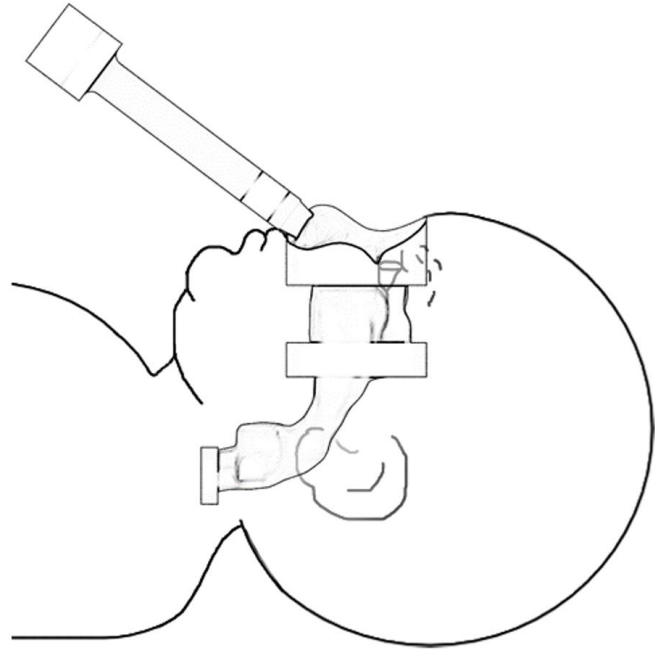


**Figure 3.4** Connection of the nasal interface to the infant NT model illustrating **(a)** angle of the nasal interface and **(b)** position of the nasal interface and NT model

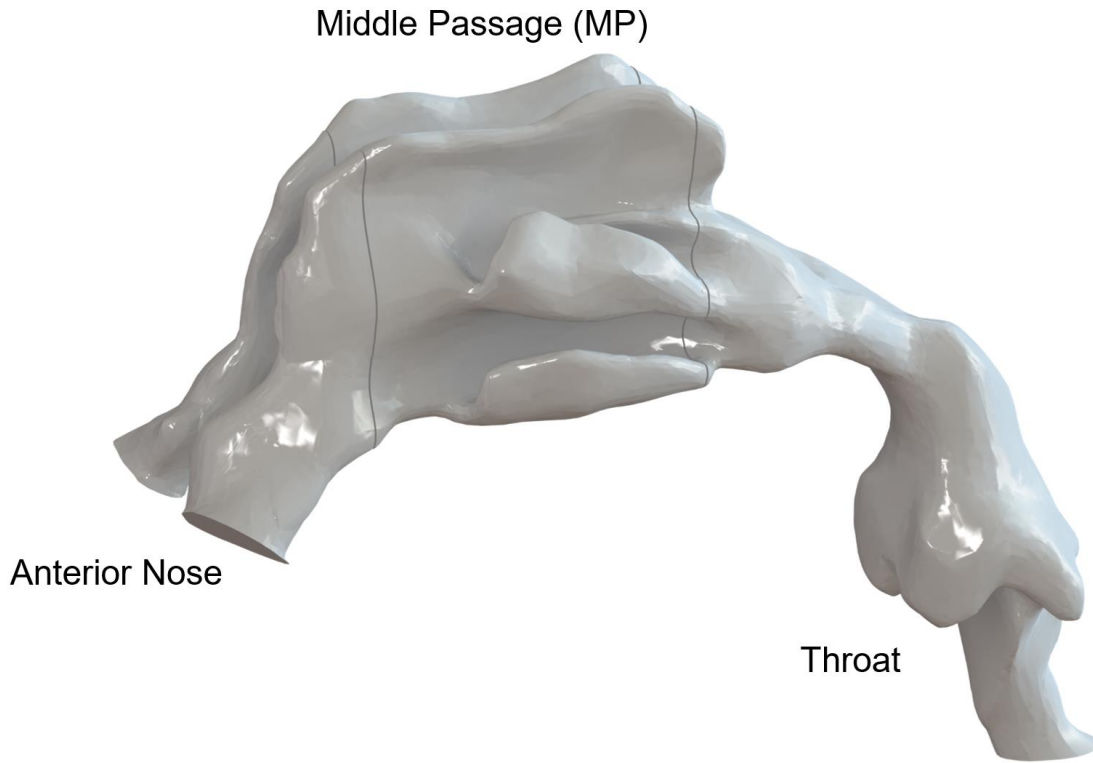


**Figure 3.5** Overview of the infant NT airway model and regional sections

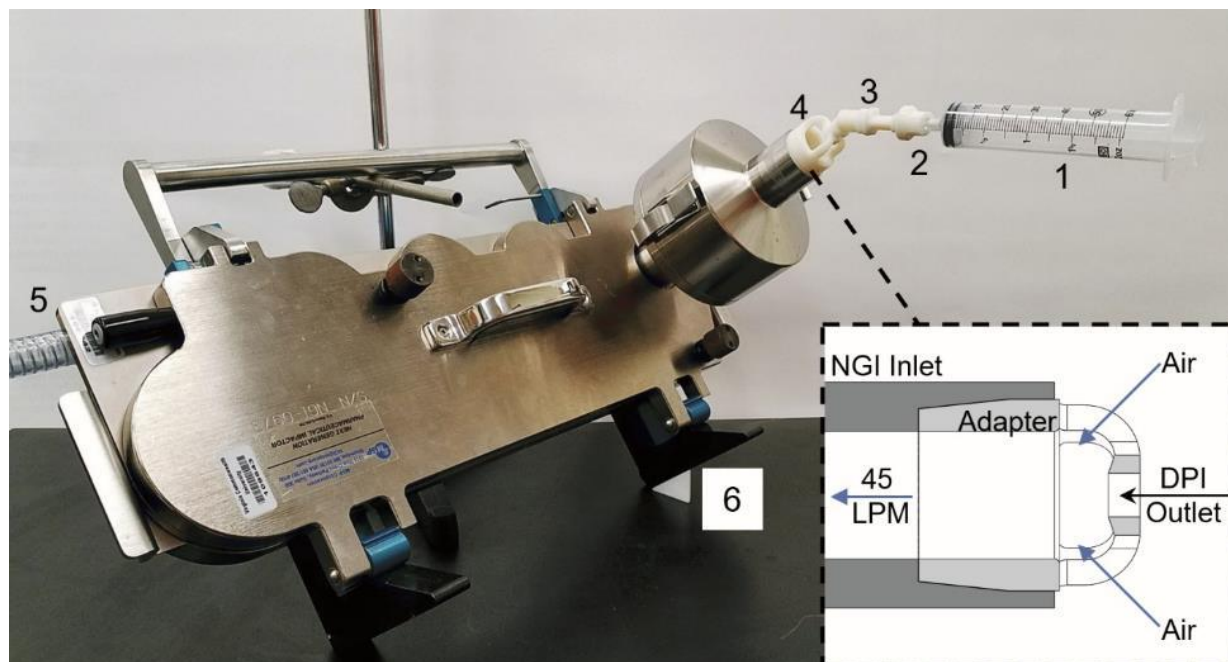


**Figure 3.6** Experimental setup for device aerosolization performance as determined by Next Generation Impactor (NGI). Parts labeled including 1. Air source (60 mL syringe), 2. Luer adapter, 3. Air-jet DPI (D2 pictured), 4. NGI adapter, 5. Vacuum for NGI (operated at 45 L/min), and 6. Guide to angle the NGI at 53° off horizontal. Expanded view of custom NGI adapter schematic allowing for co-flow room air



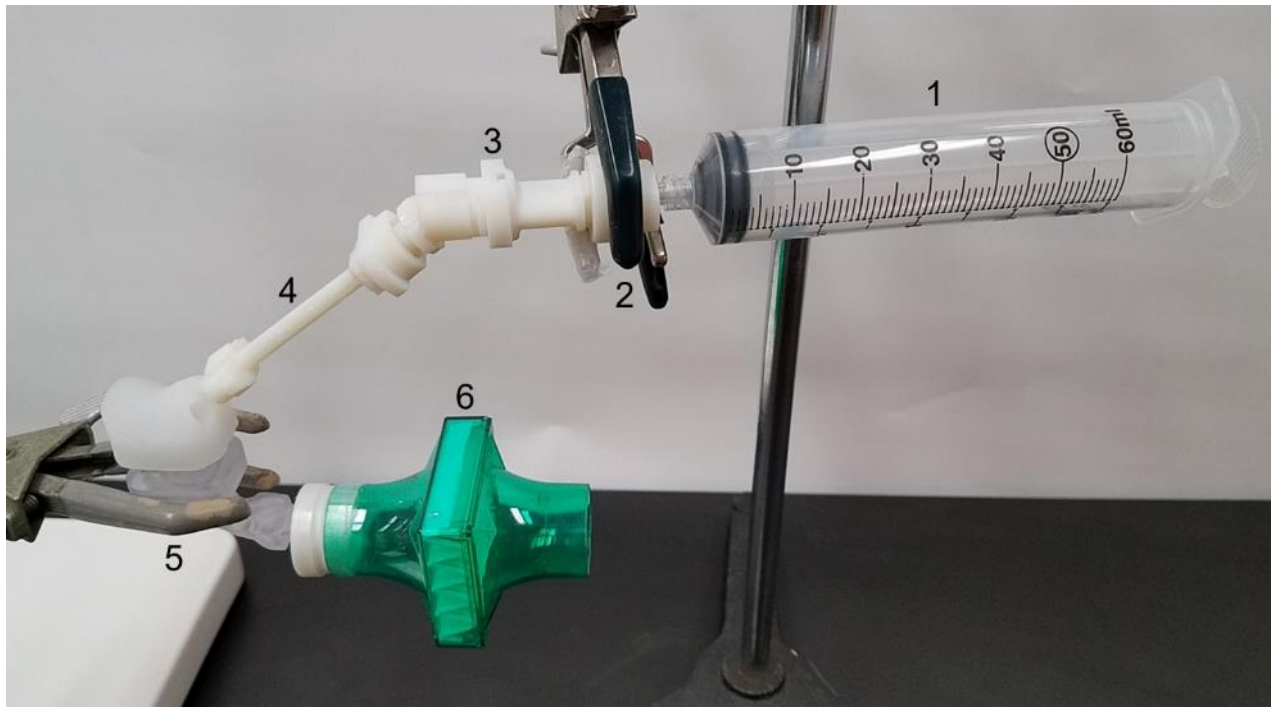


**Figure 3.7** Experimental setup for aerosol delivery efficiency testing through the infant NT model. Parts labeled including 1. Air source (60 mL syringe), 2. Luer adapter, 3. Air-jet DPI (D2 pictured), 4. Nasal interface, 5. Infant NT model, 6. Respiratory filter

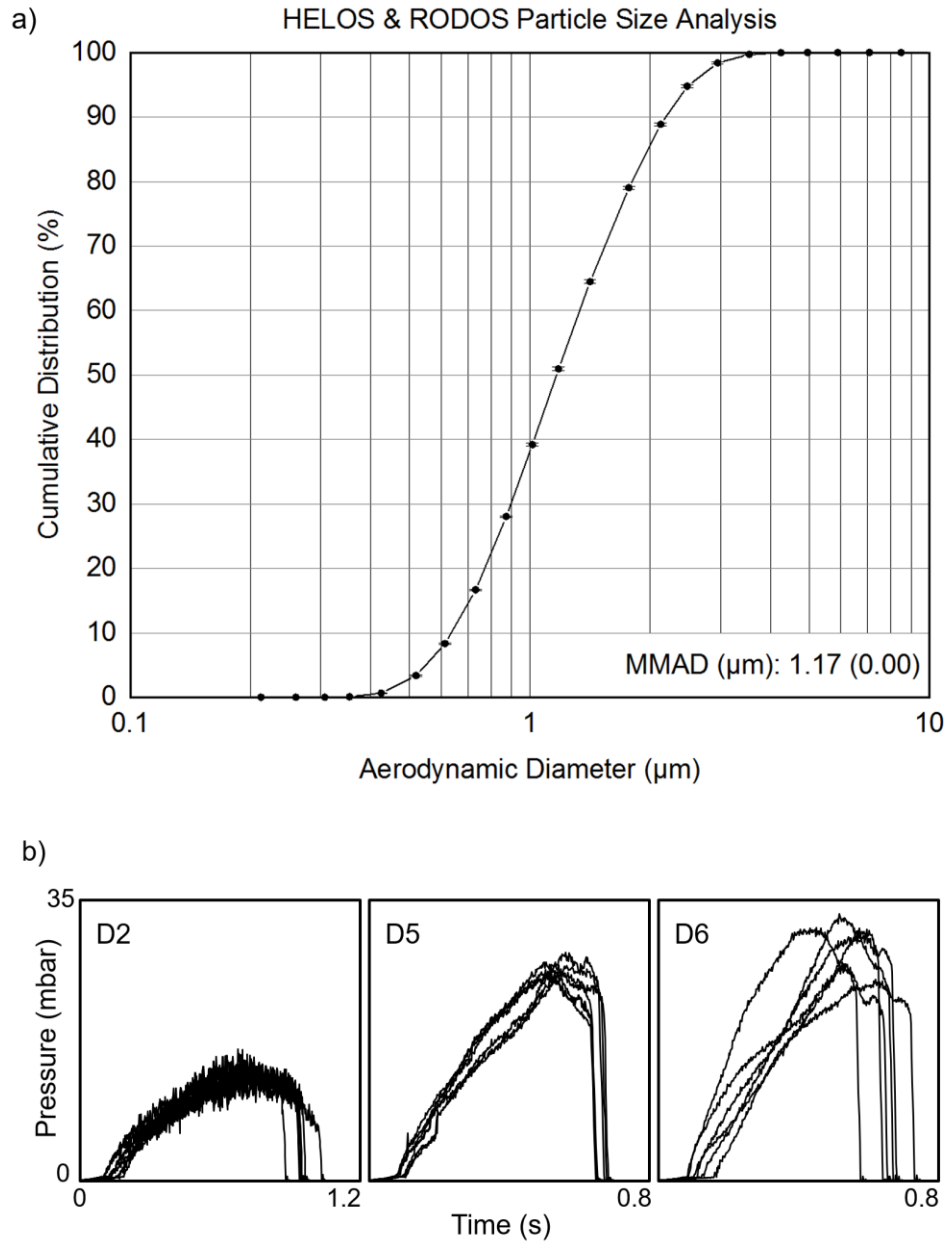


**Figure 3.8** (a) Average cumulative primary particle size distribution [n=3] of the powder based on dispersion with RODOS at a pressure of 4 bar and measured with laser diffraction as a function of aerodynamic diameter (converted based on a formulation density of 1.393 g/cm<sup>3</sup>). The resulting mean (SD) MMAD was 1.17 (0.00). (b) Pressure profile graphs of 30 mL AAVs using the hand operated syringe through devices D2, D5, and D6, measured at the air-jet DPI outlet [n=6]

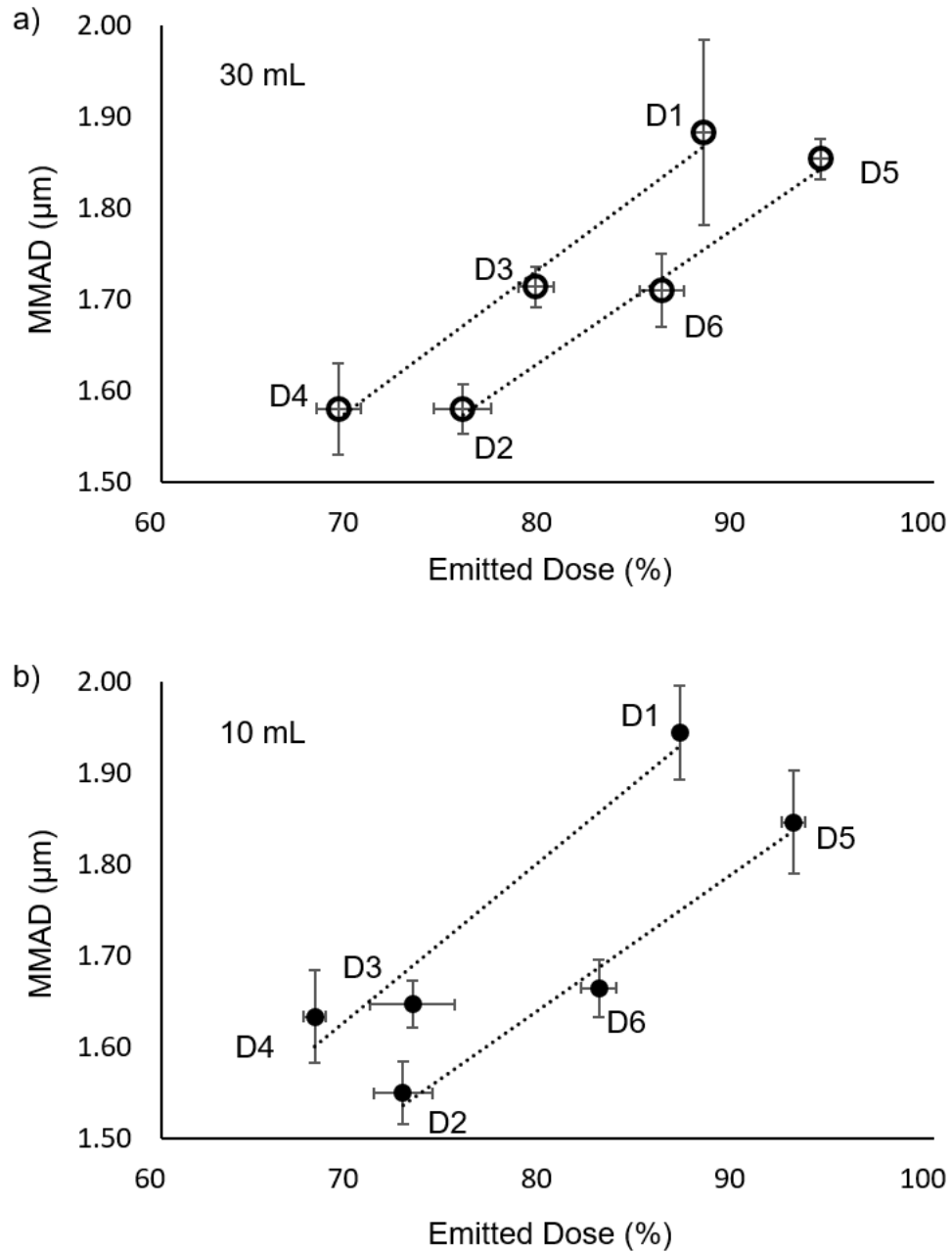


**Figure 3.9** Mean (SD) values of MMAD vs. ED based on device actuation into the NGI and AAVs of **(a)** 30 mL and **(b)** 10 mL using room-condition air. Linear best-fit trend lines are established among devices with similar performance

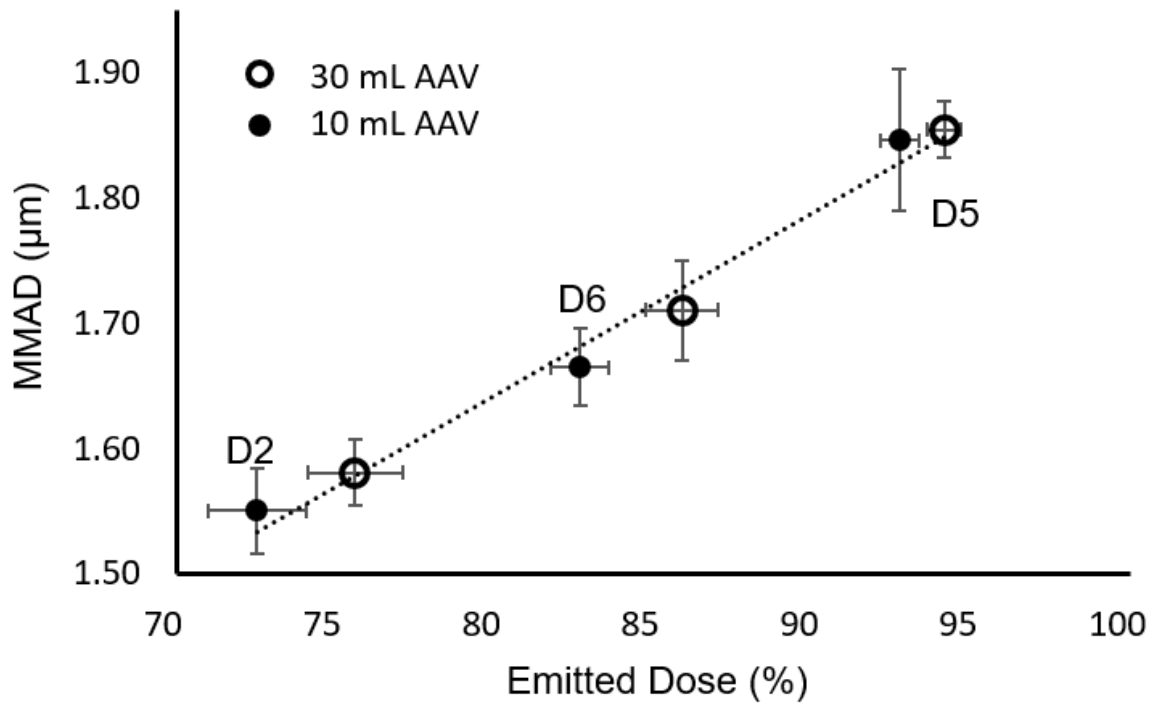


**Figure 3.10** Mean (SD) values of MMAD vs. ED based on device actuation into the NGI for the three best performing devices actuated with 30 mL (open circles) or 10 mL (filled circles) of room-condition air

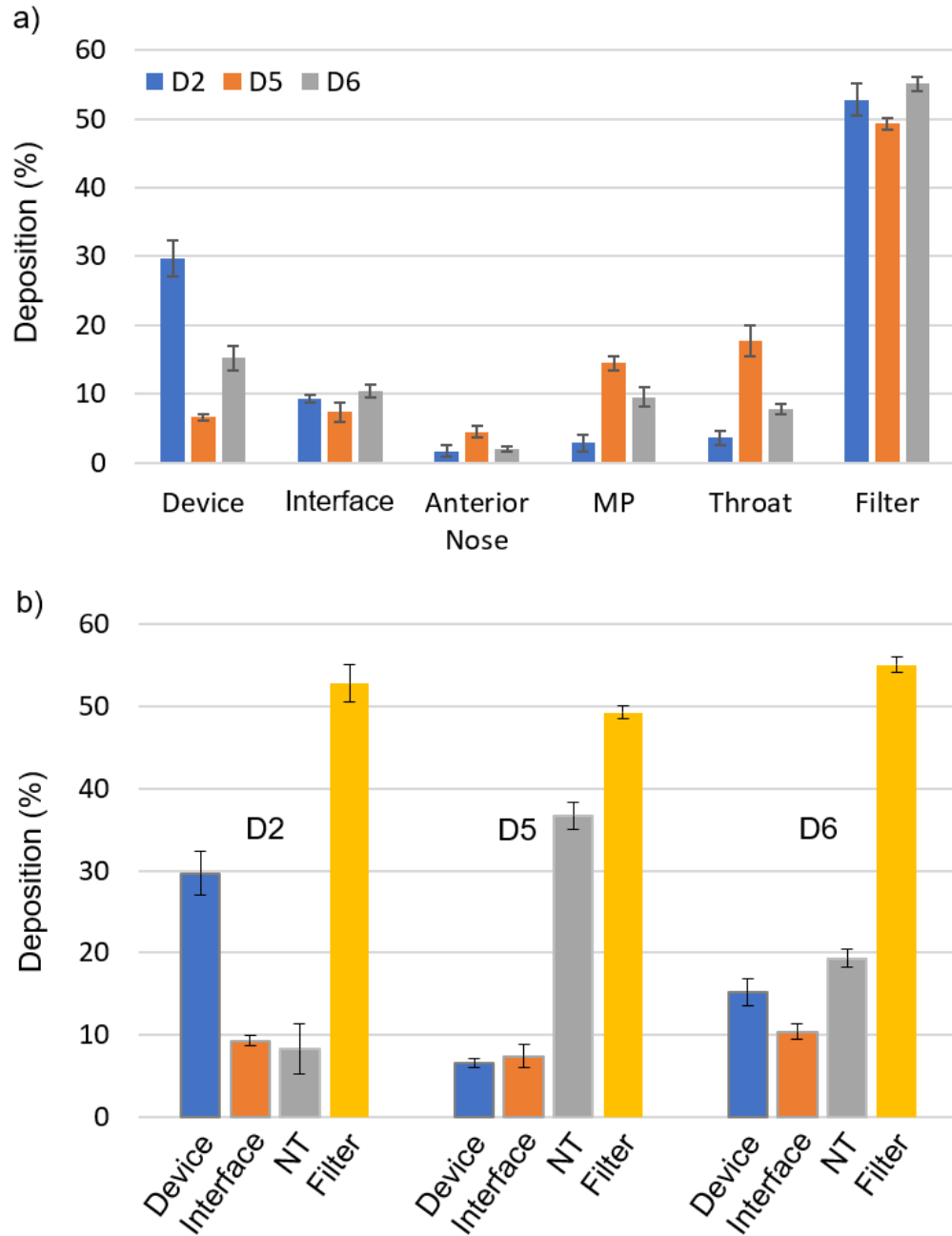


**Figure 3.11** Experimentally determined mean (SD) drug deposition fraction (based on loaded dose) grouped by **(a)** region and **(b)** device. Anterior nose, middle passage (MP), and throat deposition fractions shown in panel **(a)** are combined as NT deposition fractions in panel **(b)**

**Table 3.1** Air-jet dry powder inhaler (DPI) design parameters and configurations

<b>DPI Device</b>	<b>Inlet</b>	<b>Chamber</b>	<b>Outlet</b>
D1	R	HC	R
D2	P	HC	P
D3	F	VC	R
D4	F	S	F
D5	R/M *	HC	P
D6	P-R/M **	HC	F

Chamber parameters include horizontal cylindrical (HC), vertical cylindrical (VC), or spherical (S).

Inlet/Outlet parameters consist of rounded (R), flush (F), protruding (P), and/or multi (M).

\*Triple diverging inlet jets

\*\*Single protruding central jet, surrounded by triple parallel central jets

**Table 3.2** Aerosolization performance and measured flow rate with an air actuation volume (AAV) of 30 mL

DPI Design <sup>a</sup>	Flow Rate (L/min) <sup>1</sup>	ED (%) <sup>2</sup>	MMAD ( $\mu\text{m}$ ) <sup>2</sup>	MMAD/ED <sup>2</sup>
D1	2.0 (0.1)	88.1 (0.5)	1.88 (0.10)	0.0214 (0.0012)
D2	1.9 (0.1)	75.6 (1.5)	1.58 (0.03)	0.0210 (0.0007)
D3	2.0 (0.1)	79.4 (0.9)	1.71 (0.02)	0.0216 (0.0005)
D4	2.2 (0.1)	69.2 (1.1)	1.58 (0.05)	0.0228 (0.0010)
D5	2.7 (0.1)	94.1 (0.6)	1.86 (0.02)	0.0198 (0.0003)
D6	2.7 (0.2)	85.9 (1.1)	1.71 (0.04)	0.0200 (0.0003)

Mean values with standard deviations (SD) shown in parenthesis; <sup>1</sup>n=6, <sup>2</sup>n=3.

<sup>a</sup>p<0.05 significant effect of device design on each of the individual reported parameters (one-way ANOVA).

**Table 3.3** Aerosolization performance and measured flow rate with an AAV of 10 mL

DPI Design <sup>a</sup>	Flow Rate (L/min) <sup>1</sup>	ED (%) <sup>2</sup>	MMAD ( $\mu\text{m}$ ) <sup>2</sup>	MMAD/ED <sup>2</sup>
D1	2.1 (0.1)	86.8 (0.2)	1.95 (0.06)	0.0224 (0.0007)
D2	2.0 (0.1)	72.5 (1.5)	1.55 (0.04)	0.0214 (0.0002)
D3	2.0 (0.1)	73.0 (2.2)	1.65 (0.03)	0.0226 (0.0007)
D4	2.2 (0.1)	67.9 (0.6)	1.64 (0.05)	0.0241 (0.0007)
D5	2.6 (0.0)	92.7 (0.6)	1.85 (0.06)	0.0199 (0.0008)
D6	2.3 (0.1)	82.7 (0.9)	1.66 (0.03)	0.0201 (0.0005)

Mean values with standard deviations (SD) shown in parenthesis; <sup>1</sup>n=6, <sup>2</sup>n=3.

<sup>a</sup>p<0.05 significant effect of device design on each of the individual reported parameters (one-way ANOVA).



**Table 3.4** Comparison of best design aerosolization performance at 10 and 30 mL AAVs

<b>Description</b>	<b>10 mL AAV</b>	<b>30 mL AAV</b>
<b>D2</b>		
ED (%) <sup>a</sup>	72.5 (1.5)	75.6 (1.5)
MMAD (μm)	1.55 (0.04)	1.58 (0.03)
MMAD/ED	0.0214 (0.0002)	0.0210 (0.0007)
<b>D5</b>		
ED (%) <sup>a</sup>	92.7 (0.6)	94.1 (0.6)
MMAD (μm)	1.85 (0.06)	1.86 (0.02)
MMAD/ED	0.0199 (0.0008)	0.0198 (0.0003)
<b>D6</b>		
ED (%) <sup>a</sup>	82.7 (0.9)	85.9 (1.1)
MMAD (μm)	1.66 (0.03)	1.71 (0.04)
MMAD/ED	0.0201 (0.0005)	0.0200 (0.0003)

Mean values with standard deviations (SD) shown in parenthesis, n=3.  
<sup>a</sup>*p*<0.05 significant difference between 10 & 30 mL AAV (*t* test)

**Table 3.5** Regional deposition fractions (based on loaded dose) for air-jet DPI designs in full-term nose-throat (NT) model and 30 mL AAV

<b>Deposition Region</b>	<b>D2</b>	<b>D5</b>	<b>D6</b>
DPI Retention (%) <sup>a</sup>	29.4 (3.4)	4.5 (0.4)	14.5 (1.7)
Cannula (%) <sup>a</sup>	9.2 (0.5)	7.3 (1.2)	10.0 (0.9)
Anterior Nose (%) <sup>a</sup>	1.7 (0.7)	4.5 (0.7)	1.9 (0.4)
Middle Passage (%) <sup>a</sup>	2.9 (1.1)	14.3 (0.9)	9.1 (1.3)
Throat (%) <sup>a</sup>	3.5 (1.0)	17.4 (2.5)	7.4 (0.7)
Total Extrathoracic (%) <sup>a</sup>	8.0 (2.9)	36.1 (2.5)	18.4 (1.0)
Tracheal Filter (%)	52.2 (2.8)	48.5 (1.4)	52.6 (1.2)

Mean values with standard deviations (SD) shown in parenthesis, n=3.

Total Extrathoracic is the sum of anterior nose, middle passage and throat deposition.

<sup>a</sup>p<0.05 significant effect of device design on deposition (one-way ANOVA).

# Chapter 4 - Advancement of the Infant Air-Jet Dry Powder Inhaler (DPI): Evaluation of Different Positive-Pressure Air Sources and Flow Rates

## Task 1.2 – Published: *Pharmaceutical Research*

### 4.1 Introduction

As with adults, the use of aerosolized therapies to treat lung conditions and diseases in infants is expected to have a number of advantages such as the ability to optimize lung dose while minimizing systemic exposure and thereby reducing or eliminating off-target or side effects of the medication [57, 149-151]. Despite these advantages, aerosol delivery to the lungs of infants remains difficult across all administration platforms due to poor lung delivery efficiency, high inter-subject variability, low delivery rates, and long administration times [12, 57-59, 61, 113, 117, 118]. Across all aerosol delivery platforms, delivery efficiency to the lungs of infants remains on the order of ~1% of the aerosolized dose [12, 58, 59, 61]. Recent studies in small animal models of nose-to-lung aerosol delivery employing a new custom mesh nebulizer producing small droplets (eFlow-Neos Investigational Nebulizer system; PARI Pharma GmbH, Germany) report total lung delivery efficiencies in the range of 10-20% of the nebulized dose [66, 67, 118]. However, aerosol fractions in the upper lung lobes of side lying animals remain <5% making it unclear if the 10-20% delivery efficiency is achieved in the aerosol phase [49, 67]. The recent *in vivo* human subject study of Corcoran et al. [117] implemented a vibrating mesh nebulizer with nasal cannula interface applied to newborn infants and reported ~1% lung delivery efficiency of loaded dose over a 2 minute aerosol delivery period.

For adults and infants, DPIs offer a number of advantages in administering pharmaceutical aerosols including product stability [152], high drug mass per inhalation [153],

less susceptibility to microbial growth, and low cost [154]. Despite these advantages, DPIs are often not considered for use in applications involving infants due to the common passive inhalation design and high air volumes (1.6 – 4 L) used to operate most commercial products [154-157]. In contrast with passive DPIs that are operated with the patient's inhalation energy, active DPIs are operated with an energy source external to the user to generate an aerosol [154]. Active positive-pressure DPIs implement an upstream air source such as a ventilation bag or air-filled syringe to form the aerosol and deliver both the aerosol and air bolus to the subject [86, 87, 158, 159]. Depending on the volume of air used, these devices can be classified as high ( $\geq 200$  mL) or low ( $< 200$  mL) air actuation volume (AAV) devices [158]. In a series of studies, a new positive-pressure air-jet DPI design has been developed that can be operated with low [23, 25, 135] and high [159] AAVs. The aerosol generation unit within air-jet DPIs contains a small diameter inlet air flow passage (or passages), aerosolization chamber and small diameter outlet flow passage (or passages) [23, 159]. Positive pressure air is accelerated through the small diameter inlet and forms a high speed, turbulent, compressible and nearly sonic jet within the aerosolization chamber [21, 22]. Expansion of this jet creates secondary velocities that serve to initially fluidize the powder bed [21, 22]. The aerosolized powder then enters the high-speed jet region where further particle deaggregation occurs. Once sufficient deaggregation has occurred, particles follow flow field streamlines and exit through the outlet flow passage, which serves as a size selection filter. As shown by concurrent CFD and *in vitro* studies, air-jet DPIs have the unique attribute of producing smaller mass median aerodynamic diameters (MMADs) as internal turbulence is reduced, making them ideal for aerosol administration to infants and children with small air volumes and low air flow rates [21, 22, 160].

Based on a number of previous studies, it is expected that small particle aerosols with an MMAD of  $\sim 1.5 \mu\text{m}$  will significantly improve the lung penetration efficiency of dry powder formulations delivered to infants [79, 126, 161]. However, it is also expected that a large percentage of these particles will lack sufficient mass and momentum to deposit and will be exhaled [122]. For example, Longest et al. [122] illustrated that for nebulized aerosol delivery to an infant, an approximately  $1 \mu\text{m}$  particle would result in 32% lung deposition efficiency, but 45% of the inhaled dose would not deposit and would be exhaled. To address this high exhaled dose, the excipient enhanced growth (EEG) delivery technique can be implemented, which is one of several controlled condensational growth approaches [16, 162-165]. With EEG aerosol delivery, dry or nearly dry particles are delivered that have an initial small size and are composed of both the therapeutic agent and a hygroscopic excipient, such as mannitol (MN) or sodium chloride [16, 166]. Once the initially small particles are inside the airways, the hygroscopic excipient fosters water accumulation turning them into droplets and increasing particle/droplet diameter by a factor of 2- to 4-fold, which results in an increase of particle/droplet mass by a factor of 8- to 64-fold [15, 16, 146, 147, 166]. The properties and percentage of hygroscopic excipient can be used to control the rate and amount of particle size increase and target the region of deposition of the aerosol [146, 147, 166]. As reported by the CFD-based study of Tian et al. [123] for invasive mechanical ventilation, the EEG technique can significantly reduce the amount of aerosol that is lost in the delivery system and increase the amount of drug deposition in the lungs of infants.

Howe et al. [26] recently described the initial development of an infant air-jet DPI for nose-to-lung administration of spray-dried EEG formulations to infants. The infant air-jet DPI

was actuated with 10 mL or 30 mL volumes of air supplied from a hand-operated syringe. The aerosolization chamber was initially loaded with 10 mg powder masses of a model EEG formulation containing albuterol sulfate (AS) as a reference therapeutic that is readily quantifiable, MN as the hygroscopic excipient and l-leucine as a dispersion enhancer, based on the study of Son et al. [76]. At both 10 and 30 mL AAVs, the three best performing devices produced MMADs of 1.6-1.9  $\mu\text{m}$  and emitted doses (EDs) of 73-94% of loaded dose [26]. These three best performing devices were each connected to a gradually expanding nasal interface and an *in vitro* nose-throat (NT) model consistent with a full-term infant, and were actuated with 30 mL air volumes. In each case, ~50% of the loaded dose passed through the NT model and reached the tracheal filter, which approximated the lung delivery efficiency. While this delivery efficiency is lower than with adult air-jet applications, it is one or more orders of magnitude better than the manually operated Solovent infant positive-pressure device tested with a realistic NT model [134].

In addition to high efficiency aerosol delivery, the infant air-jet DPI is intended to make an airtight connection with the infant's lungs and provide a deep inhalation breath [26]. At inhalation volumes just above passive breathing of 7-8 mL/kg [99], deep inhalation breaths and therefore device AAVs for a 1600 g preterm and 3550 g full-term infant are 10 and 30 mL, respectively. This inhalation breath delivered with positive pressure can help to expand the infants' flexible upper airways and deliver the aerosol deep within the lungs. Developing airtight communication with the lungs is an important aspect of infant air-jet DPI operation. For single prong administration, as with Howe et al. [26], the infant's other nostril and mouth must be held closed. As with nasal cannula respiratory support, mouth closure can be accomplished

manually or with a temporary chin strap. The delivery system can be used to assist with a brief breath hold to allow for aerosol deposition (3-5 sec) and to perform a simultaneous alveoli recruitment maneuver [102]. Exhalation can be accomplished by removing the device after aerosol delivery, or with an active exhalation port in the device if multiple breaths are required.

While the previous study of Howe et al. [26] was successful at achieving high efficiency lung delivery through a NT model of a full-term infant, a number of potential advances are possible. First, delivery efficiency can potentially be further improved and needs to be evaluated through a more challenging preterm NT airway model. The preterm model limits the amount of AAV to 10 mL and has considerably smaller NT airway dimensions. Second, actuation of the device can be simplified by removing the hand-operated syringe. Use of a hand syringe is also subject to inter-operator variability. Automated air sources can potentially improve repeatability, performance and can better control the upper airway pressure compared with a hand-operated syringe. Finally, the infant air-jet DPI is intended to be operated in airtight connection with the lungs. Lung resistance and compliance may limit or slow gas flow through the device and increase device operating pressure, which could potentially impact aerosolization performance. It is important to test operation with a downstream resistance and compliance in place consistent with a preterm infant experiencing respiratory distress.

The objective of this study was to further develop the infant air-jet DPI platform by considering the effects of different air sources, flow rates, and pulmonary mechanics on aerosol generation and delivery through a preterm NT airway model. Consistent with aerosol delivery to a preterm infant with a body weight of 1600 g, device actuation was tested with ~10 mL of positive-pressure air. To maximize device performance, new designs with multiple air inlets

were assessed. Three different air sources were tested that provide different flow rate waveforms, each with actuation delivery times under 1 second, and flow rates ranging from 1-4 L/min. A gradually expanding nasal cannula was previously shown to provide low interface depositional loss, but relatively high NT loss. In order to reduce NT depositional loss, adjustment of flow rates was explored. Finally, physically realistic downstream resistance and compliance consistent with a preterm infant in respiratory distress were added to the realistic NT model. Design goals of the device include high ED ( $\geq 80\%$  loaded dose) with low interface ( $< 15\%$ ) and NT ( $< 15\%$ ) depositional loss. For the preterm infant NT model, a lung delivery efficiency of  $>50\%$  of the loaded dose is targeted.

## **4.2 Materials and Methods**

### *Powder Materials and Formulation*

Pearlitol® PF-Mannitol was donated from Roquette Pharma (Lestrem, France) and Poloxamer 188 (Leutrol F68) was donated from BASF Corporation (Florham Park, NJ). Trileucine was purchased from Bachem Americas, Inc. (Torrance, CA). Albuterol sulfate (AS), l-leucine and all other reagents were purchased from Sigma Chemical Co. (St. Louis, MO).

Albuterol sulfate excipient enhanced growth (AS-EEG) powders were obtained using a Büchi Nano B-90 HP Spray Dryer (Büchi Laboratory-Techniques, Flawil, Switzerland), and spray-dried based on the optimized method described by Son et al. [76]. AS-EEG powder formulations included 30:48:20:2% w/w ratio of AS, mannitol, l-leucine or trileucine, and Poloxamer 188, respectively. A feed solution of 250 mL containing the dissolved drug and excipients at the stated ratio was sprayed over a 5 – 6-hour period at a spray rate of 0.7 - 0.9 mL/min. The solids



concentration in the feed solution was 0.5%w/v. Throughout the spray drying process, the inlet temperature was set to 120 °C, resulting in an outlet temperature of 48-51°C. The feed solution temperature was 2-15° C during the spray drying as excess feed solution was recycled into the stock. Multiple batches of spray-dried formulations containing l-leucine as the dispersion enhancer were implemented in all experiments except for the final evaluation of pulmonary mechanics. To determine the effects of both more realistic infant pulmonary mechanics and a different dispersion enhancer, final experiments were performed with the trileucine formulation delivered through the NT model with and without inclusion of a downstream lung chamber.

#### *Platform and Experimental Overview*

The infant air-jet DPI system developed in our previous study [26] consists of three main components: the air source, the air-jet DPI, and the nasal interface, which are briefly reviewed here. The main focus of this study is the air source, which, described in detail in the next subsection, is responsible for providing the aerosolization energy to the air-jet DPI, delivering the aerosolized powder to the lungs and providing a full inhalation breath for the infant. The air-jet DPI is responsible for aerosolization of the powder and consists of small diameter flow pathways for the inlets and outlets connected by an aerosolization chamber. As the air source is actuated, high speed jets of air pass through the aerosolization chamber and over the preloaded powder bed facilitating powder aerosolization. The aerosol then passes through the nasal interface and to the infant. The nasal interface forms an airtight seal with an infant's

nostril and is inserted approximately 2 to 5 mm into the nose, consistent with short ventilation support nasal prongs.

Comparisons of the different air sources were considered in two main stages. In the first stage, aerosolization performance of four different air-jet DPI designs through the end of the air-jet outlet flow passage (excluding the nasal interface) was compared for each air source. Aerosolization performance was established as device emitted dose (ED), which is the amount of powder exiting the air-jet DPI as a percentage of the loaded dose, and the mass median aerodynamic diameter (MMAD), which was determined through the use of a next generation impactor (NGI). Figure 4.1a illustrates the experimental setup for the first stage experiments. Each air source was connected to each of the air-jet DPIs in turn, and actuated three times in succession into the NGI as described in more detail in the *“Evaluation of Air Source and Air-Jet DPI Aerosolization Performance”* subsection. In the second stage of experimentation, the performance of the platform as a whole (including nasal interface) was evaluated with use of a preterm infant nose-throat (NT) *in vitro* model. As seen in Figure 4.1b, the platform interfaces with the preterm NT model which leads to a custom low-volume filter for approximating lung delivered dose. In this setup, device ED, NT regional deposition, and lung deposition efficiency (represented by aerosol passing through the larynx and depositing on the filter) were assessed, as percentage values of the loaded dose.

### *Air Source Designs*

Three unique air sources were designed and prototyped to provide different air flow waveforms and investigate effects on aerosolization performance of the air-jet DPI. Figure 4.2

shows the three unique air sources (Timer, Pneumatic, and Spring) with main components labeled. The different air flow waveforms produced by each air source are discussed in the next subsection. In each system, the air source provides both the energy to aerosolize the dry powder and a full positive-pressure inhalation breath. In this study the full inhalation for a preterm infant was 10 mL of air, used as the air actuation volume (AAV) which equated to a tidal volume of 6.25 mL/kg. Since each air source uses positive pressure to deliver the aerosol, it is expected to help mildly expand the flexible airways while preventing exhalation back into the system. Prototyped parts were 3D printed using PLA black material or VeroWhitePlus resin.

The Timer air source (Figure 4.2a) consisted of an electronic timer control board connected to miniature electronic solenoid valves. The air source pictured and used in this study operated on standard 120 V AC power; however, a more portable rechargeable battery configuration was also developed. The inlet was connected to an upstream compressed air supply and controlled by a pressure regulator with digital gauge and flow valve. The pressure regulator and flow valve can be adjusted to produce the desired flow rate profile. The timer control board opens the air flow to the outlet connection that attaches to the air-jet DPI with accuracy to the hundredth of a second, which facilitates precise control over each actuation. The actuation was performed by either a push button on the device or through a connected cable leading to a foot pedal switch that allowed for hands free actuation. Subsequent actuations could be performed immediately without the need for a reloading action. This air source required electricity and compressed air to operate. Measuring the flow rate of air produced by the actuation, a delivered AAV was calculated based on duration and rate of air flow, and the timer was set accordingly.

The Pneumatic air source (Figure 4.2b) used a pneumatic piston to perform the actuation motion where the piston rod depresses a modified large bore syringe, very similar to a hand operated syringe actuation; however, this configuration was highly consistent, tunable and repeatable. The air source consisted of a pressure regulator with digital gauge, which connected to a compressed air source and led to a 5/3 (EC) control valve allowing for the extension, retraction or venting of the pneumatic piston. The pressures needed for the upstream compressed air for both the Timer and Pneumatic air source in this study were less than 30 psi. The pressure regulator could be tuned to produce a stronger or weaker extension of the piston rod, which results in a faster or slower actuation, respectively. A modified 140 mL syringe acted as an air reservoir chamber that could be set to a desired volume for a pre-set AAV. At the end of the air reservoir was a custom 3-way valve and outlet connection for the air-jet DPI, which allows for the system to remain closed while refilling the air reservoir. For initial actuation, the reservoir chamber was filled, the 3-way valve was set to the open position, and the air-jet DPI was attached. Next, the piston rod was extended (which performed the actuation), and then retracted using the control valve. This air source required compressed air to operate the pneumatic piston and the air reservoir chamber needed to be manually refilled between actuations, using the 3-way valve.

The Spring air source (Figure 4.2c) operated using a pre-compressed air reservoir chamber to produce the actuation upon opening a valve to the air-jet DPI. This air source was similar to the Pneumatic air source in the use of the air reservoir chamber leading to the 3-way valve and connection to the air-jet DPI. This air source had a set of springs inside the piston that when compressed, facilitated the complete emptying of the reservoir chamber. In this study, a

preset spring compression distance guide was used, but an adjustable guide can be easily implemented. More or less compression of the air and spring led to a faster or slower actuation of the device, respectively. Before initial actuation, the 3-way valve was set to the refill position and the reservoir chamber was filled with room air to the desired set volume. Next, the 3-way valve was set to the closed position and a hand clamp was used to compress the air in the reservoir and the spring by an appropriate amount set by the guide. For actuation, the air-jet DPI was connected to the infant and the 3-way valve was moved to the open position, allowing the compressed air to flow into the air-jet DPI, performing the actuation. This air source had no external requirements such as electricity or compressed gas, but was more complex to operate and needed to be manually refilled between actuations.

#### *Air Source Flow Rate Measurement*

To characterize the unique air flow waveform generated by each air source, a neonatal mass flow meter (Sensirion SFM3400, Sensirion AG, Stafa, Switzerland) was connected directly between an air source and an air-jet DPI (Figure 4.1b shows the location of the mass flow meter). The air flow was recorded at approximately 2000 samples/sec. Figure 4.3 illustrates the three unique air flow waveforms for each air source after calibration (n=3) during actuation while connected to the D1-Single air-jet device. In order to compare performance between the unique waveforms, the parameter of Q90 (the value at which 90% of the measured flow rate values fall below) was selected to be held constant among the air sources while the peak and average flow rates were allowed to vary. The plots in Figure 4.3 were based on the measured flow rate values for each air source set to a Q90 of 4 L/min. The Timer air source produced an

air flow with a square waveform while the Pneumatic air source produced more of a parabolic waveform, similar to hand actuation. The Spring air source had a sharp peak followed by a gradual decrease of the flow rate as expected for an initially compressed air reservoir.

### *Air-Jet DPI Designs*

The internal airway geometries for the air-jet DPI designs in this study are illustrated in Figure 4.4, with basic elements shown, including small diameter inlet capillaries, aerosolization chamber where the powder was loaded, and outlet capillary. All designs were influenced by our previous study and used multiple inlets with diameters of 0.5 mm [26]. The four new designs in this study are shown in Figure 4.4a-d and are referred to as D1-Single, D1-Dual, D2-Single and D2-Dual. The D2 designs implemented a horizontal cylindrical chamber based on a size 0 capsule with a volume of about 0.68 mL, whereas the D1 designs implemented a vertical cylindrical chamber of the same diameter but with reduced height resulting in a volume of approximately 0.28 mL. The Single version of each design utilized a single outlet from the aerosolization chamber leading to a hollow stainless steel (SAE 304) capillary tube to form the outlet, while the Dual versions utilized two outlets and capillary tubes. The single outlet was similar to our previous study and allowed connection to a single nasal interface with a single nasal prong while the dual outlets will allow for investigation of a dual prong interface in a future study.

As with our previous study [26], parts (including the nasal interface in the next subsection) were designed in SolidWorks (Dassault Systèmes, Paris, France), and exported as .STL files. The parts were then 3D printed at 32  $\mu\text{m}$  resolution on a Stratasys Objet24 3D Printer

(Stratasys Ltd., Eden Prairie, MN) using VeroWhitePlus resin. All parts in this study were designed to interconnect using a twist locking design with an intermediate O-ring for an airtight seal.

After construction of the devices, each design consisted of two parts to facilitate powder loading and operation. The D1 designs implemented a top/bottom configuration in which the powder was loaded into the bottom portion of the aerosolization chamber and then attached to the top with the twist lock motion. The D2 designs implemented an inlet/outlet configuration in which the aerosolization chamber was split perpendicular to the air flow path, near the outlet side to facilitate powder loading before the inlet and outlet parts were connected.

### *Nasal Interface Design*

A gradually expanding nasal interface design was used in this study based on results of previous full-term testing [26]. For the preterm infant, a shortened version of the gradually expanding interface was implemented. The nasal interface consisted of a straight gradually expanding circular cross-section with a length of 43 mm, and a final internal diameter of 3 mm. The end of the expansion transitioned to a flexible prong, made from tubing with an inner diameter of 3 mm and outer diameter of 5 mm. The air pathway of the nasal interface when attached to the air-jet DPI is illustrated in Figure 4.4e. A gradual exterior taper was included around the flexible prong to help form an airtight seal with the infant's nostril. During aerosol delivery through the NT model, the single-prong nasal interface was inserted approximately 5 mm into one nostril and the other nostril was held closed.

### *Preterm Infant Nose-Throat (NT) Model*

Aerosol delivery efficiency to the lungs was tested by the administration of the powder through a preterm NT airway model beginning at the nostrils and including the pharynx, larynx, and approximately 3/4<sup>th</sup> of the trachea, after which a custom low-volume filter housing was attached. Figure 4.5a shows the complete setup and assembly break-out of the NT model and low-volume filter housing. In this study, the smaller and more difficult to penetrate airways of a preterm infant were considered. The preterm infant airways were based on an infant weight of 1600 g and length (height) of 40.7 cm. Similar to the full-term infant NT model developed in our previous study [26], a preterm version was designed using the same method. A high-quality NT geometry of a 6-month-old infant based on CT scans provided nasal airway deposition consistent with mean values [79]. Using the infant body length (height), an appropriate geometric scaling factor of 0.6 was used to reduce the model to that of a preterm infant with weight and height of about 1600 g and 40.7 cm, respectively [167]. The resulting preterm airway, shown in Figure 4.5b, has a volume of 2.2 mL. The resulting tracheal length and diameter (proximal) were approximately 26 and 3 mm, respectively. While these parameters are known to vary, they do fall within the expected range for preterm infants of 25 to 30 weeks gestational age (GA) based on reported studies [168].

The preterm NT model was constructed with similar twist lock interfaces and O-rings as the platform, which provided air tight seals and facilitated ease of use. The low-volume filter housing was developed to accommodate the low AAV of 10 mL used for a preterm infant, which had a dead space of only 2.7 mL before the 1.5” diameter glassfiber filter. The diameter of the



filter was chosen to balance the dead space with resistance. To provide a smooth and accurate internal airway surface, the middle passage and throat sections of the preterm NT model were built using stereo-lithography (SLA) with Accura ClearVue resin through 3D Systems On Demand Manufacturing. The low-volume filter housing was 3D printed with using VeroWhitePlus resin. To facilitate nasal interface prong insertion and the formation of an airtight seal, the face and anterior nose section was molded with a skin-like silicone elastomer. The face adapter (pictured in Figure 4.5a) was printed using VeroWhitePlus resin, and was glued to the soft face mold, allowing for a secure and air-tight connection to the rest of the NT model.

#### *Evaluation of Air Source and Air-Jet DPI Aerosolization Performance*

Consistent with our previous studies, experiments used 10 mg of AS-EEG powder formulation (manually weighed) and a Next Generation Impactor (NGI: MSP, TSI Incorporated, Shoreview, MN) for aerosol particle size analysis. The powder mass was weighed and then loaded into either the inlet or bottom section of the air-jet DPI, which was then connected and sealed to its outlet or top section with a twisting motion. To assess aerosol size distribution, the air-jet DPI (without nasal interface) was attached to a custom adapter and placed in the pre-separator inlet of the NGI (Figure 4.1a). The custom adapter positioned the outlet of the air-jet DPI 1 cm away, centered and perpendicular to the inlet of the pre-separator, with open space allowing for co-flow room air to enter the NGI. The NGI was operated at a flow rate of 45 L/min using a downstream vacuum pump. The NGI was positioned 53° off horizontal to allow the device to remain level during use and maintain an inline flow path from the device outlet to the NGI inlet as would occur during administration to a supine infant. Each stage of the NGI was

coated with MOLYKOTE® 316 silicone spray (Dow Corning, Midland, MI) to minimize particle bounce and re-entrainment. The NGI flow rate of 45 L/min was chosen to ensure collection of the aerosol, minimize any effects of settling, and provide appropriate stage cutoff diameters for evaluating small aerosol sizes. Before each set of experimental runs, the flow rate was confirmed using a flow sensor (Sensirion SFM3000, Sensirion AG, Stafa, Switzerland) connected to the pre-separator inlet with an air-tight seal.

Each combination of air-jet DPI and air source was actuated into the NGI with an AAV of 10 mL 3 times, with a 5 sec pause between actuations. Three runs for each air-jet DPI and air source combination were performed in a random order. For this initial stage of experiments, the air sources were calibrated to deliver an actuation with a Q90 flow rate of 4 L/min. Analysis metrics included emitted dose (ED) and mass median aerodynamic diameter (MMAD). The parameter of MMAD/ED was also considered as a general indicator of performance, in which lower values are more desirable. ED was calculated as the mass of AS loaded into the device minus the mass of AS remaining in the device divided by the initial loaded mass of AS.

Aerosolization calculations were based on the mass of AS recovered in the NGI.

In a later stage of experiments a single device and air source were chosen for aerosolization performance testing with the NGI. In this set of experiments, the previous methods remained the same except for the use of a single combination, where the Q90 was varied instead, to investigate the effects of flow rate on aerosolization performance. All drug masses were determined using HPLC analysis, as described in the “Drug Mass Characterization Methods” subsection.

### *Evaluation of Preterm Lung Delivery Efficiency*

Based on device and air source assessment, the second stage of this study used the best performing design for preterm NT *in vitro* model testing at an AAV of 10 mL. The experimental setup was the same as with aerosolization performance in terms of actuation, powder loading, and randomization. However, instead of the device connecting to the NGI adapter, it was connected to the gradually expanding nasal interface, as seen in Figure 4.6, which was inserted approximately 5 mm into the left nostril of the infant NT model (the right nostril was manually held closed during actuation). A small amount of lubricant grease was applied to the exterior of the prong to ensure an airtight seal. All NT model segments were internally coated with silicon spray to minimize particle bounce similar to airway surface liquid. At the end of the NT model, a custom low-volume filter collected powder passing through the extrathoracic regions and represented the amount of drug delivered to the lung. The NT model was mounted horizontally while the platform was held as pictured in Figure 4.6a, with a lateral angle of approximately 5 degrees. Figure 4.6b provides images of the experimental setup without the right nostril being held closed.

Three runs for each air source were performed at the original Q90 of 4 L/min and subsequently at 2 L/min for selected air sources. Comparing the air sources in this way was used to determine if there was an effect on performance caused by the flow waveforms. Higher (4 L/min) and lower (2 L/min) flow rates were tested to investigate the effects of overall flow rate on performance in terms of lung delivery efficiency. A single air source was then chosen to test across a range flow rates to build an impaction parameter curve. The Timer air source with the D1-Single device was tested at four Q90 values for both NT model deposition and NGI size

characterization. Using the NT deposition and MMAD recorded at each flow rate, the impaction parameter of  $d_p^2Q$  was determined, which is the particle diameter ( $d_p$ ) squared (represented by the MMAD in  $\mu\text{m}$ ) times the flow rate ( $Q$ ) (represented by the Q90 value in L/min). Calculations for ED and regional deposition, including the nasal interface and in the NT model and tracheal filter (amount delivered to lung) were expressed as a percentage of the loaded dose of AS.

### *Pulmonary Mechanics Setup*

In a final stage of this study, the effects of an infant's pulmonary mechanics were considered using a trileucine EEG formulation. In all previous infant NT model testing, the model ended with a low-volume filter housing that was open to atmosphere past the filter. The filter created some resistance, but not to the extent as expected for an infant suffering from respiratory distress syndrome (RDS). Two NT model outlet conditions were considered: one as the standard filter only and then also including the down-stream pulmonary mechanics. A final experimental set was performed to directly compare each outlet condition using the best-case air source (operated at 1.7 L/min). Pulmonary mechanics (PM) considered in this study were airway resistance ( $\text{cm H}_2\text{O/L/s}$ ) and lung compliance ( $\text{mL/cm H}_2\text{O}$ ). While values for these properties are known to vary, a compliance of 0.48  $\text{mL/cm H}_2\text{O}$  was chosen for the preterm infant (of 1600 g) based on a similar value measured in infants with a weight of 1600 g [104]. For infants with RDS, airway resistance values have been reported between 100-200  $\text{cm H}_2\text{O/L/s}$  [104-107]. An adjustable chamber was built to simulate these properties for PM testing that connects with the NT model filter housing as seen in Figure 4.7.

To set the desired properties of the PM chamber, first the volume of air inside the chamber was adjusted to create compliance based on the compressibility of air. To measure compliance after the chamber was adjusted, 10 mL of room air was forced into the chamber while the change in pressure was recorded using a pressure sensor (SSCDLNN040MBGSA5, Honeywell, Sensing and Control, Golden Valley, MN). The resulting compliance was calculated to be 0.49 mL/cm H<sub>2</sub>O. Next, an adjustable orifice between the filter and compliance chamber was used to control the resistance. To measure the resistance through the filter housing and orifice, the pressure sensor was placed anterior to the filter housing while the neonatal flow meter (Sensorion SFM3000) was placed further upstream. The compliance chamber was opened to allow atmospheric pressure downstream of the orifice. The flow rate was set to 4 L/min and the pressure was recorded. The orifice was adjusted to provide resistance expected for an infant with RDS. The resulting calculated resistance was 170 cm H<sub>2</sub>O/L/s which falls within the range of expected values.

While considering PM of an infant receiving treatment, another consideration is a safe operating pressure. It is generally accepted that safe pressure ranges for infant airways are up to 25 or possibly 35 cm H<sub>2</sub>O [19, 99, 102, 169] depending on the state of the infant's lungs. During PM condition testing, the pressure sensor was also used to measure the closed system pressure during aerosol actuation to ensure safe operating conditions. The pressure port for measurement in the PM condition testing and vent port was located between the filter and resistance orifice. Venting between actuations at this location allowed for the air to exit the simulated lungs without passing back through the filter and detaching any deposited powder.

### *Drug Mass Characterization Methods*

After actuation and aerosolization, drug masses retained or collected in the air-jet DPI and NGI or nasal interface, NT model, and filter were recovered by dissolving in an appropriate volume of deionized water followed by high performance liquid chromatography (HPLC) analysis with fluorescence detection (excitation = 276 nm, emission = 609 nm). A Restek Allure PFP propyl column (5  $\mu\text{m}$ , 60  $\text{Å}$ , 150 x 2.1 mm) was used for the chromatographic separation with a mobile phase flow rate of 0.4 mL/min. The mobile phase consisted of methanol and ammonium formate buffer (20 mM, pH 3.4) in a ratio of 70:30. The sample injection volume was 10  $\mu\text{L}$ . The loaded drug mass was determined through content uniformity analysis of the AS-EEG formulation; where known masses of AS-EEG were dissolved in water and the AS content ( $\mu\text{g}/\text{mg}$  of formulation) was determined. AS quantification was performed for each deposition site and for the drug mass used to calculate the drug recovery. Drug recovery percentage was expressed as the amount of AS recovered on all deposition sites divided by the loaded AS dose for each experiment.

Based on an airflow rate of 45 L/min, the NGI stage cut-off diameters were determined using the formula specified in USP 35 (Chapter 601, Apparatus 5). The MMAD was calculated through linear interpolation between appropriate stages using a plot of cumulative percentage drug mass vs. cut-off diameter.

### *Statistical Analysis*

Statistical analysis for comparing aerosolization performance based on air source and comparisons of lung depositions were performed using JMP Pro 15 (SAS Institute Inc., Cary,

NC). Comparison of device performance based on air source and comparison of NT model filter deposition utilized one-way ANOVA followed by post hoc Tukey. Comparison of filter-only outlet condition and pulmonary mechanics outlet condition utilized Student's *t*-test. Statistical tests used a significance limit of  $P=0.05$ .

### **4.3 Results**

#### *Comparison of Air Sources*

Table 4.1 provides a comparison of each air source with a target Q90 of 4 L/min during calibration over 5 actuations. The low standard deviations of the measured values highlight the controllability and consistency of each air source. Peak values were found to vary by a small amount due to the different waveforms, while the time averaged flow rate varied by a larger degree.

#### *Air Source Effect on Air-Jet DPI Performance*

In the first stage of testing, each combination of air source and air-jet DPI was tested for aerosolization performance. For all experimental testing except for the last pulmonary mechanics set, the I-leucine EEG formulation powder was used. Figure 4.8 plots the mean values for each combination in terms of ED vs MMAD, with standard deviation bars for  $n=3$ . The legend provides the combination of air-jet DPI device and air source tested, with air sources abbreviated as Timer (Tmr), Pneumatic (Pnu), and Spring (Spr). Some combinations produced larger variability than others such as the D2 with Spring air source. A trend line of all mean values has been plotted to distinguish performance comparatively where a higher ED paired

with a lower MMAD is most desirable. Therefore, values below the trendline represent better overall performance, while values above the trendline indicate worse performance relative to the mean.

The parameter of MMAD/ED is a similar indicator with lower values indicating better performance. Table 4.2 lists the mean values of ED and MMAD as well as the MMAD/ED parameter for each combination. Considering Figure 4.8 and Table 4.2, there is no obvious distinction of an effect on performance from the unique flow rate profiles produced by each air source. For each device, statistical analysis was performed separately to compare the effect of air source on performance in terms of ED, MMAD, and MMAD/ED (Table 4.2). For each device and parameter combination there was no statistically significant effect of air source except for one instance, in which there was statistically significant difference between the MMAD produced with D1-Single when comparing the Pneumatic and Spring air source. Despite this difference, due to the surprisingly low variability of MMAD values with the Pneumatic air source, the D1-Single device produced the overall smallest range of performance values across each air source.

Results at 4 L/min indicate there is no significant effect of flow profile on aerosolization performance except possibly with the D1-Single device. All combinations reached the target ED of >80% except D2-Single with the Spring air source. The mean MMAD values fell between 1.65 – 1.80  $\mu\text{m}$ . Only the D1-Single device had all points below the trend line, indicating better performance for all air sources. For that reason and the fact that D1-Single also showed the overall lowest standard deviations and range of performance (MMAD and ED), D1-Single was chosen as the air-jet DPI for continued testing in this study.



### *Air Source Comparison with Preterm NT Model*

In the filter only outlet configuration, three replicate runs for D1-Single and each air source were actuated through the preterm NT model, using a Q90 of 4 L/min (Figure 4.9) using the I-leucine EEG formulation. Figure 4.9 illustrates the amount of powder remaining in the air-jet DPI labeled as Device, the amount deposited in the nasal interface labeled as Interface, and the combined deposition in the anterior nose, middle passage and throat labeled as NT. The amount of powder that passed through the model and reached the filter was labeled Filter, which approximates the lung delivery efficiency. For each air source at 4 L/min, the filter deposition was approximately 33-36%. There was no statistically significant difference between the lung delivery efficiencies at 4 L/min across the air sources. With the challenging preterm airway model, the best performing air-jet DPI was unable to reach the 50% lung delivery efficiency goal at 4 L/min.

It is known that the impaction parameter, which consists of the particle size and flow rate, has a strong correlation with NT deposition. While the particle size is more difficult to control, the development of these air sources made it easier to control the flow rate, which would be very difficult using a hand operated syringe. If aerosolization performance is not influenced by reducing the flow rate, then it leads to a lower impaction parameter which in turn improves NT penetration and lung delivery efficiency. The two air sources with the greatest difference (while not statistically significant), the Timer and Pneumatic, were chosen to test at half the flow rate, or a Q90 of 2 L/min. At this reduced flow rate, Figure 4.9 illustrates a large

increase in filter deposition to approximately 44% for both air sources with the D1-Single device.

#### *Effect of Flow Rate on Lung Delivery Efficiency*

Additional NT model testing was performed using the D1-Single device and Timer air source to verify the effects of lower flow rates using the l-leucine EEG formulation. In addition to the Q90 flow rates of 2 and 4 L/min, 3 L/min and 1.7 L/min were also included. A Q90 of 1.5 L/min was intended to be the lowest flow rate; however, ED performance at this flow rate was noticeably lower hence a Q90 of 1.7 L/min was selected as the lower bound. Figure 4.10 illustrates the regional depositions of the D1-Single and Timer air source at each flow rate. A clear trend appears in which lowering the flow rate decreases NT deposition and increases lung delivery efficiency. The ED or device retention remained similar across all flow rates shown and ED remained above 80%. Nasal interface deposition was also similar across all flow rates with values around 15%. From the flow rates of 4, 3, and 2 L/min, the resulting mean filter deposition was 32.7, 35.3, and 44.4%, respectively, while the total mean NT deposition was 36.8, 32.2, and 25.5%, respectively. At the lowest flow rate tested (Q90 = 1.7 L/min), the mean filter deposition was 53.6% and total mean NT deposition was 15.5% of the loaded dose. The difference in performance (in terms of filter deposition) between 4 and 3 L/min was not statistically significant, while the differences between 3 and 2 L/min and between 2 and 1.7 L/min were significant. Lowering the flow rate to improve NT penetration allowed for the platform to achieve the target goals and resulted in a >50% estimated lung delivery efficiency for the l-leucine EEG formulation.

### *Impaction Parameter*

Using the total NT deposition fractions in the previous experimental set, the data was combined with an additional set of experiments to build an impaction parameter curve. Similar to the first stage of experiments, the air-jet DPI was tested with the NGI to determine the MMAD for the aerosol produced at each respective flow rate using the l-leucine EEG formulation. Table 4.3 provides the values obtained for calculation of the impaction parameter. Figure 4.11 provides the plot of impaction parameter vs NT deposition. A surprising result is that the MMAD actually decreased with flow rates below 3 L/min (Table 4.3). At both 4 and 3 L/min, the MMAD was found to be about 1.7  $\mu\text{m}$ , then dropped slightly to a mean value of 1.65  $\mu\text{m}$  at 2 L/min, and further decreased to 1.56  $\mu\text{m}$  at 1.7 L/min. This behavior of reduced flow rate producing smaller MMAD values has been observed with other air-jet systems [22, 170] and explains the significant increase in lung delivery with reduced flow rate observed in Figure 4.10.

### *Regional Deposition for Preterm NT Model*

To highlight the effect of increased NT penetration due to the lower impaction parameter, Figure 4.12 illustrates the deposition fractions for each flow rate broken down by nasal region. Referring back to Figure 4.5, the illustration shows specifically where the regions were split in the infant NT model. For the middle passage and throat region, a steady decrease in deposition can be seen with decreasing flow rate. For each region, the deposition at 1.7 L/min was less than half than the deposition at 4 L/min.

### *Pulmonary Mechanics*

A final set of experimental data comparing the filter only outlet condition and PM outlet condition is reported in Table 4.4. Using a novel trileucine EEG formulation powder which has a lower density than the l-leucine EEG formulation, side-by-side comparisons for deposition in each region highlight the similarity in the air-jet DPI system performance with and without PM included. Two regions (Middle Passage and Total Extrathoracic) resulted in a statistically significant difference between conditions; however, these differences were less than 2 or 3% of the loaded dose. The PM condition was not found to have a statistically significant effect on filter deposition. Infant airway pressure is also a concern and Figure 4.13 shows sample pressure recordings taken during actuation, including a 5 sec breath hold. The highest pressure recorded during all actuations was 27.0 cm H<sub>2</sub>O.

### **4.4 Discussion**

A significant finding of this study is that for a consistent Q90 flow rate through the infant air-jet DPI system, different air sources with different waveforms did not impact the overall performance. In comparing tracheal filter deposition, which approximates lung delivery efficiency, there was no statistically significant difference between the air sources when testing with a preterm infant NT model. This conclusion allows for the air source to be selectable for different operating environments or based on other criteria, without compromising the performance of the platform. For example, the Timer air source would be ideal for its ease of use in a high resource setting where breathable compressed air and power are available,

whereas the Spring air source could be ideal for low resource or mobile environments where compressed air and power are not readily available. This finding also enables the possibility for additional air sources to be developed tailored to specific requirements, such as ease of use, without dependence on power or a compressed air supply. It is expected that a new air source design will not have an impact on performance provided the Q90 flow rate can be controlled as it was with the currently developed air sources in this study. As opposed to a hand operated syringe actuation, the air sources currently developed are highly controllable, repeatable and should not suffer from intra-operator variability. In this study, after it was found that the flow rate waveform did not significantly affect performance, the Timer air source was chosen for further testing for its ease of use and likely direct deployment in high resource clinical markets.

In our previous study that initially developed the infant air-jet system, 3 of the 4 horizontal aerosolization chamber designs tested were found to have improved performance compared to a vertical chamber design [26]. In the current study, the D1-Single design (implementing a vertical chamber) was found to perform better than the horizontal chambers with the addition of multiple inlet jets and a reduced volume aerosolization chamber. It is also observed that in the initial study the average flow was approximately 2-3 L/min, producing tracheal filter deposition of approximately 50% in a larger full-term NT model. While a direct comparison is difficult due to different air-jet DPI designs and AAVs, the air flow profile produced by the hand operated syringe is similar to that of the Pneumatic air source, and as reported in this study, the Pneumatic air source operated with a Q90 of 4 L/min resulted in a time-averaged flow rate of about 2 L/min. Therefore, under similar actuation conditions, there was a significant decrease in filter delivery efficiency from about 50% in the full-term model to

about 35% in the preterm model, which can be attributed to the smaller, more difficult to penetrate airways of the preterm NT geometry.

A second significant finding of this study was that lowering the actuation flow rates largely improved lung delivery efficiency for a highly dispersible particle engineered spray-dried powder formulation. To overcome challenges presented with the small preterm airways, lowering the actuation flow rate to decrease the impaction parameter was investigated. As shown in this study, lowering the flow rate provided a significant improvement in NT penetration and improved lung delivery efficiency. When the flow rate was decreased from the original Q90 of 4 L/min to a Q90 of 1.7 L/min, the lung delivery efficiency increased from about 35% to over 50% for the l-leucine EEG formulation. Thus, using the low flow rate, the platform achieved the target performance goal and performed consistently with our previous study employing full-term infant airways.

Investigation of the impaction parameter led to interesting results in which the aerosolization performance improved when decreasing the flow rate below a Q90 of 3 L/min. When the flow rates were tested at 2 and 1.7 L/min, the resulting MMAD decreased by 0.07 and 0.16  $\mu\text{m}$ , respectively, when compared to 3 and 4 L/min. This observation partially explains the significant increase in NT penetration at the lower flow rates as the particle size also decreased, while the ED remained approximately the same. It is typically held that higher turbulent energy provided by a larger flow rate should better deaggregate a dry powder formulation; however this may not be the case with the air-jet DPI design and the spray-dried formulations as recent studies on dispersion parameters have indicated [22, 170]. Another consideration for lowering flow rate to improve performance is that performance in terms of

ED will quickly drop off below a certain flow rate. In this study, testing at 1.5 L/min reduced ED performance more than two-fold compared to 4 L/min, while the reduction at 1.7 L/min was not statistically significant. While 1.7 L/min was optimal for the configuration and formulation presented in this study, it is likely to be air-jet DPI design and powder dependent, which will need further consideration in future studies.

The final portion of this study investigated the effects of downstream pulmonary mechanics on the air-jet DPI system's performance using a second spray-dried EEG formulation containing trileucine as the dispersion enhancer. With added resistance and compliance in the ranges of expected values for preterm infants with RDS, the PM outlet condition did not have a significant effect on the approximated lung delivery efficiency. This indicates the platform will deliver a therapeutic similarly between infants with varying pulmonary mechanics in terms of resistance and compliance. Another finding is the expected safety of the aerosol delivery in terms of airway pressure; the highest measured peak pressure in the airway was 27 cm H<sub>2</sub>O, while the majority of the breath hold pressure was between 20 to 25 cm H<sub>2</sub>O.

Limitations of this study include the use of a single preterm NT model, a single nasal interface, and limited number of devices compared across air sources. The use of a single preterm NT airway geometry limits the deposition data to a single point while it is known that NT deposition varies at all ages. The single nasal interface used in this study was based on the initial platform development, which performed best during initial screening of interfaces. Future studies will focus on optimizing the nasal interface, from the transport of aerosol to the prong insertion, as well as the influence of the nasal prong on aerosol transport through the nose. Finally, with only 4 unique air-jet DPI designs and 3 unique air sources being tested, it is

not known if all designs will perform similar with all air sources. However, for the devices tested in this study, and especially the D1-Single design, the air source flow rate waveforms do not significantly affect the lung delivery performance of the platform. While this is believed to be the case for future combinations of air-jet DPIs and air sources, performance of significantly different design combinations should be compared and verified. While initial development and optimization of the platform was performed with 10 mg doses of a model spray-dried formulation, performance with surfactant powders at higher doses needs to be determined.

#### **4.5 Conclusions**

In conclusion, three unique air sources were developed that can deliver consistent, repeatable, and controllable actuations for the infant air-jet DPI system containing a spray-dried EEG formulation. These air sources were found to perform similarly during *in vitro* testing using a preterm NT model and when matched at the same Q90 flow rate value. As a result, in future studies the air source implemented with the infant air-jet DPI can be based on factors such as the operating environment (high or low resource setting) without a significant impact on drug delivery performance. It was also found that the Q90 flow rate of the actuation plays a significant role in the drug delivery performance. Initial performance of the platform comparable to that of syringe hand actuation was improved, with lung delivery efficiency increasing from about 35% to 54% when the Q90 flow rate was lowered from 4 L/min to 1.7 L/min. Addition of a realistic pulmonary outlet condition (simulating the airway resistance and lung compliance of a preterm infant with RDS) did not significantly affect the lung delivery efficiency of the platform. The platform was also found to operate in safe infant airway



pressure ranges. Overall, development of the air sources led to the target goal of >50% lung delivery efficiency of a spray-dried EEG formulation in the smaller more challenging preterm NT model. Further development of the platform is expected to improve upon the current performance, allowing for a highly efficient, rapid, and non-invasive form of aerosol delivery to neonates.

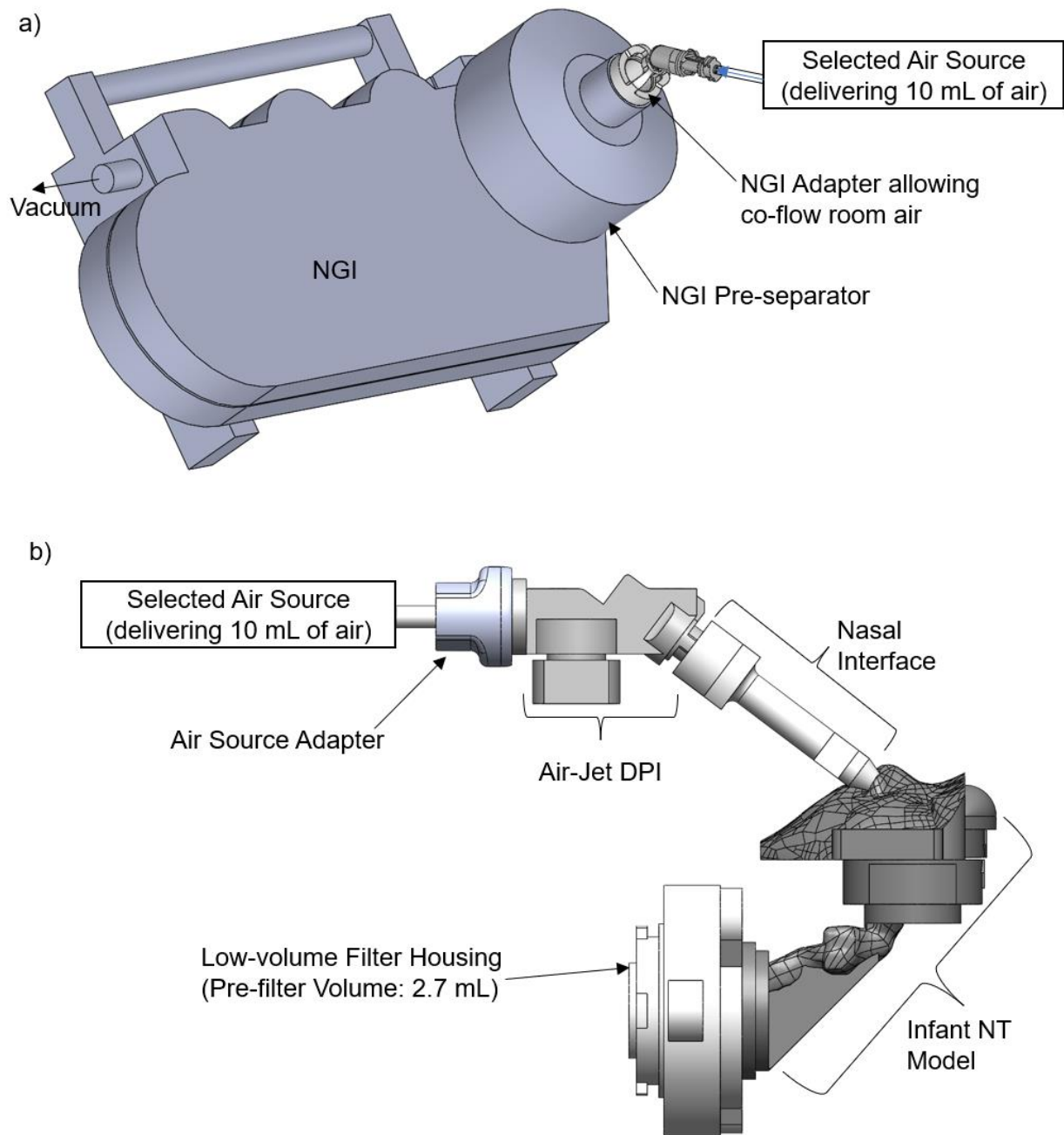
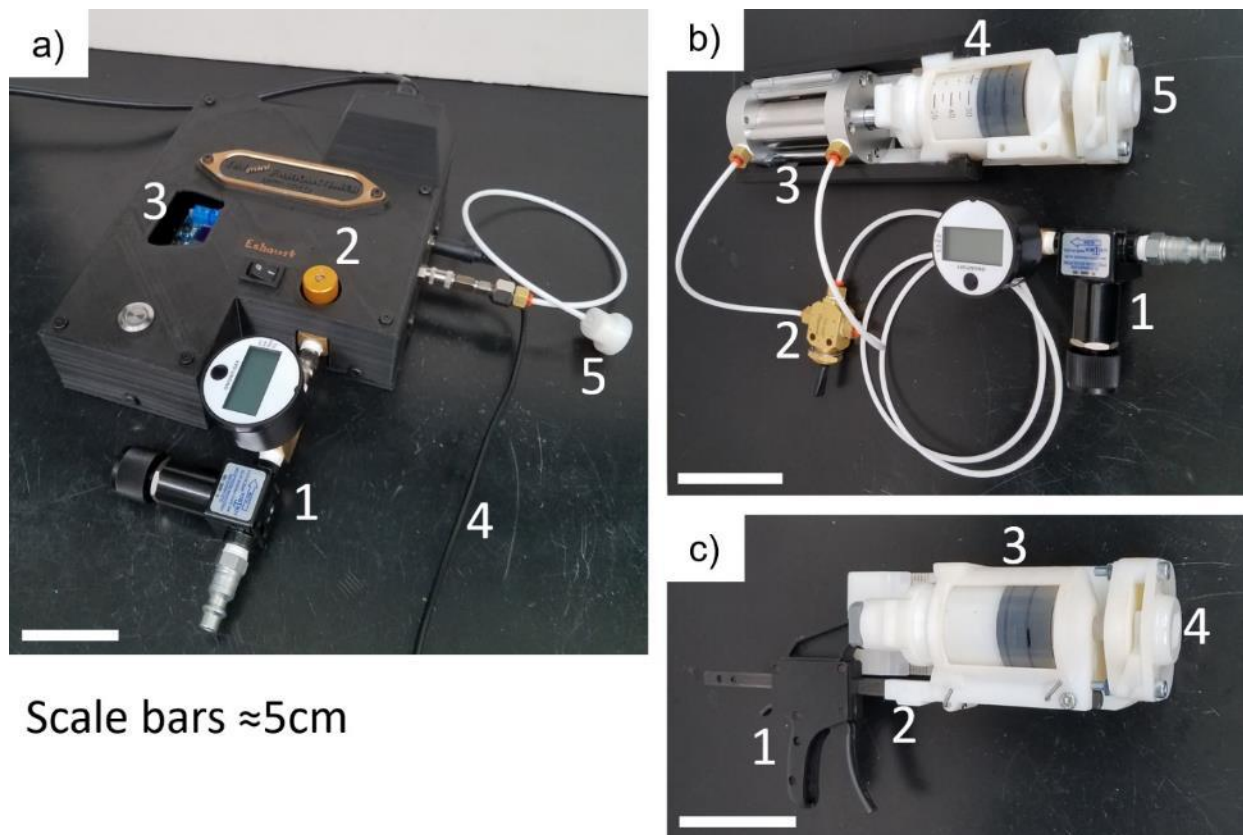


**Figure 4.1** Schematic representation of infant air-jet DPI platform in experimental setup. **(a)** Next Generation Impactor (NGI) experimental setup for aerosol size classification. **(b)** System attached to preterm nose-throat (NT) airway model for deposition and lung delivery efficiency testing



Scale bars  $\approx 5\text{cm}$

**Figure 4.2** Images of air sources with main components labeled: **(a)** Timer air source; 1. pressure regulator with digital gauge, 2. flow control valve, 3. timer control board, 4. cable to actuation foot pedal switch, 5. outlet connection to air-jet DPI. **(b)** Pneumatic air source; 1. pressure regulator with digital gauge, 2. 5/3 (EC) control valve, 3. pneumatic piston, 4. actuation air reservoir, 5. outlet connection to air-jet DPI. **(c)** Spring air source; 1. spring compression hand clamp, 2. spring compression distance guide, 3. actuation air reservoir, 4. outlet connection to air-jet DPI

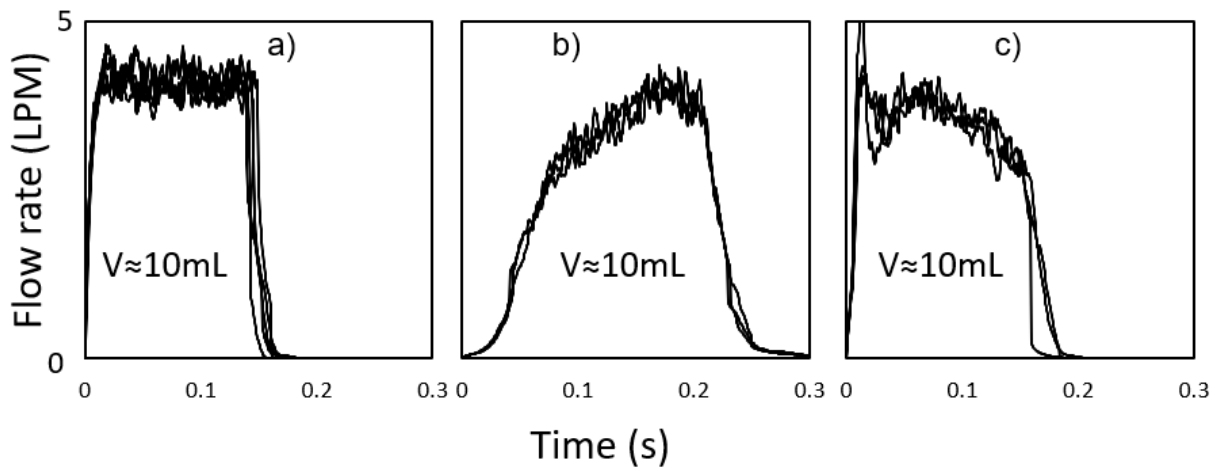


**Figure 4.3** Plots of measured flow rate (L/min) for each air source and the corresponding flow rate waveform during actuation at a  $Q_{90}$  of 4 L/min. **(a)** Timer air source **(b)** Pneumatic air source **(c)** Spring air source

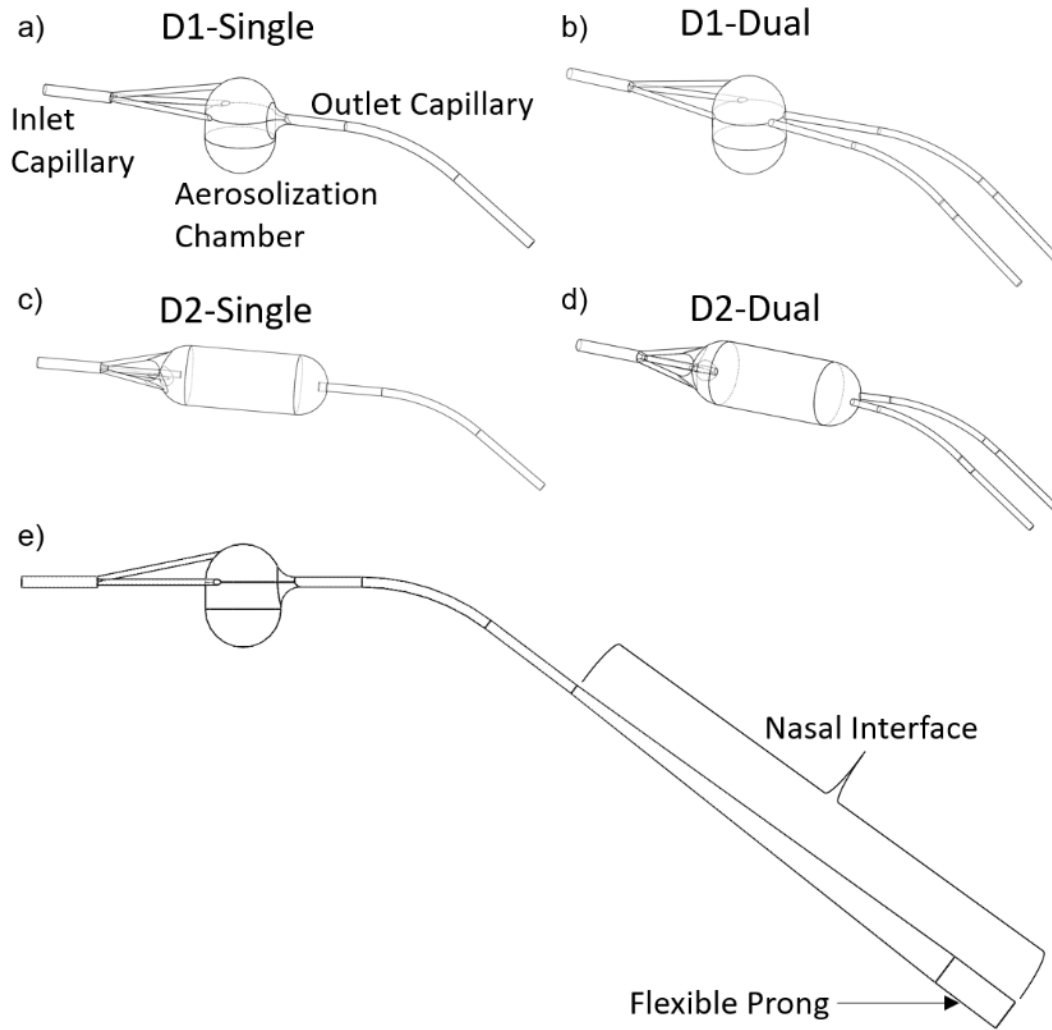


**Figure 4.4** Internal airflow geometry of each device from air source inlet (left side of each image) to the device outlet (right side of each image). **(a)-(d)** corresponds to D1-Single, D1-Dual, D2-Single, D2-Dual, respectively. **(e)** Side view of airflow geometry of D1-Single connected to the nasal interface

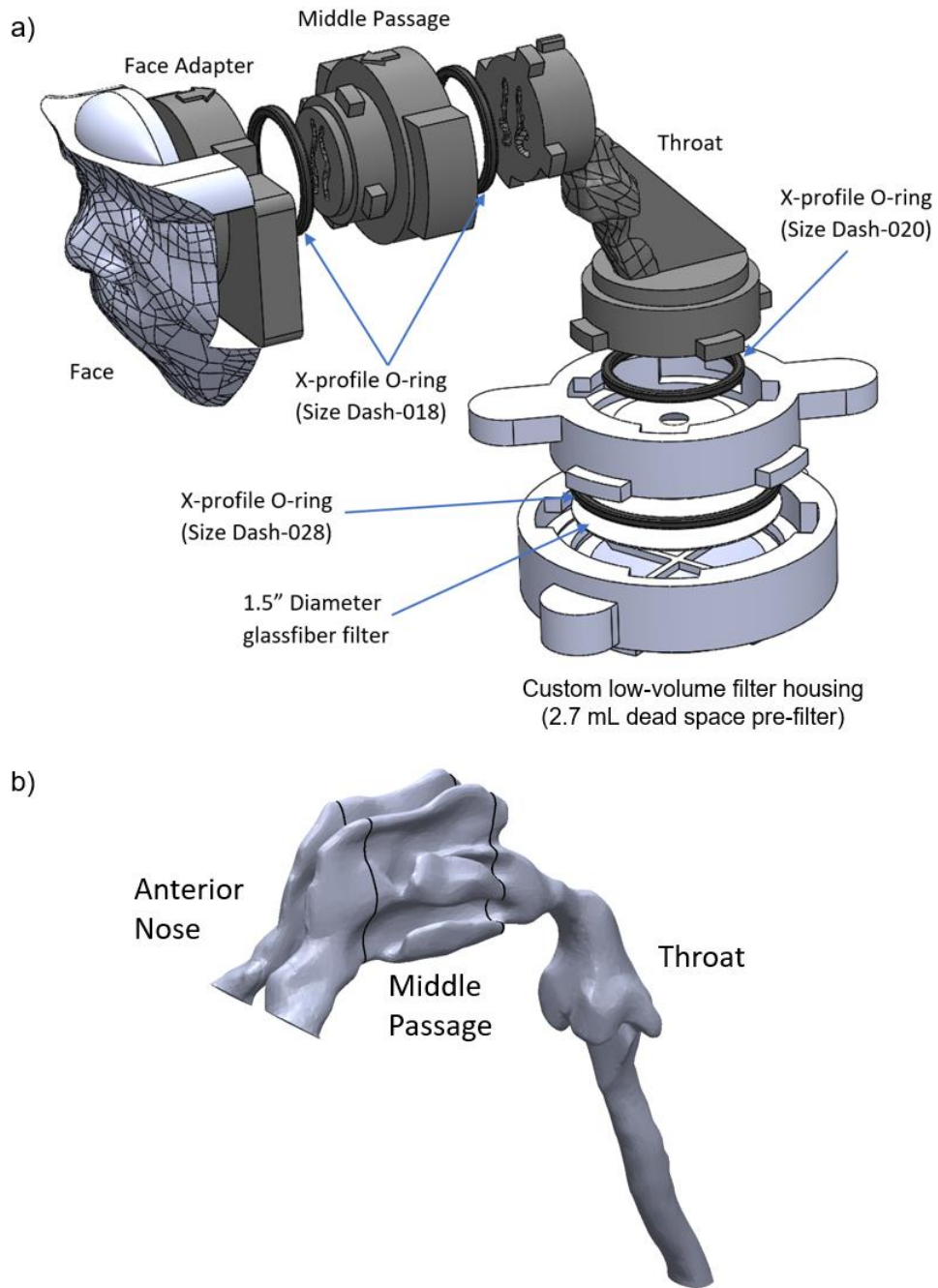


**Figure 4.5** Schematic overview of the preterm infant NT airway model and regional sections. **(a)** Assembly of infant NT model with connection to custom low-volume filter housing with parts labeled. **(b)** Internal airway geometry of the infant NT model with regions labeled

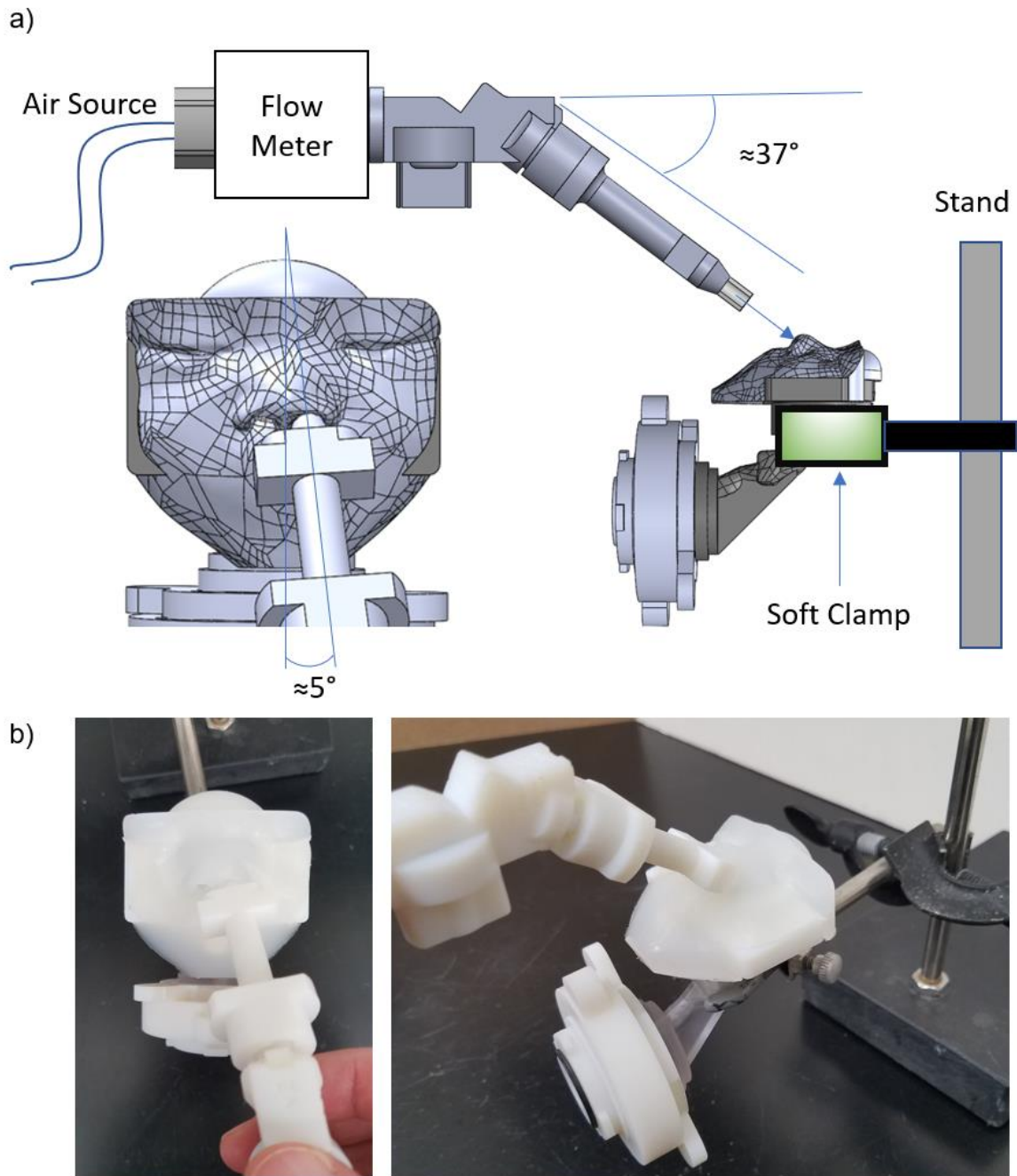


**Figure 4.6** Experimental setup for aerosol delivery efficiency testing through the infant NT model showing orientation and insertion of the platform. **(a)** Schematic representation of experimental setup and **(b)** pictures of experimental setup during NT model testing

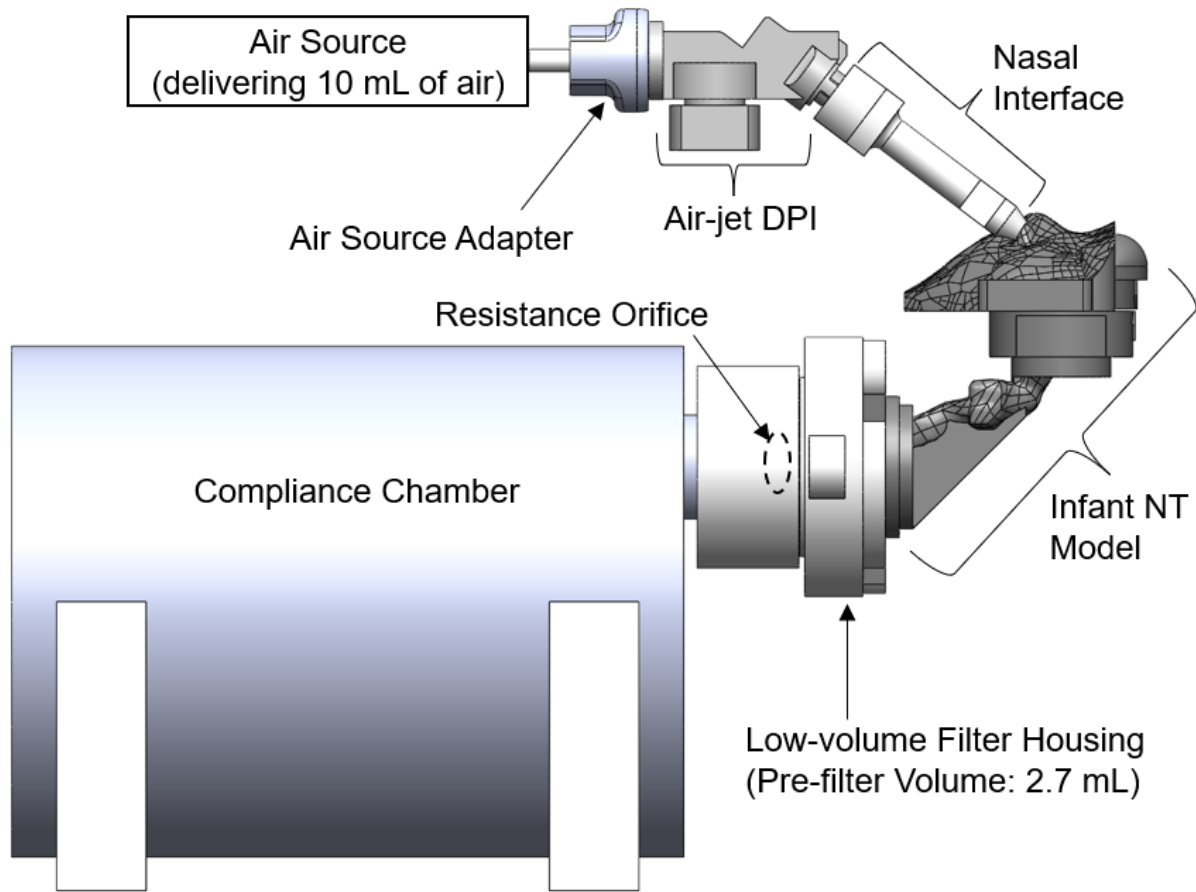


**Figure 4.7** Experimental setup for aerosol delivery efficiency testing through the infant NT model with the pulmonary mechanics (PM) outlet condition, with parts labeled



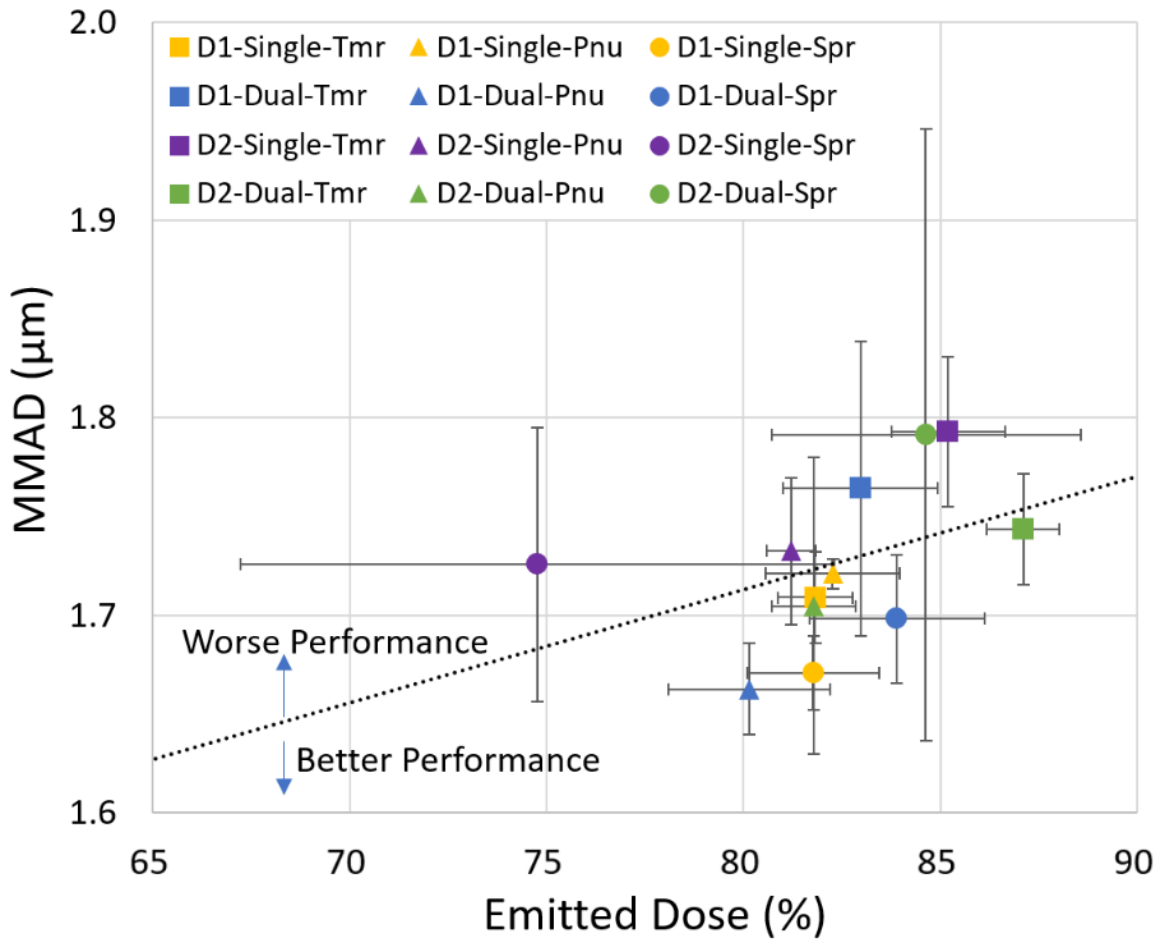


**Figure 4.8** Mean (SD) values of mass median aerodynamic diameter (MMAD) vs. emitted dose (ED) of the l-leucine EEG formulation based on device actuation into the NGI for each combination of air source and air-jet DPI [n=3]. Linear best-fit trend line establishes relative performance among the combinations

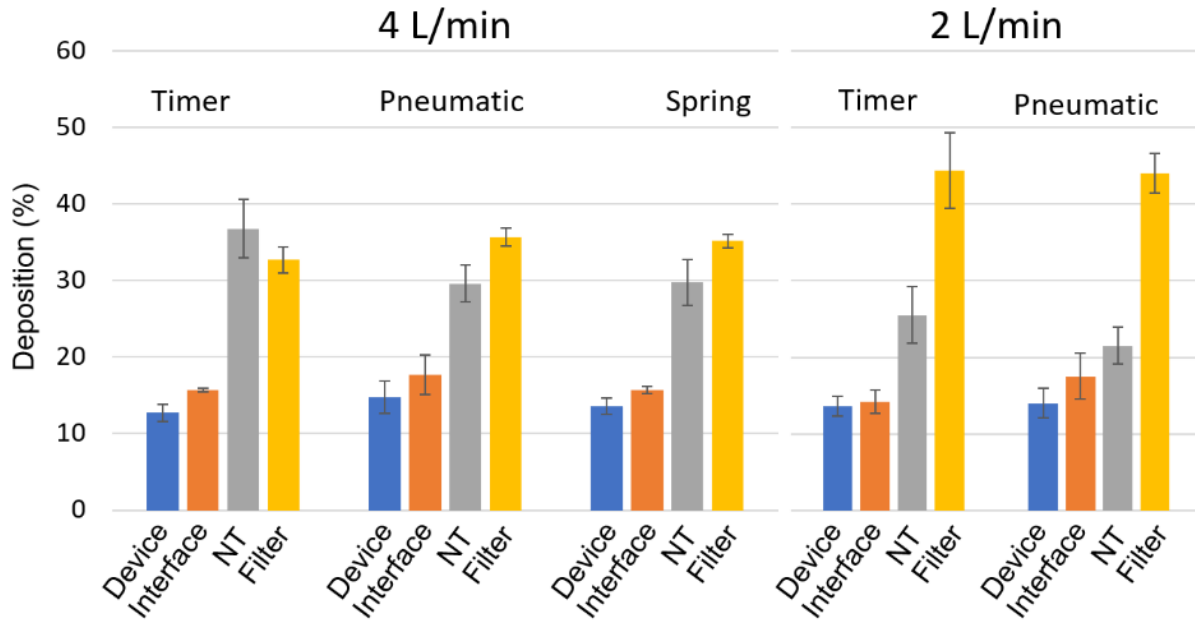


**Figure 4.9** Plot of experimentally determined mean (SD) drug deposition fractions (based on loaded dose) of the I-leucine EEG formulation grouped by air source and operated at a Q90 of either 4 L/min (left) or 2 L/min (right) [n=3]. Anterior nose, middle passage (MP), and throat deposition fractions sum to total NT deposition

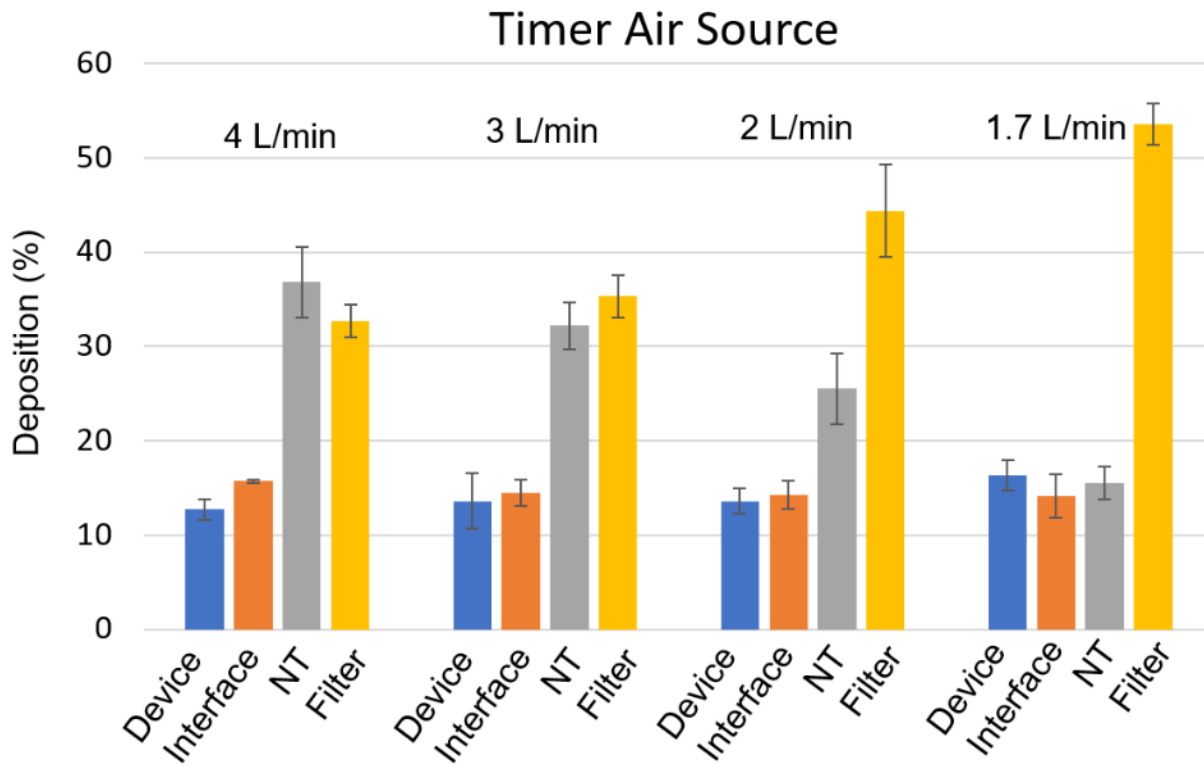


**Figure 4.10** Experimentally determined mean (SD) drug deposition fraction (based on loaded dose) of the I-leucine EEG formulation for the Timer air source operated at varied Q90 flow rates, with total NT deposition [n=3]

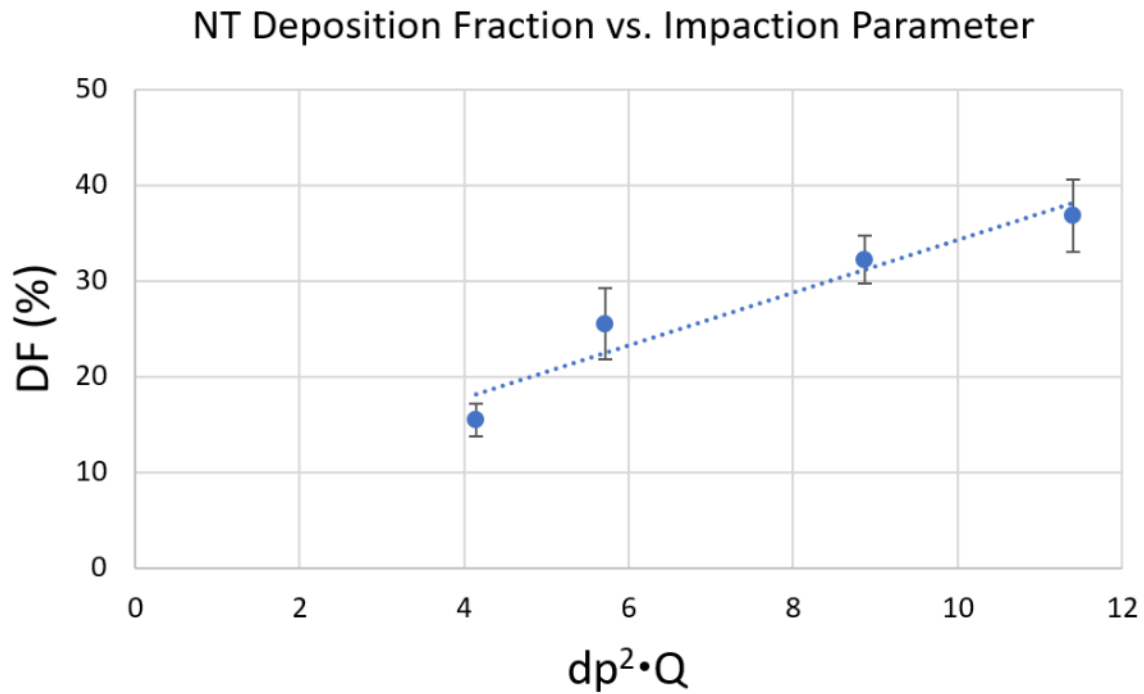


**Figure 4.11** Graph of experimentally determined mean (SD) drug deposition fraction (DF) of the l-leucine EEG formulation in the NT region compared to impaction parameter ( $d_p^2Q$ ) where  $d_p$  and  $Q$  are the MMAD at each Q90 and the Q90 for each tested value, respectively [n=3]

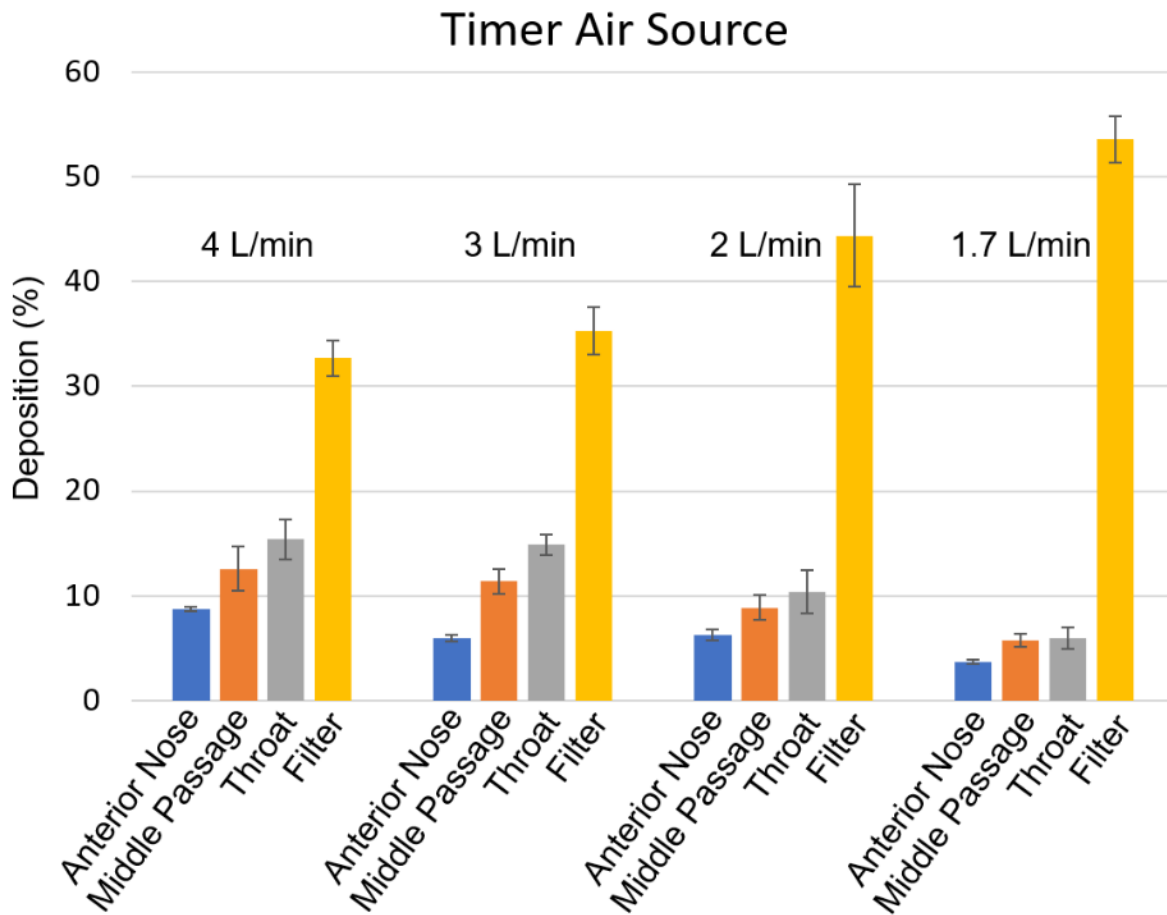


**Figure 4.12** Experimentally determined mean (SD) drug deposition fraction of the l-leucine EEG formulation (based on loaded dose) in each NT region and filter deposition for the Timer air source operated at varied Q90 flow rates [n=3]

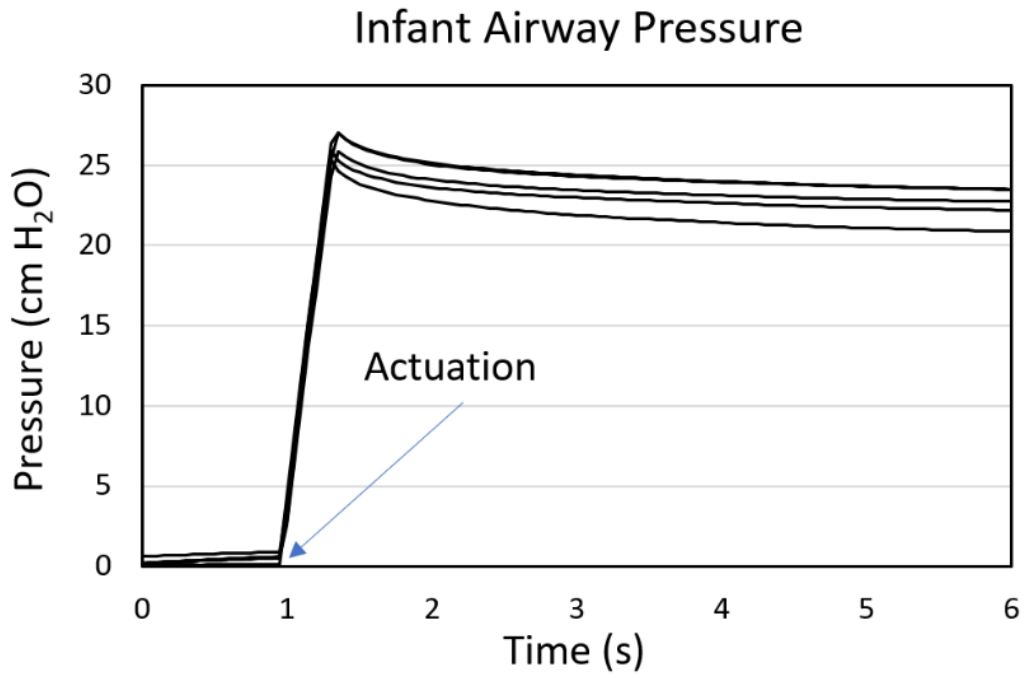


**Figure 4.13** Plot of the measured internal infant airway pressure taken during PM outlet condition experimental testing for each actuation, including a 5 sec breath hold [n=5]. Measurements were taken at a pressure port on the low-volume filter housing, between the filter and the resistance orifice

**Table 4.1** Air source flow rate properties compared at a target Q90 of 4 L/min and air actuation volume (AAV) of 10 mL, n=5 actuations

<b>Air Source</b>	<b>Q90 (L/min)</b>	<b>Peak (L/min)</b>	<b>Average (L/min)</b>
Timer	4.01 (0.05)	4.28 (0.13)	3.34 (0.25)
Pneumatic	4.04 (0.05)	4.53 (0.10)	1.95 (0.02)
Spring	3.97 (0.04)	4.62 (0.13)	2.79 (0.10)

---

Mean values with standard deviations (SD) shown in parenthesis.

---

**Table 4.2** Aerosolization performance of the l-leucine EEG formulation in the air-jet DPIs based on air source, in terms of air-jet DPI emitted dose (ED) and mass median aerodynamic diameter (MMAD) at 4 L/min (Q90)

<b>Description</b>	<b>Timer</b>	<b>Pneumatic</b>	<b>Spring</b>
<b>D1-Single</b>			
ED (%)	81.8 (1.0)	82.3 (1.7)	81.8 (1.7)
MMAD (µm) <sup>a</sup>	1.71 (0.02)	1.72 (0.01) <sup>b</sup>	1.67 (0.02)
MMAD/ED	0.021 (0.003)	0.021 (0.004)	0.020 (0.006)
<b>D1-Dual</b>			
ED (%)	83.0 (2.0)	80.1 (2.1)	83.9 (2.2)
MMAD (µm)	1.76 (0.07)	1.66 (0.02)	1.70 (0.03)
MMAD/ED	0.021 (0.007)	0.021 (0.003)	0.020 (0.007)
<b>D2-Single</b>			
ED (%)	85.2 (1.5)	81.2 (0.6)	74.8 (7.5)
MMAD (µm)	1.79 (0.04)	1.73 (0.04)	1.73 (0.07)
MMAD/ED	0.021 (0.001)	0.021 (0.003)	0.023 (0.023)
<b>D2-Dual</b>			
ED (%)	87.1 (0.9)	81.8 (1.1)	84.6 (3.9)
MMAD (µm)	1.74 (0.03)	1.70 (0.08)	1.79 (0.15)
MMAD/ED	0.020 (0.004)	0.021 (0.010)	0.021 (0.023)

Mean values with standard deviations (SD) shown in parenthesis; n=3.

<sup>a</sup> $p < 0.05$  significant effect of air source on performance (one-way ANOVA).

<sup>b</sup> $p < 0.05$  significant difference vs Spring air source (post-hoc Tukey).



**Table 4.3** Impaction Parameter details for D1-Single and Timer air source at selected Q90 flow rates using the l-leucine EEG formulation. MMAD from impaction testing and deposition fraction from preterm NT model testing

<b>Description</b>	<b>4 L/min</b>	<b>3 L/min</b>	<b>2 L/min</b>	<b>1.7 L/min</b>
MMAD ( $\mu\text{m}$ ) <sup>a</sup>	1.71 (0.02)	1.72 (0.04)	1.65 (0.05)	1.56 (0.04) <sup>b</sup>
NT Deposition Fraction (%) <sup>a</sup>	36.8 (3.8)	32.2 (2.5)	25.5 (3.7) <sup>b</sup>	15.5 (1.7) <sup>b</sup>
Impaction Parameter	11.4	8.9	5.7	4.1

Mean values with standard deviations (SD) shown in parenthesis, n=3.

Deposition Fraction is the sum of anterior nose, middle passage and throat depositions.

Impaction Parameter is mean MMAD value ( $\mu\text{m}$ ) squared times the measured Q90 flow rate (L/min).

<sup>a</sup> $p < 0.05$  significant effect of flow rate on performance (one-way ANOVA).

<sup>b</sup> $p < 0.05$  significant difference compared to 4 L/min (post-hoc Tukey).

**Table 4.4** Regional deposition fractions (based on loaded dose) of the trileucine EEG formulation for D1-Single with Timer air source at Q90 = 1.7 L/min for the filter only outlet condition and the pulmonary mechanics (PM) outlet condition

<b>Deposition Region</b>	<b>Filter Only</b>	<b>PM</b>
DPI Retention (%)	8.3 (0.4)	8.1 (0.9)
Nasal Interface (%)	5.2 (0.6)	5.0 (0.3)
Anterior Nose (%)	4.3 (1.3)	5.4 (0.2)
Middle Passage (%) <sup>a</sup>	10.2 (0.8)	12.1 (0.9)
Throat (%)	17.1 (0.1)	16.6 (1.1)
Total Extrathoracic (%) <sup>a</sup>	31.6 (0.7)	34.1 (1.1)
Tracheal Filter (%)	52.1 (0.7)	50.1 (1.5)

Mean values with standard deviations (SD) shown in parenthesis, n=3.

Total Extrathoracic is the sum of anterior nose, middle passage and throat deposition.

PM, pulmonary mechanics outlet condition.

<sup>a</sup>p<0.05 significant effect of PM on deposition (t test).

## Chapter 5 - *In Vitro* Analysis of Nasal Interface Options for High Efficiency Aerosol Administration to Preterm Infants

Task 1.3 – Published: *Journal of Aerosol Medicine and Pulmonary Drug Delivery*

### 5.1 Introduction

Nose-to-lung or transnasal aerosol administration to infants is a potentially effective route for the delivery of life-saving medications, such as lung surfactant, anti-inflammatories, antivirals, and antibiotics that can also potentially help to avoid the need for endotracheal intubation in some cases. [57-59, 61, 66, 117, 120, 171] Pharmaceutical aerosol may be administered to infants simultaneously with noninvasive ventilation (NIV) respiratory support, as with nasal continuous positive airway pressure (nCPAP), synchronized inspiratory positive airway pressure (SiPAP), and high-flow nasal cannula (HFNC) therapy. [58, 172] Alternatively, a rapid direct-to-infant technique may also be employed that administers the aerosol using specially designed nasal interfaces or masks either before, during or after NIV. [26, 134] With either the NIV-simultaneous or direct-to-infant administration strategy, delivery efficiencies of pharmaceutical aerosols to the lungs of infants are known to be low. For example, the recent *in vivo* study of Corcoran et al. [117] considered mesh nebulizer aerosol administration to 18 infants through nasal cannula interfaces while simultaneously delivering nasal cannula oxygen. At flow rates required to provide oxygen support (~2 L/min), mean lung delivery efficiency was only 0.46% of the nebulized dose with high variability. These findings are consistent with most other *in vivo* and realistic *in vitro* studies of lung delivery efficiency in infants with typical values in the range of 0%-10% of the loaded or nebulized dose. [12, 52, 58, 59, 61, 67, 114, 116] Low lung delivery efficiency makes the administration of high-dose medications difficult due to

potentially high therapeutic cost and long delivery times. Moreover, as with adults, [173] high delivery system and extrathoracic depositional losses are expected to lead to high variability in lung delivered doses, which has been observed with infant *in vivo* studies.[12, 117]

The vast majority of aerosol studies in infants have focused on the use of nebulized liquids, [53, 54, 57] with fewer studies considering dry powder formulations. [26, 51, 110, 134] Compared with nebulized liquids, dry powder formulations offer the potential for improved stability, [152] rapid administration, [23] low-cost delivery devices, [154] high-dose delivery [135] and potential high-efficiency lung delivery [25] with the possibility for inclusion of controlled condensational growth technology. [145, 166] One challenging aspect of dry powder administration to infants is forming a sufficiently small particle aerosol with very low volumes of air. Adult dry powder inhalers (DPIs) are typically used with air actuation volumes in the range of 3-4 L. [174, 175] Best-case new DPIs that can be used by some children require a minimum of 1.6 L for successful actuation. [153, 155] In contrast, infants inhale on the order of 10 mL per breath, [99] such that existing adult DPI products likely cannot be used or successfully modified. One approach that was previously developed to enable dry powder aerosol delivery to an infant was to form the aerosol with a high air volume and then contain the aerosol in a reservoir bag that was used for infant respiration over a series of breaths. However, due to high system and interface losses, lung delivery efficiency using this technique remained in the range of 1-10% of the loaded dose. [134, 176] Alternatively, the development of positive-pressure air-jet DPIs [23, 25, 91, 135] coupled with highly dispersive spray-dried powder formulations [76, 177, 178] can effectively form high quality small-particle dry powder

aerosols using actuation air volumes in the range of 4-10 mL and very short (~0.2 seconds) actuation times.

Howe et al. [26] recently developed the use of an air-jet DPI for high efficiency direct-to-infant aerosol administration using the transnasal route. In this previous study, different aerosolization chambers were explored for an air-jet DPI system with a single gradual expansion nasal interface and air actuation volumes of 10 and 30 mL. With direct-to-infant administration, the single gradual expansion and nasal prong interface was selected over a mask interface due to the fact that single prong reduced dead volume, which is highly important when very limited air volumes are available to transport the aerosol into the lungs. Masks are also expected to introduce flow pathway expansions and contractions, which are known to limit aerosol delivery efficiency. The best performing aerosolization chamber with a model spray-dried powder formulation was capable of producing >80% emitted dose (ED) from the device (based on loaded dose) and an aerosol with a mass median aerodynamic diameter (MMAD) of <1.8  $\mu\text{m}$  for both air actuation volumes.

A key feature of the positive pressure air-jet system is that the aerosol is administered together with a full inhalation breath. [26] For the single prong interface system, the prong forms an airtight seal with one of the infant's nostrils while the mouth and contralateral nostril are held closed. Device actuation requires ~0.2 seconds followed by a brief breath hold (~5 seconds) to enable lung deposition of the aerosol, after which the contralateral nostril is released to allow for exhalation. Full aerosol delivery is typically accomplished with 2-3 breaths for a 10 mg nominal powder loading. Using this approach with a realistic *in vitro* nasal model of a full-term neonate, Howe et al. [26] reported that >50% of the loaded drug mass was delivered

to a tracheal filter representing the lung delivered fraction. In a subsequent study, Howe et al. [179] evaluated the effects of the air source waveform and flow rate on aerosol administration in a much smaller preterm infant nasal model, again employing the single prong delivery approach. By reducing the infant air-jet DPI flow rate, lung delivery efficiency in the preterm model remained above 50% of the loaded dose.

The air-jet system consists of a positive-pressure air source, device inlet jet configuration, aerosolization chamber, outlet capillary configuration and nasal interface. [22, 23, 26] Previous studies have considered different aspects of the inlet and outlet configuration as well as the aerosolization chamber using both computational fluid dynamics (CFD) [21, 22, 160] and aerosol characterization experiments. [23, 25, 135] The gradual expansion patient interface was initially designed with CFD input to avoid internal flow separation; however, depositional losses are still relatively high and in the range of 10%-15% of the loaded dose. Furthermore, nasal depositional loss in both studies of Howe et al. [26, 179] were higher than expected. For example, in the full-term infant model using devices that emptied well, 20%-30% of the loaded dose was lost in the nose, which is higher than expected for an aerosol with an MMAD of  $\sim 1.8 \mu\text{m}$  (using measurement techniques that include all of the aerosol). This high loss may be due to the single prong configuration, but could also be due in part to the way the aerosol is introduced into the nasal cavity by the interface.

The patient interface of the infant air-jet DPI system can be subdivided into flow pathway and prong regions. **Figure 5.1** depicts the infant air-jet DPI and nasal interface components of the aerosol delivery system. The lower panel highlights the nasal interface region and illustrates the airflow passages of the separate flow pathway and nasal prong

components. The flow pathway transports the aerosol from the air-jet outlet capillary to the nasal prong, and the nasal prong is the component of the interface in closest contact with the nose. It is anticipated that further improvements in aerosol delivery efficiency with the infant air-jet system will require improvements to both the flow pathway and prong regions of the nasal interface.

Considering the interface flow pathway, previous studies with other air-jet DPIs operated at higher air actuation volumes have indicated that modifications to this region can significantly improve performance. For example, Bass and Longest [180] used CFD to optimize the flow pathway region of a pediatric air-jet DPI system actuated with 750 mL air volumes. A high-speed turbulent jet exiting the outlet capillary was identified to be a significant source of aerosol loss in both the interface and extrathoracic airways. [180] An optimized flow passage containing a three-dimensional (3D) rod array was shown to dissipate the turbulent jet and, compared with a base-case initial design, reduced device, interface, and mouth-throat deposition fractions by factors of eight-, three- and two-fold, respectively. [180] A subsequent *in vitro* experimental study by Farkas et al. [181] demonstrated that the 3D rod array of the optimized interface further reduced the aerosol MMAD by 20%, produced <2% mouth-throat depositional loss and transmitted >70% of the aerosol to the lung. These studies demonstrate collectively that an effective interface region for use with air-jet DPIs can (1) sufficiently dissipate the high-speed air jet without causing additional loss of the aerosol and (2) further reduce the aerosol size.

In addition to the flow pathway, the nasal prong region may also influence the depositional loss of aerosol in the nose. It is anticipated that the nasal prong can influence nasal

depositional loss due to (1) the potential for turbulent jet formation and (2) determining the initial direction of the aerosol stream. The previous study by Bass et al. [79] considered a gradually curved (streamlined) [132] nasal prong configuration for aerosol administration to an infant simultaneous with HFNC therapy. During the inhalation phase, depositional loss for a 1.4  $\mu\text{m}$  aerosol was extremely low in the interface and nasal region with over 90% lung transmission efficiency. The study of Bianco et al. [118] considered nebulized high volumes of surfactant aerosol droplets administered through two sizes of four different commercial cannulas. Both cannula size and shape significantly influenced estimated lung delivery; however, a majority of the nebulized suspension was found in a backup liquid-capture trap indicating likely droplet deposition followed by significant liquid resuspension or droplet running. In an adult transnasal aerosol delivery system employing dry powder aerosol, Farkas et al. [25] demonstrated improved lung aerosol delivery using streamlined cannulas that directed the aerosol slightly toward the septum with an elliptical outlet cross-section. In general, it is expected that a cannula with a larger diameter or outlet cross-section will result in less nasal depositional loss. [120, 135] Furthermore, with a sealed cannula system, the outer wedge on the prong and positive-pressure delivery may help to open the nasal airways and improve transmission. While previous studies point to the prong design as a potential way to improve lung transmission of an aerosol, further development is needed.

The objective of this study is to explore the impact of different nasal interface options on the lung transmission efficiency of pharmaceutical aerosols administered to preterm neonates with an air-jet DPI system. Based on previous studies, [26, 179] the air-jet DPIs selected are the D1 single and dual designs consisting of three air-jet inlets and a single or dual



outlet leading to the interface and operated with 10 mL air bursts from a timer-based air source. The evaluation criterion is the delivery efficiency of an initially loaded 10 mg spray-dried model excipient enhanced growth (EEG) formulation to the tracheal filter of a realistic preterm nose-throat (NT) model after three device actuations. While the primary goal for best-case performance is a higher lung delivery efficiency of the aerosol (estimated as tracheal filter deposition), other parameters such as ED and NT deposition are also considered.

The impact of different low-volume interface flow pathways is first explored, along with a comparison between single and dual nostril configurations. Implementing a base-case gradually expanding flow pathway, the effect of different flexible and rigid prong configurations is then evaluated. Best-case combinations of flow pathway and prong design are then considered across different flow rates and spray-dried powders. Finally, performance of the best-case interface configuration is compared with multiple *in vitro* models and spray-dried powder formulations. Based on experience with previous systems, [182] it is anticipated that modifications to the interface region of the infant air-jet DPI system can reduce interface and nasal cavity loss thereby increasing the dose delivered to the lungs.

## **5.2 Materials and Methods**

### *Powder Materials and Formulation*

Pearlitol® PF-Mannitol was donated from Roquette Pharma (Lestrem, France) and Poloxamer 188 (Leutrol F68) was donated by BASF Corporation (Florham Park, NJ). Trileucine was purchased from Bachem Americas, Inc. (Torrance, CA). Albuterol sulfate (AS), l-leucine and all other reagents were purchased from Sigma Chemical Co. (St. Louis, MO).

AS-EEG powders were obtained using a Büchi Nano B-90 HP Spray Dryer (Büchi Laboratory-Techniques, Flawil, Switzerland), and spray-dried based on the optimized method described by Son et al. [76] AS-EEG powder formulations consisted of 30:48:20:2% w/w ratio of AS, mannitol, l-leucine or trileucine, and Poloxamer 188, respectively. Throughout the spray drying process, the feed solution temperature was cooled between 2°C and 15°C while excess feed solution was recycled back into the stock. When evaluating each individual design parameter considered in this study (e.g., flow pathway design, prong design, or air flow rate), a single batch of spray-dried l-leucine formulation was implemented. However, different batches of the l-leucine formulation were required across the different system parameters with bridging experiments performed as needed. A single batch of the trileucine formulation was prepared and was sufficient for all testing utilizing this formulation. To determine the performance of multiple preterm NT models and the alternate dispersion enhancer, a final set of experiments was performed with both formulations (l-leucine and trileucine) delivered through two different NT models.

#### *Air-Jet DPI System and Designs*

The infant air-jet DPI system developed in our previous studies [26, 179] consists of three main components: the air source, the air-jet DPI, and the nasal interface. The main focus of this study is the nasal interface, which is described in detail in the Nasal Interface Designs subsection. The air source is responsible for providing the aerosolization energy to the air-jet DPI, delivering the aerosolized powder to the lungs and providing a full inhalation breath for the infant. The air-jet DPI consists of small diameter flow pathways that form the inlet(s) and

outlet(s) of the central aerosolization chamber (**Figure 5.2**). As the air source is actuated, high speed jets of air pass through the aerosolization chamber and over the preloaded powder bed facilitating powder aerosolization. The aerosol is then delivered to the infant through the nasal interface, which consists of the flow pathway and prong. The nasal interface forms an airtight seal with an infant's nostril and is inserted ~5 mm into the nose. **Figure 5.2** shows the schematic setup for the air-jet DPI platform from the air source, to the air-jet DPI and nasal interface, as well as connection with a preterm infant NT model and custom filter housing that collects the estimated lung delivery dose.

The air-jet DPI used in this study is the D1 design, which was developed in our previous study [179] with the internal flow pathways shown in the cut-out box in **Figure 5.2**. To compare a single prong and a dual prong nasal interface, two versions of the D1 design were used: the D1-Single and D1-Dual, with internal airway geometries shown in **Figure 5.3a** and **b**, respectively. In the previous study, both versions of the D1 air-jet DPI performed similarly; producing a mean ED of 81.8% and 83.0%, and a MMAD of 1.71 and 1.76  $\mu\text{m}$ , for the D1-Single and D1-Dual designs, respectively. [179] The D1-Single version has a single outlet capillary leading from the aerosolization chamber to the nasal interface with a single flow pathway, while the D1-Dual version has two outlet capillaries leading from the aerosolization chamber to the nasal interface allowing for nose-to-lung administration through both nostrils.

XAs determined in our previous air source study, [179] when using the air-jet DPI platform the tested air sources do not affect the overall performance and are interchangeable as long as the Q90 flow rate (value at which 90% of the measured flow rate values fall below) is consistent. In this study, the electromechanically controlled Timer air source was selected for high-resource

applications. Briefly, the custom Timer air source consists of a timer control board and miniature electronic solenoid valves that enable precise bursts of pressurized air for actuation of the system. These device actuations can be performed in series, without the need for a gas-source reloading action, by pressing a button or hands-free through a foot pedal. The optimal Q90 flow rate previously determined [179] and used for this study was 1.7 L/min. One additional experiment set re-examines the effect of adjusting the Q90 flow rate to higher values with the best-case nasal interface. Air flow-rate measurements and calibrations were performed using a neonatal mass flow meter (Sensirion SFM3400; Sensirion AG, Stafa, Switzerland), which was connected directly between the Timer air source and air-jet DPI as shown in **Figure 5.2**.

#### *Preterm Infant Nose-Throat (NT) Models*

Nasal interface comparisons utilized a preterm infant NT model previously developed by Howe et al. [179] for testing the aerosol delivery efficiency to the lungs and regional deposition in a representative 1600 g preterm infant. The preterm NT model consists of a soft nose interface beginning at the nostrils and includes the pharynx, larynx, and approximately three-fourths of the trachea, after which a custom low-volume filter housing was attached (**Figure 5.2**). The model was originally developed by geometrically scaling down (by a factor of 0.6) a model of a 6-month-old infant based on a relationship between infant length and airway dimensions. In this study, the preterm NT model previously developed will be referred to as the Scaled-6mo model.

In this study, a second preterm NT model was used to compare aerosol delivery performance in a different geometry. The nasal portion of this model was based on airway surfaces from a 1500 g, 28-week gestational age preterm airway model provided by Dr. Robert M. DiBlasi from Seattle Children's Hospital. [183] The DiBlasi nasal model did not include the laryngeal region, which is expected to impact lung delivery of aerosol, [184] with the model only including a short section of the nasopharynx. Therefore, a scaled version of the laryngeal region was extracted from the 6-month-old NT model, [79] and smoothly coupled to the preterm NT model to form a full model from nares through the middle passage, nasopharynx, larynx, and a section of the trachea. Smooth coupling with the preterm NT model in the nasopharynx required that the extracted 6-month-old model component be scaled by a factor of 0.6. This was the same scaling factor used in scaling the 6-month-old NT model to preterm conditions based on subject height (infant length), which gives further verification of this factor.

The hydraulic diameter through the glottis of the new preterm model was measured to be 3.2 mm, which falls within the expected range for preterm infants of 25-30 weeks gestational age. [168] The larynx was positioned in the new preterm NT model such that the glottis was a similar distance away from the main curvature in the nasopharynx as with the Scaled-6mo model. Vorperian et al. [185] reported that the most rapid change in vertical positioning of the larynx occurs from 0 to ~14 months of age. However, the difference in laryngeal descent between 0 and 6 months is only ~6 mm (measured from thyroid notch to the posterior nasal spine). Therefore, the positioning of the larynx incorporated into the new preterm NT model was deemed acceptable. In this study, the new model will be referred to as the Preterm NT model.

Side-by-side comparisons of the airways for the two NT models used in this study are provided in **Figure 5.4**. For each NT model, an isometric rendering of the airway (top panels) shows the regional definitions with lower panels providing top and side views of the airways with scale bars. **Figure 5.4a** illustrates the previously developed Scaled-6mo model, while **Figure 5.4b** illustrates the new Preterm NT model. All experimental sets utilized the Scaled-6mo model, with an experimental set also using the Preterm NT model in the final section for comparison.

The NT models were constructed with twist lock interfaces and O-ring seals, which provided air tight conditions. To provide a smooth and accurate internal airway surface, the middle passage and throat sections were built using stereolithography with Accura ClearVue resin (3D Systems On Demand Manufacturing, Rockhill, SC), printed at high resolution with a layer thickness of 0.05 mm. The low-volume filter housing was 3D printed using VeroWhitePlus resin. To facilitate nasal interface prong insertion and the formation of an airtight seal, the combined face and anterior nasal region was molded with a skin-like silicone elastomer (Dragon Skin™; Smooth-On, Macungie, PA). The anterior nose was glued to the rigid section of the model, allowing for a secure and air-tight connection without interfering with the smooth internal surfaces.

### *Nasal Interface Designs*

The nasal interface implemented in our previous preterm study [179] consisted of a straight gradually expanding diffuser with a circular cross-section over a length of 43 mm with a beginning diameter of 0.89 mm and a final internal diameter (ID) of 3 mm. The end of the

expansion transitioned to a flexible prong, made from tubing with an ID of 3 mm and outer diameter of 5 mm. **Figure 5.5a** depicts the internal air pathway of the gradual expansion nasal interface (also depicted in **Figure 5.1**). A gradual exterior taper was included around the flexible prong to help form an airtight seal with the infant's nostril. In this study, new nasal interface designs are compared with this previously established (base case) single prong gradual expansion design (GE-S). As described below, five different sets of experiments were performed evaluating various interface design parameters with the goal of improving aerosol delivery to the lungs compared with the base-case GE-S design.

Interface Set 1: The first set of experiments focuses on dissipating the aerosol jet exiting the air-jet DPI through different interface flow pathway designs, as illustrated in **Figure 5.5**. In three of the designs, a metal mesh (MM) was implemented in various configurations to dissipate the air-jet passing through the interface. The MM screen was formed by linear patterned circular holes  $\sim 0.15$  mm in diameter with  $\sim 28\%$  open area, and the screen was  $\sim 0.12$  mm thick. **Figure 5.5b-d** illustrates the flow pathways of the three metal mesh designs; MM-1, MM-2, and MM-3, respectively. The gray shaded area in each illustration indicates the location of the MM. MM-1 and MM-2 both have 0.89 mm diameter capillary outlets from the air-jet DPI forming the flow pathway inlet with the mesh located in the 3 mm diameter section of the interface.

The MM-3 design employs a 1.2 mm diameter flow pathway inlet, with the mesh located just before the expansion, and was assembled to connect directly to the aerosolization chamber, combining the air-jet DPI and nasal interface as a single part. **Figure 5.5e** shows the air pathway of the direct capillary (DC) design, which has three 0.6 mm diameter capillary tubes

leading directly from the aerosolization chamber to the flexible prong, and was also assembled as a single part. The final ID of each flow pathway was 3 mm and circular at the point of prong connection.

Interface Set 2: Using the dual outlet air-jet DPI design, dual prong nasal interface configurations were also tested, which were initially designed to match the gradual expansion interface. **Figure 5.6** shows a cross-sectional view of the dual prong interfaces, from interface inlet (left side of image), through the gradually expanding flow pathway, and to the prong (right side of image). Solid hatches represent rigid material while the dashed hatches represent the flexible prong tubing. Two interfaces were designed; one to exactly match the single gradual expansion flow pathway, but duplicated side by side to be inserted into both nostrils (GE-Dual, **Figure 5.6a**), and a second to have an extended flexible prong section of 3 cm to facilitate easier control of the insertion (GE-Dual-Flex, **Figure 5.6b**). Rigid wedge-shaped rings were attached to the 3 cm flexible prongs to guide the ~5 mm insertion into the nostrils and aid in forming an airtight seal.

Interface Set 3: The third set of experiments focused on the prong design to better direct the aerosol flow through the nasal cavity. Instead of the initial straight flexible prong, multiple curved prong designs were prototyped. Two sets of small curvature (~20°) prongs were printed as either rigid or flexible, and standard or larger diameter (3 or 4 mm ID, respectively). The curvature was chosen to maintain a streamlined redirection of the airflow away from the roof of the nasal cavity while maintaining a similar insertion distance. The rigid prongs were 3D printed along with the nasal interface flow pathway as a single piece, while the flexible prongs



were custom molded using a urethane rubber and glued to the nasal interface in a similar manner as the original straight prong tubing.

Interface Set 4: The main focus of the Set 4 experiments was to test the impact of the trileucine formulation in the GE-S and Rigid-3 (best case from Set 3) prong configurations. This step was performed to determine if improvements with the Rigid-3 prong observed with l-leucine were maintained with a different powder. These data can also be compared with the Set 3 results to determine the relative performance of trileucine powder compared with l-leucine across two prong configurations. As a secondary test in Set 4, an additional curved prong was then considered with an extended length to potentially better direct the aerosol to the pharynx. The resulting Large Curve prong maintained the same radius of curvature as Rigid-3, but extended the curvature arc to  $\sim 40^\circ$ . **Figure 5.7** illustrates the air pathways of the small (Rigid-3, **Figure 5.7a**) and large (Large Curve, **Figure 5.7b**) curvature prongs and interface. The standard 3 mm ID interfaces use the same flow pathway as the original gradual expansion interface, while the 4 mm ID interfaces increased the length of flow pathway by 10 mm while keeping the angle of expansion approximately the same.

Interface Set 5: The last nasal interface set of experiments combined the best performing flow pathways, including the MM designs (MM-1 and MM-3), with the best performing prong. **Figure 5.8** illustrates the airways of the two combined interfaces with the mesh shaded in gray. The two new interfaces are labeled MM-1-C (**Figure 5.8a**) and MM-3-C (**Figure 5.8b**) with the added “-C” to denote the curved prong (from Rigid-3) has replaced the initial MM prong. The new interfaces were compared with the original gradual expansion as

well as to the interface with the original gradual expansion flow pathway with the rigid small curved prong (Rigid-3).

During aerosol delivery through the NT model, single-prong nasal interfaces were inserted approximately 5 mm (~7 mm for the large curved prong) into one nostril and the other nostril was held closed. For dual prong configurations, each prong was inserted into a nostril and the wedge was gently held against the nares to form air-tight communication with the infant model. For aerosol delivery to an infant, exhalation with the single-prong configuration is enabled by release of the contralateral nostril, which is held closed along with the mouth during device actuation, while the delivery prong remains in place for multiple actuations. With dual prong delivery, an exhalation port will be added to the flow pathways, which in preliminary experiments was found to not influence aerosol delivery efficiency.

#### *Evaluation of Lung Delivery in the Preterm NT Model*

Consistent with our previous studies, experiments used 10 mg of AS-EEG powder formulation (manually weighed) and a preterm NT model. The powder mass was weighed and loaded into the bottom section of the air-jet DPI, which was then connected and sealed to the top section with a twisting motion. After connecting to the selected nasal interface, the prong portion was inserted ~5 mm into the left nostril of each preterm NT *in vitro* model, whereas the other nostril was held closed during each actuation. A small amount of lubrication was applied to the exterior of the prong to improve insertion and ensure an airtight seal. The aerosol delivery system was operated with an air actuation volume of 10 mL followed by a 5-second pause before releasing the right nostril to simulate a brief breath hold period. This process of

system actuation and simulated breath hold was repeated three times to empty the loaded powder. All NT model segments were internally coated with MOLYKOTE® 316 silicone spray (Dow Corning, Midland, MI) to minimize particle bounce similar to airway surface liquid. At the end of each NT model, a custom low-volume filter housing and high-efficiency fiber filter collected powder passing through the extrathoracic regions and represented the amount of drug delivered to the lung. The NT models were mounted as pictured in **Figure 5.9** with the air-jet DPI held horizontally as represented in **Figure 5.2** (Scaled-6mo NT model pictured).

Three runs for each data set were performed at the optimal Q90 of 1.7 L/min for all experiments except for a flow rate sensitivity experiment which compared the performance at higher flow rates (2.5 and 4 L/min). Calculations for ED and regional deposition, including the nasal interface and within the NT model and tracheal filter (lung dose) were expressed as a percentage of the loaded dose of AS. Drug masses were determined using high-performance liquid chromatography (HPLC) analysis of AS, as described in the next section.

#### *Drug Mass Characterization Methods*

After actuation and aerosolization, drug masses retained or collected in the air-jet DPI, nasal interface, NT model regions, and filter were recovered by dissolving the deposited powder in an appropriate volume of deionized water followed by HPLC analysis with fluorescence detection. The loaded drug mass was determined through content uniformity analysis of the AS-EEG formulation, where known masses of AS-EEG were dissolved in water and the AS content ( $\mu\text{g}/\text{mg}$  of formulation) was determined. AS quantification was performed for each deposition site and for the total drug mass used to calculate the drug recovery. Drug

recovery percentage was expressed as the amount of AS recovered on all deposition sites divided by the calculated loaded AS dose for each experiment, with nearly all values over 95%, representing valid collection and quantification. The metric of Total ED was used to represent the percentage of loaded dose that enters the infant NT model and was calculated as 100% minus the sum of the DPI retention and nasal interface deposition percentages. The metric of Total NT deposition was used to represent the sum of the regional deposition percentages (expressed as a percentage of the loaded dose) in each infant NT model.

### *Statistical Analyses*

Statistical analyses for comparing aerosol delivery performance and estimated lung delivery efficiencies were performed using JMP Pro 16 (SAS Institute, Inc., Cary, NC). Comparison of nasal interface designs utilized one-way analysis of variance ANOVA followed by Student's *t*-test when compared with the initial base-case design (GE-S interface). Comparison of NT models also utilized Student's *t*-test. Statistical tests used a significance limit of  $p = 0.05$ .

## **5.3 Results**

### *Comparison of Nasal Interface Flow Pathways (Interface Set 1)*

Comparisons of the flow pathway designs (**Figure 5.5**) implement the D1-Single air-jet DPI and 5 mm flexible prong. A single batch of l-leucine AS-EEG formulation (Batch 1) was employed. To compare device retention and nasal interface deposition across the different designs, the Total ED was used, which accounted for the total dose (as a percentage of the loaded dose) exiting the nasal prongs and entering the infant model. **Table 5.1** presents the

aerosol delivery performance for each flow pathway design. Using the l-leucine EEG formulation, the original GE-S interface combined with the D1-Single air-jet DPI resulted in a Total ED of 67.0%, with a lung delivery efficiency of 44.3% and a total NT deposition of 22.3%. Two designs, MM-2 and DC did not improve performance when compared with the GE-S interface, with no statistically significant difference for all regions in the DC design. The MM-2 design produced a statistically significant lower throat and total NT deposition; however, when combined with a higher nasal interface deposition, the mean filter deposition was slightly lower, with no statistically significant difference from the GE-S interface.

In comparison, the MM-1 design significantly lowered the Total NT deposition to 9.8%, and despite a lower Total ED of 58.4%, produced a statistically significant improvement in lung delivery efficiency with a filter deposition of 48.2%. The MM-3 design produced a mean filter deposition of 46.5%; however, the only statistically significant difference was a slightly lower throat deposition compared with the GE-S interface. Designs MM-1 and MM-3 were chosen for future testing incorporating prong design changes based on reduced Total NT loss or increased Tracheal Filter delivery efficiency.

#### *Dual Prong Nasal Interface (Interface Set 2)*

To compare the aerosol delivery performance of a dual interface to the single prong approach, two designs were created with the same flow pathway as the single, one with identical prongs, and one with extended prongs to facilitate easier insertion and sealing with the nostrils (**Figure 5.6**). The two flow pathways connected to the D1-Dual air-jet DPI and were labeled GE-Dual and GE-Dual-Flex (for the extended more flexible prongs). Using the same

batch of l-leucine EEG formulation (Batch 1), **Table 5.2** provides the aerosol delivery performance for the two dual nasal interfaces compared with the single interface (GE-S). Both GE-Dual designs had statistically significant increases in Total NT deposition resulting in lower filter deposition, when compared with the GE-S design. While the GE-Dual design provided a similar Total ED value (66.6%) compared with the GE-S (67.0%), the GE-Dual-Flex had a lower Total ED of 59.1%, likely due to the extended prongs. With filter depositions approximately 10%-15% lower and Total NT deposition about 8% higher than with the single prong case, the dual interfaces were not considered for further testing.

#### *Comparison of Nasal Interface Prongs (Interface Sets 3 and 4)*

Interface set 3 experiments investigated prong adjustments to help direct and streamline the aerosol entering the nasal cavity. Four curved prong designs: Soft-3, Soft-4, Rigid-3, and Rigid-4, were developed to streamline the prong of the nasal interface using the original GE-S flow pathway. Each prong had the same curvature, and was constructed with either soft (flexible) or rigid material, and ended with an outlet ID of 3 or 4 mm. The naming convention was a combination of the material type (Soft or Rigid) and prong outlet ID. Using a second batch of l-leucine EEG formulation (Batch 2), the GE-S and new curved prong designs were connected to the D1-Single air-jet DPI and tested for aerosol delivery performance. **Table 5.3** summarized the performance of each design with statistical comparisons made to the original GE-S design using the Batch 2 formulation. In terms of Total ED, all interfaces performed similarly with no statistical difference between the curved designs and the original GE-S design, which was around 60%.

The Soft-3 interface produced a significant increase in Total NT deposition whereas the other curved designs produced similar Total NT deposition when compared with the noncurved prong. Each of the curved prong designs increased the mean lung delivery efficiency; however, only the rigid prongs produced a statistically significant improvement, increasing the filter deposition from 40.9% with the GE-S, to about 49% with Rigid-3. While improvements were similar between the two rigid designs, the larger diameter (Rigid-4) produced larger variability between the trials and was therefore not chosen for further testing.

Interface Set 4 utilized an additional curved prong interface, based on the Rigid-3 design, with an extended curvature through 40°, as illustrated in **Figure 5.7**. For this set of experiments, the performance of a trileucine EEG formulation was investigated for aerosol delivery through the original GE-S interface, Rigid-3, and the extended curvature version of Rigid-3 (labeled “Large Curve”). **Table 5.4** compared the aerosol delivery performance of each interface connected to the D1-Single air-jet DPI, using the trileucine EEG formulation, with statistical comparisons to the GE-S design. The Total ED and Total NT values for each interface were similar, around 85%-87% and 29%-31% of the loaded dose, respectively. The Rigid-3 interface was found to have a statistically significant higher mean filter deposition of 56.8% compared with the GE-S interface of 52.1%. The Large Curve design did not improve the lung delivery efficiency. The Rigid-3 prong design (with small curvature) was chosen for continued testing.

#### *Combining Best Flow Pathways and Prongs (Interface Set 5)*

The best-performing flow pathways (determined from Interface Set 1) and prong (resulting from Interface Sets 3 and 4) were then combined to create two new interfaces; labeled MM-1-C and MM-3-C, with the small curved prong (Rigid-3) attached to the MM-1 and MM-3 flow pathways, respectively. Using a third batch of the l-leucine EEG formulation (Batch 3), **Table 5.5** presents the aerosol delivery performance of the combined nasal interfaces, as well as the Rigid-3 design, with statistical comparisons to the original GE-S design. With Batch 3 of spray-dried l-leucine formulation, the original GE-S interface connected to the D1-Single air-jet DPI produced a mean filter deposition and Total NT loss of 43.3% and 29.5% of the loaded dose, respectively, whereas the mean Total ED was 71.9%. For the MM-3-C design, performance was similar with a nearly identical mean filter deposition of 43.1%. The MM-1-C design led to statistically significant improvements in Total NT (lowered to a mean value of 11.9%) and tracheal filter (increased to a mean value of 48.7%) deposition; however, the mean Total ED dropped to 60.1% of the loaded dose. The Rigid-3 design also led to statistically significant improvements in Total NT (lowered to a mean value of 21.7%) and tracheal filter (increased to a mean value of 50.8%) deposition, while the mean Total ED remained similar. Overall, the MM-1-C and Rigid-3 designs both show improvements to the estimated lung delivery efficiency when compared with the original GE-S design; however, the Rigid-3 design was chosen for the remaining testing.

#### *Flow Rate Sensitivity*

Using the Rigid-3 nasal interface as the best-performing design (in terms of tracheal filter deposition) in this study, a flow rate sensitivity study was performed. Two higher Q90 flow



rate values of 2.5 and 4 L/min were chosen to test aerosol delivery performance using the D1-Single air-jet DPI, Rigid-3 nasal interface and Batch 3 of the l-leucine EEG formulation. When the flow rate was increased from 1.7 to 2.5 L/min and 4 L/min, there were significant changes in Total NT and Filter depositions (**Figure 5.10**). With increasing flow rates, Total NT deposition increases from 21.7% at 1.7 L/min to 30.8% and 37.1% at 2.5 and 4 L/min, respectively, whereas the Filter deposition decreased from 50.8% to 36.4% and 32.3%, respectively. With increasing flow rate, there were no statistically significant differences between depositions in the nasal interface region. Hence, the lower flow rate remains ideal for the current platform.

#### *Comparison of Infant NT Models and Two Powder Formulation*

In a final set of experiments, the aerosol delivery performance of the best-case (D1-Single with Rigid-3, at 1.7 L/min) setup was considered in two different NT models (the original Scaled-6mo model and the new Preterm NT model). Two powder formulations were also compared with an l-leucine EEG formulation (Batch 4) and the trileucine EEG formulation.

**Figure 5.11** illustrates the regional deposition results of each combination of powder formulation and infant model. The trileucine formulation produced ~55% filter deposition and 30% Total NT loss in both infant models, while the l-leucine formulation produced ~48% filter deposition and less than 20% Total NT loss in both infant models. When comparing each formulation in both infant models separately, there was no statistically significant difference in aerosol delivery to the lung or Total NT deposition between the two models. It is noted that comparison of the two models only considers the Total NT deposition and not the regional

segments due to the different construction of the Preterm NT model compared with the Scaled-6mo model.

#### 5.4 Discussion

A primary outcome of this study is the increased lung delivery efficiency that can be achieved with an infant air-jet DPI through modifications of the nasal interface flow pathway and prong configuration. This increase in lung delivery efficiency arises not only from improved prong ED, but also from reduced NT depositional loss. In our previous preterm study, [179] the initially developed best-performing nasal interface (GE-S) consisted of a gradually expanding flow pathway that connected to a straight flexible prong, as shown in **Figure 5.1**. In the current study, two main components provided improved performance in terms of estimated lung delivery efficiency. First, adding a MM to aid in the dissipation of the aerosol jet exiting air-jet DPI in the MM-1 configuration (**Figure 5.5b**) was found to be effective. In the initial set of experiments, the MM-1 design was able to deliver about 4% more powder to the tracheal filter, while lowering the NT depositional loss by a factor of over two-fold, from about 22% to 10%, compared with the gradual expansion interface. The second component was replacing the straight flexible prong with a curved rigid design.

The data set reported in **Table 5.3** shows a tracheal filter deposition increase of almost 9% (absolute difference) when replacing the prong with the Rigid-3 design. Interestingly, combining the MM-1 flow pathway with the rigid curved prong did not improve the filter deposition beyond that of replacing the prong alone. The final interface comparison data set reported in **Table 5.5** shows the MM-1-C configuration and Rigid-3 compared with the original

GE-S design, with mean filter deposition improvements of about 5% and 7% (absolute difference), respectively. However, it should also be noted that the MM-1-C Total NT depositional loss was 10% lower than the Rigid-3 design, indicating the potential of the MM designs if ED can be increased, perhaps through more open area meshes. Future studies will investigate additional mesh configurations and sizes.

A second primary finding of this study was similar lung delivery efficiencies between two very different NT models. In two separate experimental sets, using two different EEG powder formulations, there was no statistically significant difference in aerosol delivery performance between the two infant models used in this study. The two models are considered distinct and represent a range of expected preterm geometries. The Scaled-6mo model is based on a 6-month-old infant's computed tomography (CT) scan with developed nasal turbinates and complex nasal cavity geometry, while the nasal component of the Preterm NT model is based on a CT scan of a preterm infant with underdeveloped turbinates and other nasal structures. The ability to deliver consistent aerosol therapeutic doses to the lungs may be an advantage over other infant aerosol delivery approaches, like nebulized administration, where variability in lung aerosol delivery is expected to be very high. [12, 117] Comparing two different formulations has shown similarity in lung delivery efficiency, despite trade-offs between ED and NT deposition, which may guide device-drug combination selections in future studies.

As with our previous study in preterm NT models, [179] the performance of the air-jet platform was found to be highly influenced by the Q90 flow rate with a preference for delivering the aerosol at 2 L/min or below. Previously, lowering the flow rate from 4 to 3 L/min produced little difference in lung delivery efficiency, while lowering to 2 L/min and then 1.7

L/min produced significant improvements. Despite this trend, further lowering the flow rate to 1.5 L/min did not sufficiently aerosolize the powder and device retention had a negative impact on lung delivery. In this study, increasing the flow rate from 1.7 to 2.5 L/min reduced performance in terms of filter deposition by about 14%, and by an additional 4% at 4 L/min. These results indicate a narrow window of tunability with the lowest flow rate maintaining sufficient energy to aerosolize the powder producing the best performance. While interesting, these findings may be limited to the specific air-jet DPI and formulation combination considered and will need to be reconsidered for different device and formulation combinations.

The dual prong delivery configurations tested in this study were not found to be beneficial. The design of the GE-Dual interface was a side-by-side version identical to the original GE-S interface. While the two interfaces performed similarly in terms of device retention and interface deposition, they increased deposition in the nose and throat region compared with the single passage designs. Possible reasons for this include the additional surface area to which the aerosol is exposed to, as well as both prongs being inserted into the nostril parallel to each other as opposed to the slight inward lateral angle using in the single prong configuration. A second dual prong interface was designed with an extended flexible prong segment, which allowed for an angled insertion. While the second design improved aerosol delivery through the anterior nose region, there was additional depositional losses in the nasal interface and continued under performance compared with the single prong design. Although the dual designs tested in this study did not improve aerosol delivery performance, other designs such as shorter angled and curved prongs or bifurcating designs may be worth investigating.

During the initial curved prong testing, all prongs were found to improve the estimated lung delivery efficiency when compared with the GE-S straight flexible prong. However, the rigid curved prongs improved the tracheal filter deposition approximately 8%-9% while the improvement from the soft curved prongs was only approximately 2%-4%. A possible reason the rigid prongs performed better could be due to increased deformation of the airway geometry with the prong slightly opening the soft nasal passage model. When comparing the two rigid prongs, of 3 or 4 mm ID, the lung delivery efficiency was similar; however, the 4 mm prong produced a larger standard deviation and was not chosen for additional experimentation. It is possible the performance is more sensitive to the fit and positioning of the larger prong in the NT model. CFD simulations may be useful to further explore these issues.

A potential limitation of this study is the sequential nature of the design analysis. The effects of different flow pathway geometries and dual pathway configurations were first assessed with fixed nasal prongs. Different prong designs were then assessed for a fixed flow pathway. Best-performing flow pathways and prongs were then combined as potential lead interface designs and tested. This sequential approach provides considerable experimental savings compared with assessing a full design matrix that pairs every flow pathway option with every nasal prong design considered. While efficient, a potential downside of this sequential approach is that some untested combinations of flow pathways and prongs may perform better than the tested combinations. Nevertheless, the selected sequential study design achieved the objective of finding a flow pathway and prong combination to produce a nasal interface that improved lung delivery efficiency of the aerosol by a statistically significant amount.

As with the sequential design comparisons, a second powder formulation (containing trileucine) was also considered on a limited basis. Performance of the air-jet system with the trileucine formulation was first tested in Set 4 to ensure improved performance of the Rigid-3 prong design. Based on this comparison it was determined that the Rigid-3 prong significantly improves performance compared with the GE-S design with the trileucine formulation (**Table 5.4**) just as with the l-leucine formulation (**Table 5.3**). This finding provided confidence that trends observed with the l-leucine formulation when comparing different designs should hold with other highly dispersible spray-dried formulations. With **Figure 5.11**, no statistical difference was observed in tracheal filter delivery efficiency between the two infant geometries for both the trileucine and l-leucine formulations. In this case, consideration of two powder formulations provides support to the claim that lung delivery efficiency of EEG formulations with infant air-jet DPIs are largely independent of airway geometry. Still, it cannot be ruled out that some different EEG powders may produce differences in lung delivery efficiency across different airway models.

Limitations of this study include the relatively small number of nasal interface configurations, absence of downstream lung resistance and compliance, use of static *in vitro* airway models, and implementation of a model spray-dried powder formulation. While a wide range of design features and combinations were tested, a full matrix for the selected features would not have been feasible; however, two designs (Rigid-3 and MM-1-C) containing features of both flow path and prong modifications have shown similar improvements to delivery efficiency and will be used for future studies. In a previous study we demonstrated that including downstream resistance and compliance consistent with infants in respiratory distress

did not impact delivery of aerosols with the infant air-jet system. [179] Hence, the downstream resistance and compliance chamber was not included in this study.

While two anatomically realistic NT models were implemented, *in vivo* nasal and pharyngeal structures can be highly dynamic with actions such as breathing and swallowing. The timing of the actuation is to be performed by the respiratory technician; however, it is possible for an out-of-sync actuation and while this has not been studied, aerosol delivery was not previously affected by the addition of downstream resistance and compliance. Moreover, *in vivo* nasal passages can be mucus filled, which would need to be suctioned before nose-to-lung aerosol administration, as regularly performed before infant nasal continuous positive airway pressure (nCPAP) ventilation. Finally, the AS-EEG formulation was considered as a model spray-dried powder that can be accurately quantified with low cost and low risk. Envisioned applications include administration of surfactants, antibiotics and antivirals as dry powder aerosols. These formulations will require additional device optimization and well as additional design modifications to efficiency aerosolize higher powder masses. Another consideration regarding the EEG formulation is the lack of a realistically humidified airway in the NT model, however, a previous study [182] has shown nasal depositional losses remain low and were not statistically significantly different when comparing room (~33%) and airway (~99%) relative humidity through a pediatric NT model.

## 5.5 Conclusions

In conclusion, this study has improved aerosol delivery efficiency of the infant air-jet DPI platform through modifications of the nasal interface. The rigid curved prong design (Rigid-3)

increased the estimated lung delivery efficiency of the platform nearly 5% and 10% for the trileucine and l-leucine EEG formulations, respectively. Modification to the flow pathway, including a MM to dissipate the aerosol jet, also produced improved tracheal filter deposition by about 5% while significantly lowering the Total NT loss by over half with the MM-1-C design. With the addition of the Preterm NT model testing, it was found that for both EEG formulations, there was no statistically significant difference between aerosol delivery performance (Total ED, Total NT, and Tracheal Filter percentages) in the different infant airway geometries. Continued development of the platform, with optimizations to the air-jet DPI and nasal interface are expected to facilitate a rapid, highly efficient, and noninvasive form of aerosol delivery to neonates.



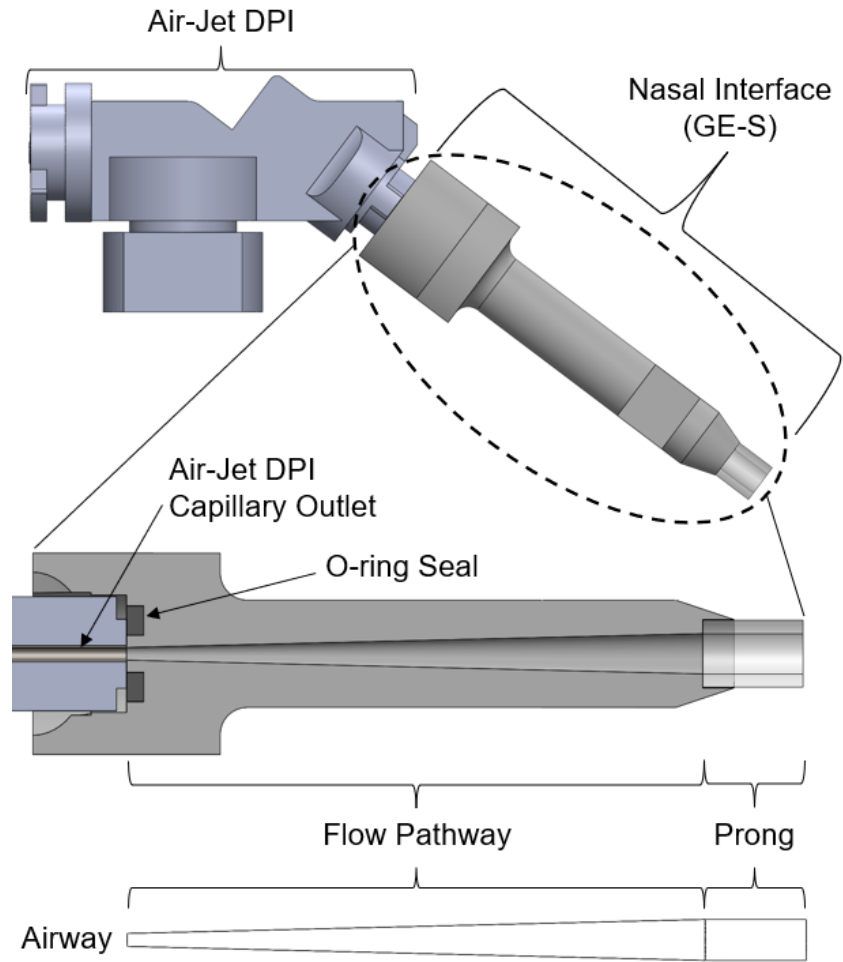


**Figure 5.1** Overview of air-jet DPI and nasal interface connection with expanded internal view, illustrating attachment to the outlet of the air-jet DPI. Expanded view depicts interface flow pathway and prong regions as a midplane sectioned view and as a flow passage outline

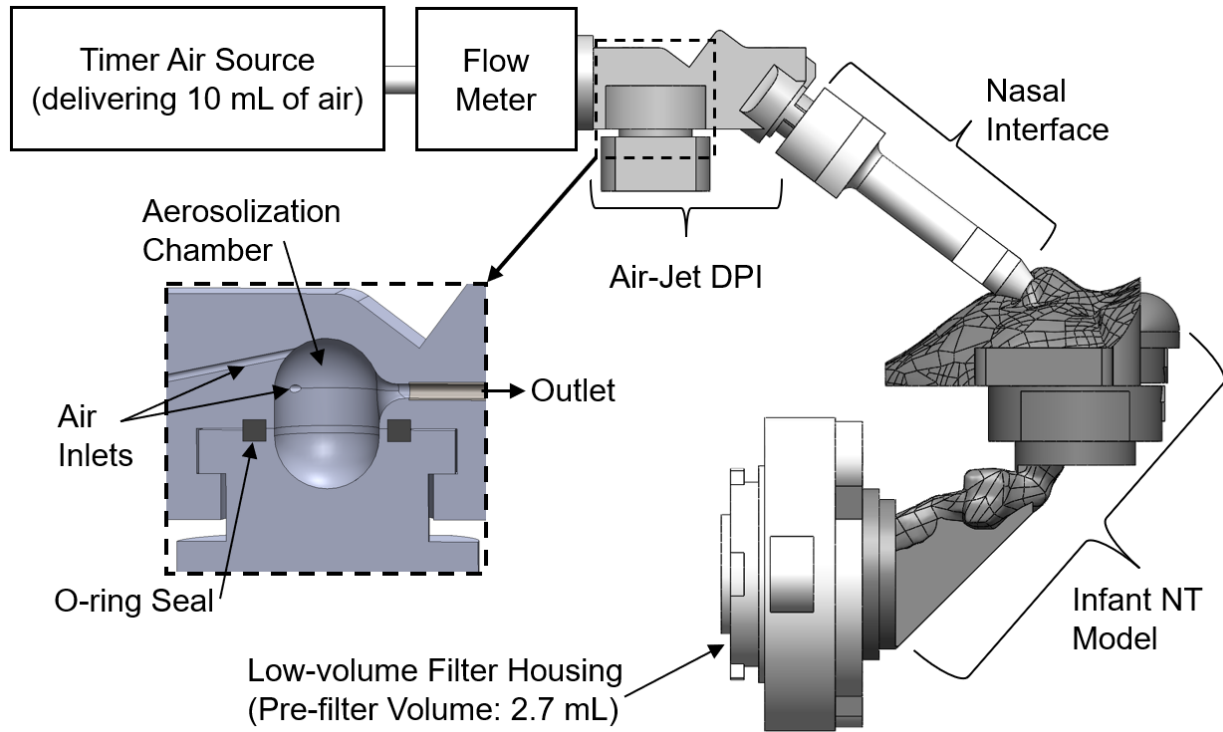


**Figure 5.2** Overview of the infant air-jet DPI aerosol delivery system connected to a preterm infant nose-throat (NT) airway model. Expanded view of the air-jet DPI illustrates internal components including the aerosolization chamber

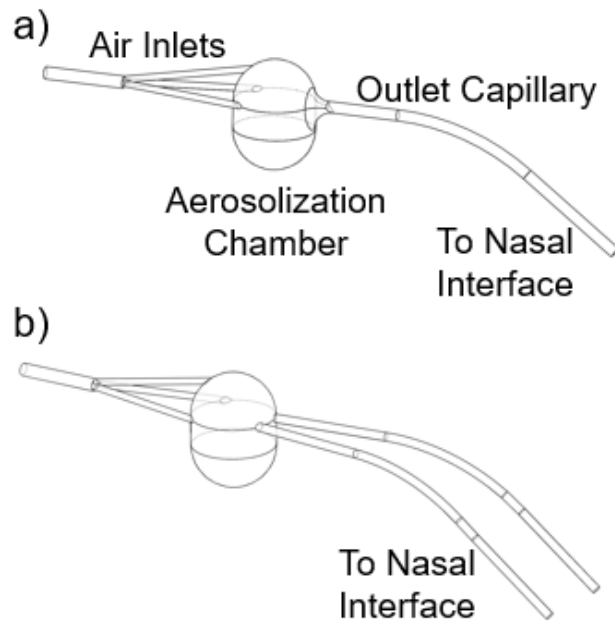


**Figure 5.3** Internal airflow geometries of each air-jet DPI from device inlet (left side of each image) to the device outlet(s) (right side of each image) and central aerosolization chamber. **(a)** D1-Single and **(b)** D1-Dual. The outlet capillaries lead to the inlet of the nasal interfaces

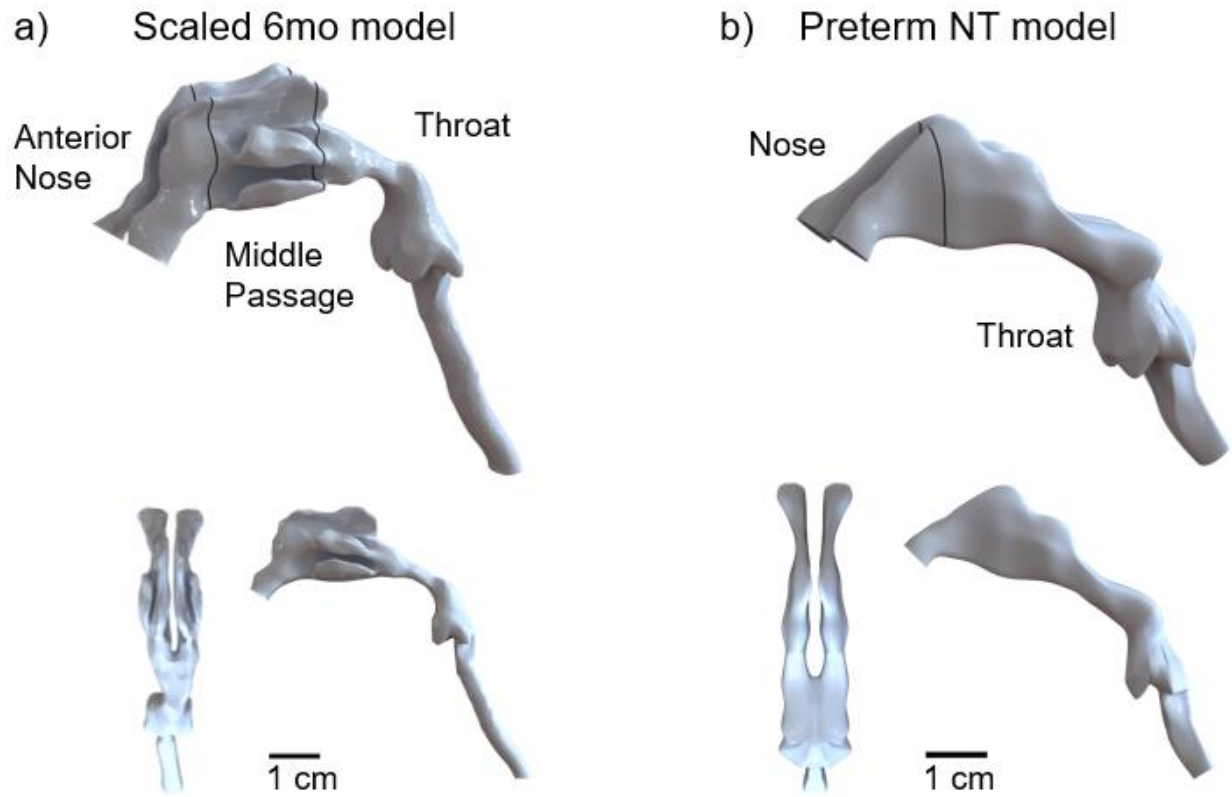


**Figure 5.4** Overview of the infant NT airway model and regional sections. Top panels provide isometric views of regional sections, and lower panels provide top and side views of the same nasal models with 1 cm scale bars. **(a)** Scaled-6mo model and **(b)** Preterm NT model

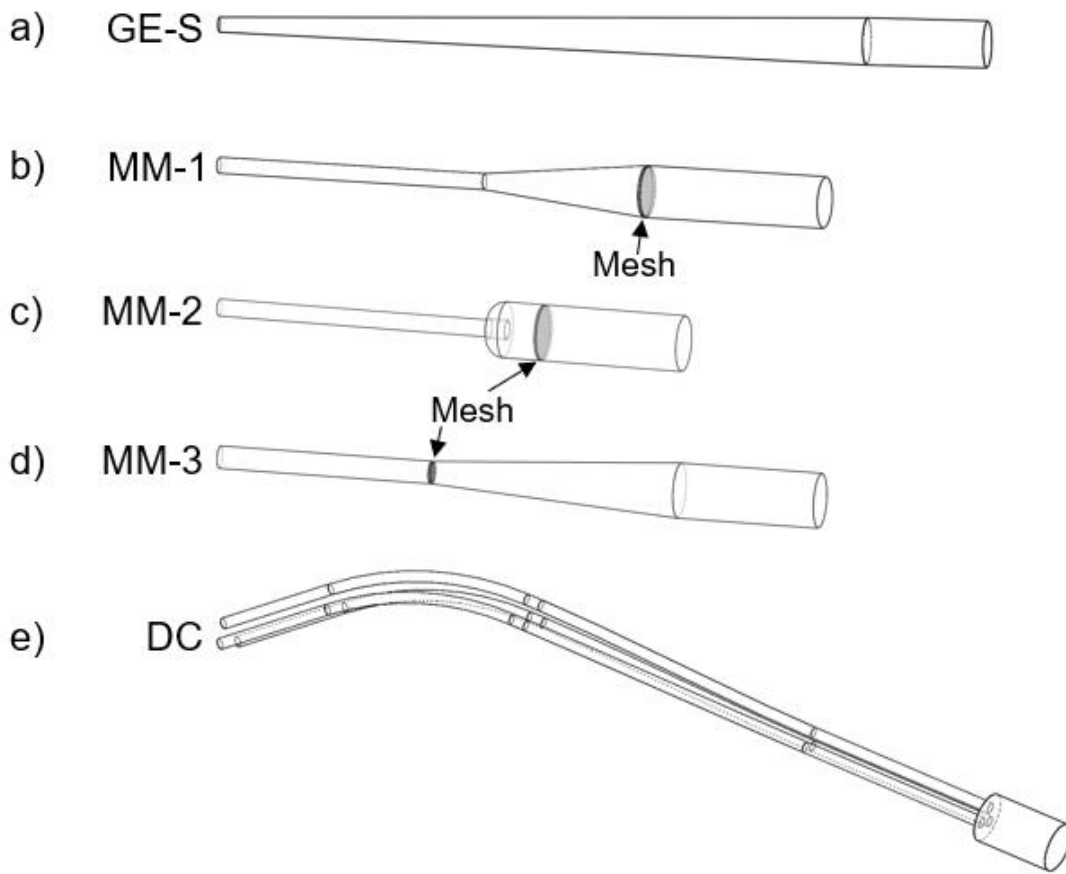


**Figure 5.5** Interface Set 1: Nasal interface designs (internal surfaces) beginning with the air-jet DPI outlet capillary (left side), followed by different flow pathways and ending with the same flexible straight prong. **(a)** Original GE-S, **(b)** MM design 1 (MM-1), **(c)** MM design 2 (MM-2), **(d)** MM design 3 (MM-3), and **(e)** DC design. All designs shown have a 3 mm internal prong diameter. Gray shaded area indicates location of MM for MM designs **((b) – (d))**. DC, direct capillary; GE-S, single gradual expansion; MM, metal mesh

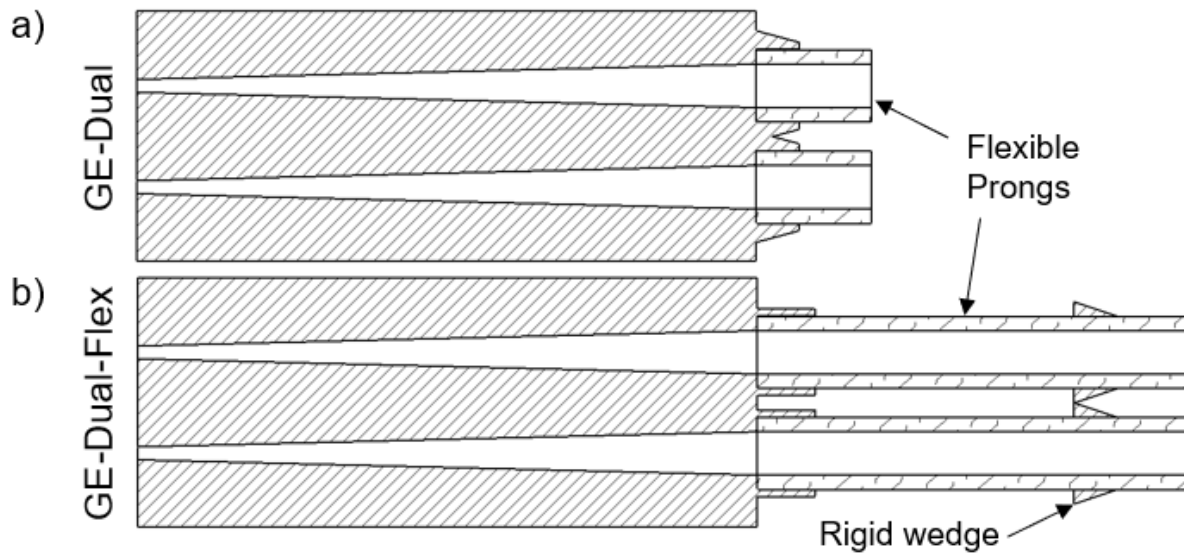


**Figure 5.6** Interface Set 2: Axial sectioned view of dual prong nasal interface designs from air-jet outlet capillary (left side of each image) to the straight flexible prongs (right side of each image). **(a)** Initial (GE-Dual) design and **(b)** Extended prong (GE-Dual-Flex) design

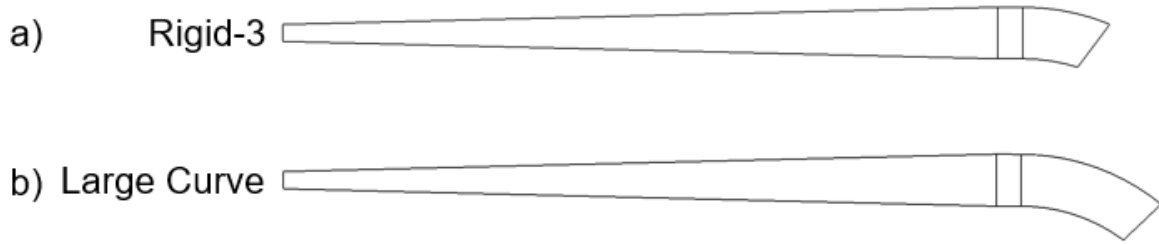


**Figure 5.7** Interface Sets 3 and 4: Internal airflow geometry of curved prong designs from air-jet outlet capillary (left side of each image) to the curved prong (right side of each image). Pictured are the **(a)** 3 mm inner diameter versions for the short curve prongs used in Interface Set 3 (Rigid-3) and **(b)** large curve prong used in Interface Set 4 (Large Curve)

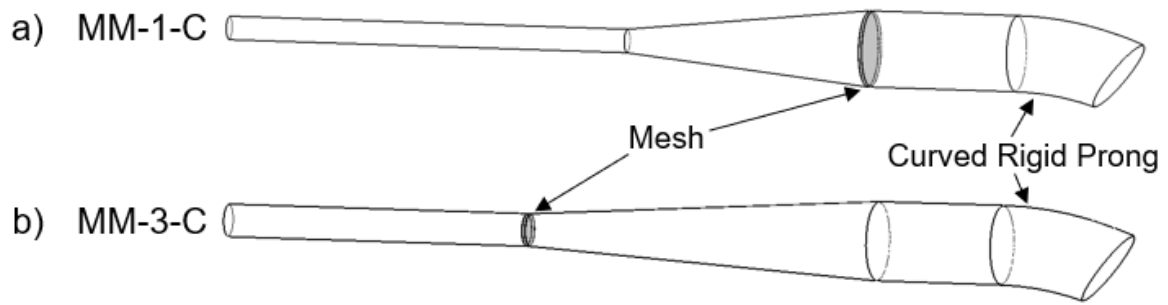


**Figure 5.8** Interface Set 5: Internal airflow geometry of combined flow pathway and curved prong designs from air-jet outlet capillary (left side of each image) to the curved prong (right side of each image). **(a)** MM-1-C design and **(b)** MM-3-C design. Gray shaded area indicates location of MM



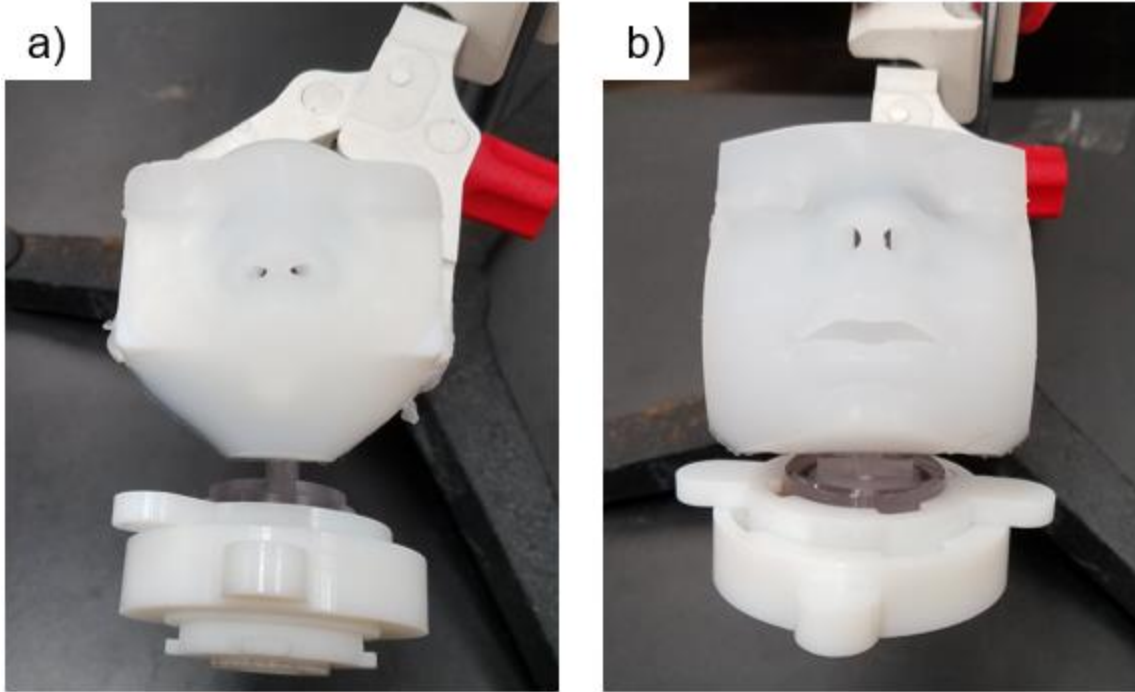


**Figure 5.9** Pictures of infant NT models during *in vitro* experimental setup for the **(a)** Scaled-6m model and **(b)** Preterm NT model

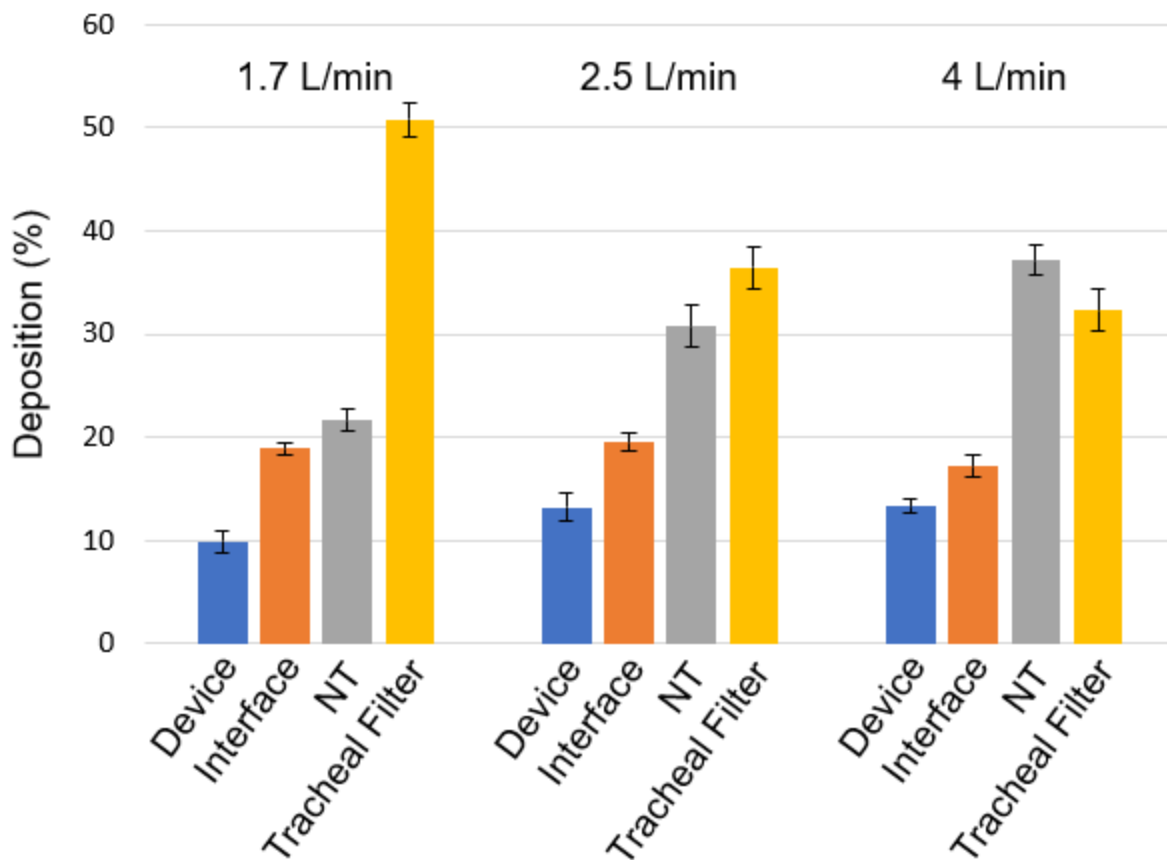


**Figure 5.10** Experimentally determined mean drug deposition fractions (based on loaded dose) of the I-leucine formulation (Batch 3) using the D1-Single air-jet DPI and Rigid-3 nasal interface across different Q90 flow rates. Anterior nose, MP, and throat deposition fractions were combined as total nose-throat (NT) deposition. Tracheal filter deposition is an estimate of lung delivery efficiency. Error bars denote  $\pm 1$  standard deviation. MP, middle passage

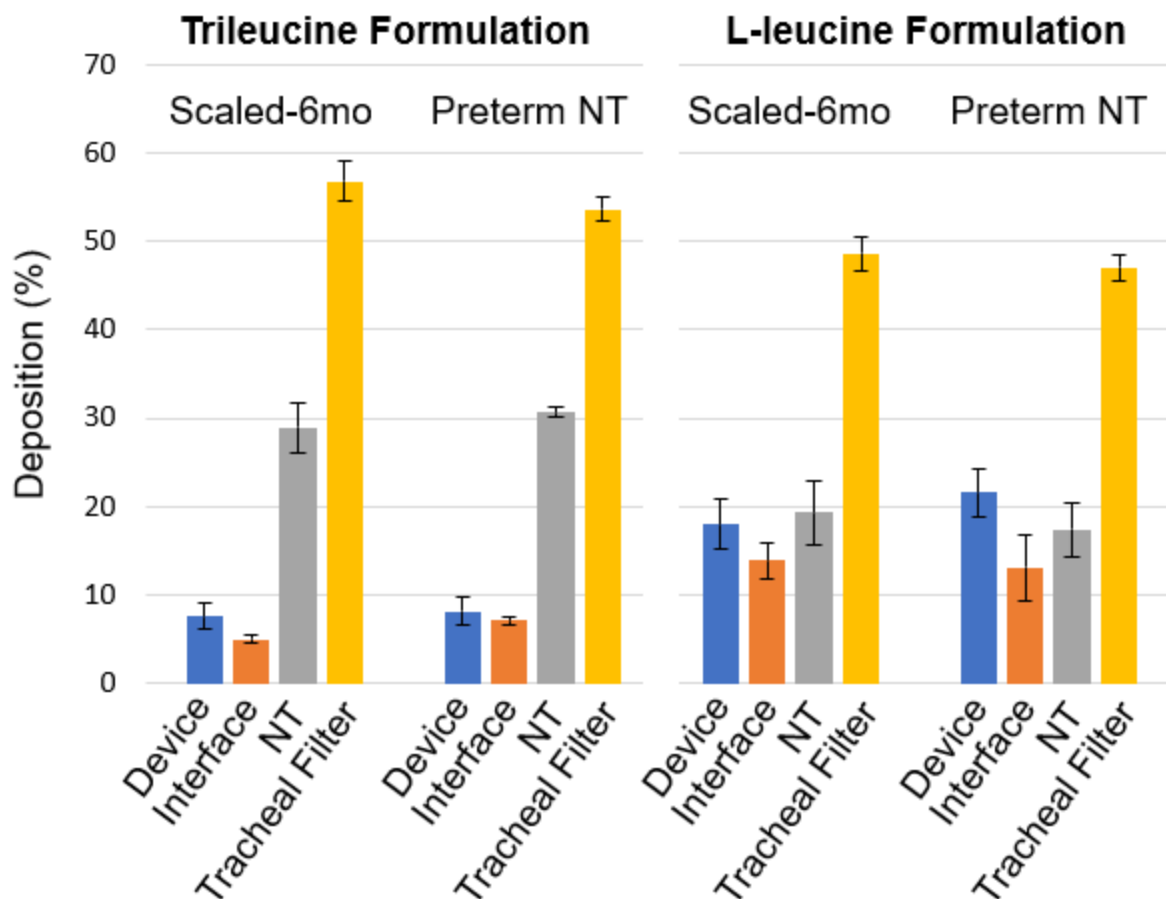


**Figure 5.11** Experimentally determined mean drug deposition fraction (based on loaded dose) using the D1-Single air-jet DPI and Rigid-3 nasal interface. Total nose-throat (NT) deposition represents sum of infant NT regional deposition fractions for each respective model. Tracheal filter deposition is an estimate of lung delivery efficiency. Comparison of aerosol delivery performance presented side by side for each formulation (trileucine on the left and Batch 4 l-leucine on the right) in two different infant NT models. Error bars denote  $\pm 1$  standard deviation

**Table 5.1** Interface Set 1: Lung delivery efficiencies (estimated as Tracheal Filter %) and regional deposition fractions (based on loaded dose) for the l-leucine EEG formulation (Batch 1) and an initial round of nasal interface designs with differing flow pathways and the same straight flexible prong with 3 mm internal diameter

<b>Deposition Region</b>	<b>GE-S</b>	<b>MM-1</b>	<b>MM-2</b>	<b>MM-3 *</b>	<b>DC *</b>
DPI Retention (%)	21.3 (1.5)	22.4 (2.3)	21.4 (4.4)	33.4 (3.8)	32.5 (4.4)
Nasal Interface (%) <sup>a</sup>	11.7 (2.1)	19.3 (0.9) <sup>b</sup>	14.8 (0.8) <sup>b</sup>	-	-
Total ED (%) <sup>a</sup>	67.0 (0.5)	58.4 (1.7) <sup>b</sup>	63.8 (5.1)	66.6 (3.8)	67.5 (4.4)
Anterior Nose (%) <sup>a</sup>	5.3 (1.1)	2.2 (0.2) <sup>b</sup>	5.2 (0.8)	5.7 (0.7)	6.4 (0.7)
Middle Passage (%) <sup>a</sup>	8.1 (1.1)	3.3 (0.7) <sup>b</sup>	7.9 (1.4)	6.8 (0.9)	7.8 (0.8)
Throat (%) <sup>a</sup>	9.9 (0.6)	4.3 (0.1) <sup>b</sup>	5.4 (1.7) <sup>b</sup>	7.1 (1.1) <sup>b</sup>	9.1 (1.1)
Total NT (%) <sup>a</sup>	22.3 (2.5)	9.8 (0.9) <sup>b</sup>	18.5 (3.5) <sup>b</sup>	19.5 (1.9)	23.2 (1.8)
Tracheal Filter (%) <sup>a</sup>	44.3 (1.5)	48.2 (0.2) <sup>b</sup>	41.3 (2.5)	46.5 (2.9)	43.8 (3.2)

Mean values with SDs shown in parenthesis, n=3.

\*DPI and nasal interface constructed as single piece, only Total ED is considered for statistical comparison for these deposition regions.

<sup>a</sup>p<0.05 significant effect of design on deposition region (one-way ANOVA).

<sup>b</sup>p<0.05 significant difference compared with GE-S case (t test).

DC, direct capillary; GE-S, single gradual expansion; MM, metal mesh

**Table 5.2** Interface Set 2: Lung delivery efficiencies (estimated as Tracheal Filter %) and regional deposition fractions (based on loaded dose) for the l-leucine EEG formulation (Batch 1) and Dual interface designs connected to the dual outlet version of the air-jet DPI, compared with initial GE-S results

<b>Deposition Region</b>	<b>GE-S</b>	<b>GE-Dual</b>	<b>GE-Dual-Flex</b>
DPI Retention (%)	21.3 (1.5)	23.4 (1.4)	23.3 (6.9)
Nasal Interface (%)	11.7 (2.1)	10.0 (1.1)	17.6 (5.1)
Total ED (%) <sup>a</sup>	67.0 (0.5)	66.6 (1.2)	59.1 (1.8) <sup>b</sup>
Anterior Nose (%) <sup>a</sup>	5.3 (1.1)	8.2 (1.7) <sup>b</sup>	6.8 (0.6)
Middle Passage (%)	8.1 (1.1)	9.7 (2.0)	9.7 (1.8)
Throat (%) <sup>a</sup>	9.9 (0.6)	12.8 (1.4)	13.4 (2.3) <sup>b</sup>
Total NT (%) <sup>a</sup>	22.3 (2.5)	30.7 (3.0) <sup>b</sup>	30.0 (4.1) <sup>b</sup>
Tracheal Filter (%) <sup>a</sup>	44.3 (1.5)	33.8 (2.3) <sup>b</sup>	29.5 (0.8) <sup>b</sup>

Mean values with SDs shown in parenthesis, n=3.

<sup>a</sup> $p < 0.05$  significant effect of design on deposition region (one-way ANOVA).

<sup>b</sup> $p < 0.05$  significant difference compared with GE-S case (*t* test).

**Table 5.3** Interface Set 3: Lung delivery efficiencies (estimated as Tracheal Filter %) and regional deposition fractions (based on loaded dose) for the l-leucine EEG formulation (Batch 2) and comparison of curved prong nasal interface configurations with 3 or 4 mm internal diameter

<b>Deposition Region</b>	<b>GE-S</b>	<b>Soft-3</b>	<b>Soft-4</b>	<b>Rigid-3</b>	<b>Rigid-4</b>
DPI Retention (%) <sup>a</sup>	27.5 (2.9)	18.8 (4.9) <sup>b</sup>	26.0 (2.1)	21.7 (1.6)	19.2 (3.9) <sup>b</sup>
Nasal Interface (%) <sup>a</sup>	11.5 (0.8)	14.3 (2.4)	14.9 (3.1)	16.9 (0.6) <sup>b</sup>	17.1 (2.8) <sup>b</sup>
Total ED (%)	61.0 (2.9)	66.9 (7.4)	59.2 (5.0)	61.5 (1.7)	63.7 (5.5)
Anterior Nose (%)	3.6 (0.4)	3.3 (0.7)	3.0 (0.6)	3.1 (0.4)	2.7 (0.5)
Middle Passage (%) <sup>a</sup>	5.6 (0.8)	4.9 (0.7)	2.5 (0.3) <sup>b</sup>	4.2 (0.3) <sup>b</sup>	3.0 (0.6) <sup>b</sup>
Throat (%) <sup>a</sup>	5.1 (0.6)	10.1 (1.8) <sup>b</sup>	6.1 (0.9)	6.5 (1.0)	6.1 (0.9)
Total NT (%) <sup>a</sup>	14.3 (1.7)	18.3 (2.5) <sup>b</sup>	11.5 (1.7)	13.7 (0.9)	11.8 (1.4)
Tracheal Filter (%) <sup>a</sup>	40.9 (1.1)	44.4 (3.5)	42.3 (3.6)	49.6 (2.6) <sup>b</sup>	48.7 (6.4) <sup>b</sup>

Mean values with SDs shown in parenthesis, n=3.

<sup>a</sup>p<0.05 significant effect of design on deposition region (one-way ANOVA).

<sup>b</sup>p<0.05 significant difference compared with GE-S case (t test).

**Table 5.4** Interface Set 4: Lung delivery efficiencies (estimated as Tracheal Filter %) and regional deposition fractions (based on loaded dose) for trileucine EEG formulation and comparison of small versus large curvature prong

<b>Deposition Region</b>	<b>GE-S</b>	<b>Rigid-3</b>	<b>Large Curve</b>
DPI Retention (%)	8.3 (0.4)	7.6 (1.5)	6.3 (1.2)
Nasal Interface (%) <sup>a</sup>	5.2 (0.6)	5.0 (0.4)	8.8 (2.0) <sup>b</sup>
Total ED (%)	86.5 (0.7)	87.4 (1.7)	84.8 (2.1)
Anterior Nose (%)	4.3 (1.3)	5.5 (1.4)	2.6 (0.3)
Middle Passage (%) <sup>a</sup>	10.2 (0.8)	9.2 (2.0)	3.8 (0.4) <sup>b</sup>
Throat (%) <sup>a</sup>	17.1 (0.1)	14.3 (1.3)	24.5 (2.1) <sup>b</sup>
Total NT (%)	31.6 (0.7)	29.0 (2.8)	30.9 (1.9)
Tracheal Filter (%) <sup>a</sup>	52.1 (0.7)	56.8 (2.2) <sup>b</sup>	51.0 (1.2)

Mean values with standard deviations (SD) shown in parenthesis, n=3.

<sup>a</sup> $p < 0.05$  significant effect of design on deposition region (one-way ANOVA).

<sup>b</sup> $p < 0.05$  significant difference compared with GE-S case ( $t$  test).

**Table 5.5** Interface Set 5: Lung delivery efficiencies (estimated as Tracheal Filter %) and regional deposition fractions (based on loaded dose) for the l-leucine EEG formulation (Batch 3) and comparison of nasal interface design effect

<b>Deposition Region</b>	<b>GE-S</b>	<b>MM-1-C</b>	<b>MM-3-C *</b>	<b>Rigid-3</b>
DPI Retention (%) <sup>a</sup>	15.1 (1.1)	12.7 (1.6)	31.9 (2.7)	9.9 (1.1) <sup>b</sup>
Nasal Interface (%) <sup>a</sup>	13.1 (0.1)	27.2 (2.5) <sup>b</sup>	-	18.9 (0.7) <sup>b</sup>
Total ED (%) <sup>a</sup>	71.9 (1.2)	60.1 (3.3) <sup>b</sup>	68.1 (2.7)	71.2 (1.6)
Anterior Nose (%) <sup>a</sup>	6.7 (1.4)	3.0 (0.2) <sup>b</sup>	7.3 (1.0)	5.0 (0.1) <sup>b</sup>
Middle Passage (%) <sup>a</sup>	10.4 (0.3)	3.9 (0.2) <sup>b</sup>	8.3 (1.0) <sup>b</sup>	6.4 (0.7) <sup>b</sup>
Throat (%) <sup>a</sup>	12.4 (0.4)	5.0 (0.6) <sup>b</sup>	12.2 (2.2)	10.3 (1.7)
Total NT (%) <sup>a</sup>	29.5 (1.2)	11.9 (0.3) <sup>b</sup>	27.8 (2.7)	21.7 (1.1) <sup>b</sup>
Tracheal Filter (%) <sup>a</sup>	43.3 (0.8)	48.7 (1.1) <sup>b</sup>	43.1 (1.2)	50.8 (1.7) <sup>b</sup>

Mean values with standard deviations (SD) shown in parenthesis, n=3.

\*DPI and nasal interface constructed as single piece, only Total ED is considered for statistical comparison for these deposition regions.

<sup>a</sup>p<0.05 significant effect of design on deposition region (one-way ANOVA).

<sup>b</sup>p<0.05 significant difference compared with GE-S case (t test).



## Chapter 6 - Development of a High-Dose Infant Air-Jet Dry Powder Inhaler (DPI) with Passive Cyclic Loading of the Formulation

### Task 2.1 – Published: *Pharmaceutical Research*

#### 6.1 Introduction

Challenges associated with pharmaceutical aerosol delivery to infants include poor lung delivery efficiency, high inter-subject dose variability and long administration times [53-57]. For example, in the *in vivo* study of Fok et al. [12], a group of 13 spontaneously breathing infants received radio-labelled salbutamol delivered through a metered dose inhaler (MDI) with a valved holding chamber and facemask. With two actuations of the MDI, the mean lung dose was 1.35  $\mu\text{g}$  across the population, with lung delivery efficiencies to all infants <2.5% of the loaded dose. Perhaps even more concerning than poor lung delivery efficiency is high inter-subject variability, where in the study of Fok et al. [12] one infant received a lung dose of only 0.25  $\mu\text{g}$  and another received 4.52  $\mu\text{g}$ , indicating the dose received may be approximately 5-fold lower or 3-fold higher than the mean of 1.35  $\mu\text{g}$ . A more recent example of poor infant lung delivery efficiency is the *in vivo* study of Corcoran et al. [117], in which a radiopharmaceutical aerosol was administered to 18 infants via mesh nebulizer through a nasal cannula interface while simultaneously receiving nasal cannula oxygen. It was estimated that only 0.46% of the nebulized dose reached the lungs at a cannula flow rate of 2 L/min, with an overall high variability in delivered dose. These findings are consistent with most other *in vivo* and realistic *in vitro* infant studies, resulting in lung delivery efficiency values in the range of 0-10% of the loaded or nebulized dose [52, 58, 59, 61, 67, 114-116] across multiple inhalation platforms.

These low lung delivery efficiencies combined with high inter-subject variabilities can often result in extended treatment times, poor clinical response and elevated off-target effects, especially when administering medications that require relatively high lung doses or that have a narrow therapeutic window.

To better address the challenges associated with pharmaceutical aerosol delivery to infants, our group [26-28] is developing an infant air-jet dry powder inhaler (DPI) platform. Overall, the infant air-jet DPI is designed to provide a full inhalation breath along with the aerosol to the lungs of an infant through the nasal route. The platform consists of an air source (providing aerosolization energy and inhalation breath), the air-jet DPI (responsible for holding and aerosolizing the loaded powder), and the nasal interface, which transports the aerosol from the DPI to the infant's nasal passage and forms an airtight seal with the infants' nostrils. Previous studies of the infant air-jet DPI have evaluated the effects of the aerosolization chamber geometry [26], air source and flow rate [27], and infant nasal interfaces [28]. Overall, the best performing configuration of the infant air-jet DPI platform was able to deliver ~57% of the loaded dose to the tracheal filter through an *in vitro* preterm NT model [28]; however, this configuration held only ~10-20 mg of the dry powder formulation before needing to be reloaded.

The infant air-jet DPI is viewed as a general aerosol delivery platform with multiple potential applications. These potential uses of the platform where high efficiency lung delivery of a pharmaceutical aerosol may be beneficial include administering inhaled surfactant in surfactant replacement therapy [91, 177], inhaled antibiotics to treat bacterial pneumonia [186], and inhaled antivirals to treat RSV and severe viral pneumonia [187, 188]. In each of

these envisioned applications, relatively high doses of powder, typically in the range of 10 mg and above for an infant, are expected to be required to generate a sufficient biological response. Even in adults, the availability of high dose DPIs is limited, with some newer devices administering >10 mg of drug [135, 189-191]. However, these devices are designed to operate with very large inhaled air volumes (on the order of ~2 L and above), high airflow rates (typically 45 L/min and above), and may incur significant extrathoracic depositional losses. Alternatively, higher dose delivery is often accomplished by requiring the patient to use a relatively low dose device and load multiple capsules with repeated inhalations over multiple cycles [153, 192], which increases the difficulty of device operation as well as the opportunity for user errors [193]. Ideally, a general high dose DPI platform should allow for different powder mass loadings without significantly impacting performance or operation, and will likely require multiple breaths to maintain an acceptable lung deposited powder mass with each inhalation. Considering the infant air-jet DPI applied to high dose applications, what is needed is a system that will enable increased powder mass loadings without impacting the previously achieved high lung delivery efficiency.

Options to increase the aerosolized dose of the infant air-jet DPI include (i) use of a larger aerosolization chamber to accommodate more loaded powder or (ii) development of a cyclic loading strategy that is employed automatically by the device. Preliminary experiments have indicated that increasing the infant air-jet DPI aerosolization chamber volume to accommodate higher mass loadings negatively impacts aerosol performance (with current chamber designs) especially when only 10 mL of air is available to aerosolize the powder. Furthermore, repeated exposure of dry powder formulations to aerosolization forces within the

device creates aggregates that are then difficult to disperse with subsequent actuations. As an alternative to simply increasing the aerosolization chamber volume, we propose a *passive cyclic loading strategy* that employs separate powder reservoir and aerosolization chamber components. Variable powder doses may be loaded into the powder reservoir, which connects to the aerosolization chamber. This enables the aerosolization chamber to maintain previously established dimensions and flow conditions that have been shown to be conducive for high efficiency aerosolization [26-28]. A combination of the connection design leading from the reservoir and a potential metering system may control the dose loaded into the aerosolization chamber that is then converted to an aerosol with each actuation.

With a passive cyclic loading strategy, introduction of a *metering element*, such as a *powder tray*, may be used to further control the amount of powder that is aerosolized with each actuation. Goals of the passive cyclic loading system include metering a consistent amount of powder for each actuation while protecting the powder in the reservoir from aggregate formation. If designed properly, the result should be a single device that can accommodate a variable range of powder doses and aerosolize a relatively consistent amount of dose with each actuation, while remaining insensitive to the amount of powder loaded (above a certain threshold). Accomplishing this goal with forces already present in the device and very small volumes of actuation air presents a significant challenge for infant aerosol delivery.

The objective of this study was to expand the infant air-jet DPI with a passive cyclic loading strategy that provides high efficiency lung delivery of an aerosol and is insensitive to powder mass loadings in the range of 10-30 mg as well as the presence of downstream pulmonary mechanics. As a secondary objective, this study will also explore the impact of

different powder reservoir sizes, formulation types and actuation gas flow rates on performance of the new device. The study begins by comparing four new air-jet DPIs with a passive cyclic loading design using the initial 10 mg powder mass. The best designs (based on highest tracheal filter deposition percentage, which estimates the lung delivery efficiency) are then loaded with a 30 mg powder mass and performance is re-examined. The goal of the new designs is to produce similar aerosolization performance and lung delivery efficiencies independent of the loaded powder mass (10 vs 30 mg). A secondary goal is to improve upon our previous best performing infant air-jet DPI platform configuration by reaching a lung delivery efficiency of 60% using a highly dispersible spray-dried model excipient enhanced growth (EEG) formulation and realistic preterm nose-throat model. Next, a single design is chosen for continued sensitivity analysis including downstream pulmonary mechanics and powder reservoir volume size (the initial standard vs an extended volume size). Finally, the performance of the platform with a spray-dried Surfactant-EEG formulation [177] is investigated, as well as a re-examination of the effect of flow rate.

## **6.2 Materials and Methods**

### *Powder Materials and Formulation*

Albuterol sulfate (AS) and l-leucine were purchased from Sigma Chemical Co. (St. Louis, MO). Pearlitol® PF-Mannitol was donated from Roquette Pharma (Lestrem, France) and Poloxamer 188 (Leutrol F68) was donated from BASF Corporation (Florham Park, NJ). Trileucine was purchased from Bachem Americas, Inc. (Torrance, CA). Sodium chloride, ethanol and methanol were purchased from Fisher Scientific Co. (Hanover Park, IL). Survanta® (beractant)

intratracheal suspension was purchased from Cardinal Health, Inc. (Greensboro, NC).

Throughout the study, freshly collected deionized water was used.

A batch of AS excipient enhanced growth (AS-EEG) powder was obtained using a Büchi Nano B-90 HP Spray Dryer (Büchi Laboratory-Techniques, Flawil, Switzerland), and spray-dried based on the optimized method described by Son et al. [76]. The AS-EEG powder formulation included 30:48:20:2% w/w ratio of AS, mannitol, trileucine, and Poloxamer 188, respectively. A feed solution of 150 mL containing the dissolved drug and excipients at the stated ratio was sprayed over a 4-hour period at a spray rate of 0.6 mL/min. The solids concentration in the feed solution was 0.5% w/v. Throughout the spray drying process, the inlet temperature was set to 120 °C, resulting in an outlet temperature of 49 °C. The feed solution temperature was 5-15 °C during the spray drying as excess feed solution was recycled into the stock.

Two batches of Survanta<sup>®</sup> based Surfactant-EEG powders were prepared by spray drying of the feed dispersions containing Survanta<sup>®</sup>, mannitol, sodium chloride and l-leucine at a ratio of 40:30:10:20% w/w using the Buchi Nano Spray Dryer B-90 HP (Büchi Labortechnik AG, Flawil, Switzerland). The feed dispersions were prepared with 0.125% w/v solids by addition of all the formulation components to 5% v/v ethanol in water followed by 40 min sonication in a heated water bath (Fisher Scientific™ CPXH, Hanover Park, IL) at 45-55°C. The prepared feed dispersions were spray-dried with the spray dryer in an open mode configuration using the small nozzle and the following optimized operating conditions reported by Boc et al. [90]. Throughout the spray drying process, the inlet temperature was set to 70 °C, resulting in an outlet temperature of 35-38 °C. The spray-dried powders were collected from the electrostatic

precipitator into glass vials and stored in a desiccator (0% RH) in the freezer (-20 °C) when not in use.

### *Infant Air-Jet Platform and Experimental Overview*

The infant air-jet DPI platform [26-28] is comprised of three main components: the air source, the air-jet DPI, and the nasal interface (**Figure 6.1**). The air source is responsible for providing the aerosolization energy to the air-jet DPI, as well as delivering the aerosolized powder to the lungs while providing a full inhalation breath for the infant. For all experiments, the electronic *Timer* air source was utilized as developed and described by Howe et al. [27]. The air source at baseline conditions delivers an air actuation volume (AAV) of 10 mL bursts at a Q90 flow rate of 1.7 L/min. For each trial, a neonatal mass flow meter (Sensirion SFM3400, Sensirion AG, Stafa, Switzerland) was used to calibrate and verify the air source actuation parameters. **Figure 6.1** shows the location of the mass flow meter connected between the air source and air-jet DPI. The air-jet DPI consists of small diameter flow pathways for the inlets and outlets connected by an aerosolization chamber (**Figure 6.2**) and is responsible for aerosolization of the powder as well as holding the full dose of powder. In this study, as the air source is actuated, high speed jets of air pass through the aerosolization chamber and either around or through the preloaded powder facilitating powder aerosolization and a passive cyclic loading action. Four unique air-jet DPI designs (**Figure 6.2**) were developed and are described in more detail in the “*Air-Jet DPI Designs*” subsection. After exiting the air-jet DPI, the formed aerosol then passes through the nasal interface and to the infant (**Figure 6.1**). The prong of the

nasal interface is inserted approximately 5 mm into the nose, consistent with short ventilation support nasal prongs and forms an airtight seal with the nostril.

A single nasal interface was used for all experiments in this study consisting of a gradually expanding flow pathway and rigid curved prong (**Figure 6.3**) based on results of previous nasal interface testing [28]. Slight modifications were made to the nasal interface based on additional testing. The nasal interface in this study consisted of a straight gradually expanding circular cross-section with a length of 48 mm, and a final internal diameter of 3.6 mm. The end of the expansion transitioned to a rigid curved prong (**Figure 6.3**), with an inner diameter of 3.6 mm and outer diameter of 4.6 mm. The outer diameter of the prong was based on a Hudson Prong Size 2, commonly used for preterm infant nasal continuous positive airway pressure (CPAP) administration. A gradual exterior taper was included at the base of the prong, forming a wedge to help facilitate an airtight seal with the infant's nostril (**Figure 6.3**). The nasal interface was built using stereo-lithography (SLA) with Accura ClearVue resin through 3D Systems On Demand Manufacturing.

The main portion of this study compares the different air-jet DPI designs using a preterm infant nose-throat (NT) *in vitro* model and a 10 mg loaded powder mass of AS-EEG formulation. As seen in **Figure 6.1**, the platform interfaces with the preterm NT model which leads to a custom low-volume filter for approximating lung delivered dose. In this setup, device ED, nasal interface deposition, NT regional depositions, and lung delivery efficiency (represented by aerosol passing through the larynx and a portion of the trachea and depositing on the filter) were assessed, as percentage values of the loaded dose. The best performing devices were then selected for dose loading sensitivity in which a 30 mg loaded powder mass



was also tested. A pulmonary mechanics sensitivity comparison was also performed to test the performance of the platform while connected to an infant lung simulator that provided realistic downstream resistance and compliance. To enable larger mass loadings for high dose applications or lower density powder formulations, a loading chamber volume sensitivity experiment was also performed. As a final step, this study explored the use of a Surfactant-EEG formulation in the best performing device. Sensitivity of the platform to powder formulation was explored as well as the effect of flow rate on the new formulation.

#### *Preterm Infant Nose-Throat (NT) Model*

For all experiments in this study, a previously developed [27, 28] preterm NT *in vitro* model was used. The scaled 6-month preterm NT airway model includes flexible nostrils and anterior nose connected to a rigid middle passage, throat and approximately 3/4<sup>th</sup> of the trachea, which then connects to a custom low-volume filter housing. **Figure 6.4a** illustrates the setup and assembly break-out of the NT model and low-volume filter housing. Briefly, the preterm infant airway geometries were scaled down to an infant with a weight of 1600 g and length (height) of 40.7 cm, based on a high-quality CT scan of a 6-month-old infant NT geometry [79]. Using the infant body length (height), an appropriate geometric scaling factor of 0.6 was applied to the 6-month-old NT airway to reduce the model to that of a preterm infant with weight and height of about 1600 g and 40.7 cm, respectively [167]. The resulting preterm airway, shown in **Figure 6.4b**, has a tracheal length and diameter (proximal) of approximately 26 and 3 mm, respectively. While these parameters are known to vary, they do fall within the

expected range for preterm infants of 25 to 30 weeks gestational age (GA) based on reported studies [168].

The scaled 6-month preterm NT model was constructed with twist lock interfaces and O-rings that provided air tight seals and facilitated ease of use. The low-volume filter housing accommodated the low AAV of 10 mL used for a preterm infant, with a dead space of only 2.7 mL before the 1.5" diameter glass-fiber filter. To provide a smooth and accurate internal airway surface, the middle passage and throat sections of the preterm NT model were built using SLA printing with Accura ClearVue resin (3D Systems). The low-volume filter housing was 3D printed using VeroWhitePlus resin. To facilitate nasal interface prong insertion and the formation of an airtight seal, the face and anterior nose section were molded with a skin-like silicone elastomer. The face adapter (pictured in **Figure 6.4a**) was printed using VeroWhitePlus resin, and was glued to the soft face mold, allowing for a secure and air-tight connection to the rest of the NT model. The three distinct airway regions of the NT model used for regional deposition quantification (anterior nose, middle passage, and throat) are illustrated in **Figure 6.4b**.

#### *Air-Jet DPI Designs*

Four unique air-jet DPIs were designed and prototyped to investigate passive cyclic loading for the platform. **Figure 6.2** shows the internal airway geometries of each air-jet DPI passive design (PD), labeled as PD-1 through PD-4, with basic elements including small diameter inlet flow passage(s), aerosolization chamber, powder reservoir (where the powder was initially loaded), and outlet capillary. In each design, the powder reservoir was positioned above (with respect to gravity) the aerosolization chamber, centered perpendicular to the direction of

primary air flow. In this study, the powder reservoir was filled with the desired dose (mass of powder) and then connected to the air-jet DPI with a twist-lock and O-ring seal. The initial standard powder reservoir could accommodate a powder volume up to 0.55 mL. Each air-jet PD had identical connections for powder reservoir attachment, while the inlets, aerosolization chamber geometries, and outlets differed. Several rounds of preliminary screening were performed for each of the four designs in this study leading to a relative best case for each PD geometry. For the initial comparison of the four unique air-jet DPI designs, the number of actuations to clear the device was also recorded, in which actuations continued until two consecutive visibly clear (no aerosol visible passing through the nasal interface) actuations were observed. This metric helps distinguish future ease of use and speed of delivery, with a lower number of actuations indicating quicker delivery times and less work to administer a full dose.

All designs were influenced by our previous studies with modifications made to explore passive cyclic loading. As with previous infant air-jet DPIs, the four new designs in this study (**Figure 6.2a-d**) all used a single outlet capillary from the aerosolization chamber (inner diameter of 0.89 mm and a flush or protruding configuration) comprised of a hollow stainless steel (SAE 304) capillary tube. After exiting the aerosolization chamber, this capillary tube included a 37-degree downward bend prior to connection with the nasal interface. All devices used a flush (capillary does not protrude into the aerosolization chamber) outlet configuration with the exception of PD-3, in which the capillary tube protruded into the aerosolization chamber by 0.5 mm. PD-1 and PD-4 used a single inlet of 0.6 mm diameter while PD-2 and PD-3 used multiple inlets with 0.5 mm diameters. These inlet geometries were formed into the structure of the air-jet device during 3D printing. One subtle difference in inlet configurations

was that PD-2 had four inlets, all directing the inlet airflow around the initial powder bed. PD-3 had three inlets with one directing a portion of the inlet flow toward the powder bed and the other two directing the airflow through the lower region of the aerosolization chamber.

Considering the aerosolization chambers, PD-1 included a small spherical geometry (diameter of 4.8 mm) with a 3 mm diameter connection to the powder reservoir. PD-2 and PD-3 both had a horizontal capsule shaped aerosolization chamber with a volume  $\sim 0.68$  mL, and a powder shelf or tray placed directly below the powder reservoir to facilitate dose metering. The PD-2 device used a 3 mm diameter opening to the powder reservoir with the shelf positioned to provide an approximate 0.026 mL volume for the powder to rest during each actuation. The PD-3 device used a 2.7 mm diameter opening to the powder reservoir with the shelf positioned to provide an approximate 0.013 mL volume for powder metering. PD-4 used a small aerosolization chamber of  $\sim 0.05$  mL with two small (1 mm diameter) openings to the powder reservoir, spaced equidistance between the inlet/outlet and center of the chamber (as pictured in **Figure 6.2d**).

All air-jet DPI parts (as well as nasal interface and NT model parts) were designed in SolidWorks (Dassault Systèmes, Paris, France), and exported as .STL files. The parts were then 3D printed at either 32  $\mu\text{m}$  resolution on a Stratasys Objet24 3D Printer (Stratasys Ltd., Eden Prairie, MN) using VeroWhitePlus resin, or with stereo-lithography (SLA) using Accura ClearVue resin through 3D Systems On Demand Manufacturing with a layer thickness of 0.05 mm. All parts were designed to interconnect using a twist lock mechanism with an intermediate O-ring for an air-tight seal.

### *In Vitro Evaluation of Preterm Lung Delivery Efficiency*

To assess the aerosol transmission through the nose and throat, and effective lung delivery efficiency (drug deposited on the filter), all experiments utilized the scaled 6-month preterm NT *in vitro* model. The nasal interface, as seen in **Figure 6.3**, was inserted approximately 5 mm into the left nostril of the infant NT model while the right nostril was manually held closed during actuation. A small amount of lubricant grease was applied to the exterior of the prong to ensure an airtight seal. The internal airways of all NT model segments were coated with a silicon spray to minimize particle bounce and simulate airway surface liquid. At the end of the NT model, a custom low-volume filter collected powder passing through the extrathoracic regions and represented the amount of drug delivered to the lung. Calculations for ED and regional depositions, including the nasal interface and in the NT model regions and tracheal filter, were expressed as a percentage of the manually weighed loaded dose of AS. All experiments were performed in triplicate for the calculation of mean and standard deviation values. More detail on the regional deposition fractions can be found in the “*Drug Mass Characterization Methods*” subsection.

### *Sensitivity Analysis*

Impact of Loaded Dose: To determine potential sensitivity to powder loading between the initial mass of 10 mg and a larger mass of 30 mg, additional experiments were performed for the two best case designs (PD-2 and PD-3), in which a 30 mg powder mass loading was used. All experimental procedures remained the same as with the air-jet DPI comparison set, except for the manual weighing of 30 mg of powder instead of 10 mg. Likewise, actuations continued

until no powder was visible passing through the system and one subsequent clear actuation was performed. The total number of actuations used in all cases was recorded.

Impact of Downstream Pulmonary Mechanics: To test sensitivity of the platform to downstream pulmonary mechanics, the PD-3 air-jet DPI design was chosen and retested while connected to an infant Michigan Lung simulator (Adult/Infant Model, Michigan Instruments, Grand Rapids, MI). Two NT model outlet conditions were considered: one as the standard filter only (used in all other experiments) and then also including the downstream pulmonary mechanics, connected to the lung simulator. This experiment was performed to directly compare the large dose loading condition including downstream pulmonary mechanics in a breathing lung simulator, as pictured in **Figure 6.5**. Using the air source operated at 1.7 L/min, and a 30 mg powder mass loading, the platform was actuated during the inhalation cycle of the lung simulator, while all other methods remained the same. Pulmonary mechanics (PM) considered in this study were lung compliance (mL/cm H<sub>2</sub>O), airway resistance (cm H<sub>2</sub>O/L/s), breath cycle (sec), and tidal volume (mL). The compliance, breath cycle, and tidal volume were manually set on the lung simulator, and a custom resistance orifice adapter was used to adjust the airway resistance.

While values for these properties are known to vary, our previous study examining pulmonary mechanics [27] used a compliance of 0.49 mL/cm H<sub>2</sub>O for a 1600 g preterm infant based on similar values measured in infants with a weight of 1600 g [104]. For this study, the infant lung simulator was set to its lowest compliance setting of 1 mL/cm H<sub>2</sub>O. The inspiratory time was set to 0.5 sec, with a 1 sec breath hold and exhalation period resulting in a ~2.5 sec breath cycle. With the direct-to-infant delivery protocol used in this study, one nostril was

connected to the device while the contralateral nostril and mouth were held closed, enabling the use of a breath hold period. The tidal volume was adjusted to approximately 10-11 mL. For infants with RDS, airway resistance values have been reported between 100-200 cm H<sub>2</sub>O/L/s [104-107]. An adjustable resistance orifice was built to set the desired airway resistance downstream of the filter. To measure airway resistance through the filter housing and orifice, a pressure sensor (SSCDLNN040MBGSA5, Honeywell, Sensing and Control, Golden Valley, MN) was placed anterior to the filter housing while the neonatal flow meter (Sensirion SFM3400) was placed further upstream. The downstream side of the resistance orifice was opened to atmospheric pressure while a steady upstream flow rate of 2 L/min was set. The pressure was recorded while the orifice was adjusted to provide a total airway resistance expected for an infant with RDS. The resulting calculated resistance was 172 cm H<sub>2</sub>O/L/s which falls within the range of expected values.

As with our previous study including pulmonary mechanics [27], air flow from exhalation of the lung simulator was prevented from passing back through the filter and detaching any deposited powder. The use of one-way valves and a bifurcation downstream of the resistance orifice allowed for venting the exhalation gas, as seen in **Figure 6.5**.

Impact of Powder Reservoir Volume: To enable larger dose loadings of powder, an extended powder reservoir was also considered. Both powder reservoirs had similar geometry with a half capsule shape of 7.1 mm diameter, differing by length only. The standard powder reservoir had a loading volume of 0.55 mL, while the extended volume was 1.5 mL, and both reservoirs were fabricated using the SLA method to produce clear parts for viewing of powder behavior during actuation. Images of the two translucent powder reservoirs connected to the

opaque PD-3 device can be seen in **Figure 6.6**. The standard powder reservoir could accommodate dose loadings between 10-50 mg of the AS-EEG formulation used in this study, which had a bulk density of  $\sim 0.1 \text{ g/cm}^3$  and up to  $\sim 150 \text{ mg}$  with the extended version. For this experiment, PD-3 was chosen with a 10 mg powder mass loading, while all other parameters remained the same as the initial experimental set.

Impact of Surfactant Formulation: Different dry powder formulations containing specific active pharmaceutical ingredients for a target disease state are expected to have different properties and different aerosolization characteristics. For this study, the Surfactant-EEG formulation was chosen for comparison with the model AS-EEG formulation. The PD-3 design was chosen for formulation sensitivity of the platform using a 10 mg mass loading of Surfactant-EEG. All other experimental parameters remained the same.

Impact of Surfactant Formulation Across Different Flow Rates: As mentioned in the previous air source study [27], the ideal flow rate is likely device and/or formulation dependent. While a Q90 flow rate of 1.7 L/min was ideal for dispersion and delivery of the AS-EEG formulation, it may not be ideal for the case of Surfactant-EEG. Two additional flow rates (i.e., 4 and 6 L/min) were chosen to compare aerosol delivery performance with the PD-3 device and the Surfactant-EEG formulation. To generate these flow rates, the Timer air source was adjusted to 0.15 and 0.1 second delivery times, respectively, which maintained the  $\sim 10 \text{ mL}$  AAV in each case.

#### *Drug Mass Characterization Methods*



For the AS-EEG formulation, after approximately 4 to 8 actuation cycles, drug masses retained or deposited on the air-jet DPI, nasal interface, NT model, and filter were recovered by dissolving in an appropriate volume of deionized water followed by high performance liquid chromatography (HPLC) analysis with fluorescence detection (excitation = 276 nm, emission = 609 nm). A Restek Allure PFP propyl column (5  $\mu\text{m}$ , 60  $\text{\AA}$ , 150 x 2.1 mm) was used for the chromatographic separation with a mobile phase flow rate of 0.4 mL/min. The mobile phase consisted of methanol and ammonium formate buffer (20 mM, pH 3.4 through addition of formic acid) in a ratio of 70:30, and the sample injection volume was 10  $\mu\text{L}$ . The loaded drug mass was determined through content uniformity analysis of the AS-EEG formulation; where known masses of AS-EEG were dissolved in water and the AS content ( $\mu\text{g}/\text{mg}$  of formulation) was determined. AS quantification was performed for each deposition site and for the total drug mass used to calculate the drug recovery. Drug recovery percentages were expressed as the sum of the amount of AS recovered in each deposition region divided by the loaded AS dose for each experiment.

For the Surfactant-EEG formulation, the surfactant content was determined based on the content of dipalmitoylphosphatidylcholine (DPPC). The DPPC content was quantified using a liquid chromatography–mass spectrometry (LC-MS) method adapted from Li et al. [194]. The system consisted of the Quattro micro™ mass spectrometer linked to an Alliance 2695 Separations Module with data acquisition software, MassLynx v4.1 (all from Waters Corporation, Milford, MA). The chromatographic separation was achieved using the Atlantis hydrophilic interaction liquid chromatography (HILIC) silica column (5  $\mu\text{m}$ , 50×1.0 mm; Waters Corporation, Milford, MA). The isocratic mobile phase consisted of acetonitrile and 5 mM

ammonium formate in water with 0.1% formic acid (88:12% v/v) pumped at a flow rate of 0.3 mL/min. The injection volume was 10  $\mu$ L. Following optimization of the ionization settings of the mass spectrometer, selected ion monitoring (SIM) analysis (for  $m/z = 735$ ) with positive electrospray ionization mode was applied to detect and quantify DPPC (molecular weight = 734 Daltons) following chromatographic separation. The DPPC stock standard solution (20  $\mu$ g/mL) was prepared by dissolving sufficient amount of DPPC (Avanti Polar Lipids, Inc., Alabaster, AL) in methanol. The diluted standard solutions of DPPC in the concentration range of 2 to 20  $\mu$ g/mL were prepared by dilution of the stock standard solution in methanol. The prepared stock standard and diluted standard solutions were injected as calibration standards. To determine the content uniformity of the Surfactant-EEG powder, approximately 1 mg of the powder was dissolved in 25 mL of methanol and quantitatively analyzed for the DPPC content by the LC-MS method described above. The mean amount of DPPC per mg of Surfactant-EEG formulations was determined. Triplicate samples were prepared and analyzed for each of the powder samples. The loaded drug (DPPC) mass was determined through content uniformity analysis of the Surfactant-EEG powder. The mass of DPPC was also determined from all the deposition sites, and the recovered dose was the total mass recovered from all the deposition sites.

The bulk density of each powder batch was determined using a 1 mL plastic syringe. Briefly, powder mass was calculated as the weight difference between the weight of the empty syringe and the weight of the syringe containing powder. The mass was then divided by the volume occupied by the powder inside the syringe to calculate the powder bulk density. The resulting densities were  $\sim 0.10$  g/cm<sup>3</sup> for the AS-EEG formulation and  $\sim 0.18$  g/cm<sup>3</sup> for the Survanta<sup>®</sup> based Surfactant-EEG formulation.

### *Statistical Analysis*

All experiments were performed with three or more replicates. Statistical analysis was performed using JMP Pro 16 (SAS Institute Inc., Cary, NC). Comparison of air-jet DPI device performance and surfactant formulation sensitivity to flow rate utilized one-way ANOVA followed by post hoc Tukey. Direct comparisons of sensitivity cases utilized Student's *t*-test. Statistical tests used a significance limit of  $P=0.05$ .

## **6.3 Results**

### *Comparison of Air-Jet DPI Design*

Performance of the four unique PD designs (**Figure 6.2**) was initially evaluated using the 10 mg mass loading of the AS-EEG powder formulation. **Table 6.1** provides the deposition fractions within each region based on the loaded formulation mass, as well as the number of actuations required to provide two consecutive clear actuations (no powder visible exiting the air-jet DPI). PD-2 and PD-3 produced the lowest DPI retention (~11-13%) and the highest tracheal filter deposition of ~60%, which met the goal of achieving 60% estimated lung delivery efficiency. PD-2 and PD-3 also had statistically similar performance across all deposition regions with the only difference being that PD-2 required one extra actuation to clear the device. PD-4 did not perform as well as the other devices and had the highest variability, based on mean (SD) DPI retention and tracheal filter delivery of 33.2 (5.5) % and 46.2 (2.1) %, respectively. This device also required the highest number of actuations. PD-1 had a mid-range performance with a mean tracheal filter deposition of ~53% and a DPI retention ~17%. PD-1 was also in the mid-

range in terms of consistency with larger standard deviations than PD-2 and PD-3, but less than seen with PD-4. Due to the similar and best performance of PD-2 and PD-3, both devices were selected for sensitivity analysis of loaded dose in the next step.

#### *Sensitivity Analysis: Impact of Loaded Dose*

To determine if the devices perform similar when loaded with a larger dose of powder, the results of the initial 10 mg powder mass were compared to a 30 mg loaded powder mass of the same formulation. For PD-2 and PD-3, **Table 6.2** compares the results with 10 mg powder mass loadings from **Table 6.1** with additional data using 30 mg loadings. For both designs, there was a slight but statistically significant reduction in nasal interface deposition (~2% absolute difference) with the larger loaded dose. PD-3 also produced a slight but statistically significant reduction in the anterior nose deposition region (~1%) with the larger loaded dose. All other regions for both designs remained statistically equivalent, indicating these two designs are not sensitive to the loaded dose for the values tested. It is also observed that the dose delivered on each actuation appears to be consistent. Due to the experimental procedure of delivery, requiring two consecutive visibly clear actuations before ending the trial, it can be inferred that performance will remain similar when PD-2 is actuated 3 and 9 times, and while PD-3 is actuated 2 and 6 times, for a 10 and 30 mg powder mass loading, respectively. For both designs, a 3-fold increase in powder mass also required a 3-fold increase in number of actuations to empty the device, which indicates a similar dose per actuation between the two loaded dose masses. Since both devices performed similarly with the increased loaded dose,

only PD-3 was chosen for additional sensitivity analysis in this study to reduce material and time costs of the experiments.

#### *Sensitivity Analysis: Impact of Downstream Pulmonary Mechanics*

The second sensitivity analysis utilized the results of PD-3 with a 30 mg powder mass loading of the AS-EEG formulation (from **Table 6.2**; denoted filter-only), compared to a pulmonary mechanics (PM) outlet condition. All other parameters of the experiment were identical, including number of actuations. The comparison of regional drug deposition for filter-only and PM outlet conditions is presented in **Table 6.3**. Performance across all deposition regions was statistically similar except for the nasal interface, which decreased by ~1% (absolute difference). The PM outlet condition was not found to have a statistically significant effect on the estimated lung deliver efficiency, which remained about 60%, but demonstrated an increasing trend in lung delivery efficiency (i.e., 60.5% filter only vs. 62.6% PM outlet). Overall, the performance was found to be insensitive to the addition of the PM outlet condition.

#### *Sensitivity Analysis: Impact of Powder Reservoir Volume*

The powder reservoir volume sensitivity analysis used the PD-3 device and 10 mg powder mass loading with the AS-EEG formulation. A comparison of the initial results using the standard powder reservoir (**Table 6.2** data) with additional data using the extended volume powder reservoir is shown in **Table 6.4**. The extended volume was not found to have an impact on the deposition found in the nasal interface and nose-throat regions; however, a statistically

significant difference was found for the DPI retention (also affecting Total ED) and the tracheal filter. The mean DPI retention increased from 10.9% to 15.5% while the mean tracheal filter deposition decreased from 60.9% to 54.5% with the extended powder reservoir. The nearly 3-fold increase of dead space in the powder reservoir was found to impact the performance of the system by lowering the emitted dose and consequently the tracheal filter deposition by approximately 5% (absolute difference).

#### *Sensitivity Analysis: Impact of Surfactant Formulation*

Using the results of the initial PD-3 test with 10 mg of the AS-EEG powder formulation, **Figure 6.7** compares the difference in deposition with the Survanta<sup>®</sup> based Surfactant-EEG powder formulation under similar conditions. In **Figure 6.7**, the total NT deposition represents the sum of the three nose-throat regions of the preterm infant model. A side-by-side comparison is made for the mean deposition fractions within different regions for both formulations, with +/- 1 standard deviation error bars. While the formulation was not found to have a statistically significant effect on device retention, all other regions indicated a statistical difference. Most notable were the differences in Total NT and Filter deposition. Changing from the AS-EEG to the Surfactant-EEG formulation increased the mean Total NT deposition from 23.3% to 47%, and decreased the mean Filter deposition from 60.9% to 30.2%. Due to this significant change in performance, the flow rate was re-evaluated for the Surfactant-EEG formulation as performance has been previously shown to be sensitive to flow rate [27].

#### *Sensitivity Analysis: Impact of Surfactant Formulation Across Different Flow Rates*

As a final sensitivity analysis, the effect of flow rate on performance for the Surfactant-EEG formulation was explored, using the two additional Q90 flow rates of 4 and 6 L/min. **Figure 6.8** provides mean deposition fractions across the regions of interest, with +/- 1 standard deviation error bars grouped by flow rate. Statistical analysis using one-way ANOVA ( $p < 0.05$ ) showed no significant effect of flow rate on Device retention or Interface deposition, which remained about 11-13% and 3-4%, respectively. The total NT and Filter deposition were, however, found to be affected by the flow rate. Statistical analysis using post-hoc Tukey ( $p < 0.05$ ) showed a significant increase in tracheal filter deposition for the 4 L/min case, and a significant increase in NT deposition for the 6 L/min case, when compared to the original 1.7 L/min. The results of the flow rate sensitivity analysis for the Surfactant-EEG powder formulation demonstrated best performance at a Q90 of 4 L/min, which improved the mean estimated lung delivery efficiency to 38.6%.

#### **6.4 Discussion**

A significant outcome of this study is the advancement of the infant air-jet DPI system to enable high dose powder loadings using a passive cyclic loading approach. Four new passive design (PD) devices were implemented and two of the designs (PD-2 and PD-3) resulted in improved estimated lung delivery efficiencies over the previously developed system (e.g., Howe et al. [27] with ~50% lung delivery efficiency), while also enabling high dose delivery. Both PD-2 and PD-3 performed similarly when loaded with a 10 and 30 mg mass of AS-EEG formulation, and were able to deliver ~60% of the loaded dose to the tracheal filter through a preterm NT model. Based on the observation that tripling the loaded dose did not have an impact on lung

delivery efficiency, it is projected that mass loadings can be increased even further without negative impacts. Furthermore, tripling the volume of the powder reservoir resulted in only a minor reduction in lung delivery efficiency from ~60% to ~55%. As a result, the passive cyclic loading strategy appears capable of delivering a range of drug masses from ~10 mg through ~150 mg (at a powder bulk density of 0.1 g/cm<sup>3</sup>) with only minor changes in lung delivery efficiency. Including downstream pulmonary mechanics consistent with a preterm infant was also observed to produce a negligible impact on platform performance and lung delivery efficiency of the aerosol. Considered collectively, results of this study indicate that the infant air-jet DPI expanded with passive cyclic loading is expected to exhibit consistent performance across a range of loaded doses and is largely insensitive to pulmonary mechanics.

In contrast with loaded dose, reservoir volume size and downstream conditions, performance of the infant air-jet DPI was found to be sensitive to characteristics of the loaded formulation, as expected. While the platform using the PD-3 device was able to achieve 60% lung delivery efficiency with the AS-EEG formulations, performance was significantly different when delivering the Surfactant-EEG powder. The powder formulations had similar primary particle size characteristics with Dv50's of 1.24 and 1.14  $\mu\text{m}$  for the Surfactant-EEG and AS-EEG formulations, respectively, when measured using laser diffraction (Sympatec HELOS with RODOS/M disperser at 4 bar; Sympatec GmbH, Clausthal-Zellerfeld, Germany). However, the Surfactant-EEG formulation produced a ~2-fold increase in total NT deposition as well as an equivalent decrease in tracheal filter deposition, at the 1.7 L/min flow rate. Differences in powder dispersion properties are likely the driving cause for the change in performance, and increasing the flow rate provides a means to provide additional energy to better deaggregate



the formulation and produce the aerosol. As mentioned in our previous study [27], the optimal flow rate is likely to be device and formulation dependent, and therefore an additional sensitivity analysis was performed for the PD-3 device and the Surfactant-EEG formulation. Lung delivery performance was found to improve when increasing the flow rate to 4 L/min, and then fall when further increased to 6 L/min, likely due to additional turbulence and impaction aerosol losses in the interface and NT airways. Out of the three flow rates tested, the estimated lung delivery efficiency for Surfactant-EEG peaked at nearly 40% with the 4 L/min flow rate; however, NT deposition remained high, between 40-50%.

Additional ways to improve performance with the Surfactant-EEG formulation include the use of a mesh interface or adjusting the shelf height in the aerosolization chamber. Previous investigation on nasal interface design has shown that using a metal mesh incorporated into the nasal interface can significantly reduce NT deposition [28]. With the high NT deposition found with the Surfactant-EEG formulation, inclusion of a mesh may significantly improve performance. Furthermore, the shelf inside the aerosolization chamber of PD-2 and PD-3 has been optimized for the AS-EEG formulation. For example, the shelf in the PD-2 device is positioned such that ~2.6 mg of the AS-EEG powder can fall and rest on the shelf for each actuation. Compared to the density of the AS-EEG powder (~0.10 g/cm<sup>3</sup>), the Survanta<sup>®</sup> based Surfactant-EEG powder was more dense, at approximately 0.18 g/cm<sup>3</sup>, resulting in ~4.7 mg of powder resting on the shelf between actuations, which may diminish aerosolization or create cloud motion phenomenon, which increases the deposition of all elements in the cloud [195, 196]. Adjusting the shelf spacing for each formulation and respective density may prove beneficial.

Limitations of this study include the use of a single preterm NT model, a single nasal interface, and limited number of devices. The use of a single preterm NT airway geometry limits the deposition data to a single point; however, in a previous study investigating nasal interfaces [28], the performance of the infant air-jet platform remained statistically similar across two preterm NT models with very different airway features. Also guided by the previous nasal interface study [28], only a single nasal interface was used in this study, whereas the inclusion of a mesh based design may improve results, specifically for the Surfactant-EEG formulation. Finally, with only 4 unique passive cyclic loading air-jet DPI designs, the range of performance this selection captures are unknown. However, for the devices tested in this study, especially PD-2 and PD-3, the performance meets the initially established lung delivery efficiency goal of 60% with the AS-EEG formulation. Additional testing and modification will need to be explored for other formulations to further improve lung delivery efficiency. While it is anticipated that lung delivery performance will remain relatively unchanged up to dose loadings of 150 mg at a powder bulk density of 0.1 g/cm<sup>3</sup>, this evaluation was not performed in this study.

Considering the example of surfactant replacement therapy using the Survanta<sup>®</sup> based Surfactant-EEG formulation, Kamga Gninzeko [197] evaluated efficacy in an animal model of surfactant depleted rats. Significant improvements in rat pulmonary mechanics were observed with the Surfactant-EEG formulation at a phospholipid (PL) dose of 1.5 mg per kg of animal body weight. Assuming that 1.5 mg/kg of PL will be effective in a human infant, the required Surfactant-EEG powder mass for a body weight of 1.6 kg would be ~20 mg, factoring in 25% PL loading in the formulation and a 50% lung delivery efficiency. Assuming the same conditions, the powder mass loading for a full-term infant with a weight of 3.55 kg would be ~44 mg. Based

on the results of this study, the infant air-jet DPI with passive cyclic loading appears capable of delivering this range of powder dose with minimal expected change in lung delivery performance. Other recent studies on the use of aerosol surfactant replacement therapy in animal models have indicated much higher required doses for positive efficacy, in the range of 100 to 240 mg/kg [198-200] and higher [66, 68, 201]. Through the use of an expanded powder reservoir, it appears that the passive cyclic loading approach could also be used to deliver powder versions of these much higher doses with a single loading of the device and potentially at a controlled rate.

## 6.5 Conclusions

In conclusion, a passive cyclic loading approach was successfully implemented for the infant air-jet DPI platform. During *in vitro* testing using a preterm NT model and AS-EEG formulation, the platform performed consistently when the loaded dose increased from 10 mg to 30 mg and also when connected to the pulmonary mechanics outlet condition. The optimal PD devices (PD-2 and PD-3) achieved an estimated lung delivery efficiency of ~60% when administered through a 1600 g preterm NT model. The performance was notably different when the Surfactant-EEG powder was used, which led to an increase in NT deposition and decrease in tracheal filter deposition. It is likely adjustments to the aerosolization chamber and passive cyclic loading system will be needed for each new formulation. In this study, modifying the flow rate alone produced an increased estimated lung delivery efficiency from 30% to nearly 40% at flow rates of 1.7 and 4.0 L/min, respectively. Additional modifications will likely further improve performance when using a Surfactant-EEG formulation. Further optimization of

the platform with passive cyclic loading will allow for a highly efficient, rapid, and non-invasive form of aerosol delivery to neonates with selectable dosage and expected consistent performance.

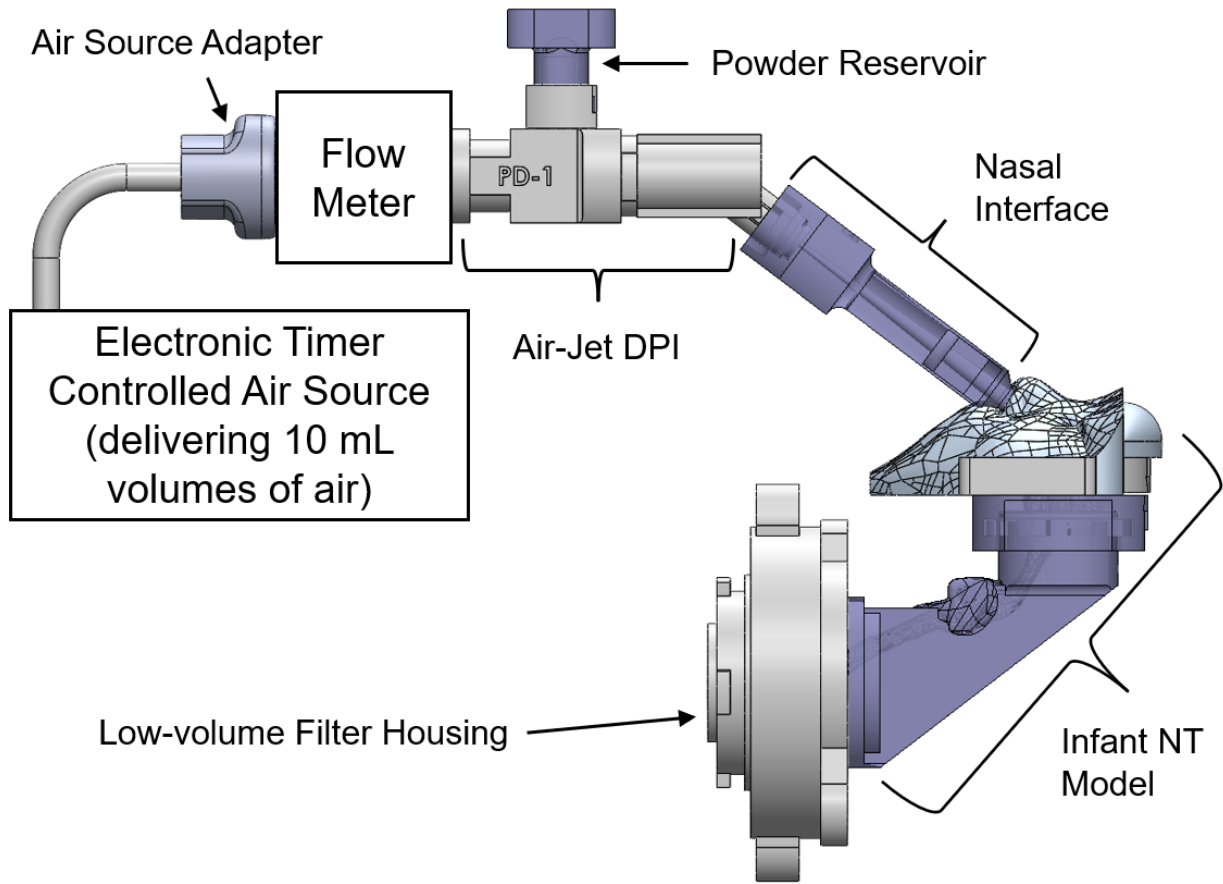


**Figure 6.1** Graphical overview of the experimental setup including the infant air-jet DPI platform with passive cyclic loading

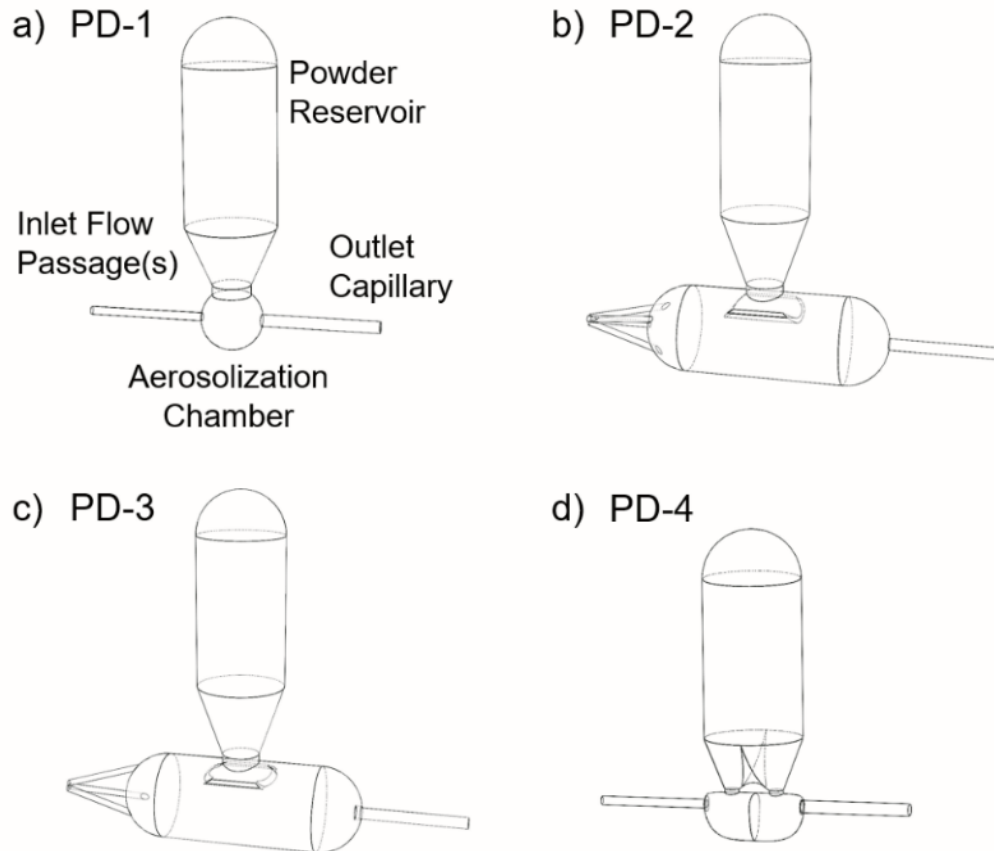


**Figure 6.2** Internal airflow geometry of each infant air-jet DPI passive design (PD) from air source inlet (left side of each image) to the device outlet (right side of each image). Panels **(a)**-**(d)** correspond to PD-1, PD-2, PD-3, and PD-4, respectively

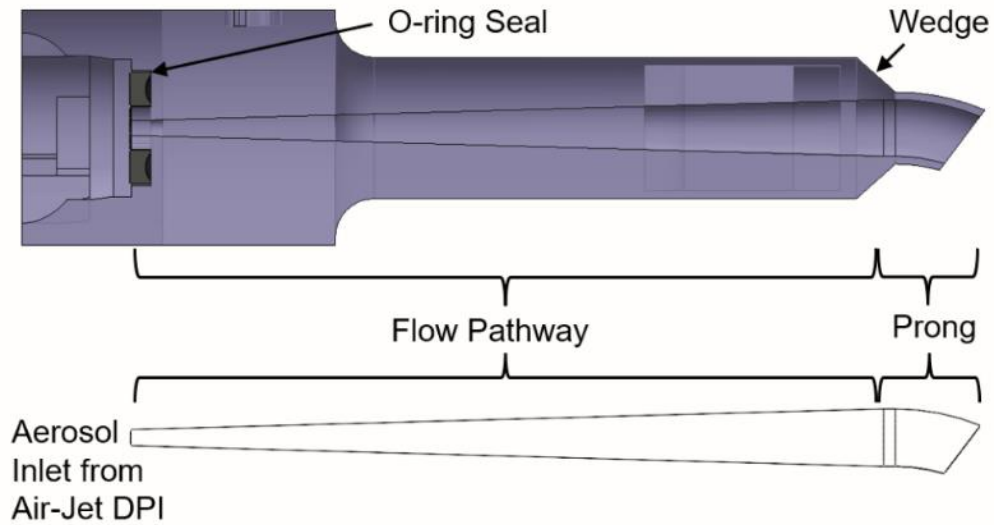


**Figure 6.3** Overview of the single nasal interface used in this study illustrating the flow pathway and prong regions. A cross sectional view rendering (above) depicts interface features including O-ring seal and exterior prong wedge, while the internal airway geometry is pictured below. The nasal prong employed a short curve and was produced in rigid material

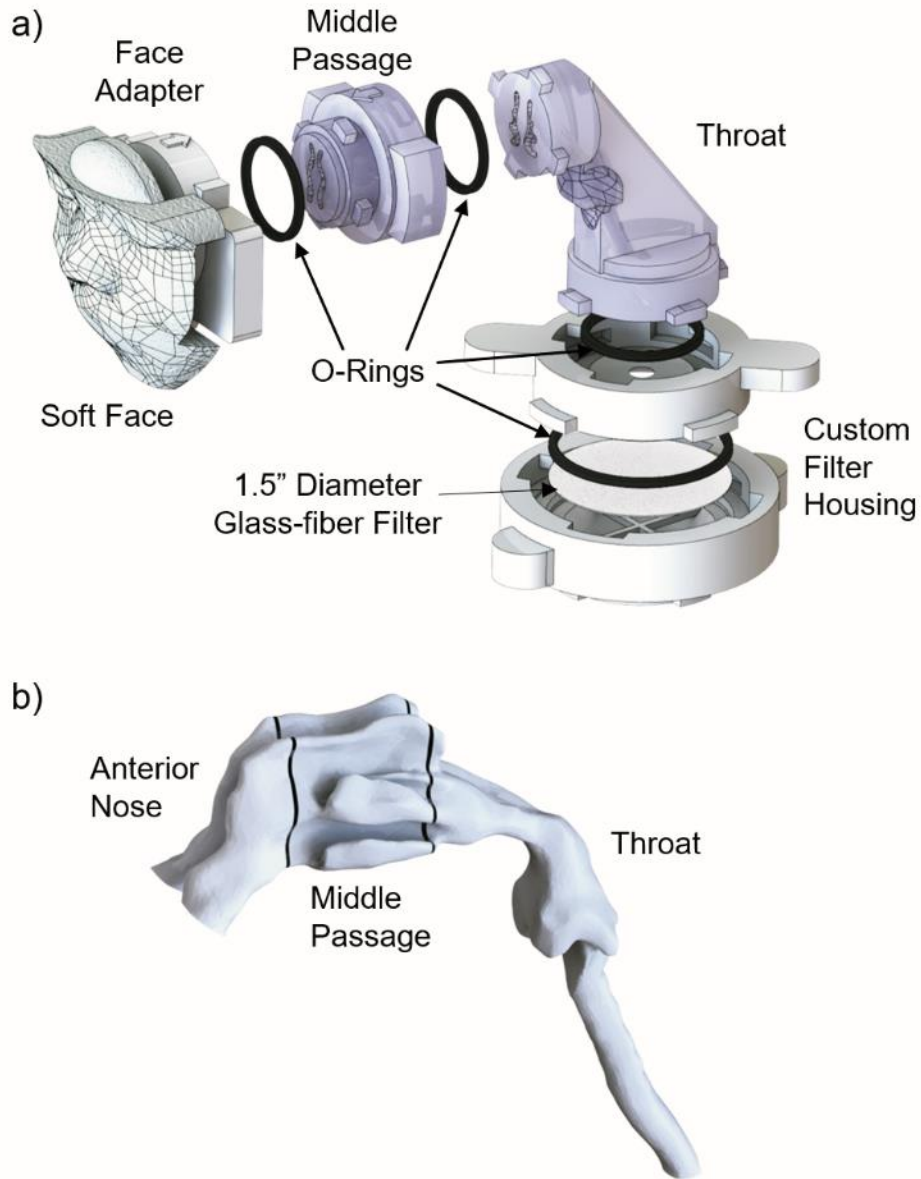


**Figure 6.4** Schematic overview of the preterm infant NT airway model and regional sections. **(a)** Assembly of infant NT model with connection to custom low-volume filter housing with parts labeled (the Soft Face and Face Adapter segments are glued together before use and represent the Anterior Nose airway region). **(b)** Internal airway geometry of the infant NT model with assessed regions including the anterior nose, middle passage and throat



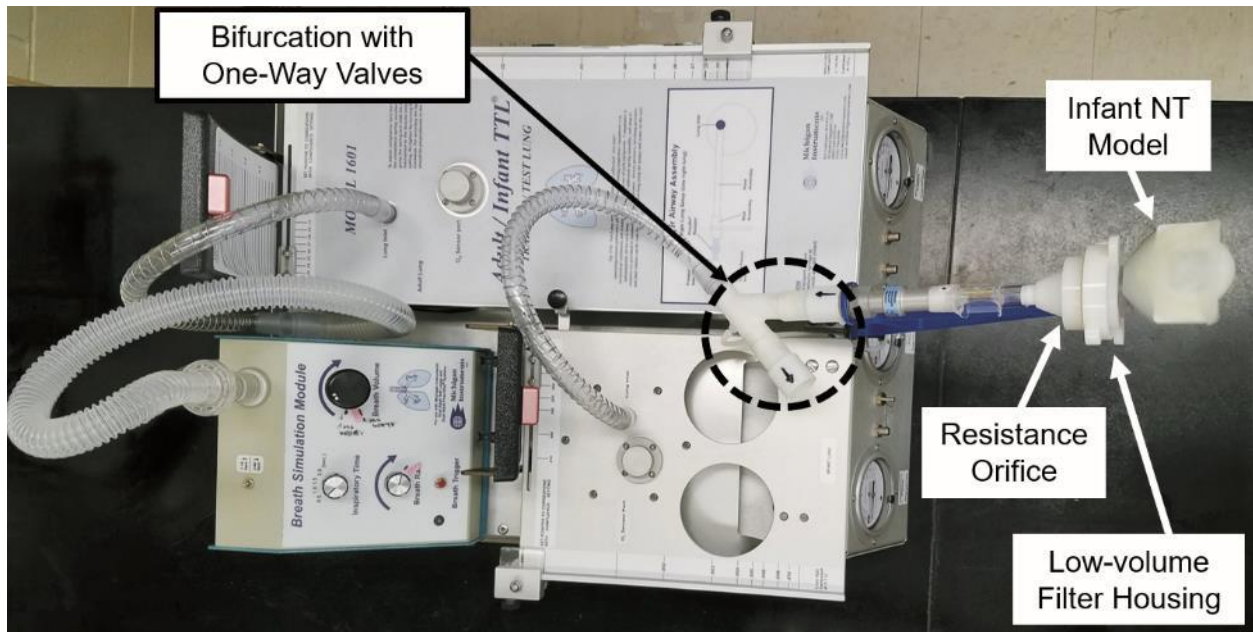


**Figure 6.5** Experimental setup for sensitivity analysis testing with the infant NT model connected to the infant pulmonary mechanics (PM) outlet condition and breathing simulator. All custom components are labeled

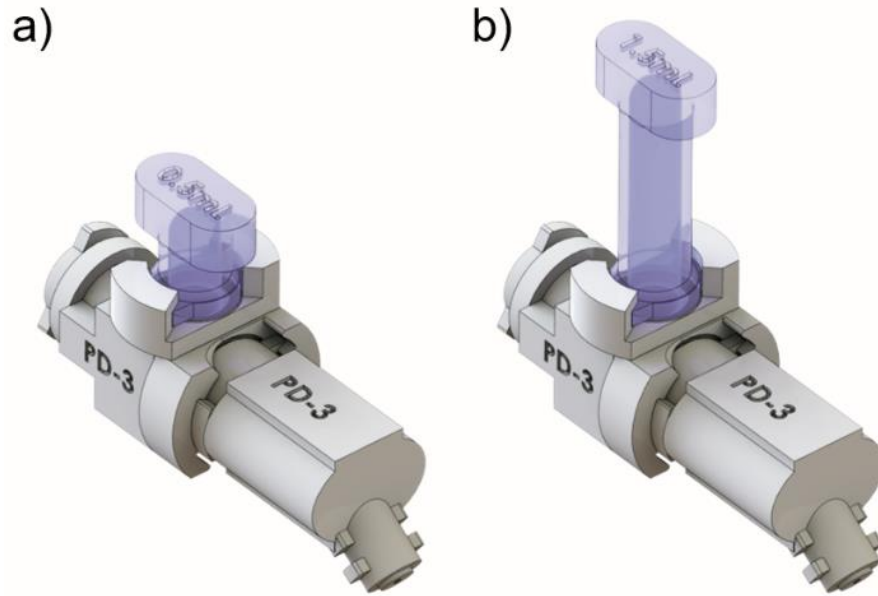
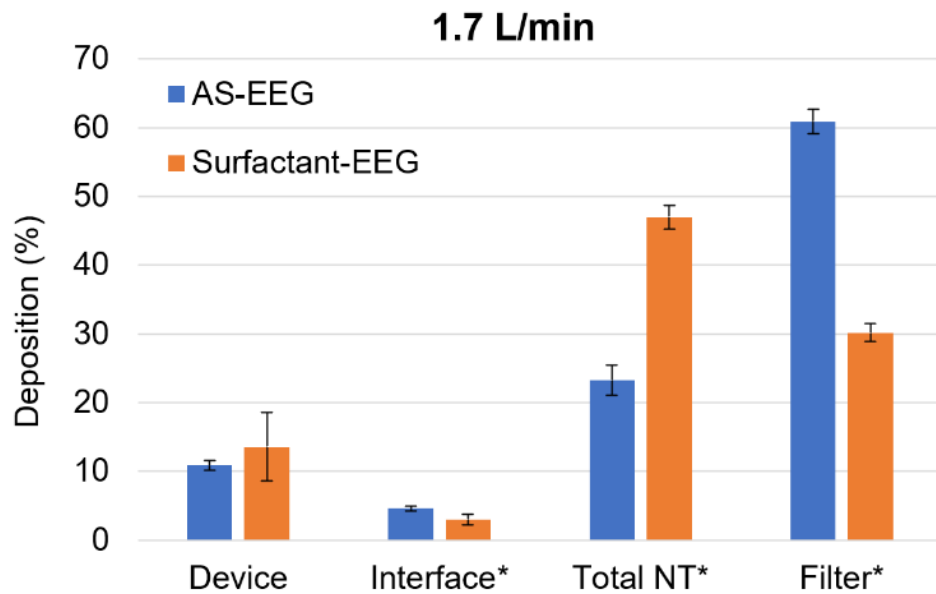
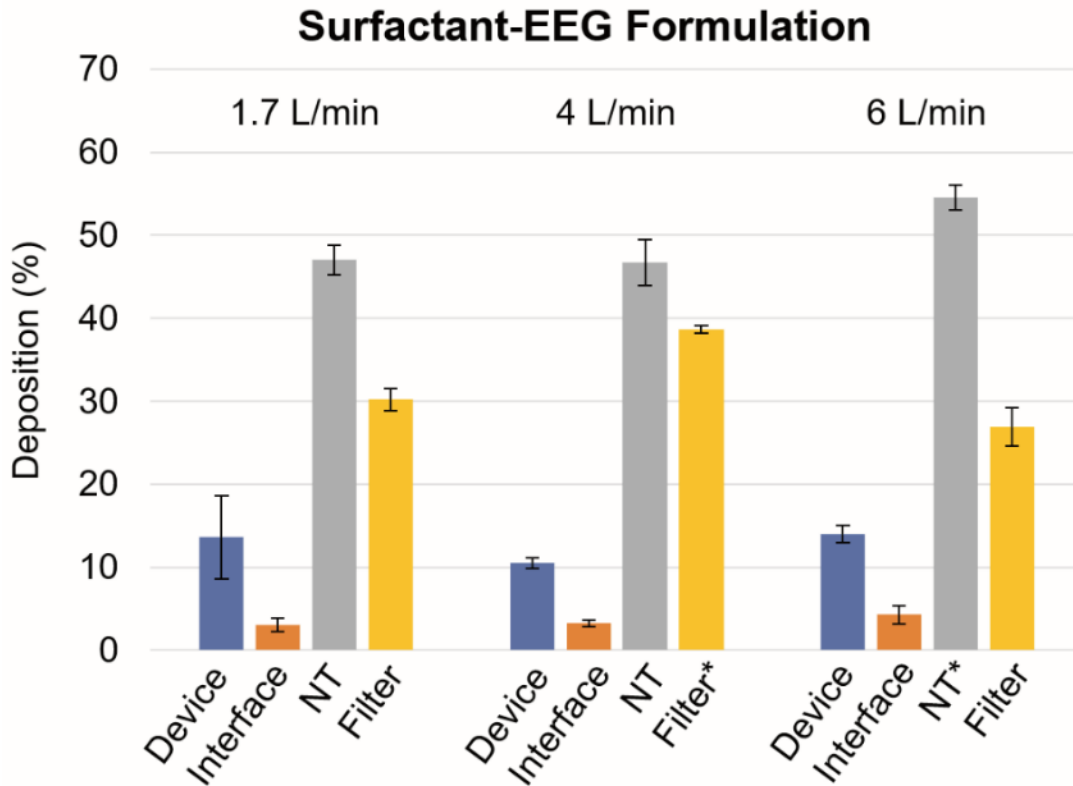


**Figure 6.6** Renderings of the two device configurations for the powder reservoir sensitivity analysis. **(a)** PD-3 device with standard (0.55 mL) volume reservoir attached and **(b)** PD-3 device with extended (1.5 mL) volume reservoir attached



\* $p < 0.05$  significant effect of formulation on deposition region (t-test).

**Figure 6.7** Plot of experimentally determined mean (SD) drug deposition fractions (based on loaded dose) of the AS-EEG formulation compared with the Surfactant-EEG formulation grouped by deposition region, at a Q90 flow rate of 1.7 L/min [n=3]. Anterior nose, middle passage (MP), and throat deposition fractions were summed to form the total NT deposition. Significant effect ( $p < 0.05$ ) of formulation found in the interface, total NT, and filter deposition regions (t test)



\* $p < 0.05$  significant difference compared with 1.7 L/min flow rate (one-way ANOVA followed by post-hoc Tukey).

**Figure 6.8** Experimentally determined mean (SD) drug deposition fractions (based on loaded dose) of the Surfactant-EEG formulation for different Q90 flow rates [n=3]. Anterior nose, middle passage (MP), and throat deposition fractions were summed to form the total NT deposition. Significant difference ( $p < 0.05$ ) found for filter deposition at 4 L/min and for NT at 6 L/min when compared to the original 1.7 L/min case (one-way ANOVA followed by post-hoc Tukey)

**Table 6.1** Lung delivery efficiencies (estimated as Tracheal Filter %) and regional deposition fractions (based on 10 mg loaded dose) for the AS-EEG formulation and an initial round of different device designs

	<b>PD-1</b>	<b>PD-2</b>	<b>PD-3</b>	<b>PD-4</b>
<b># of Actuations</b>	4	5	4	6
<b>Deposition Region</b>				
DPI Retention (%) <sup>a</sup>	16.8 (4.8)	12.9 (1.1)	10.9 (0.7)	33.2 (5.5) <sup>b</sup>
Nasal Interface (%)	5.2 (0.4)	4.3 (0.2)	4.6 (0.3)	4.0 (1.1)
Total ED (%) <sup>a</sup>	77.9 (4.6)	82.8 (1.2)	84.5 (0.4)	62.8 (5.5) <sup>b</sup>
Anterior Nose (%)	4.8 (1.0)	5.4 (1.6)	4.5 (0.3)	3.2 (1.1)
Middle Passage (%) <sup>a</sup>	7.8 (0.9)	7.8 (0.4)	8.4 (1.4)	5.0 (1.3) <sup>b</sup>
Throat (%)	11.5 (3.1)	9.1 (0.9)	10.4 (1.3)	6.3 (4.6)
Total NT (%)	24.1 (4.9)	22.3 (1.1)	23.2 (2.1)	14.4 (7.0)
Tracheal Filter (%) <sup>a</sup>	53.1 (1.7)	60.0 (0.6) <sup>b</sup>	60.9 (1.9) <sup>b</sup>	46.2 (2.1) <sup>b</sup>

Mean values with standard deviations (SD) shown in parenthesis, n=3.

<sup>a</sup> $p < 0.05$  significant effect of design on deposition region (one-way ANOVA).

<sup>b</sup> $p < 0.05$  significant difference compared to PD-1 case (post-hoc Tukey).

PD, passive design

**Table 6.2** Lung delivery efficiencies (estimated as Tracheal Filter %) and regional deposition fractions (based on loaded dose) for the AS-EEG formulation and comparisons of 10 vs 30 mg loaded powder in lead devices

	PD-2		PD-3	
	10mg	30mg	10mg	30mg
<b># of Actuations</b>	5	11	4	8
<b>Deposition Region</b>				
DPI Retention (%)	12.9 (1.1)	16.1 (2.1)	10.9 (0.7)	12.2 (2.9)
Nasal Interface (%)	4.3 (0.2)	2.4 (0.1) <sup>a</sup>	4.6 (0.3)	2.8 (0.4) <sup>a</sup>
Total ED (%)	82.8 (1.2)	81.5 (2.0)	84.5 (0.4)	85.0 (3.3)
Anterior Nose (%)	5.4 (1.6)	3.3 (0.3)	4.5 (0.3)	3.7 (0.5) <sup>a</sup>
Middle Passage (%)	7.8 (0.4)	8.2 (0.3)	8.4 (1.4)	8.3 (0.5)
Throat (%)	9.1 (0.9)	10.6 (0.9)	10.4 (1.3)	12.3 (1.3)
Total NT (%)	22.3 (1.1)	22.1 (1.0)	23.2 (2.1)	24.4 (1.3)
Tracheal Filter (%)	60.0 (0.6)	58.5 (1.3)	60.9 (1.9)	60.5 (1.6)

Mean values with standard deviations (SD) shown in parenthesis, n=3.

<sup>a</sup>p<0.05 significant difference in deposition region compared with 10 mg case (*t* test).

**Table 6.3** Lung delivery efficiencies (estimated as Tracheal Filter %) and regional deposition fractions (based on loaded dose) of the AS-EEG formulation and 30 mg dose loadings with the PD-3 device and filter-only vs. pulmonary mechanics (PM) outlet conditions

<b>Deposition Region</b>	<b>Filter-Only</b>	<b>PM</b>
DPI Retention (%)	12.2 (2.9)	10.5 (1.1)
Nasal Interface (%)	2.8 (0.4)	1.7 (0.5) <sup>a</sup>
Total ED (%)	85.0 (3.3)	87.8 (1.4)
Anterior Nose (%)	3.7 (0.5)	3.7 (0.4)
Middle Passage (%)	8.3 (0.5)	7.9 (0.9)
Throat (%)	12.3 (1.3)	12.3 (0.7)
Total NT (%)	24.4 (1.3)	23.9 (0.7)
Tracheal Filter (%)	60.5 (1.6)	62.6 (1.4)

Mean values with standard deviations (SD) shown in parenthesis, n=3.

<sup>a</sup> $p < 0.05$  significant difference between filter-only and PM outlet condition for nasal interface deposition (*t* test).

PM, pulmonary mechanics outlet condition

**Table 6.4** Lung delivery efficiencies (estimated as Tracheal Filter %) and regional deposition fractions (based on loaded dose) for the AS-EEG formulation and comparisons of standard (0.55 mL) vs extended (1.5 mL) powder reservoir volume with the PD-3 device

<b>Deposition Region</b>	<b>Standard</b>	<b>Extended</b>
DPI Retention (%)	10.9 (0.7)	15.5 (0.9) <sup>a</sup>
Nasal Interface (%)	4.6 (0.3)	4.5 (0.3)
Total ED (%)	84.5 (0.4)	79.9 (1.1) <sup>a</sup>
Anterior Nose (%)	4.5 (0.3)	4.9 (0.8)
Middle Passage (%)	8.4 (1.4)	9.6 (0.2)
Throat (%)	10.4 (1.3)	11.1 (0.8)
Total NT (%)	23.2 (2.1)	25.6 (1.0)
Tracheal Filter (%)	60.9 (1.9)	54.5 (2.3) <sup>a</sup>

Mean values with standard deviations (SD) shown in parenthesis, n=3.  
<sup>a</sup>p<0.05 significant difference between standard and extended chamber volume (*t* test).



# Chapter 7 - Advancement of the Infant Air-Jet DPI Platform with Passive Cyclic Loading and Passive Metering Elements for Various Formulations

## Task 2.2 – Publication Pending

### 7.1 Introduction

Delivery of pharmaceutical aerosol to infants has seen significant challenges, most notably poor lung delivery efficiency, high inter-subject dose variability and long administration times [53-57]. Poor lung delivery efficiencies have been documented in most *in vivo* and realistic *in vitro* infant studies, resulting in lung delivery efficiency values in the range of 0-10% of the loaded or nebulized dose [52, 58, 59, 61, 67, 114-116] across multiple inhalation platforms. A recent example of poor infant lung delivery efficiency is the *in vivo* study of Corcoran et al. [117], in which a nebulized radiopharmaceutical aerosol was administered to 18 infants while receiving nasal cannula oxygen, and it was estimated that only 0.46% of the nebulized dose reached the lungs at a cannula flow rate of 2 L/min. Poor lung delivery efficiency as well as high inter-subject variability has been observed in the *in vivo* study of Fok et al. [12], in which a group of 13 spontaneously breathing infants received two actuations of radio-labelled salbutamol delivered through a metered dose inhaler (MDI). Lung delivery efficiencies across the population were all <2.5% of the loaded dose, with one infant receiving a dose of 0.25 µg and another 4.52 µg, indicating an order of magnitude difference between doses received by different subjects. Similar high inter-subject dose variability has also been observed for nebulized aerosol delivered via nasal prongs; in the study of Linner et al. [49], 8 piglets

received between 2% and 40% of the nebulized dose (radio-labelled surfactant), furthermore, with most of the dose found in the dependent lung it is uncertain if the dose to the dependent lung was delivered in aerosol form. Low lung delivery efficiencies and high inter-subject variabilities can often lead to extended treatment times, and when administering medications that require relatively high lung doses or that have a narrow therapeutic window, poor clinical responses or elevated off-target effects can be expected.

To better address the challenges associated with pharmaceutical aerosol delivery to infants, our group [26-29] is developing an infant air-jet dry powder inhaler (DPI) platform for rapid and efficient administration. Overall, the infant air-jet DPI is designed to provide a full inhalation breath along with the aerosol to the lungs of an infant through the nasal route. The platform consists of an air source (providing aerosolization energy and inhalation breath), the air-jet DPI (responsible for holding the loaded powder and aerosolizing metered doses per actuation), and the nasal interface which transports the aerosol from the DPI to the infant's nasal passage, forming an airtight seal with the infant's nostrils. Previous development of the infant air-jet DPI platform have evaluated the effects of the aerosolization chamber geometry [26], air source and flow rate [27], infant nasal interfaces [28], and a passive cyclic loading scheme [29].

In the most recent study by Howe et al. [29], a passive design (PD) for the air-jet DPI was developed as a passive cyclic loading scheme, which utilized already present gravity and hydrodynamic forces. The PD air-jet DPI employed an initial powder reservoir capable of holding up to ~50 mg of a model powder formulation while an extended volume reservoir (~3-fold larger) was also explored, and found to produce a slight decrease in performance. Overall,

the best performing configurations of the infant air-jet DPI platform were able to deliver >60% of the loaded dose to a tracheal filter through an *in vitro* preterm nose-throat (NT) model and was found to be insensitive to increasing the loaded powder mass from 10 to 30 mg, as well as being insensitive to downstream pulmonary mechanics [29]. While previous configurations worked well for the model formulation, adjustments will likely be needed for different formulations.

The infant air-jet DPI platform is viewed as a general aerosol delivery platform capable of providing high efficiency lung delivery of pharmaceutical aerosols. Initial development of the platform revolved around administering inhaled surfactant for surfactant replacement therapy [91, 177], however, additional potential applications include inhaled antibiotics to treat bacterial pneumonia [186], and inhaled antivirals to treat RSV and severe viral pneumonia [187, 188]. Different dry powder pharmaceutical formulations and doses would be needed for each envisioned application. While the previously developed PD air-jet DPI [29] is expected to perform similarly when delivering 10-50 mg of model powder, continued consistent performance will likely be needed for a larger range to accommodate larger dose requirements or lower density powder formulations. Considering the infant air-jet DPI platform applied to various therapeutic applications, what is needed are design parameters will enable increased powder mass loadings as well as different powder formulation loadings without impacting the high lung delivery efficiency.

While maintaining previously established dimensions and flow conditions conducive for high efficiency aerosolization [26-28], the PD-2 air-jet DPI device [29] employed a powder reservoir located above a powder shelf in the aerosolization chamber as a means to control the

dose loaded into the aerosolization chamber for each actuation while protecting the bulk of the powder. To enable consistent performance of the platform across multiple powder formulations, *passive metering elements* will need to be identified to allow for tuning of the air-jet DPI without significant device changes. The positioning or volume (amount of powder that can rest on the shelf inside the aerosolization chamber) of the powder shelf is a potential metering element, as well as the geometry or diameter of the powder reservoir opening into the aerosolization chamber. Adjustment of the two elements mentioned should allow for controlling the amount of powder transferring from the powder reservoir to the aerosolization chamber during each actuation, which could affect the aerosolization performance and ED per actuation. If the *passive metering elements* can adjust the performance of the air-jet DPI across multiple formulations, then the platform should be tunable for different therapeutic applications. The goal is to identify configurations based on modification of the metering elements which can later be implemented as adjustable features of a single air-jet DPI design able deliver various dry powder formulations with high efficiency. Accomplishing this goal with the given conditions presents a significant challenge in aerosol delivery.

The objective of this study was to advance the infant air-jet DPI with a passive cyclic loading to enable a high dose powder reservoir with no performance loss and establish design modification parameters for different formulations, and characterize aerosol performance with relative best case configures for multiple formulations. This study also explored the air-jet DPI emptying characteristics as far as the emitted dose (ED) per actuation for both 10 and 30 mg powder mass loadings. The study begins by obtaining baseline excipient enhanced growth (EEG) formulation aerosolization characteristics (*in vitro* preterm NT model performance and particle

sizing) using the model spray-dried (EEG) formulation and PD air-jet DPI actuated at 4 L/min. Next, to overcome slight performance changes previously seen with a larger powder reservoir, and adjustable volume powder reservoir is investigated as well as the air-jet DPI emptying characteristics. Finally, passive metering elements are investigated and the aerosolization characteristics of relative best-case configurations for each formulation determined and compared.

## **7.2 Materials and Methods**

### *Powder Materials and Formulation*

Albuterol sulfate (AS) and l-leucine were purchased from Sigma Chemical Co. (St. Louis, MO). Pearlitol® PF-Mannitol was donated from Roquette Pharma (Lestrem, France) and Poloxamer 188 (Leutrol F68) was donated from BASF Corporation (Florham Park, NJ). Trileucine was purchased from Bachem Americas, Inc. (Torrance, CA). Sodium chloride, ethanol and methanol were purchased from Fisher Scientific Co. (Hanover Park, IL). Survanta® (beractant) intratracheal suspension was purchased from Cardinal Health, Inc. (Greensboro, NC). Dipalmitoylphosphatidylcholine (DPPC) and B-YL (surfactant protein B mimic peptide) were purchased from Avanti Polar Lipids, Inc. (Alabaster, AL) and CSBio (Menlo Park, CA), respectively. Throughout the study, freshly collected deionized water was used.

A batch of AS excipient enhanced growth (AS-EEG) powder was obtained using a Büchi Nano B-90 HP Spray Dryer (Büchi Laboratory-Techniques, Flawil, Switzerland), and spray-dried based on the optimized method described by Son et al. [76]. The AS-EEG powder formulation included 30:48:20:2% w/w ratio of AS, mannitol, trileucine, and Poloxamer 188, respectively. A

feed solution of 150 mL containing the dissolved drug and excipients at the stated ratio was sprayed at a spray rate of 0.64 mL/min. The solids concentration in the feed solution was 0.5% w/v. Throughout the spray drying process, the inlet temperature was set to 120 °C, resulting in an outlet temperature of 47-49 °C. The feed solution temperature was <15 °C during the spray drying as excess feed solution was recycled into the stock.

Two batches of Survanta<sup>®</sup> based surfactant EEG (Survanta-EEG) powders were prepared by spray drying of the feed dispersions containing Survanta<sup>®</sup>, mannitol, sodium chloride and l-leucine at a ratio of 40:30:10:20% w/w using the Buchi Nano Spray Dryer B-90 HP (Büchi Labortechnik AG, Flawil, Switzerland). The feed dispersions were prepared with 0.125% w/v solids by addition of all the formulation components to 5% v/v ethanol in water followed by 40 min sonication in a heated water bath (Fisher Scientific™ CPXH, Hanover Park, IL) at 45-55°C. The prepared feed dispersions were spray-dried with the spray dryer in an open mode configuration using the small nozzle and the following optimized operating conditions reported by Boc et al. [90]. Throughout the spray drying process, the inlet temperature was set to 70 °C, resulting in an outlet temperature of 36-38 °C. The spray-dried powders were collected from the electrostatic precipitator into glass vials and stored in a desiccator (0% RH) in the freezer (-20 °C) when not in use.

The synthetic lung surfactant powder formulation (DPPC-BYL3-EEG) was prepared by spray drying of feed dispersions containing DPPC, B-YL, hygroscopic excipients (mannitol and sodium chloride) and dispersion enhancer (l-leucine) (at a ratio of 25:3:42:10:20) using the Buchi Nano Spray Dryer B-90 HP (Büchi Labortechnik AG, Flawil, Switzerland) following the same procedure as previously reported [177]. Briefly, the feed dispersions of 0.125% w/v solids

were prepared by addition of all the formulation components to an ethanol-water (5:95% v/v) co-solvent system followed by 40 min sonication in a heated water bath (45-55°C) with every 10 min intermittent manual shaking. The prepared feed dispersions were spray-dried using the small nozzle at a spray rate of 0.5 L/min. Throughout the spray drying process, the inlet temperature was set to 70 °C, resulting in an outlet temperature of 35-39 °C. During spray drying, the feed dispersion was continuously stirred using a magnetic stirrer as excess feed dispersion was recycled into the stock. The spray-dried powders were collected from the electrostatic precipitator into glass vials and stored in a desiccator (0% RH) in the freezer (-20 °C) by keeping the glass vial's lid closed.

#### *Infant Air-Jet Platform and Experimental Overview*

The infant air-jet DPI platform initially developed [26-28] is comprised of three main components: the air source, the air-jet DPI, and the nasal interface. The air source provides the aerosolization energy to the air-jet DPI, and delivers the aerosolized powder to the lungs while providing a full inhalation breath for the infant. For all experiments in this study, the electronic *Timer* air source was utilized as developed and described by Howe et al. [27]. The air source at baseline conditions delivers an air actuation volume (AAV) of 10 mL bursts at a Q90 flow rate of 4 L/min. A neonatal mass flow meter (Sensirion SFM3400, Sensirion AG, Stafa, Switzerland) was used to calibrate and verify the air source actuation parameters. **Figure 7.1** shows the location of the mass flow meter connected between the air source and air-jet DPI, as well as the overall infant nose-throat (NT) experimental setup. The air-jet DPI (PD-2 device) developed for passive cyclic loading [29] consists of small diameter flow pathways for the inlets and outlet connected

by an aerosolization chamber with a powder reservoir above (**Figure 7.2**) and is responsible for aerosolization of the powder as well as metering and holding the full dose of powder. **Figure 7.2b** highlights the small diameter flow pathway configuration for the inlets, with two upward angled jets positioned to pass below the metering shelf. After exiting the air-jet DPI, the aerosolized powder then passes through the nasal interface and to the infant (**Figure 7.1**). The prong of the nasal interface was inserted approximately 5 mm into the nose, consistent with short ventilation support nasal prongs and forms an airtight seal with an infant's nostril.

As with our previous study developing the passive design (PD) air-jet DPI [29], a single nasal interface was used for all experiments in this study consisting of a gradually expanding flow pathway and rigid curved prong (**Figure 7.3**). A gradual exterior taper was included at the base of the prong, forming a wedge to help facilitate an airtight seal with the infant's nostril. **Figure 7.3** shows a rendering of the nasal interface (above) connected to the outlet of the air-jet DPI, with an axial cross section below. The nasal interface was built using stereo-lithography (SLA) with Accura ClearVue resin through 3D Systems On Demand Manufacturing.

All custom parts (air-jet DPI, nasal interface, NT model, and filter housing/collection assembly parts) were designed in SolidWorks (Dassault Systèmes, Paris, France), and exported as .STL files. The parts were then 3D printed at either 32  $\mu\text{m}$  resolution on a Stratasys Objet24 3D Printer (Stratasys Ltd., Eden Prairie, MN) using VeroWhitePlus resin, or with stereo-lithography (SLA) using Accura ClearVue resin through 3D Systems On Demand Manufacturing with a layer thickness of 0.05 mm. All parts were designed to interconnect using a twist lock mechanism with an intermediate O-ring for an air-tight seal.



In our previous study developing the passive cyclic loading platform, a slight, but statistically significant decrease in performance (~5% lower lung delivery efficiency) was observed [29] when increasing the powder reservoir volume to accommodate large powder doses and lower density formulations. The initial portion of this study investigates device performance of the PD-2 air-jet DPI operated at 4 L/min, and a different powder reservoir approach to mitigate the decrease in performance with various reservoir volumes. The emitted dose (ED) per actuation of the platform is also considered, as dose delivery and variability are a potential concern for rapid administration of a dry powder aerosol. Initial platform performance is determined using a preterm infant nose-throat (NT) *in vitro* model and a 10 mg loaded powder mass of AS-EEG formulation. As seen in **Figure 7.1**, the platform interfaces with the preterm NT model which leads to a custom low-volume filter for approximating lung delivered dose. In this setup, device ED, nasal interface deposition, NT regional depositions, and lung delivery efficiency (represented by aerosol passing through the larynx and portion of the trachea and depositing on the filter) were assessed, as percentage values of the loaded dose. Aerosol characteristics of the air-jet DPI (excluding nasal interface), in terms of mass median aerodynamic diameter (MMAD) and fine particle fractions (FPFs), are determined through impaction testing using a next generation impactor (NGI). The main portion of this study then explored dose metering element configuration across multiple EEG formulations to achieve best or similar performance compared to the model AS-EEG formulation. Two metering elements were found to significantly affect the performance of the platform across different formulation which include the shelf height (volume of powder allowed to rest on the shelf

between actuations) and the diameter of the powder reservoir connection to the aerosolization chamber (affecting number of required actuations for lower density powders).

#### *Preterm Infant Nose-Throat (NT) Model*

A single preterm NT *in vitro* model was used in this study as previously developed [27, 28]. The scaled 6-month preterm NT airway model includes flexible nostrils and anterior nose affixed to a rigid adapter piece that connects to a rigid middle passage and throat region that extends through approximately 3/4<sup>th</sup> of the trachea. The NT model then connects to a custom low-volume filter housing. Briefly; the preterm infant airway geometries were scaled down to an infant with a weight of 1600 g and length (height) of 40.7 cm, based on a high-quality CT scans of 6-month-old infant NT geometry [79], using a geometric scaling factor of 0.6 based on Fenton preterm growth charts [167]. **Figure 7.4a** shows side, front, and top views of the resulting preterm airway geometry, which had a tracheal length and diameter (proximal) of approximately 26 and 3 mm, respectively, which falls within the range for preterm infants of 25 to 30 weeks gestational age (GA) based on reported studies [168]. **Figure 7.4a** also depicts the regional segments used for analysis (anterior nose, middle passage, and throat regions).

The scaled 6-month preterm NT model was constructed with twist lock interfaces and O-rings that provided air tight seals and facilitated ease of use. The low-volume (LV) filter housing accommodated the low AAV of 10 mL used for a preterm infant, with a dead space of only 2.7 mL before the 1.5" diameter glass-fiber filter. To provide a smooth and accurate internal airway surface, the middle passage and throat sections of the preterm NT model were built using SLA printing with Accura ClearVue resin (3D Systems). The low-volume filter housing was 3D printed

with using VeroWhitePlus resin. To facilitate nasal interface prong insertion and the formation of an airtight seal, the face and anterior nose section were molded with a skin-like silicone elastomer and glued to a rigid adapter piece (printed using VeroWhitePlus resin), which allowed for a secure and air-tight connection to the rest of the NT model. The three distinct airway regions of the NT model used for regional deposition quantification (anterior nose, middle passage, and throat) are illustrated in **Figure 7.4a** and **b**. **Figure 7.4b** presents a rendering of the assembled NT model connected to the LV filter housing with a custom cross-sectional cut to highlight the airway geometry starting at the left nostril and moving through the left nasal passage, then continuing through the trachea and leading to the filter housing.

#### *In Vitro Evaluation of Preterm Lung Delivery Efficiency*

To determine aerosol deposition in the nose-throat regions, and effective lung delivery efficiency (drug deposited on the filter), experiments utilized the scaled 6-month preterm NT *in vitro* model. The nasal interface, shown in **Figure 7.3**, was inserted approximately 5 mm into the left nostril of the infant NT model and during the actuation and breath hold, the right nostril was manually held closed. A small amount of lubricant grease was applied to the exterior of the prong before insertion to ensure an airtight seal. Before assembly, all internal airways of the NT model segments were coated with a silicon spray to minimize particle bounce and simulate airway surface liquid. At the end of the NT model, the custom LV housing collected powder passing through the extrathoracic regions and depositing on the filter, represented the amount of drug delivered to the lung. Calculations for ED and regional depositions, including the nasal interface and in the NT model regions and tracheal filter, were expressed as a percentage of the

manually weighed loaded dose. All experiments were performed in triplicate for the calculation of mean and standard deviation values. More detail on the regional deposition fractions can be found in the “*Drug Mass Characterization Methods*” subsection.

#### *Adjustable Powder Reservoir*

To enable consistent performance across a range of loaded doses, several large volume (1.5 mL) powder reservoir designs were investigated. The lead design utilized a powder reservoir with an open top and sliding insert for an adjustable volume reservoir depending on the loaded dose. **Figure 7.5** shows the standard volume reservoir (0.55 mL) and the adjustable volume reservoir (up to 1.5 ml). For a smooth interior wall, the adjustable powder reservoir was constructed in the same manner as the standard volume reservoir, using SLA printing with Accura ClearVue resin (3D Systems). The initial prototype and testing version of the adjustable insert was 3D printed using VeroWhitePlus resin, with two concentric O-rings at the tip to provide an airtight seal, and a central hole allowing for venting during position adjustment and required sealing (placing a finger on top) during actuation. The adjustable powder reservoir is designed to allow loading any volume of powder (up to 1.5 mL) and then remove the dead space in the powder reservoir by positioning the adjustable insert just above the resting powder. The venting hole remained open during positioning to allow dead space air to exit through the insert and not compress or force the loaded powder into the aerosolization chamber. While the procedures for the initial test design were manageable in a laboratory setting, a final version would utilize an automatic vent seal scheme in which opening the vent

for positioning would require a push or squeeze button configuration that seals automatically after positioning.

#### *Device Emptying Characterization*

To address concerns of delivering large doses too quickly or inconsistently over the course of a full dose administration, a device emptying characterization study was performed with the AS-EEG formulation. An aerosol collection assembly was designed and 3D printed using VeroWhitePlus resin and is assembled with intermediate O-ring seals for an airtight seal, as pictured in **Figure 7.6**. The air-jet DPI was inserted into the collection assembly as pictured which allowed the aerosol exiting the outlet of the air-jet DPI to be collected on the filter as co-flow room air was being pulled through the collection assembly at 45 L/min. **Figure 7.6b** shows an inside cut view of the collection assembly with glass-fiber filter and O-ring locations. The emptying characterization was performed in triplicate for both small (10 mg) and large (30 mg) powder loadings. For the 10 mg loaded dose, the air-jet DPI was actuated 5 times, while the 30 mg loaded dose used 10 actuations. Between each actuation of the air-jet DPI, the collection assembly was opened to replace the filter, such that the emitted dose for each actuation could be quantified individually.

#### *Aerosolization Performance and Characterization*

Consistent with previous studies by our group, the air-jet DPI aerosol performance and characterization experiments utilized a Next Generation Impactor (NGI; MSP, TSI Incorporated, Shoreview, MN) for aerosol particle size analysis. To assess the aerosol size distribution, the air-

jet DPI (without the nasal interface) was attached to the pre-separator inlet of the NGI using a custom adapter, as seen in **Figure 7.7**. The adapter positioned the outlet of the air-jet DPI one cm away, perpendicular from the center of the pre-separator inlet with open space allowing for co-flow room air to enter the NGI, which was operated at a flow rate of 45 LPM using a downstream vacuum pump. The NGI was positioned 53° off horizontal using an angle guide (#6, **Figure 7.7**) to allow the device to remain level during use and maintain an inline flow path from the device outlet to the NGI inlet as would be during administration to a supine infant. Each stage of the NGI was coated with MOLYKOTE® 316 silicone spray (Dow Corning, Midland, MI) to minimize particle bounce and re-entrainment. The NGI flow rate of 45 LPM was chosen to ensure collection of the aerosol, minimize any effects of settling, and provide appropriate stage cutoff diameters for evaluating small aerosol sizes. Before each set of experimental runs, the flow rate was confirmed using a flow sensor (Sensirion SFM3000, Sensirion AG, Stafa, Switzerland) connected to the NGI inlet.

The air-jet DPI was loaded with 10 mg of powder and actuated into the NGI via the electronic Timer air source using a 10 ml AAV. Three replicate runs for each experiment were performed. Analysis metrics included emitted dose (ED), mass median aerodynamic diameter (MMAD), fine particle fraction (FPF), and geometric standard deviation (GSD). ED was calculated as the mass of AS in the loaded dose minus the mass of AS remaining in the device divided by the initial loaded mass of AS. Aerosolization calculations were based on the mass of AS recovered in the NGI (including pre-separator fractions if possible). Based on an airflow rate of 45 L/min, the NGI stage cut-off diameters were determined using the formula specified in USP 35 (Chapter 601, Apparatus 5). The MMAD was calculated through linear interpolation

between appropriate stages using a plot of cumulative percentage drug mass vs. cut-off diameter. The FPF, either 5 or 1  $\mu\text{m}$ , was calculated as the fraction of recovered particles with an aerodynamic diameter  $\leq$  5 or 1  $\mu\text{m}$ , respectively. The GSD was calculated as the square root of the ratio of the 84.1 percentile over the 15.9 percentile of the cumulative drug mass percentage. Drug masses were determined using HPLC analysis, as described in the next subsection.

#### *Drug Mass Characterization Methods*

After the final actuation for the AS-EEG formulation, drug masses retained or deposited on each deposition region (air-jet DPI, nasal interface, NT model regions, NGI stages, and/or filters) were recovered by dissolving in an appropriate volume of deionized water followed by high performance liquid chromatography (HPLC) analysis with fluorescence detection (excitation = 276 nm, emission = 609 nm). A sample injection volume of 10  $\mu\text{L}$  was used, and a Restek Allure PFP propyl column (5  $\mu\text{m}$ , 60  $\text{\AA}$ , 150 x 2.1 mm) produced chromatographic separation with a mobile phase flow rate of 0.4 mL/min. The mobile phase consisted of methanol and ammonium formate buffer (20 mM, pH 3.4 through addition of formic acid) in a ratio of 70:30. The loaded drug mass was determined through content uniformity analysis of the AS-EEG formulation; where known masses of AS-EEG were dissolved in water and the AS content ( $\mu\text{g}/\text{mg}$  of formulation) was determined. AS quantification was performed for each deposition site and for the total drug mass used to calculate the drug recovery. Drug recovery percentages were expressed as the sum of the amount of AS recovered in each deposition region divided by the loaded AS dose for each experiment.

For the Survanta-EEG and DPPC-BYL3-EEG formulation, the surfactant content was determined based on the content of dipalmitoylphosphatidylcholine (DPPC). The DPPC content was quantified using a liquid chromatography–mass spectrometry (LC-MS) method adapted from Li et al. [194]. The system consisted of the Quattro micro™ mass spectrometer linked to an Alliance 2695 Separations Module with data acquisition software (Waters Corporation, Milford, MA) and used an injection sample volume of 10 µL. The chromatographic separation was achieved using the Atlantis hydrophilic interaction liquid chromatography (HILIC) silica column (5 µm, 50×1.0 mm; Waters Corporation, Milford, MA). The isocratic mobile phase was pumped at a flow rate of 0.3 mL/min and consisted of acetonitrile and 5 mM ammonium formate in water with 0.1% formic acid (88:12% v/v). Following chromatographic separation and optimization of the ionization settings of the mass spectrometer, selected ion monitoring (SIM) analysis (for  $m/z = 735$ ) with positive electrospray ionization mode was applied to detect and quantify DPPC (molecular weight = 734 Daltons). A DPPC stock standard solution (20 µg/mL) was prepared by dissolving sufficient amount of DPPC (Avanti Polar Lipids, Inc., Alabaster, AL) in methanol. The diluted standard solutions of DPPC in the concentration range of 2 to 20 µg/mL were prepared by further dilution of the stock standard solution in methanol. The prepared stock standard and diluted standard solutions were injected as calibration standards. To determine the content uniformity of each formulation, approximately 1 mg of each powder was dissolved in 25 mL of methanol and quantitatively analyzed for the DPPC content by the LC-MS method described above. Triplicate samples were prepared and analyzed for each of the powder formulation samples and the mean amount of DPPC per mg of powder formulation was determined. The loaded drug (DPPC) mass was determined through content



uniformity analysis of the powder formulations. The mass of DPPC was also determined from all the deposition sites, and the recovered dose was the total mass recovered from all the deposition sites.

The bulk density of each powder formulation was determined using a 1 mL plastic syringe, in which powder mass was calculated as the weight difference between the weight of the empty syringe and the weight of the syringe containing powder. The mass was then divided by the volume occupied by the powder inside the syringe to calculate the powder bulk density. The primary particle size (Dv50) of each formulation was determined by laser diffraction using the Sympatec HELOS with RODOS/M disperser at 4 bar, and ASPIROS sample feeder (Sympatec GmbH, Clausthal-Zellerfeld, Germany). Testing at the high pressure of 4 bar was intended to produce maximum particle dispersion and show primary particle size.

### *Statistical Analysis*

All experiments were performed with three or more replicates. Statistical analysis was performed using JMP Pro 16 (SAS Institute Inc., Cary, NC). Direct comparison of two cases utilized Student's *t*-test, while comparison of multiple cases utilized one-way ANOVA followed by post hoc Tukey. Statistical tests used a significance limit of  $P=0.05$ .

## **7.3 Results**

### *Baseline AS-EEG Formulation Characteristics*

In our previous study [29], the PD-2 air-jet DPI achieved 60% estimated lung delivery efficiencies with both 10 and 30 mg powder loading of the AS-EEG formulation when operated

at 1.7 L/min. Previous investigations of surfactant-based EEG formulation indicated a higher flow rate produced improved aerosolization (around 4 L/min), so for a baseline comparison in this study, the AS-EEG formulation was characterized at a flow rate of 4 L/min. Triplicate runs were performed for both experimental setups; the preterm infant NT model (**Figure 7.1**) and NGI sizing of aerosol (**Figure 7.7**). In all cases, the PD-2 air-jet DPI with 10 mg of powder loaded in the standard powder reservoir was actuated 5 times with a flow rate of 4 L/min.

Performance and characteristics of the aerosol are presented in **Table 7.1**, which provides the deposition fractions within each region based on the loaded formulation mass and the sizing properties of the aerosol as emitted from the air-jet DPI outlet. The PD-2 device produced a tracheal filter deposition of ~45% while operated at the 4 L/min flow rate, and a mean MMAD of 1.63  $\mu\text{m}$ , while the PPFs for 5 and 1  $\mu\text{m}$  were ~85% and ~25%, respectively.

#### *Adjustable Powder Reservoir*

From our previous study [29], the powder reservoir volume sensitivity analysis showed a slight but statistically significant difference in performance when the volume of the powder reservoir was increased from 0.55 mL to 1.5 mL. The nearly 3-fold increase of dead space in the powder reservoir lowered the emitted dose and consequently the tracheal filter deposition by approximately 5% (absolute difference). To overcome the sensitivity to the added dead space, the adjustable powder reservoir was developed (**Figure 7.5b**). Investigation was performed on other methods not presented in this study (i.e., various weight or covers to rest on top of the loaded powder mass), however only the adjustable powder reservoir was found to produce similar performance with a larger reservoir. The operating principle behind this design was to

remove the excess dead space and vent the air in the reservoir for different initial powder mass loadings, by positioning the slider just above the powder bed. To determine if the device performs similar when utilizing the extended volume powder reservoir, the results of the initial baseline regional deposition study were compared to a similar setup, but utilizing the adjustable powder reservoir. **Table 7.2** compares the baseline results from **Table 7.1** with additional data using the adjustable powder reservoir and 10 mg powder mass loadings. All regions for both configurations remained statistically equivalent, indicating the adjustable powder reservoir approach will allow for different powder volumes (up to 1.5 mL for this study) to be loaded and aerosolized with similar performance. As the platform has been shown to be insensitive to loaded dose (10 to 30 mg) and now insensitive to the adjustable powder reservoir, continuation with 10 mg powder loadings and the initial static powder reservoir were deemed reasonable.

#### *Device Emptying Characteristics*

A major design goal for the infant air-jet DPI platform is to deliver consistently over the full intended delivered dose. As such, it should show reliability of dose per actuation, or at least a plateau so a max dose per actuation can be determined. An initial experimental set utilized the setup pictured in **Figure 7.6** to determine the ED per actuation for a 10 mg powder mass loading. For the 10 mg loading, the device was actuated 5 times into 5 separate collection filters, with the results plotted in **Figure 7.8a**. As expected, nearly all of the total ED was emitted in the first 3 actuations, however, they were not equivalent. The mean ED for the first and third actuation were nearly the same at about 15% or 1.5 mg, while the mean ED for the

second actuation was over twice as large at about 40% or 4.0 mg. To determine if the ED per actuation plateaus to a maximum, a second experimental set using a 30 mg powder mass loading was performed. With an identical setup, 30 mg of powder was loaded and 10 actuations were performed into 10 separate collection filters. The results of the 30 mg loading are plotted in **Figure 7.8b**, in which the ED per actuation does appear to plateau around 4.5 – 5 mg. The trends for both cases indicate the ED per actuation has a ramp up process in the initial actuations followed by a plateau and drop off at the end. While there is some variability, it is expected to hold that device emptying will occur with 3 actuations per 10 mg of loaded powder, and the maximum ED per dose is about 5 mg over the course of a treatment with current device parameters and an AAV of 10 mL.

#### *Metering Element Tuning per Formulation*

Previous development of the passive cyclic loading strategy [29] optimized the geometry of the PD-2 device for the AS-EEG formulation, resulting in a ~60% lung delivery efficiency when actuated at 1.7 L/min. In this study, the same device achieved ~45% lung delivery efficiency when actuated at 4 L/min, and further optimization was not performed as it was used for a baseline comparison. The three formulations tested in this study each have unique properties; the primary particle size (Dv50) and approximate bulk density for each formulation are presented in **Table 7.3** for comparison.

Initial results of the PD-2 device and Survanta-EEG formulation produced a low lung delivery efficiency ~20%. One of the driving factors for the lower performance was likely the density of the formulation; the shelf in the PD-2 device was positioned directly below the

powder reservoir creating a volume gap of  $\sim 26 \mu\text{L}$  (PD-2-26), resulting in  $\sim 2.6 \text{ mg}$  of the AS-EEG powder ( $\sim 0.10 \text{ g/cm}^3$ ) able to fall and rest on the shelf for each actuation, and  $\sim 4.7 \text{ mg}$  of the Survanta-EEG powder ( $\sim 0.18 \text{ g/cm}^3$ ), nearly double that of the AS-EEG powder, which may diminish aerosolization or create cloud motion phenomenon, which increases the deposition of all elements in the cloud [195, 196]. By reducing the volume of the shelf gap, and likewise the amount of powder able to rest on the shelf between actuations, performance may be improved. Various decreasing shelf volumes were investigated ( $\sim 20$ ,  $\sim 16$ , and  $\sim 8 \mu\text{L}$ ) and the best performance was observed with a shelf volume  $\sim 16 \mu\text{L}$  (PD-2-16), which equates to  $\sim 2.9 \text{ mg}$  of powder able to rest on the shelf between actuations. Reducing the shelf volume for the Survanta-EEG formulation nearly double the estimated lung delivery efficiency to  $\sim 38\%$ .

Initial results of the PD-2 device and DPPC-BYL3-EEG formulation produced a high lung delivery efficiency of  $\sim 50\%$ , but when increasing the shelf volume to account for the lower density ( $\sim 0.04 \text{ g/cm}^3$ ), performance was not improved. Also, emptying the device required 9-10 actuations opposed to only 3 with the AS-EEG formulation. For a small dose ( $\sim 10 - 20 \text{ mg}$ ) this is likely acceptable, but for large doses ( $\sim 90 \text{ mg}$ ) an extended delivery time may not be desirable. For example; an actuation ( $\sim 0.2 \text{ sec}$ ), breath hold period ( $\sim 5 \text{ sec}$ ), and exhalation ( $\sim <1 \text{ sec}$ ) produces an approximate 6 second cycle per action. With the AS-EEG formulation requiring 3 actuations per 10 mg, a 90 mg loaded powder dose would take less than 3 minutes to administer, whereas the DPPC-BYL3-EEG formulation requiring 10 actuations per 10 mg, would take about 9 minutes to administer a 90 mg dose. To increase the speed of delivery, instead of adjusting the shelf volume, the diameter of the powder reservoir opening into the aerosolization chamber was increased. The initial diameter of 3 mm was increased to 3.5 mm

and labelled as PD-2-26'. The resulting configuration was able to deliver the 10 mg loaded dose in ~3 actuations while still maintaining a high lung delivery efficiency of ~48%, and the slight decrease in performance was considered favorable to the significant reduction in required actuations to empty. Using the 3.5 mm diameter opening, a larger shelf volume was again tested for the lower density powder, however, improvements were still not seen.

The best configurations per formulation based on the testing performed in this study are consider PD-2-26, PD-2-16, and PD-2-26' for the AS-EEG, Survanta-EEG, and DPPC-BYL3-EEG formulation, respectively. **Table 7.4** presents the regional deposition fractions from the *in vitro* preterm infant NT model testing for each formulation using the relative best configuration air-jet DPI. While it was possible to tune the DPPC-BYL3-EEG formulation to match (no statistically significant difference) the base-line AS-EEG formulation performance, the Survanta-EEG formulation was not, and underperformed in terms of lung delivery efficiency by ~7%.

#### *Best Case Performance by Formulation*

Using the relative best passive metering element configurations for each formulation, **Table 7.4** compares the regional deposition fractions (based on 10 mg loaded powder mass) of the *in vitro* preterm infant NT experiment, and side-by-side performance comparisons can be seen for each formulation. The DPPC-BYL3-EEG formulation performed nearly identical (no statistically significant difference) to the AS-EEG formulation with the metering element modifications. However, the Survanta-EEG was not able to perform as well with the modifications tested. Despite having a higher Total ED (~9% absolute difference) than seen with

the AS-EEG formulation, the Survanta-EEG had larger NT depositions leading to a decrease (~7% absolute difference) in Tracheal Filter deposition.

The best configurations for the surfactant powder formulations were then tested for aerosol characterization using the NGI experimental setup. **Table 7.5** compares the characteristics of the aerosol exiting the air-jet DPI, as well as the NGI Pre-separator Fraction. The AS-EEG formulation had a mean MMAD of 1.63  $\mu\text{m}$  with a  $\text{FPF}_{5\mu\text{m}}$  and  $\text{FPF}_{1\mu\text{m}}$  of ~85% and 25%, respectively. Surprisingly, despite similar performance in the NT model, the DPPC-BYL3-EEG formulation had significantly different aerosol characteristics with a larger MMAD of 2.36  $\mu\text{m}$  and smaller FPFs ( $\text{FPF}_{5\mu\text{m}} \approx 60\%$  and  $\text{FPF}_{1\mu\text{m}} \approx 16\%$ ). The Survanta-EEG formulation produced the largest aerosol sizes as indicated by the large NGI Pre-separator Fraction of nearly 50%. Due to a large pre-separator fraction, certain calculations could not include this deposition region including the MMAD and GSD in some cases. For example, the mean MMAD of the Survanta-EEG formulation was 1.91  $\mu\text{m}$ , though it could not account for nearly half of the powder deposited in the pre-separator. The FPFs of the Survanta-EEG however, provide a clear picture as to why the lung delivery efficiency was lower than the other formulations, with a  $\text{FPF}_{5\mu\text{m}}$  and  $\text{FPF}_{1\mu\text{m}}$  of ~37% and 6%, respectively. **Figure 7.9** depicts the aerodynamic particle size distribution (APSD) for each formulation based on the NGI results, as well as the NGI Pre-separator Fractions, also highlighting the importance of considering the pre-separator fraction. The left Y-axis depicts the APSD with corresponding sizes on the X-axis, while the right Y-axis represents the pre-separator deposition fraction which is the total accumulation of all particle sizes over 9.4  $\mu\text{m}$  (initial cut-off size based on the NGI operating at 45 L/min).

## 7.4 Discussion

A significant outcome of this study is the advancement of the infant air-jet DPI platform with passive cyclic loading to enable variable low to high dose powder loadings without performance loss and identification of passive metering elements to tune the air-jet DPI for different formulations. A single device (PD-2), as previously developed [29] was used throughout this study, with modifications made to the identified metering elements. The adjustable powder reservoir design enabled the platform to be insensitive to the powder reservoir volume (from the standard 0.55 mL to the larger 1.5 mL). While only a 10 mg powder mass loading was investigated in this study, it is expected to perform similar with loadings up to 100 mg as the adjustable reservoir is designed to eliminate the dead space above the loaded powder (in the range of 0.5 – 1.5 mL), however, future studies will be needed for confirmation.

Evaluating the device emptying characteristics also lead to positive results, in which a maximum ED per actuation of ~5 mg was observed. While the ED per actuation was not identical across the entire treatment (a ramp-up period was shown), the overall total ED had small deviations and a plateau effect was seen; for example, with 30 mg of loaded powder, the mean Total ED for 3 trials was 84.1% with a SD of 0.88%, and the 3 highest ED per actuation were 4.4, 4.6, and 4.8 mg. Concerns for rapid administration of dry powder have been shown in a pilot study by Pohlmann et al. [110], in which mechanically ventilated pigs received ~1000 mg of dry surfactant aerosol delivered through a thin catheter in an endotracheal tube, resulting in a soft aggregate clot forming in the lower trachea. Unfortunately, the delivery rate was not reported, however, the dose delivered was 1-2 orders of magnitude larger than the total expected dose for the air-jet DPI platform, and a <5 mg per actuation dose is believed to be



safe. Future *in vivo* studies will need to be performed to investigate the safety of delivery speed.

Two passive metering elements have been identified in this study, which are the shelf volume and the powder reservoir opening size. Initial tuning of the shelf volume was investigated based on the powder density. Since the Survanta-EEG formulation had a higher bulk density, a smaller shelf volume was used for tuning. Reducing the shelf volume incrementally showed improved performance up to a certain point. The decreased volumes (~20 and ~16  $\mu\text{L}$ ) improved performance, after which it dropped at ~8  $\mu\text{L}$ . It is likely the aerosolization chamber needs a minimum shelf volume between 8 – 16  $\mu\text{L}$  for effective aerosolization. On the other hand, when the shelf volume was increased for the DPPC-BYL3-EEG formulation (lower bulk density), performance did not improve, indicating the shelf geometry will impede effective aerosolization beyond a certain volume (between 26 – 40  $\mu\text{L}$ ). Careful tuning of the shelf volume should allow for optimal performance with each formulation. The second metering element was the powder reservoir opening size. While tuning the device for the DPPC-BYL3-EEG formulation, improvement was not seen with increased shelf volumes, so the opening was instead increased. Increasing the diameter of the opening from 3 to 3.5 mm maintained the high lung delivery efficiency while significantly decreasing the required number of actuations to empty. With a low-density powder (~0.04  $\text{g}/\text{cm}^3$ ), a larger opening was needed to aid the powder transfer from reservoir to aerosolization chamber. With tuning of the metering elements, a surfactant-EEG powder formulation was found to perform similar to the model AS-EEG formulation.

Limitations of this study include the use of a single preterm NT model, a single nasal interface, and limited number of metering element configurations. The use of a single preterm NT airway geometry cannot show inter-subject variability; however, in a previous study investigating nasal interfaces [28], the performance of the platform remained statistically similar across two preterm NT models with very different airway features. Also based on previous studies [28, 29], only a single (previously best performing) nasal interface was used in this study, whereas new nasal interface approaches such as co-flow designs may improve results. Finally, with only several passive metering element configurations tested, the range of tunability this selection captures are unknown. However, for the configurations tested in this study, key insights for two metering elements have been observed; including lowering the shelf volume based on formulation density, with an estimated shelf volume limit equivalent to <3 mg of powder being ideal, and increasing the powder reservoir opening diameter for low density powders. While additional flow rate tuning was not investigated in this study, it has been observed to have a significant effect on performance [27-29] and should be considered for future tuning per formulation.

## **7.5 Conclusions**

In conclusion, modifications to passive metering elements were successfully implemented for the infant air-jet DPI platform. Two metering elements identified in this study were the shelf volume and the powder reservoir opening size. An adjustable powder reservoir was also developed, which should enable the platform to be performed consistently with loaded dose between 10 mg to 150 mg (based on a bulk density of 0.10 g/cm<sup>3</sup>). The platform was also

found to produce a maximum ED per actuation of ~5 mg, which should prevent overly rapid aerosol administration. During *in vitro* testing using a preterm NT model, an additional formulation (DPPC-BYL3-EEG) was found to perform similar to the model AS-EEG formulation when the metering elements were tuned, both providing a >45% lung delivery efficiency. While the Survanta-EEG formulation slightly underperformed, tuning of the metering elements nearly double the performance; increasing the lung delivery efficiency from ~20% to ~38%. Further tuning of the passive metering elements and flow rate are expected to improve the performance of the Survanta-EEG formulation. Overall, configuring the passive metering elements enable tuning of the infant air-jet DPI platform for use with different formulations. Two general metrics for best performance include a shelf volume limit equivalent to <3 mg of powder, and increasing the powder reservoir opening diameter for low density formulations ( $\sim < 0.05 \text{ g/cm}^3$ ). While each new formulation will require tuning of the platform for consistent performance, significant re-designs should not be necessary. Future development of the air-jet DPI will include a manually adjustable shelf and reservoir opening to enable easy tuning for any future formulations.

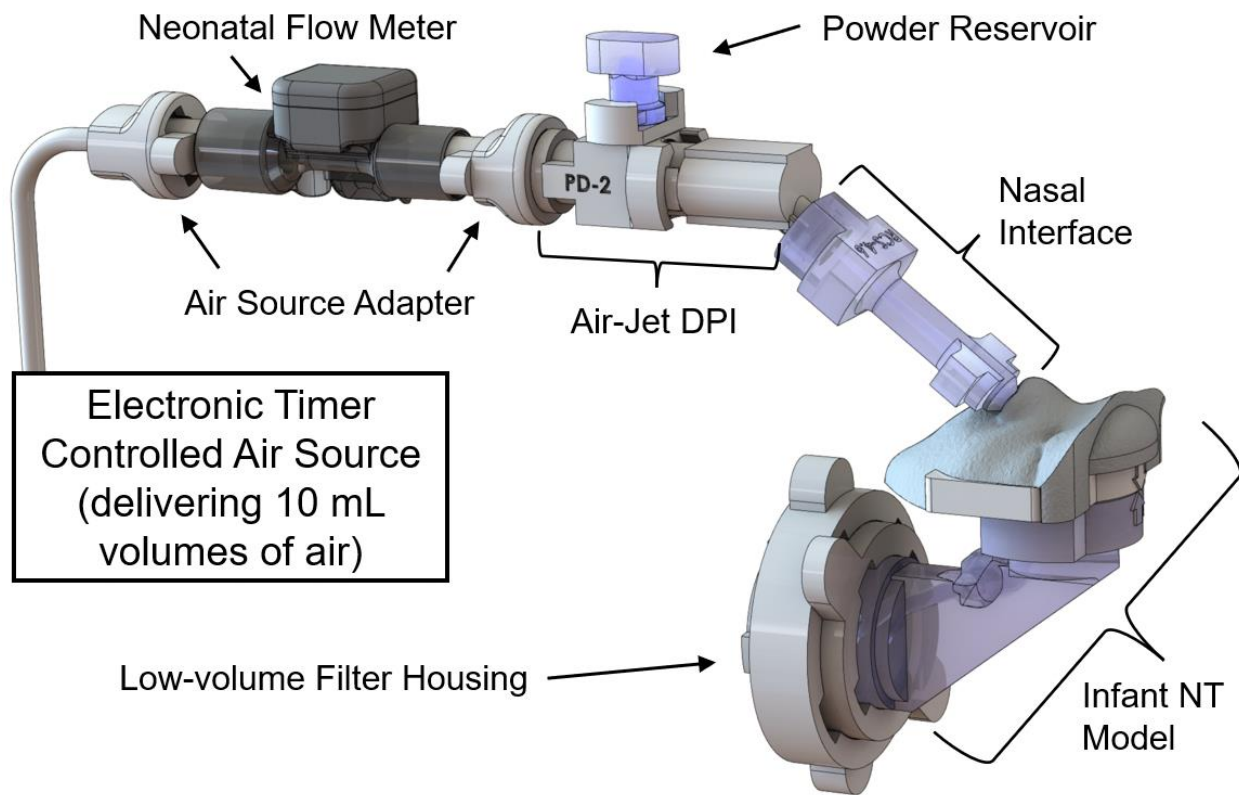


**Figure 7.1** Graphical rendering of the experimental setup including the infant air-jet DPI platform with passive cyclic loading in connection to a preterm infant model

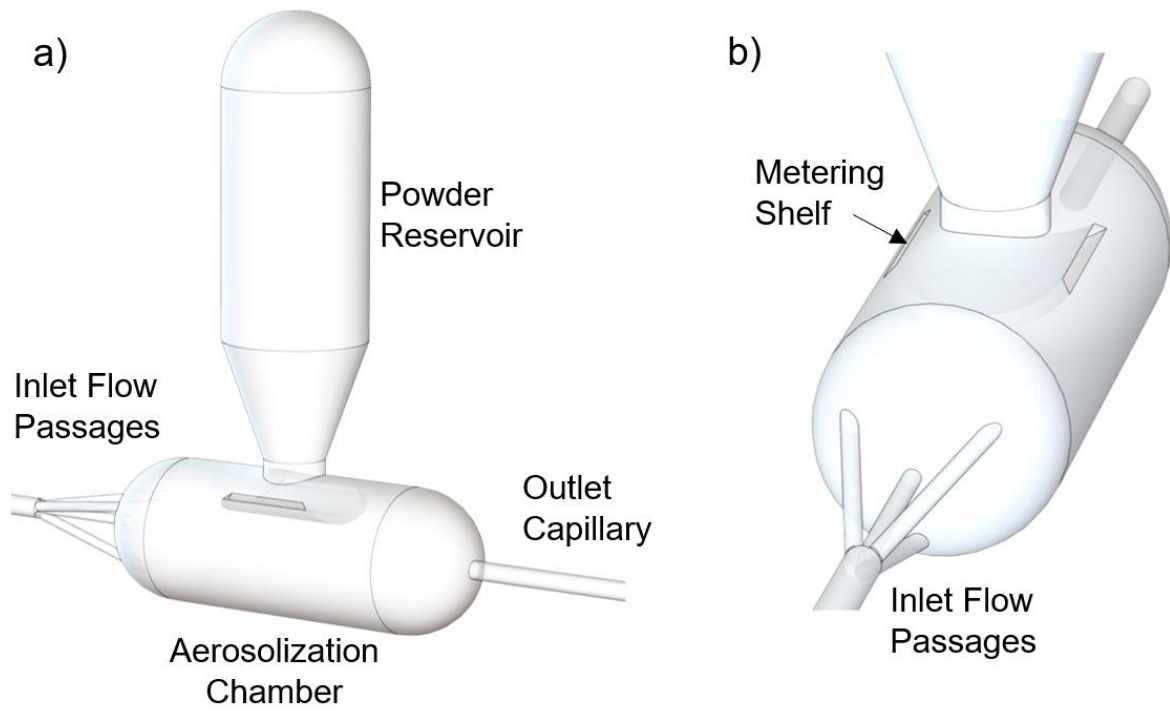


**Figure 7.2** Internal airflow geometry of the air-jet DPI. Panel (a) showing air source inlet (left side of image) to the device outlet (right side of image). Panel (b) highlights the inlet jet configuration

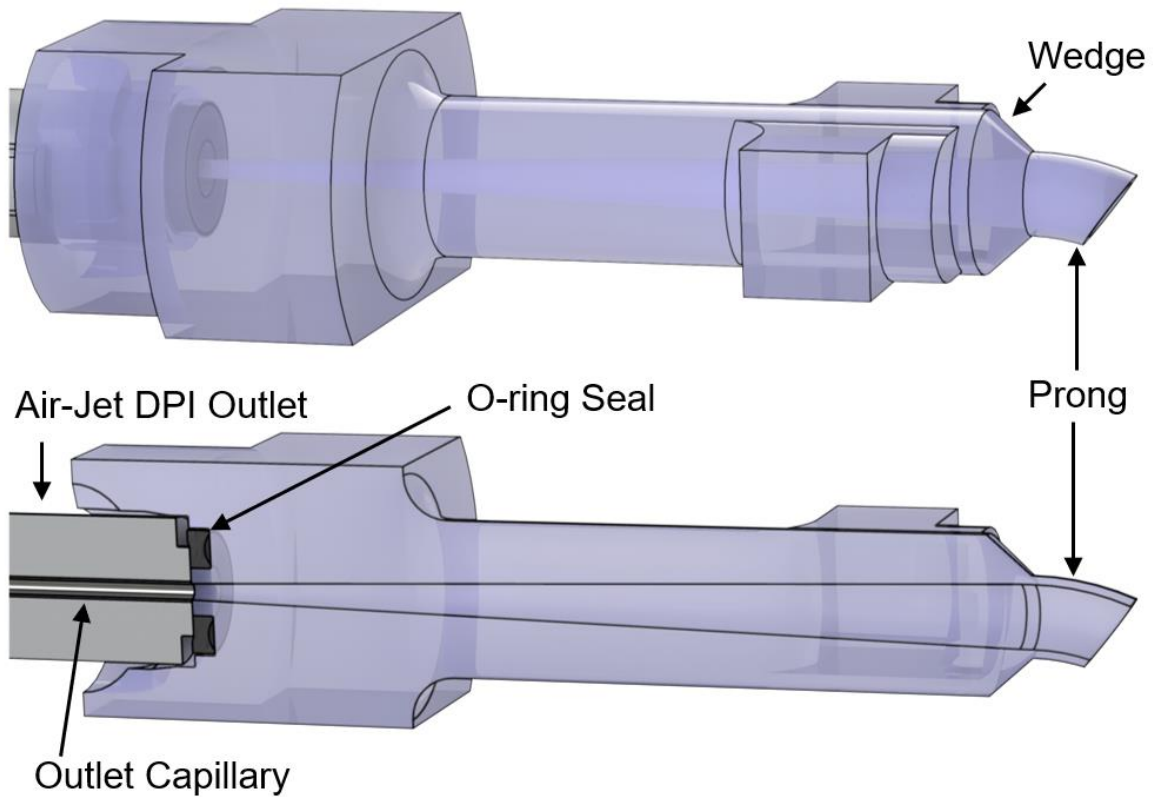


**Figure 7.3** Overview of the single nasal interface used in this study. The nasal interface was 3D printed (SLA) as a single piece in a translucent rigid material. A rendering (above) depicts external features including the short curved prong and wedge, while an axial cross-sectional rendering (pictured below) shows the internal airway geometry and connection to the outlet of the air-jet DPI with O-ring seal

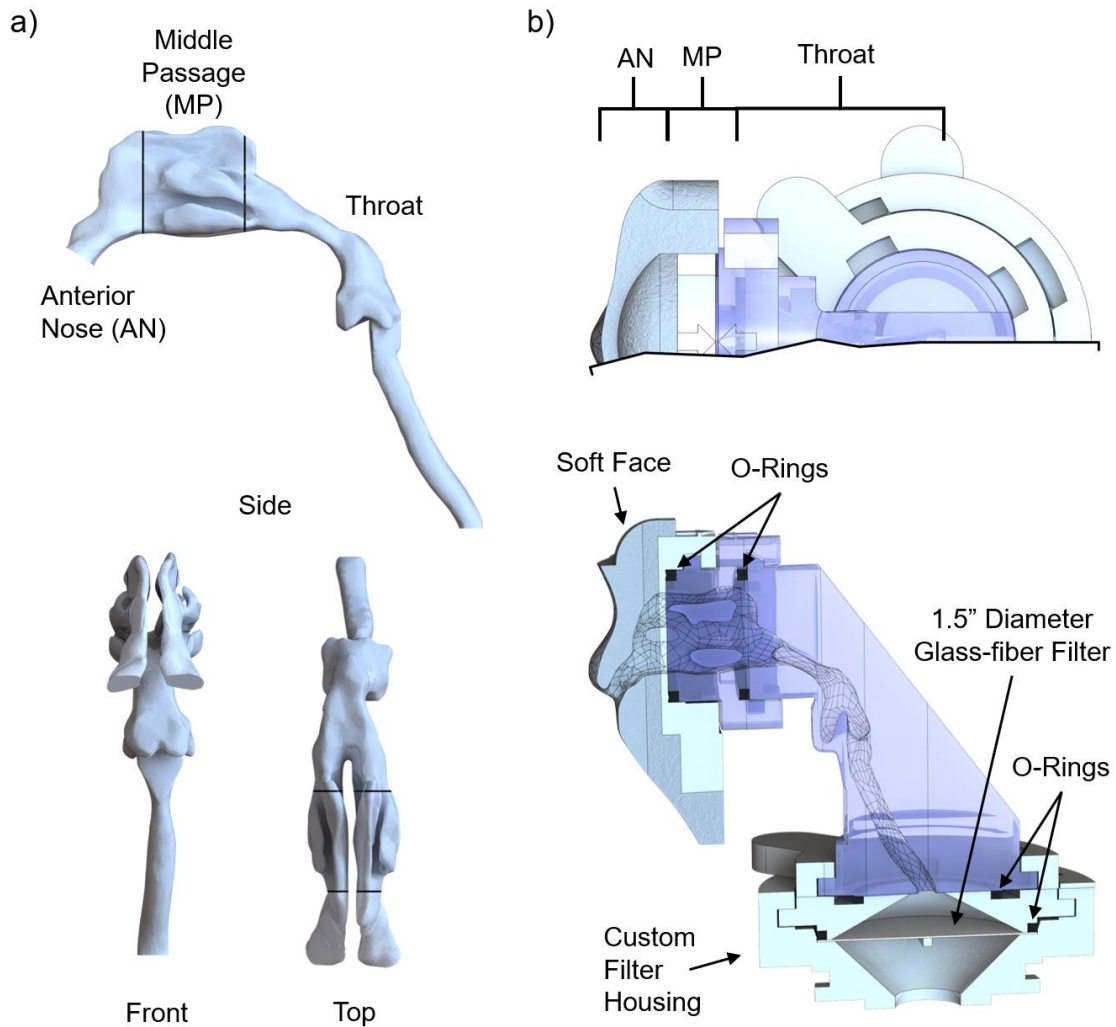
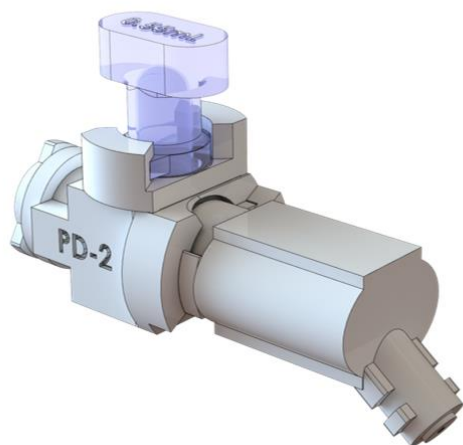


**Figure 7.4** Graphical renderings of infant NT airway geometry with regional sections and model assembly connected to custom low-volume (LV) filter housing. **(a)** Internal airway geometry of the infant NT model with assessed regions including the anterior nose, middle passage and throat, with top panel showing the side view, and front/top views shown below. **(b)** Assembled infant NT model in connection to LV filter housing with parts and regions labeled (the Soft Face segment is glued to a rigid Face Adapter segment before use and represent the Anterior Nose airway region), with custom cross-section (above) to show internal airway path through the left nostril and nasal cavity through to the filter housing (below)

a)



b)

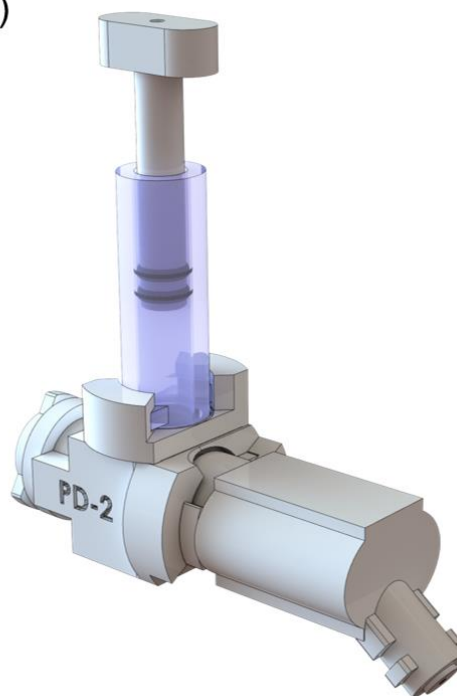


**Figure 7.5** Renderings of the two powder reservoir configurations. **(a)** PD-2 device with standard (0.55 mL volume) reservoir attached and **(b)** PD-2 device with adjustable powder reservoir (up to 1.5 mL volume) attached



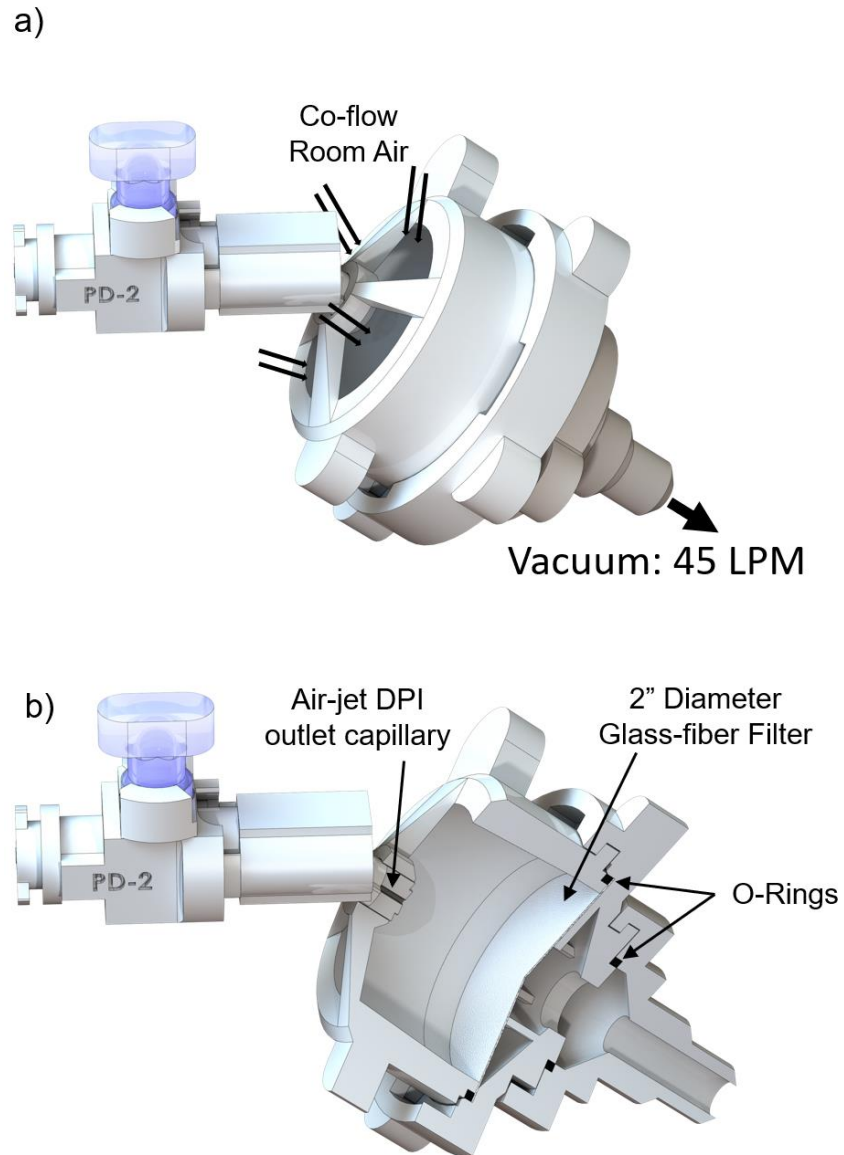


**Figure 7.6** Rendering of air-jet DPI connected to aerosol collection assembly for emitted dose (ED) per actuation experimental study. Panel **(a)** shows air-jet DPI connected to the aerosol collection assembly with hose connection to vacuum pump operated at 45 L/min. Panel **(b)** shows cross sectional view of the inside of the collection assembly and outlet connection of the air-jet DPI

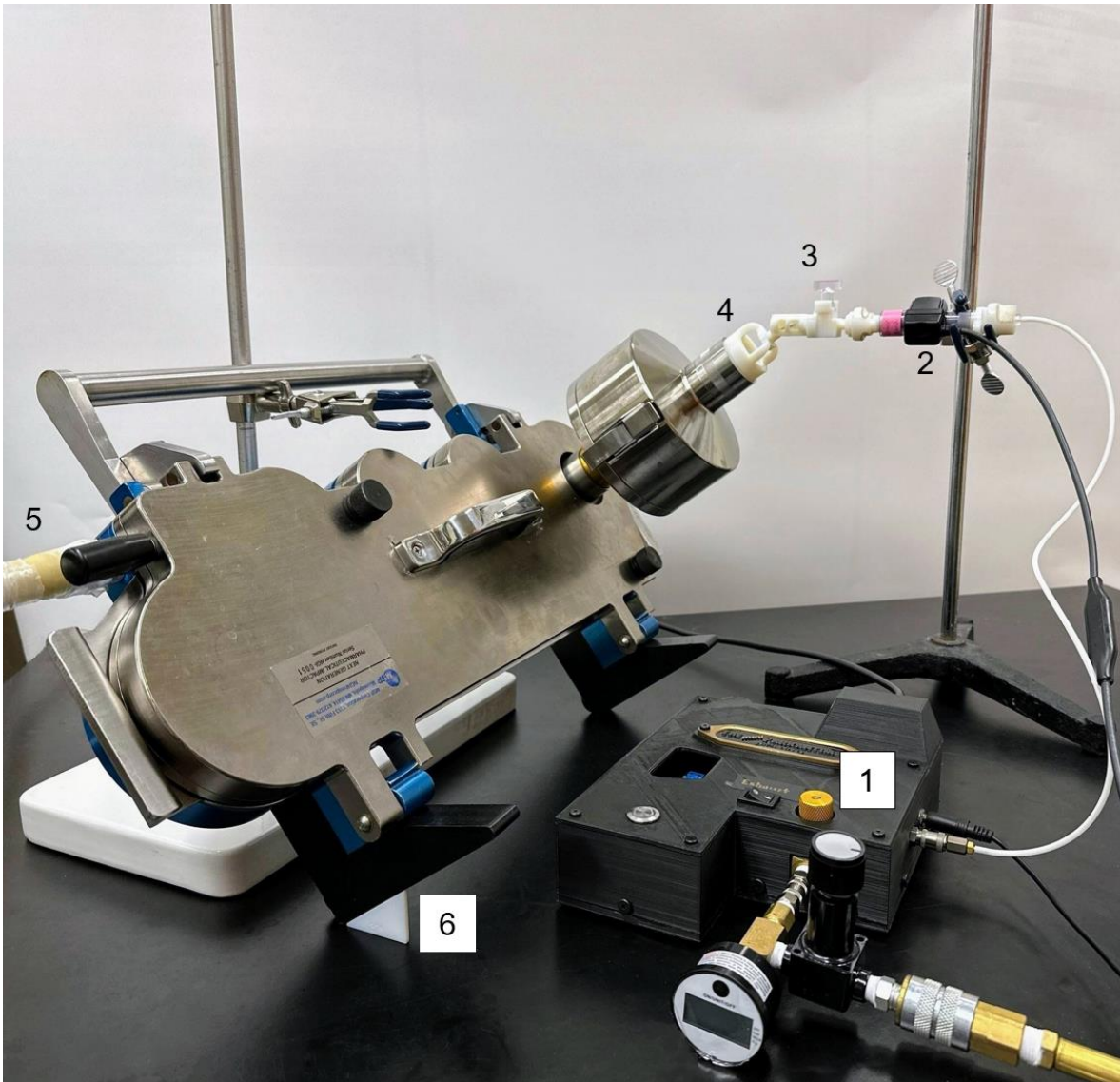


**Figure 7.7** Image of experimental setup for device aerosolization performance as determined by Next Generation Impactor (NGI). Parts labeled including 1. Electronic Timer air source, 2. Neonatal mass flow meter, 3. Air-jet DPI (PD2 with standard 0.55 mL powder reservoir pictured), 4. NGI adapter, 5. Vacuum for NGI (operated at 45 LPM), and 6. Guide to angle the NGI at 53° off horizontal

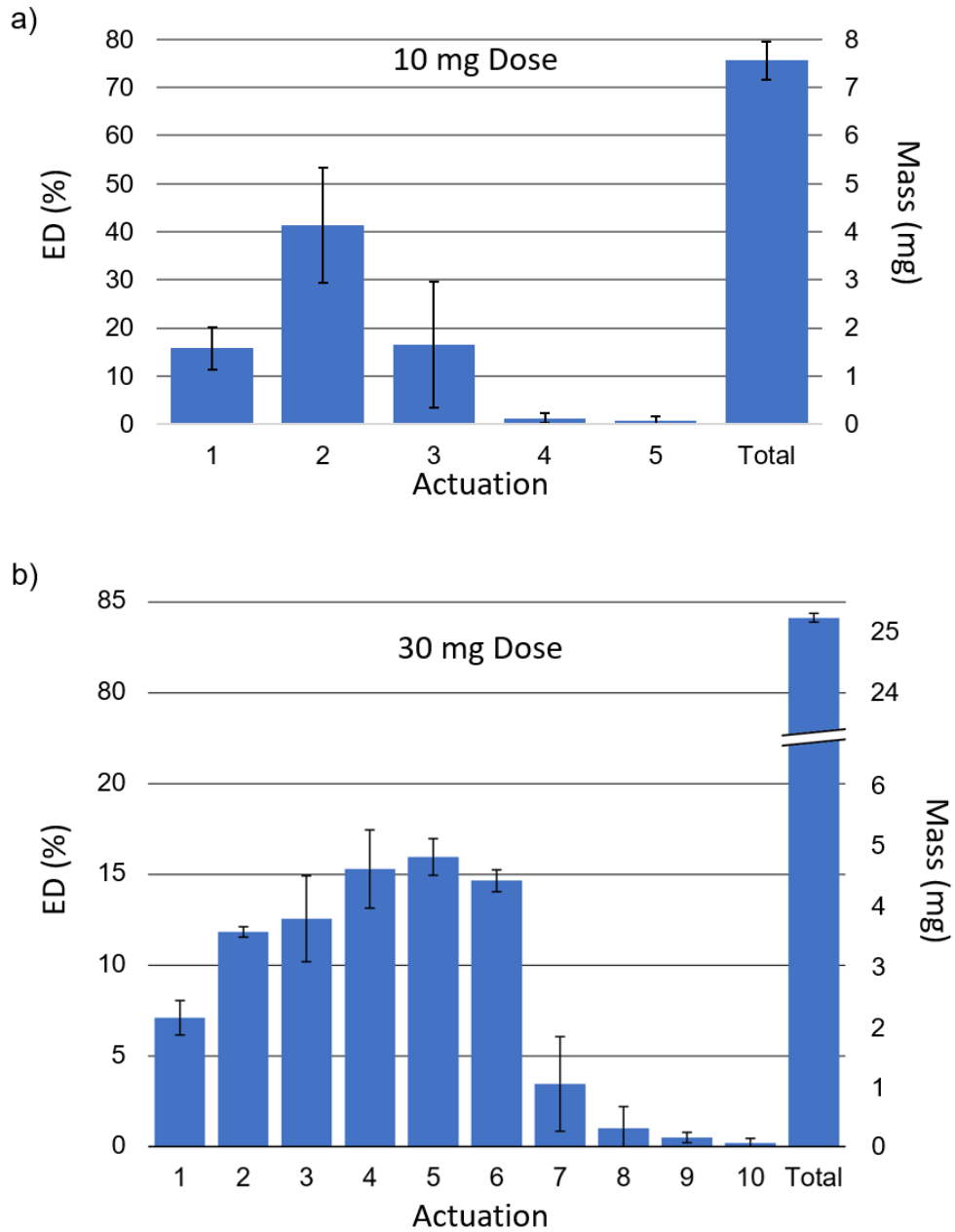


**Figure 7.8** Plot of experimentally determined mean and  $\pm 1$  SD error bars for emitted-dose (ED) per actuation and total ED (based on loaded dose) of the AS-EEG formulation, at a Q90 flow rate of 4 L/min [n=3]. **(a)** Results of 10 mg powder loading and **(b)** 30 mg powder loading

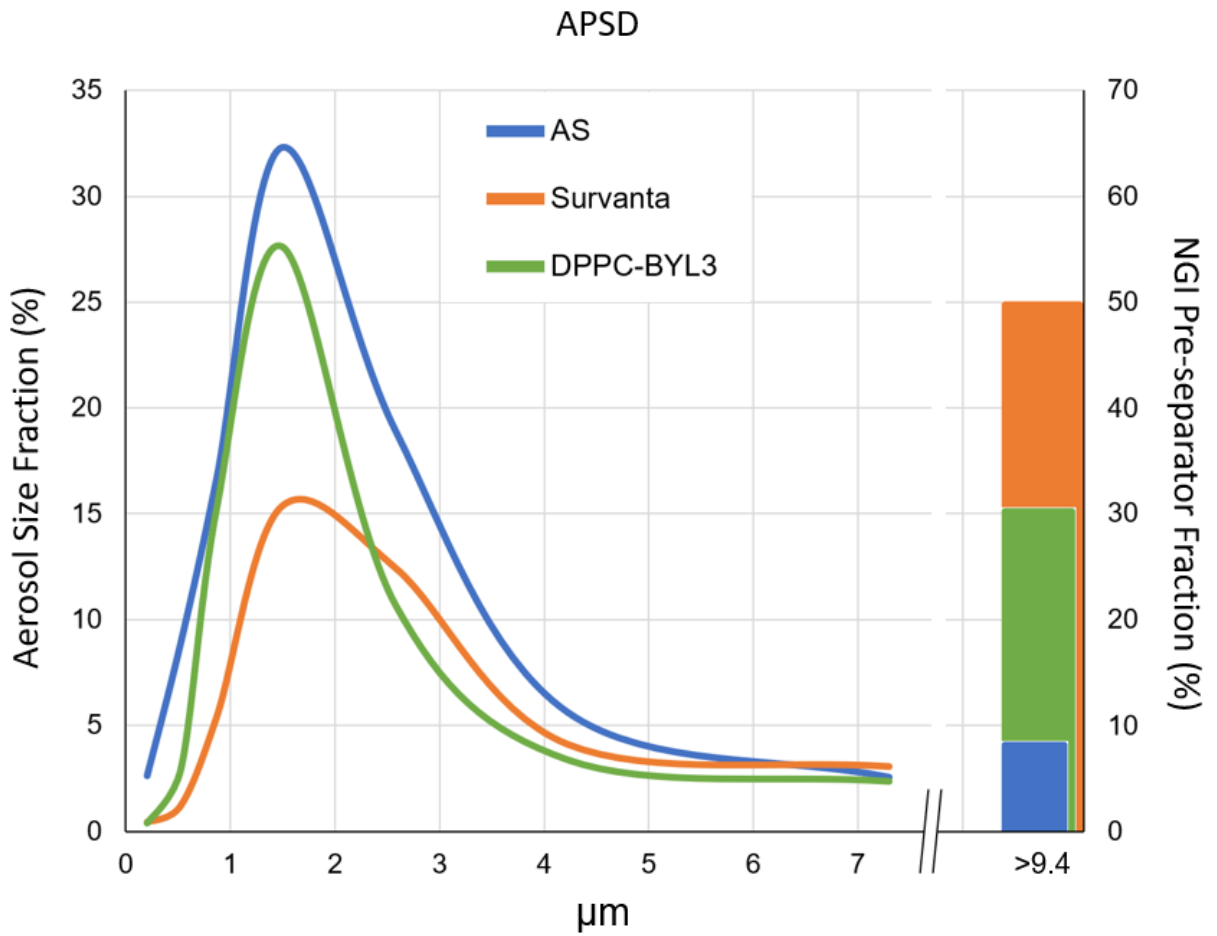


**Figure 7.9** Experimentally determined mean aerodynamic particle size distribution (APSD – left Y-axis) and NGI pre-separator deposition fraction (right Y-axis) of each formulation (based on loaded dose) for the PD-2 device and 10 mg powder loading[n=3]

**Table 7.1** Lung delivery efficiencies (estimated as Tracheal Filter %) and regional deposition fractions (based on 10 mg loaded dose) for the AS-EEG formulation and NGI determined particle size characteristics for PD-2 device

<b>PD-2</b>			
<b>Deposition Region</b>		<b>Size Characteristics</b>	
DPI Retention (%)	15.8 (3.0)	DPI Retention (%)	16.5 (1.5)
Nasal Interface (%)	5.8 (1.0)		
Total ED (%)	78.4 (2.4)	MMAD ( $\mu\text{m}$ )	1.63 (0.07)
		GSD	2.1 (0.1)
Anterior Nose (%)	7.2 (0.3)	FPF <sub>5<math>\mu\text{m}</math></sub> (%)	84.7 (2.1)
Middle Passage (%)	10.2 (0.4)	FPF <sub>1<math>\mu\text{m}</math></sub> (%)	24.9 (2.1)
Throat (%)	14.0 (1.7)		
Total NT (%)	31.4 (1.2)		
Tracheal Filter (%)	45.2 (2.2)		

Mean values with standard deviations (SD) shown in parenthesis, n=3.

DPI, dry powder inhaler; ED, emitted dose; FPF, fine particle fraction; GSD, geometric standard deviation; MMAD, mass median aerodynamic diameter; NT, nose-throat; PD, passive design.

**Table 7.2** Lung delivery efficiencies (estimated as Tracheal Filter %) and regional deposition fractions (based on loaded dose) for the AS-EEG formulation and comparisons of 0.55 mL (standard) vs 1.5 mL (adjustable) powder reservoir with PD-2 device

<b>Deposition Region</b>	<b>Standard</b>	<b>Adjustable</b>
DPI Retention (%)	15.8 (3.0)	15.6 (2.8)
Nasal Interface (%)	5.8 (1.0)	3.7 (0.4)
Total ED (%)	78.4 (2.4)	80.7 (2.8)
Anterior Nose (%)	7.2 (0.3)	6.3 (1.4)
Middle Passage (%)	10.2 (0.4)	11.0 (2.0)
Throat (%)	14.0 (1.7)	15.7 (2.8)
Total NT (%)	31.4 (1.2)	33.0 (5.8)
Tracheal Filter (%)	45.2 (2.2)	45.5 (4.0)

Mean values with standard deviations (SD) shown in parenthesis, n=3.  
 No significant difference found between deposition regions (*t* test)

**Table 7.3** Powder properties for each formulation based on primary particle size (geometric) and approximate bulk density

	<b>AS</b>	<b>Survanta</b>	<b>DPPC-BYL3</b>
Dv50 ( $\mu\text{m}$ )	1.13 (0.03)	1.15 (0.03)	1.03 (0.00)
Bulk Density ( $\text{g}/\text{cm}^3$ )	0.10	0.18	0.04

Mean values with standard deviations (SD) shown in parenthesis, n=3.

**Table 7.4** Lung delivery efficiencies (estimated as Tracheal Filter %) and regional deposition fractions (based on loaded dose) for each formulation with 10 mg powder loadings and relative best metering element configuration PD-2 device

<b>Deposition Region</b>	<b>AS</b>	<b>Survanta</b>	<b>DPPC-BYL3</b>
DPI Retention (%)	15.8 (3.0)	7.7 (0.5)	12.2 (2.0)
Nasal Interface (%)	5.8 (1.0)	4.9 (1.4)	4.0 (0.6)
Total ED (%) <sup>a</sup>	78.4 (2.4)	87.4 (1.7) <sup>b</sup>	83.8 (2.3)
Anterior Nose (%) <sup>a</sup>	7.2 (0.3)	12.5 (1.7) <sup>b</sup>	7.3 (0.4)
Middle Passage (%)	10.2 (0.4)	13.5 (4.2)	11.9 (2.0)
Throat (%) <sup>a</sup>	14.0 (1.7)	18.2 (0.8)	14.1 (2.3)
Total NT (%) <sup>a</sup>	31.4 (1.2)	44.2 (6.1) <sup>b</sup>	33.3 (4.3)
Tracheal Filter (%) <sup>a</sup>	45.2 (2.2)	38.0 (4.0) <sup>b</sup>	46.7 (1.4)

Mean values with standard deviations (SD) shown in parenthesis, n=3.

<sup>a</sup> $p < 0.05$  significant effect of design on deposition region (one-way ANOVA).

<sup>b</sup> $p < 0.05$  significant difference compared to AS formulation (post-hoc Tukey).



**Table 7.5** Aerosol characterization based on next generation impactor (NGI) testing for each formulation with 10 mg powder loadings and the best metering element configuration PD-2 device (aerosol at air-jet DPI device outlet)

<b>Deposition Region</b>	<b>AS</b>	<b>Survanta</b>	<b>DPPC-BYL3</b>
DPI Retention (%) <sup>a</sup>	16.5 (1.5)	6.7 (0.4) <sup>b</sup>	9.1 (0.6) <sup>b</sup>
Pre-separator Fraction (%) <sup>a</sup>	8.3 (1.0)	49.8 (2.6) <sup>b</sup>	30.2 (1.2) <sup>b</sup>
MMAD (μm) <sup>a</sup>	1.63 (0.07)	1.91 (0.14) *	2.36 (0.29) <sup>b</sup>
GSD <sup>a</sup>	2.53 (0.28)	2.01 (0.08) * <sup>b</sup>	1.85 (0.04) * <sup>b</sup>
FPF <sub>5μm</sub> (%) <sup>a</sup>	84.7 (2.1)	38.6 (2.0) <sup>b</sup>	60.1 (1.6) <sup>b</sup>
FPF <sub>1μm</sub> (%) <sup>a</sup>	24.9 (2.1)	6.0 (1.1) <sup>b</sup>	15.6 (0.5) <sup>b</sup>

Mean values with standard deviations (SD) shown in parenthesis, n=3.

\*Calculations exclude pre-separator deposition due to large deposition fraction.

<sup>a</sup>p<0.05 significant effect of design on deposition region (one-way ANOVA).

<sup>b</sup>p<0.05 significant difference compared to AS formulation (post-hoc Tukey).

## Chapter 8 - Conclusions and Future Work

The objectives and tasks described in Chapter 1 have each been accomplished. The following is a summary of each task accomplished: (1.1) a range of new air-jet DPI designs were tested using an *in vitro* full-term infant NT model; (1.2) three unique air sources were characterized for flow and platform performance using an *in vitro* preterm infant NT model; (1.3) nasal interface options were explored using *in vitro* methods; (2.1) the best performing platform configurations as developed in Objective 1 were expanded to include a passive cyclic loading strategy to allow for dose selection with consistent performance; (2.2) a best performing passive design (PD) device from Task 2.1 was chosen to investigate passive metering options to enable tunable parameters for use across various powder formulations. Conclusions, limitations, and possible future studies, based on the results of these objectives, are summarized below in more detail.

### **8.1 Objective 1: Development and optimization of an air-jet DPI platform for aerosol drug delivery to infants**

The infant air-jet DPI platform was initially developed using a manually operated syringe for actuation. The first optimization efforts focused on the aerosolization engine (design and geometries of the air-jet DPI component; aerosolization chamber and inlet/outlet flow passages). Out of six initial and varied designs, the leading three were found to produce similar lung delivery efficiencies of ~50% through an *in vitro* full-term infant NT model. Advantageous design options found for the air-jet DPI were identified as a horizontal and cylindrical

aerosolization chamber, flush or protruding outlet, and multiple inlet flow passages. While three of the initial devices performed well, performance in the more challenging preterm infant airways needed to be investigated. After much use of the manually operated syringe as an air source, consistent performance was achieved in the laboratory setting; however, it is expected that manual hand operation of a syringe (without an additional aid such as a lever actuator, guide or flow limiter) across different operators and environments will vary significantly, leading to the need for an automated air source or other alternatives to unify operation.

To overcome expected operator variability, the next study focused on development and optimization of an automatic air source (actuation occurs with a push button, switch, or other simple action). Three automatic air sources were investigated, producing unique actuation flow rate profiles, or waveforms. The electronic *Timer* air source produced a relatively square waveform while the *Pneumatic* air source produced more of a parabolic waveform, similar to the profile produced by manual hand actuation of a syringe. The compressed *Spring* air source had a sharp peak followed by a gradual decrease of the flow rate as expected for an initially compressed air reservoir. Each air source could be calibrated to consistently deliver an air actuation at set volumes and flow rates, and when matched by the Q90 flow rate value, all three air sources were found to produce similar aerosolization results in the platform. This was a significant finding since it will allow for interchangeability of the air source depending on delivery setting; i.e., the more convenient Timer air source can be used in a high resource setting, while the manually loaded Spring air source can be used in a setting where electricity and compressed air are not readily available, with expected similar performance. Future development of the air sources would allow for easy configuration of the actuation delivery

(e.g., setting the AAV and the Q90 flow rate). The ability to configure the actuation flow rate of the automated air sources facilitated investigation of the effect of flow rate on performance which was not feasible with a manually operated syringe. It was found that the Q90 flow rate of the actuation plays a significant role in the drug delivery performance. Initial performance of the platform comparable to that of syringe hand actuation was significantly improved in the *in vitro* preterm infant NT model, with lung delivery efficiencies increasing from about 35% to 54% when the Q90 flow rate was lowered from 4 L/min to 1.7 L/min. Another significant finding of this study was that the addition of a realistic pulmonary outlet condition, simulating the airway resistance (170 cm H<sub>2</sub>O/L/s) and lung compliance (0.49 mL/cm H<sub>2</sub>O) of a preterm infant with RDS, did not significantly affect the lung delivery efficiency of the platform, and the highest measured peak pressure in the airway was 27 cm H<sub>2</sub>O, while the majority of the breath hold pressure was between 20 to 25 cm H<sub>2</sub>O, indicating safe and reliable aerosol delivery. While inter-operator variability was addressed in this study, inter-subject variability was still a concern.

The final study for Objective 1 sought to investigate nasal interface optimization and inter-subject variability. While exploring various nasal interface design options (flow pathway and prong configurations) two design parameters were found which improved estimated lung delivery efficiency. Using a rigid curved prong design (Rigid-3), the estimated lung delivery efficiency of the platform increased 5% to 10% for different AS-EEG formulations, when compared to a straight flexible prong. Modification to the flow pathway, including a metal mesh (MM) to dissipate the aerosol jet, also produced improved tracheal filter deposition by about 5% while significantly lowering the Total NT deposition by over half with the MM-1-C design. One direction for future development on nasal interface designs is a co-flow approach.

With a co-flow design, the nasal interface geometry contains a cylindrical air flow surrounding the outlet connection from the air-jet DPI, Figure 8.1 shows an example cross section view of a co-flow design approach, with mesh flow diffusors. Potential benefits with this approach include (i) decreasing aerosol-wall interactions in the nasal interface and possibly extending through the anterior nose, leading to lower deposition fractions, (ii) decreased aerosol build-up on the walls inside the nasal interface, and (iii) addition particle break-up may occur as the aerosol cloud exits a rapid expansion from the air-jet DPI outlet capillary into the co-flow air.

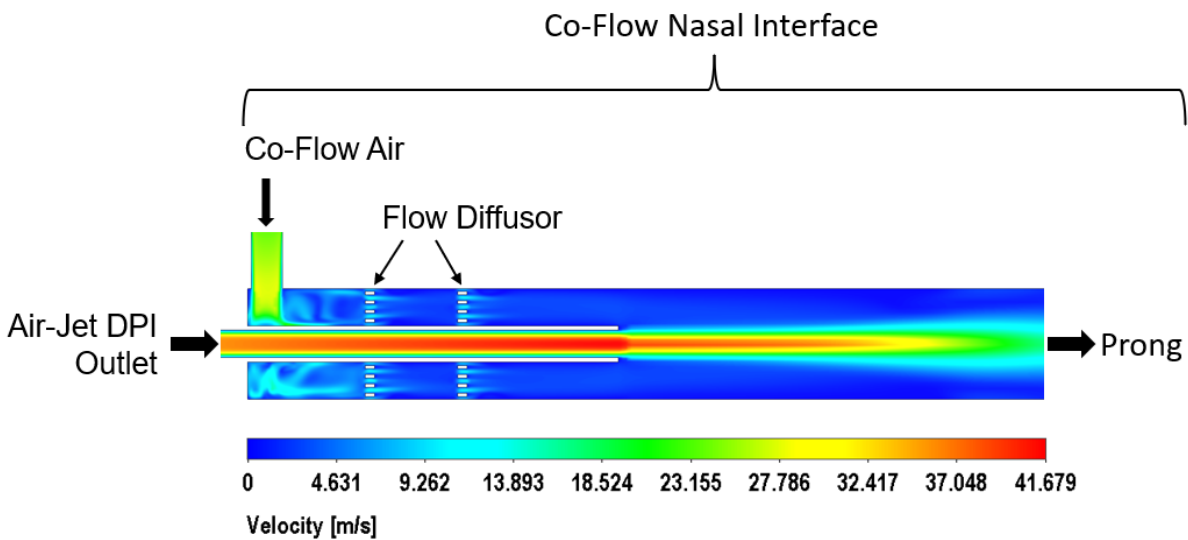


**Figure 8.1** Axial cross section view of CFD simulated air flow velocity profile for a co-flow nasal interface design

Also, in the final study of Objective 1, an additional preterm infant NT model was used and it was found that for two different AS-EEG formulations, there was no statistically significant difference between aerosol delivery performance (Total ED, Total NT, and Tracheal Filter percentages) when delivered to the two different infant airway geometries, which is encouraging for low inter-subject variability. Overall, modifications to the nasal interface of the

infant air-jet DPI platform improved the aerosol delivery, with the lead design delivering ~57% of the loaded dose to the tracheal filter, and performance across two unique preterm airway geometries remained statistically similar. While these results were encouraging for the minimization of inter-subject variability, the range of airway geometries that these two models represent is unknown, however, a prototype infant air-jet DPI platform has been successfully developed and was able to deliver a model EEG formulation aerosol with high efficiency (~57%) through an *in vitro* preterm infant model.

## **8.2 Objective 2: Expansion of the infant air-jet DPI platform to include capabilities for high powder mass loadings with minimal change and potential enhancements in aerosolization performance**

While the efforts of Objective 1 produced a highly efficient infant air-jet DPI platform, powder mass loadings >30 mg would require a reloading action. To enable a variety of loaded doses (investigational range of ~10 – 100 mg) and formulations, Objective 2 was to expand the infant air-jet DPI platform with a passive cyclic loading strategy. Design goals of the passive cyclic loading strategy were to meter a consistent amount of powder for each actuation while protecting the powder in the reservoir from aggregate formation, resulting in a single air-jet DPI device that can accommodate a variable range of powder doses with consistent performance. In the first study for Objective 2, 4 initial passive design (PD) approaches were investigated and two devices (PD-2 and PD-3) achieved an estimated lung delivery efficiency of ~60% when administered through a 1600 g preterm NT model. Additional testing with an *in vitro* preterm NT model and AS-EEG formulation, showed the platform performed consistently when the

loaded dose increased from 10 mg to 30 mg as well as when connected to the pulmonary mechanics outlet condition, using an infant lung with breath simulator. While the developed infant air-jet DPI platform had excellent performance with a highly dispersible model EEG formulation, the performance of other formulations needed to be determined. When switching to a surfactant-EEG formulation, performance was notably different in which an increase in NT deposition led to a decrease in tracheal filter deposition. The platform's performance with the AS-EEG formulation (which had an estimated lung delivery efficiency of ~60%), dropped by roughly half when using the surfactant-EEG formulation (about 30% lung delivery efficiency), likely due to the surfactant-EEG formulation being less dispersible. For a less dispersible powder, adding more aerosolization energy can facilitate further deaggregation, and was achieved in the form of a higher actuation flow rate. By simply increasing the flow rate from 1.7 L/min to 4.0 L/min, the estimated lung delivery efficiency increased from 30% to nearly 40%. However, the lower performance with the surfactant formulation led to a need for identifying other parameters that could be adjusted to accommodate varying formulations. Another area for improvement included the ability to perform consistently across a large range of loaded doses. In this study, the platform was found insensitive to varying doses in the range of 10 – 30 mg, but a slight sensitivity was found when increasing the capacity up to ~150 mg. The extended powder reservoir could hold a relatively large volume of powder, but when implemented, there was a slight (~5% absolute difference) but statistically significant decrease in lung delivery efficiency. While this difference is likely acceptable, a solution with no performance loss was still desired.

To enable the platform to operate consistently across a range of formulations and large powder loadings, the second study in Objective 2 explored modified extended powder reservoirs and passive metering elements. Of the powder reservoirs investigated, the adjustable powder reservoir was able to hold a bulk volume of powder up to 1.5 mL and when loaded with 10 mg of the AS-EEG formulation, it performed similarly to the standard 0.55 mL volume powder reservoir. Positioning of the sliding part of the reservoir allowed for minimization of the dead space in the reservoir and preserved performance for smaller powder mass loadings (i.e., 10 mg). While the prototype version worked well, a more convenient push/squeeze button vent system should be employed for formulations requiring >0.55 mL of powder volume to be loaded. **Figure 8.2** depicts concept models for automatic venting systems.

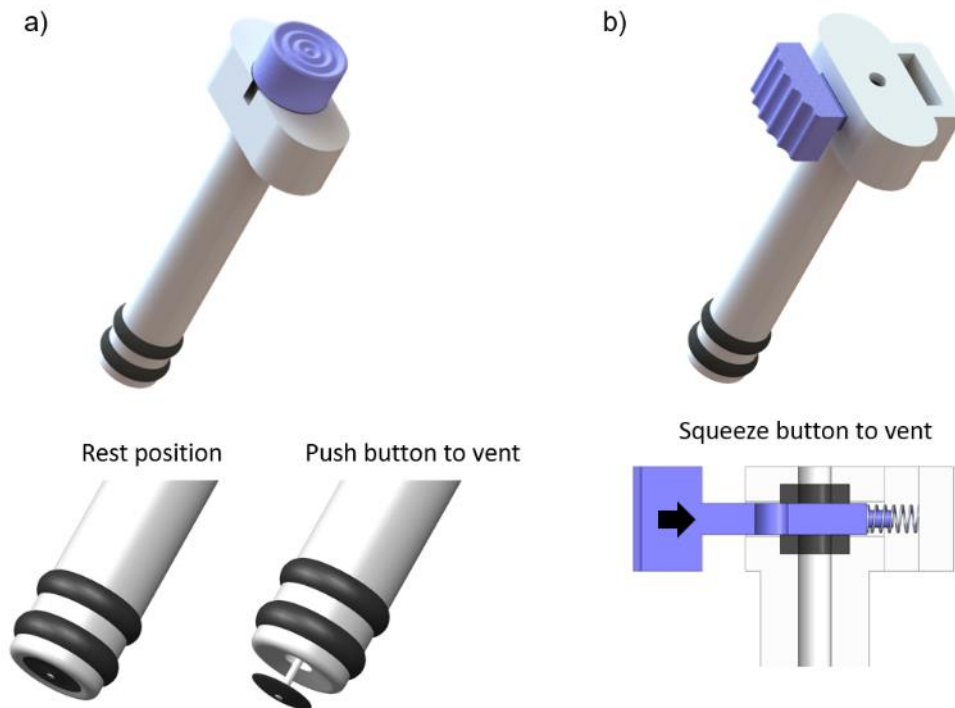


**Figure 8.2** Automatic venting schemes for the slider in the adjustable powder reservoir. **(a)** Push button and **(b)** Squeeze button configuration



To address concerns of overly rapid administration of a dry powder aerosol, this study also investigated the device emptying characteristics. Utilizing the AS-EEG formulation, the ED per actuation was determined for a 10 and 30 mg powder mass loading. The infant air-jet DPI platform was found to produce a maximum ED per actuation of ~5 mg, regardless of loaded dose, while total ED across all actuations for each case were consistent. In the main portion of this study, two passive metering elements were identified that were able to tune the performance of the air-jet DPI across multiple formulations, which were the shelf volume and powder reservoir opening size. Three formulations were investigated with varied powder properties; AS-EEG, Survanta-EEG, and DPPC-BYL3-EEG. Operated a Q90 flow rate of 4 L/min, and through tuning of the metering elements, the DPPC-BYL3-EEG formulation performed nearly identical to the model AS-EEG formulation, resulting in an estimated lung delivery efficiency ~45%. The Survanta-EEG formulation did not perform as well with the best test configuration providing an estimated lung delivery efficiency ~38%. Additional investigation of the metering elements as well as flow rate may improve the performance of the Survanta-EEG formulation to be comparable with the others. From the investigation in this study, tuning of the shelf volume is expected to produce desired performance within certain ranges. When adjusting the shelf volume based on powder formulation density, a volume equivalent up to <3 mg of powder should be implemented. However, for the aerosolization chamber to maintain high efficiency aerosolization, a maximum shelf volume between 26 – 40  $\mu$ L should be used for various formulations. The second passive metering element identified, powder reservoir opening size, is also a significant tuning parameter. While not fully explored in this study, adjusting the diameter of the opening can promote or restrict the powder flow from the

reservoir to the aerosolization chamber; for example, the low-density formulation ( $\sim 0.04 \text{ g/cm}^3$ ) required 9-10 actuation to fully empty a 10 mg powder mass loading, indicating a restrictive reservoir opening. When the opening was increased from 3 to 3.5 mm diameter, only 3 actuations were need for emptying, while still preserving aerosolization performance, indicating free flowing powder from the reservoir to the aerosolization chamber. The opposite may also be beneficial for higher density formulations, whereas decreasing the opening when using the Survanta-EEG formulation may slow the powder flow from the reservoir and possibly promote better aerosolization.

### 8.3 Synopsis and Future Directions

Overall, an infant air-jet DPI platform has been developed that can safely (based on presented metrics) deliver a variable (estimated 10 – 100 mg) dose of dry powder formulation with high efficiency ( $\sim 45 - 60\%$ ) to preterm infants (1600 g *in vitro* model) with consistent performance across multiple formulations, which has not been previously achieved. Limitations of this work include lack of *in vivo* experimentation results; however, *in vitro* results are promising, and *in vivo* testing is next step. Aside from *in vivo* testing, future work on this project can be categorized in three main areas. First, an easy to adjust passive metering element design will need to be implemented. This can be achieved through a manually adjustable shelf height, in which a highly precise threaded screw adjustment scheme could raise or lower the shelf inside the aerosolization chamber thereby increasing or decreasing the shelf volume. Also, a highly precise circular shutter scheme could be used to adjust the diameter of the powder reservoir opening. A dynamic reservoir opening may be more complex, requiring a flexible

funnel piece leading to the opening, and as such, a stepwise selection of different diameter openings as interchangeable parts may be more feasible for different formulations. **Figure 8.3** depicts a concept model for adjustable passive metering elements. For the shelf volume, a floating shelf is attached to threaded ring, that can precisely lower or raise the shelf by turning the ring to a specific marked volume. As for the reservoir opening size, this would most easily be adjusted by selecting from a range of pre-made sizes that are easily interchangeable.

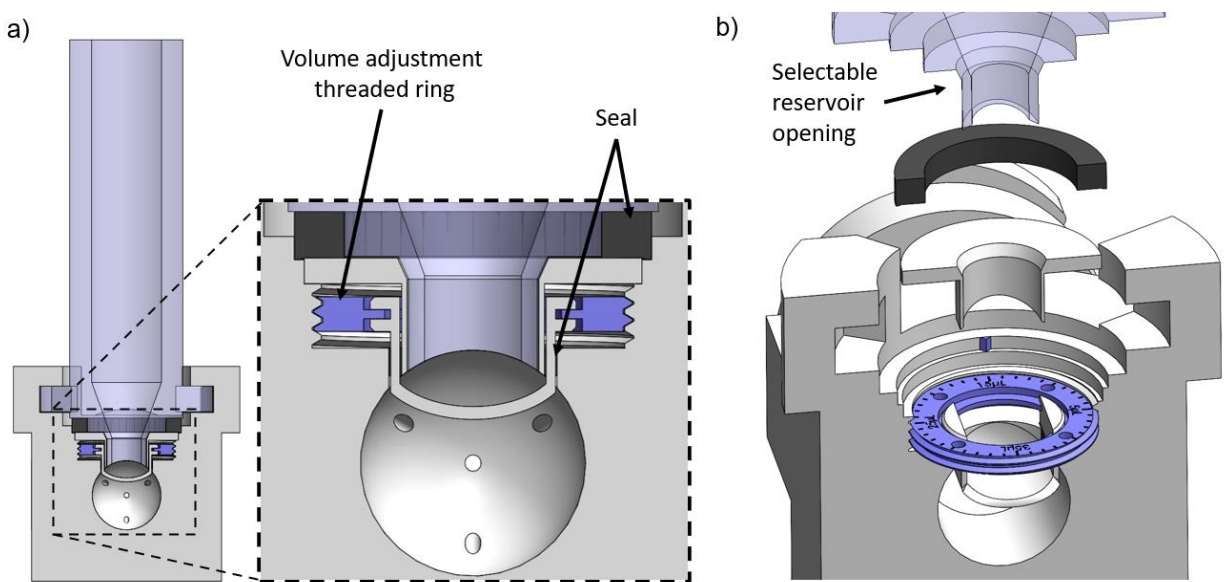


**Figure 8.3** Concept model renderings for adjustable passive metering elements. **(a)** Shows a 2-D cross-sectional cut while **(b)** shows an isometric view with full ring and shelf parts

The second area for future work is development of the co-flow nasal interface. Aside from the previously mention possible benefits, a co-flow nasal interface design also enables the ability for varied air delivery. Over the course of an actuation, the co-flow approach could be setup to aerosolize the powder for a portion of actuation, followed by a period of only air, effectively producing *chase air* after the aerosol. Chase air could be used to advance aerosol still suspended in the dead spaces of the interface and infant upper airways into the lung,

potentially increasing the lung delivery efficiency and decreasing deposition in unwanted areas, as well as lowering chances for off-target drug delivery or upper airway aggregate accumulation. The third and potentially most significant area for future work on this project would be the development and correlation of a dispersibility/density parameter of formulations for the calibration of the air-jet DPI platform. If a parameter based on powder density and an easily tested dispersibility metric could be determined and correlated to the three main tuning metrics developed in this study (flow rate, shelf volume, and reservoir opening size) then the platform could be tuned to optimal performance with minimal need for laboratory testing and investigation; the powder properties would be sufficient for preliminary adjustment of tuning elements for the infant air-jet DPI platform.

## List of References

## List of References

1. El-Gendy, N., et al., *Delivery and performance of surfactant replacement therapies to treat pulmonary disorders*. Ther. Deliv., 2013. **4**(8): p. 951-980.
2. Willson, D.F. and R.H. Notter, *The future of exogenous surfactant therapy*. Respiratory Care, 2011. **56**(9): p. 1369-1388.
3. Shah, S., *Exogenous surfactant: intubated present, nebulized future?* World Journal of Pediatrics, 2011. **7**(1): p. 11-15.
4. Pfister, R.H. and R.F. Soll, *Initial respiratory support of preterm infants - The role of CPAP, the INSURE method, and noninvasive ventilation*. Clin Perinatol, 2012. **39**: p. 459-481.
5. Peterson, S.W., *Understanding the sequence of pulmonary injury in the extremely low birth weight, surfactant-deficient infant*. Neonatal Network, 2009. **28**(4): p. 221-229.
6. O'Donnell, C.P.F., et al., *Endotracheal intubation attempts during neonatal resuscitation: Success rates, duration, and adverse effects*. Pediatrics, 2006. **117**(1): p. E16-E21.
7. Murdoch, E. and S. Kempley, *Randomized trial examining cerebral haemodynamics following artificial or animal surfactant*. Acta Paediatr., 1998. **87**: p. 411-415.
8. Maheshwari, R., et al., *Neonatal endotracheal intubation: how to make it more baby friendly*. Journal of paediatrics and child health, 2016. **52**(5): p. 480-486.
9. Walsh, B.K., et al., *AARC clinical practice guideline. Surfactant replacement therapy: 2013*. Respiratory care, 2013. **58**(2): p. 367-375.
10. Griscom, N.T. and M.E.B. Wohl, *Dimensions of the growing trachea related to age and gender*. American Journal of Roentgenology, 1986. **146**(2): p. 233-237.
11. Berggren, E., et al., *Pilot study of nebulized surfactant therapy for neonatal respiratory distress syndrome*. Acta Paediatr., 2000. **89**(4): p. 460-464.
12. Fok, T.F., et al., *Efficiency of aerosol medication delivery from a metered dose inhaler versus jet nebulizer in infants with bronchopulmonary dysplasia*. Pediatric Pulmonology, 1996. **21**(5): p. 301-309.
13. Finer, N.N., et al., *Early CPAP versus Surfactant in Extremely Preterm Infants*. New England Journal Of Medicine, 2010. **362**(21): p. 1970-1979.
14. Longest, P.W. and M. Hindle, *Condensational growth of combination drug-excipient submicrometer particles: Comparison of CFD predictions with experimental results*. Pharmaceutical Research, 2012. **29**(3): p. 707-721.
15. Longest, P.W., et al., *Performance of combination drug and hygroscopic excipient submicrometer particles from a softmist inhaler in a characteristic model of the airways*. Annals of Biomedical Engineering, 2012. **40**(12): p. 2596-2610.
16. Hindle, M. and P.W. Longest, *Condensational growth of combination drug-excipient submicrometer particles for targeted high efficiency pulmonary delivery: Evaluation of formulation and delivery device*. Journal of Pharmacy and Pharmacology, 2012. **64**(9): p. 1254-1263.
17. Walenga, R.L., et al., *Variability in nose-to-lung aerosol delivery*. Journal of Aerosol Science, 2014. **78**: p. 11-29.
18. Son, Y.-J., P.W. Longest, and M. Hindle, *Aerosolization characteristics of dry powder inhaler formulations for the enhanced excipient growth application: Effect of spray drying conditions*. Respiratory Drug Delivery 2012, 2012. **3**: p. 899-902.
19. Black, C.P., *Neonatal assessment and resuscitation*, in *Perinatal and Pediatric Respiratory Care*, B.K. Walsh, M.P. Czervinske, and R.M. DiBlasi, Editors. 2010, Saunders Elsevier: St. Louis.

20. O'Donnell, C.P. and B.J. Stenson. *Respiratory strategies for preterm infants at birth*. in *Seminars in Fetal and Neonatal Medicine*. 2008. Elsevier.
21. Longest, W. and D. Farkas, *Development of a New Inhaler for High-Efficiency Dispersion of Spray-Dried Powders Using Computational Fluid Dynamics (CFD) Modeling*. The AAPS Journal, 2019. **21**(2): p. 25.
22. Longest, W., et al., *Use of Computational Fluid Dynamics (CFD) Dispersion Parameters in the Development of a New DPI Actuated with Low Air Volumes*. *Pharmaceutical Research*, 2019. **36**(8): p. 110.
23. Farkas, D., M. Hindle, and P.W. Longest, *Development of an inline dry powder inhaler that requires low air volume*. *Journal of Aerosol Medicine and Pulmonary Drug Delivery*, 2018. **31**(4): p. 255-265.
24. Farkas, D., M. Hindle, and P.W. Longest, *Application of an inline dry powder inhaler to deliver high dose pharmaceutical aerosols during low flow nasal cannula therapy*. *International Journal of Pharmaceutics*, 2018. <https://doi.org/10.1016/j.ijpharm.2018.05.011>.
25. Farkas, D., M. Hindle, and P.W. Longest, *Efficient Nose-to-Lung Aerosol Delivery with an Inline DPI Requiring Low Actuation Air Volume*. *Pharmaceutical Research*, 2018. **35**(10): p. 194.
26. Howe, C., et al., *Initial Development of an Air-Jet Dry Powder Inhaler for Rapid Delivery of Pharmaceutical Aerosols to Infants*. *Journal of Aerosol Medicine and Pulmonary Drug Delivery*, 2021. **34**(1): p. 57-70.
27. Howe, C., et al., *Advancement of the Infant Air-Jet Dry Powder Inhaler (DPI): Evaluation of Different Positive-Pressure Air Sources and Flow Rates*. *Pharmaceutical Research*, 2021. **38**(9): p. 1615-1632.
28. Howe, C., et al., *In Vitro Analysis of Nasal Interface Options for High-Efficiency Aerosol Administration to Preterm Infants*. *Journal of Aerosol Medicine and Pulmonary Drug Delivery*, 2022. <https://doi.org/10.1089/jamp.2021.0057>.
29. Howe, C., et al., *Development of a High-Dose Infant Air-Jet Dry Powder Inhaler (DPI) with Passive Cyclic Loading of the Formulation*. *Pharmaceutical Research*, 2022: p. 1-14.
30. Organization, W.H., *March of Dimes; The partnership for maternal, newborn & child health; save the children*. *Born too soon: the global action report on preterm birth*, 2012: p. 1-124.
31. Smith, L.J., et al., *Normal development of the lung and premature birth*. *Paediatric respiratory reviews*, 2010. **11**(3): p. 135-142.
32. Notter, R.H., *Lung surfactants: basic science and clinical applications*. 2000: CRC Press.
33. Ma, C.C.-H. and S. Ma, *The role of surfactant in respiratory distress syndrome*. *The open respiratory medicine journal*, 2012. **6**: p. 44.
34. Seger, N. and R. Soll, *Animal derived surfactant extract for treatment of respiratory distress syndrome*. *Cochrane Database Syst Rev*, 2009. **Art. No.: CD007836**.
35. Soll, R.F. and F. Blanco, *Natural surfactant extract versus synthetic surfactant for neonatal respiratory distress syndrome*. *Cochrane Database of Systematic Reviews*, 2001. **Art. No. CD000144**.
36. Suresh, G.K. and R.F. Soll, *Overview of surfactant replacement trials*. *Journal of perinatology*, 2005. **25**(2): p. S40-S44.
37. Liechty, E.A., et al., *Reduction of neonatal mortality after multiple doses of bovine surfactant in low birth weight neonates with respiratory distress syndrome*. *Pediatrics*, 1991. **88**(1): p. 19-28.
38. Kumar, P., S.E. Denson, and T.J. Mancuso, *Clinical report-Premedication for nonemergency endotracheal intubation in the neonate*. *Pediatrics*, 2010. **125**(3): p. 608-615.
39. Estol, P., et al., *Assessment of pulmonary dynamics in normal newborns: a pneumotachographic method*. *Journal of Perinatal Medicine-Official Journal of the WAPM*, 1988. **16**(3): p. 183-192.

40. Fuchs, O., et al., *Normative data for lung function and exhaled nitric oxide in unsedated healthy infants*. European respiratory journal, 2011. **37**(5): p. 1208-1216.
41. Schermuly, R., et al., *Ultrasonic nebulization for efficient delivery of surfactant in a model of acute lung injury impact on gas exchange*. Am. J. Respir. Crit. Care Med., 1997. **156**(2): p. 445-453.
42. Cowan, F., et al., *Cerebral blood-flow velocity changes after rapid administration of surfactant*. Archives Of Disease In Childhood, 1991. **66**(10): p. 1105-1109.
43. Raju, T.N.K. and P. Langenberg, *Pulmonary hemorrhage and exogenous surfactant therapy - a metaanalysis*. Journal Of Pediatrics, 1993. **123**(4): p. 603-610.
44. Robertson, B. and H.L. Halliday, *Principles of surfactant replacement*. Biochimica et Biophysica Acta (BBA)-Molecular Basis of Disease, 1998. **1408**(2-3): p. 346-361.
45. Jobe, A.H., et al., *Decreased indicators of lung injury with continuous positive expiratory pressure in preterm lambs*. Pediatric Research, 2002. **52**(3): p. 387-392.
46. Polin, R.A. and R. Sahni, *Newer experience with CPAP*. Semin Neonatol, 2002. **7**(5): p. 379-389.
47. Avery, M.E., et al., *Is chronic lung-disease in low-birth-weight infants preventable - A survey of 8 centers*. Pediatrics, 1987. **79**(1): p. 26-30.
48. Herting, E., C. Härtel, and W. Göpel, *Less invasive surfactant administration (LISA): chances and limitations*. Archives of Disease in Childhood-Fetal and Neonatal Edition, 2019. **104**(6): p. F655-F659.
49. Linner, R., V. Perez-de-Sa, and D. Cunha-Goncalves, *Lung deposition of nebulized surfactant in newborn piglets*. Neonatology, 2015. **107**(4): p. 277-282.
50. Mahmoud, R.A., C.C. Roehr, and G. Schmalisch, *Current methods of non-invasive ventilatory support for neonates*. Paediatric respiratory reviews, 2011. **12**(3): p. 196-205.
51. Morley, C.J., et al., *Dry artificial lung surfactant and its effect on very premature babies*. The Lancet, 1981. **317**(8211): p. 64-68.
52. Fok, T.F., et al., *Pulmonary deposition of salbutamol aerosol delivered by metered dose inhaler, jet nebulizer, and ultrasonic nebulizer in mechanically ventilated rabbits*. Pediatric Research, 1997. **42**(5): p. 721-727.
53. Willson, D.F., *Aerosolized surfactants, anti-inflammatory drugs, and analgesics*. Respiratory Care, 2015. **60**(6): p. 774-793.
54. DiBlasi, R.M., *Clinical controversies in aerosol therapy for infants and children*. Respiratory Care, 2015. **60**(6): p. 894-916.
55. Everard, M.L., *Inhaler devices in infants and children: Challenges and solutions*. Journal of Aerosol Medicine-Deposition Clearance and Effects in the Lung, 2004. **17**(2): p. 186-195.
56. Fink, J.B., *Aerosol delivery to ventilated infant and pediatric patients*. Respiratory Care, 2004. **49**(6): p. 653-665.
57. Fink, J.B., *Delivery of inhaled drugs for infants and small children: a commentary on present and future needs*. Clinical Therapeutics, 2012. **34**(11): p. S36-S45.
58. Sunbul, F.S., et al., *Comparison of HFNC, bubble CPAP and SiPAP on aerosol delivery in neonates: An in-vitro study*. Pediatric Pulmonology, 2015. **50**(11): p. 1099-1106.
59. El Taoum, K.K., et al., *In vitro evaluation of aerosols delivered via the nasal route*. Respiratory Care, 2015. **60**(7): p. 1015-1025.
60. Lin, H.-L., et al., *In vitro comparison of aerosol delivery using different face masks and flow rates with a high-flow humidity system*. 2015. **60**(9): p. 1215-1219.
61. Réminiac, F., et al., *Nasal high flow nebulization in infants and toddlers: an in vitro and in vivo scintigraphic study*. Pediatric Pulmonology, 2017. **52**(3): p. 337-344.
62. Fok, T.F., et al., *Delivery of metered dose inhaler aerosols to paralyzed and nonparalyzed rabbits*. Critical Care Medicine, 1997. **25**(1): p. 140-144.



63. El Taoum, K.K., et al., *In vitro evaluation of aerosols delivered via the nasal route*. Respiratory Care, 2016. **10.4187/respcare.03606**.
64. Lewis, J.F., et al., *Aerosolized surfactant treatment of preterm lambs*. J Appl Physiol, 1991. **70**: p. 869-876.
65. Fok, T.F., et al., *Nebulisation of surfactants in an animal model of neonatal respiratory distress*. Archives of Disease in Childhood-Fetal and Neonatal Edition, 1998. **78**(1): p. F3-F9.
66. Bianco, F., et al., *From bench to bedside: in vitro and in vivo evaluation of a neonate-focused nebulized surfactant delivery strategy*. Respiratory Research, 2019. **20**(1): p. 134.
67. Nord, A., et al., *Lung deposition of nebulized surfactant in newborn piglets: Nasal CPAP vs Nasal IPPV*. Pediatric Pulmonology, 2019.
68. Hutten, M.C., et al., *Nebulization of Poractant alfa via a vibrating membrane nebulizer in spontaneously breathing preterm lambs with binasal continuous positive pressure ventilation*. Pediatric Research, 2015. **78**(6): p. 664-669.
69. Rey-Santano, C., et al., *Dose-response study on surfactant nebulization therapy during nasal continuous positive airway pressure ventilation in spontaneously breathing surfactant-deficient newborn piglets*. Pediatric Critical Care Medicine, 2020. **21**(7): p. e456.
70. Berggren, E., et al., *Pilot study of nebulized surfactant therapy for neonatal respiratory distress syndrome*. Acta Paediatrica, 2000. **89**(4): p. 460-464.
71. Finer, N.N., et al., *An Open Label, Pilot Study of Aerosurf (R) Combined with nCPAP to Prevent RDS in Preterm Neonates*. Journal Of Aerosol Medicine And Pulmonary Drug Delivery, 2010. **23**(5): p. 303-309.
72. Minocchieri, S., C.A. Berry, and J.J. Pillow, *Nebulised surfactant to reduce severity of respiratory distress: a blinded, parallel, randomised controlled trial*. Archives of Disease in Childhood-Fetal and Neonatal Edition, 2019. **104**(3): p. F313-F319.
73. Sood, B.G., et al., *Aerosolized surfactant in neonatal respiratory distress syndrome: Phase I study*. Early Human Development, 2019. **134**: p. 19-25.
74. Hinds, W.C., *Aerosol Technology: Properties, Behavior, and Measurement of Airborne Particles*. 1999, New York: John Wiley and Sons.
75. Chow, A.H., et al., *Particle engineering for pulmonary drug delivery*. Pharmaceutical research, 2007. **24**(3): p. 411-437.
76. Son, Y.-J., P.W. Longest, and M. Hindle, *Aerosolization characteristics of dry powder inhaler formulations for the excipient enhanced growth (EEG) application: Effect of spray drying process conditions on aerosol performance*. International Journal of Pharmaceutics, 2013. **443**: p. 137-145.
77. Isayama, T., et al., *Association of noninvasive ventilation strategies with mortality and bronchopulmonary dysplasia among preterm infants: a systematic review and meta-analysis*. Jama, 2016. **316**(6): p. 611-624.
78. Newman, S., *Respiratory Drug Delivery: Essential Theory and Practice*. 2009, Richmond: RDD Online.
79. Bass, K., et al., *High-Efficiency Nose-to-Lung Aerosol Delivery in an Infant: Development of a Validated Computational Fluid Dynamics Method*. Journal of Aerosol Medicine and Pulmonary Drug Delivery, 2019. **32**(3): p. 132-148.
80. Behara, S.R.B., et al., *Development and comparison of new high-efficiency dry powder inhalers for carrier-free formulations*. Journal of Pharmaceutical Sciences, 2014. **103**: p. 465-477.
81. Longest, P., et al., *Reviving Positive Pressure DPIs for Efficient and Reproducible Aerosol Delivery to Infants and Children*. Respiratory Drug Delivery, 2020. **1**(2020): p. 71-80.

82. Longest, P.W., et al., *Aerodynamic factors responsible for the deaggregation of carrier-free drug powders to form micrometer and submicrometer aerosols*. *Pharmaceutical Research*, 2013. **30**: p. 1608-1627.
83. Harper, N.J., et al., *The design and performance of the Exubera® pulmonary insulin delivery system*. *Diabetes technology & therapeutics*, 2007. **9**(S1): p. S-16-S-27.
84. Agarkhedkar, S., et al., *Safety and immunogenicity of dry powder measles vaccine administered by inhalation: a randomized controlled Phase I clinical trial*. *Vaccine*, 2014. **32**(50): p. 6791-6797.
85. Hoppentocht, M., et al., *In vitro evaluation of the DP-4M PennCentury insufflator*. *European Journal of Pharmaceutics and Biopharmaceutics*, 2014. **88**(1): p. 153-159.
86. Behara, S.R.B., et al., *Development of high efficiency ventilation bag actuated dry powder inhalers*. *International Journal of Pharmaceutics*, 2014. **465**: p. 52-62.
87. Longest, P.W., et al., *Efficient nose-to-lung (N2L) aerosol delivery with a dry powder inhaler*. *Journal of Aerosol Medicine and Pulmonary Drug Delivery*, 2015. **28**(3): p. 189-201.
88. Farkas, D., et al., *Development of an inline dry powder inhaler for oral or trans-nasal aerosol administration to children*. *Journal of aerosol medicine and pulmonary drug delivery*, 2019.
89. Boc, S.T., et al., *Aerosolization of spray dried pulmonary surfactant powder using a novel low air volume actuated dry powder inhaler*. *Respiratory Drug Delivery* 2018, 2018. **2**: p. 639-642.
90. Boc, S.T., et al., *Spray dried pulmonary surfactant powder formulations: Development and characterization*. *Respiratory Drug Delivery* 2018, 2018. **2**: p. 635-638.
91. Boc, S., et al., *Performance of Low Air Volume Dry Powder Inhalers (LV-DPI) when Aerosolizing Excipient Enhanced Growth (EEG) Surfactant Powder Formulations*. *AAPS PharmSciTech*, 2021. **22**(4): p. 1-12.
92. Xu, Z., et al., *Heterogeneous Particle Deaggregation and Its Implication for Therapeutic Aerosol Performance*. *Journal of Pharmaceutical Sciences*, 2010. **99**(8): p. 3442-3461.
93. Xu, Z., et al., *Dry Powder Aerosols Generated by Standardized Entrainment Tubes From Drug Blends With Lactose Monohydrate: 1. Albuterol Sulfate and Disodium Cromoglycate*. *Journal Of Pharmaceutical Sciences*, 2010. **99**(8): p. 3398-3414.
94. Xu, Z., et al., *Dry Powder Aerosols Generated by Standardized Entrainment Tubes From Drug Blends With Lactose Monohydrate: 2. Ipratropium Bromide Monohydrate and Fluticasone Propionate*. *Journal Of Pharmaceutical Sciences*, 2010. **99**(8): p. 3415-3429.
95. Coates, M.S., et al., *Effect of design on the performance of a dry powder inhaler using computational fluid dynamics. Part 1: Grid structure and mouthpiece length*. *Journal of Pharmaceutical Sciences*, 2004. **93**(11): p. 2863-2876.
96. Coates, M.S., et al., *Effect of design on the performance of a dry powder inhaler using computational fluid dynamics. Part 2: Air inlet size*. *Journal of Pharmaceutical Sciences*, 2006. **95**(6): p. 1382-1392.
97. Coates, M.S., et al., *Influence of air flow on the performance of a dry powder inhaler using computational and experimental analyses*. *Pharmaceutical Research*, 2005. **22**(9): p. 1445-1453.
98. Voss, A.P. and W.H. Finlay, *Deagglomeration of dry powder pharmaceutical aerosols*. *International Journal of Pharmaceutics*, 2002. **248**: p. 39-40.
99. Walsh, B.K. and R.M. DiBlasi, *Mechanical ventilation of the neonate and pediatric patient*, in *Perinatal and Pediatric Respiratory Care*, B.K. Walsh, M.P. Czervinske, and R.M. DiBlasi, Editors. 2010, Saunders Elsevier: St. Louis. p. 325-347.
100. Björklund, L., et al., *Lung recruitment at birth does not improve lung function in immature lambs receiving surfactant*. *Acta anaesthesiologica scandinavica*, 2001. **45**(8): p. 986-993.
101. Lindner, W., et al., *Delivery room management of extremely low birth weight infants: spontaneous breathing or intubation?* *Pediatrics*, 1999. **103**(5): p. 961-967.

102. te Pas, A.B. and F.J. Walther, *A randomized, controlled trial of delivery-room respiratory management in very preterm infants*. *Pediatrics*, 2007. **120**(2): p. 322-329.
103. O'Donnell, C.P., P.G. Davis, and C.J. Morley, *Resuscitation of premature infants: what are we doing wrong and can we do better?* *Neonatology*, 2003. **84**(1): p. 76-82.
104. Bhutani, V.K., F.W. Bowen, and E.M. Sivieri, *Postnatal changes in pulmonary mechanics and energetics of infants with respiratory distress syndrome following surfactant treatment*. *Neonatology*, 2005. **87**(4): p. 323-331.
105. Snepvangers, Y., et al., *Respiratory outcome in preterm ventilated infants: importance of early respiratory system resistance*. *European Journal of Pediatrics*, 2004. **163**(7): p. 378-384.
106. Choukroun, M., et al., *Early respiratory system mechanics and the prediction of chronic lung disease in ventilated preterm neonates requiring surfactant treatment*. *Neonatology*, 2003. **83**(1): p. 30-35.
107. Volsko, T.A., et al., *High flow through a nasal cannula and CPAP effect in a simulated infant model*. *Respiratory Care*, 2011. **56**(12): p. 1893-1900.
108. Wada, K., A.H. Jobe, and M. Ikegami, *Tidal volume effects on surfactant treatment responses with the initiation of ventilation in preterm lambs*. *Journal of Applied Physiology*, 1997. **83**(4): p. 1054-1061.
109. Davis, J.M., et al., *Changes in pulmonary mechanics after the administration of surfactant to infants with respiratory distress syndrome*. *New England Journal of Medicine*, 1988. **319**(8): p. 476-479.
110. Pohlmann, G., et al., *A novel continuous powder aerosolizer (CPA) for inhalative administration of highly concentrated recombinant surfactant protein-C (rSP-C) surfactant to perterm neonates*. *Journal of Aerosol Medicine and Pulmonary Drug Delivery*, 2013. **26**(6): p. 370-379.
111. Fleming, F.S., et al., *Development and optimization of a novel pulsed dry powder nebulizer using in vitro studies that mimic in vivo conditions*. *Respiratory Drug Delivery* 2012, 2012. **1**: p. 377-386.
112. Fink, J. and A. Ari, *Aerosol delivery to intubated patients*. *Expert Opinion on Drug Delivery*, 2013. **10**(8): p. 1077-1093.
113. Mazela, J. and R.A. Polin, *Aerosol delivery to ventilated newborn infants: historical challenges and new directions*. *Eur. J. Pediatr.*, 2011. **170**: p. 433-444.
114. Amirav, I., et al., *Beta-agonist aerosol distribution in respiratory syncytial virus bronchiolitis in infants*. *Journal of Nuclear Medicine*, 2002. **43**(4): p. 487-491.
115. Chua, H., et al., *The influence of age on aerosol deposition in children with cystic fibrosis*. *European Respiratory Journal*, 1994. **7**(12): p. 2185-2191.
116. Mallol, J., et al., *Aerosol deposition in infants with cystic fibrosis*. *Pediatric Pulmonology*, 1996. **21**(5): p. 276-281.
117. Corcoran, T.E., et al., *Deposition studies of aerosol delivery by nasal cannula to infants*. *Pediatric Pulmonology*, 2019. **54**(8): p. 1319-1325.
118. Bianco, F., et al., *Extended Pharmacopeial Characterization of Surfactant Aerosols Generated by a Customized eFlow Neos Nebulizer Delivered through Neonatal Nasal Prongs*. *Pharmaceutics*, 2020. **12**(4): p. 319.
119. Nord, A., et al., *Lung deposition of nebulized surfactant in newborn piglets: Nasal CPAP vs Nasal IPPV*. *Pediatric Pulmonology*, 2020. **55**(2): p. 514-520.
120. Bhashyam, A.R., et al., *Aerosol delivery through nasal cannulas: An in vitro study*. *Journal of Aerosol Medicine and Pulmonary Drug Delivery*, 2008. **21**(2): p. 181-187.
121. Kaviratna, A., et al., *Evaluation of Bio-relevant Mouth-Throat Models for Characterization of Metered Dose Inhalers*. *AAPS PharmSciTech*, 2019. **20**(3): p. 130.

122. Longest, P.W., M. Azimi, and M. Hindle, *Optimal delivery of aerosols to infants during mechanical ventilation*. Journal of Aerosol Medicine and Pulmonary Drug Delivery, 2014. **27**(5): p. 371-385.
123. Longest, P.W. and G. Tian, *Development of a new technique for the efficient delivery of aerosolized medications to infants on mechanical ventilation*. Pharmaceutical Research, 2015. **32**: p. 321-336.
124. Schuepp, K.G., et al., *In vitro determination of the optimal particle size for nebulized aerosol delivery to infants*. Journal of Aerosol Medicine-Deposition Clearance And Effects In The Lung, 2005. **18**(2): p. 225-235.
125. Clark, A.R., C. McKenna, and R. MacLoughlin, *Aersol delivery in term and preterm infants: The final frontier*. Respiratory Drug Delivery 2018, 2018. **1**: p. 159-168.
126. Tavernini, S., et al., *Deposition of micrometer-sized aerosol particles in neonatal nasal airway replicas*. Aerosol Science and Technology, 2018. **52**(4): p. 407-419.
127. Longest, P.W., et al., *Comparison of ambient and spray aerosol deposition in a standard induction port and more realistic mouth-throat geometry*. Journal of Aerosol Science, 2008. **39**(7): p. 572-591.
128. Storey-Bishoff, J., M. Noga, and W.H. Finlay, *Deposition of micrometer-sized aerosol particles in infant nasal airway replicas*. Aerosol Science, 2008. **39**: p. 1055-1065.
129. Golshahi, L., et al., *In vitro deposition measurement of inhaled micrometer-sized particle in extrathoracic airways of children and adolescents during nose breathing*. Journal of Aerosol Science, 2011. **42**: p. 474-488.
130. Longest, P.W., et al., *Production of inhalable submicrometer aerosols from conventional mesh nebulizers for improved respiratory drug delivery*. Journal of Aerosol Science, 2012. **51**: p. 66-80.
131. Spence, B.M., et al., *Development of a high flow nasal cannula (HFNC) and pharmaceutical aerosol combination device*. Journal of Aerosol Medicine and Pulmonary Drug Delivery, 2019. **32**(4): p. 224-41.
132. Longest, P.W., L. Golshahi, and M. Hindle, *Improving pharmaceutical aerosol delivery during noninvasive ventilation: Effects of streamlined components*. Annals of Biomedical Engineering, 2013. **41**(6): p. 1217-1232.
133. Dhapare, S., et al., *Breath-synchronized delivery of aerosols to infants using a very low volume mixer-heater*. Respiratory Drug Delivery 2018, 2018. **1**: p. 643-646.
134. Laube, B.L., et al., *Deposition of dry powder generated by solvent in Sophia Anatomical infant nose-throat (SAINT) model*. Aerosol Science and Technology, 2012. **46**: p. 514-520.
135. Farkas, D., M. Hindle, and P.W. Longest, *Application of an inline dry powder inhaler to deliver high dose pharmaceutical aerosols during low flow nasal cannula therapy*. International Journal of Pharmaceutics, 2018. **546**(1-2): p. 1-9.
136. Tavernini, S., et al., *Scaling an Idealized Infant Nasal Airway Geometry to Mimic Inertial Filtration of Neonatal Nasal Airways*. Journal of Aerosol Science, 2018. **118**: p. 14-21.
137. Hofmann, W., *Mathematical model for the postnatal growth of the human lung*. Respiration Physiology, 1982. **49**: p. 115-129.
138. Phalen, R.F., et al., *Postnatal enlargement of human tracheobronchial airways and implications for particle deposition*. Anat. Rec., 1985. **212**: p. 368-380.
139. Hofmann, W., T.B. Martonen, and R.C. Graham, *Predicted deposition of nonhygroscopic aerosols in the human lung as a function of subject age*. Journal of Aerosol Medicine, 1989. **2**(1): p. 49-67.
140. ICRP, *Human Respiratory Tract Model for Radiological Protection*. Annals of the ICRP. Vol. 66. 1994, New York: Elsevier Science Ltd.
141. NCRP, *Deposition, Retention and Dosimetry of Inhaled Radioactive Substances*. NCRP Report No. 125. 1997, Bethesda: National Council on Radiation Protection and Measurements.

142. National-Centers-for-Health-Statistics, *Length-for-age and Weight for age percentiles*. <http://www.cdc.gov/growthcharts>, 2000.
143. Xi, J., et al., *Growth of nasal and laryngeal airways in children: implications in breathing and inhaled aerosol dynamics*. *Respiratory Care*, 2014. **59**(2): p. 263-273.
144. Zhou, Y., et al., *Nasal deposition in infants and children*. *Journal of Aerosol Medicine and Pulmonary Drug Delivery*, 2014. **27**(2): p. 110-116.
145. Son, Y.-J., et al., *Evaluation and modification of commercial dry powder inhalers for the aerosolization of submicrometer excipient enhanced growth (EEG) formulation*. *European Journal of Pharmaceutical Sciences*, 2013. **49**: p. 390-399.
146. Longest, P.W. and M. Hindle, *Numerical model to characterize the size increase of combination drug and hygroscopic excipient nanoparticle aerosols*. *Aerosol Science and Technology*, 2011. **45**: p. 884-899.
147. Tian, G., M. Hindle, and P.W. Longest, *Targeted lung delivery of nasally administered aerosols*. *Aerosol Science and Technology*, 2014. **48**(4): p. 434-449.
148. Martonen, T.B., Y. Yang, and D. Hwang, *Hygroscopic behaviour of secondary cigarette smoke in human nasal passages*. *S.T.P. Pharma. Sciences*, 1994. **4**: p. 69-76.
149. Dolovich, M.B. and R. Dhand, *Aerosol drug delivery: developments in device design and clinical use*. *Lancet*, 2011. **377**(9770): p. 1032-1045.
150. Rubin, B.K. and J.B. Fink, *Aerosol therapy for children*. *Respir Care Clin N Am*, 2001. **7**(2): p. 175-213.
151. Rubin, B.K. and R.W. Williams, *Emerging aerosol drug delivery strategies: from bench to clinic*. *Advanced Drug Delivery Reviews*, 2014. **75**: p. 141-148.
152. LiCalsi, C., et al., *Dry powder inhalation as a potential delivery method for vaccines*. *Vaccine*, 1999. **17**(13-14): p. 1796-1803.
153. Geller, D.E., J. Weers, and S. Heuerding, *Development of an inhaled dry-powder formulation of Tobramycin using PulmoSphere™ technology*. *Journal of Aerosol Medicine and Pulmonary Drug Delivery*, 2011. **24**(4): p. 175-182.
154. Islam, N. and M.J. Cleary, *Developing an efficient and reliable dry powder inhaler for pulmonary drug delivery - A review for multidisciplinary researchers*. *Medical Engineering and Physics*, 2012. **34**: p. 409-427.
155. Weers, J.G., et al., *Idealhalers versus realhalers: Is it possible to bypass deposition in the upper respiratory tract?* *Journal of Aerosol Medicine and Pulmonary Drug Delivery*, 2019. **32**(2): p. 55-69.
156. Moon, C., et al., *Delivery technologies for orally inhaled products: an update*. *AAPS PharmSciTech*, 2019. **20**(3): p. 117.
157. Newman, S.P. and W.W. Busse, *Evolution of dry powder inhaler design, formulation, and performance*. *Respiratory Medicine*, 2002. **96**: p. 293-304.
158. Longest, P.W., et al., *Reviving Positive Pressure DPIs for Efficient and Reproducible Aerosol Delivery to Infants and Children*. *Respiratory Drug Delivery 2020*, 2020. **Volume 1, 71-80**.
159. Farkas, D., et al., *Development of an inline dry powder inhaler for oral or trans-nasal aerosol administration to children*. *Journal of Aerosol Medicine and Pulmonary Drug Delivery*, 2020. **33**(2): p. 83-98.
160. Bass, K., D. Farkas, and W. Longest, *Optimizing Aerosolization Using Computational Fluid Dynamics in a Pediatric Air-Jet Dry Powder Inhaler*. *AAPS PharmSciTech*, 2019. **20**(8): p. 329.
161. Golshahi, L., et al., *Deposition of inhaled ultrafine aerosols in replicas of nasal airways of infants*. *Aerosol Science and Technology*, 2010. **44**: p. 741-752.

162. Hindle, M. and P.W. Longest, *Evaluation of enhanced condensational growth (ECG) for controlled respiratory drug delivery in a mouth-throat and upper tracheobronchial model*. *Pharmaceutical Research*, 2010. **27**(9): p. 1800-1811.
163. Longest, P.W. and M. Hindle, *CFD simulations of enhanced condensational growth (ECG) applied to respiratory drug delivery with comparisons to in vitro data*. *Journal of Aerosol Science*, 2010. **41**: p. 805-820.
164. Longest, P.W., J.T. McLeskey, and M. Hindle, *Characterization of nanoaerosol size change during enhanced condensational growth*. *Aerosol Science and Technology*, 2010. **44**: p. 473-483.
165. Longest, P.W., et al., *Engineered drug targeting to the lungs: Ensuring growth and deposition of submicrometer aerosols through device design and formulation*. *Respiratory Drug Delivery* 2012, 2012. **1**: p. 61-72.
166. Tian, G., et al., *Targeting aerosol deposition to and within the lung airways using excipient enhanced growth*. *Journal of Aerosol Medicine and Pulmonary Drug Delivery*, 2013. **26**(5): p. 248-265.
167. Fenton, *Fenton Preterm Growth Charts*. <https://live-ucalgary.ucalgary.ca/resource/preterm-growth-chart/preterm-growth-chart>, 2013.
168. Dave, M.H., et al., *Pediatric airway dimensions—A summary and presentation of existing data*. *Pediatric Anesthesia*, 2019. **29**(8): p. 782-789.
169. DiBlasi, R.M. and P. Richardson, *Continuous positive airway pressure*, in *Perinatal and Pediatric Respiratory Care*, B.K. Walsh, M.P. Czervinske, and R.M. DiBlasi, Editors. 2010, Saunders Elsevier: St. Louis.
170. Longest, P.W. and D. Farkas, *Development of a new inhaler for high-efficiency dispersion of spray-dried powders using computational fluid dynamics (CFD) modeling*. *The AAPS Journal*, 2018. DOI: **10.1208/s12248-018-0281-y**.
171. Bianco, F., et al., *Aerosol drug delivery to spontaneously-breathing preterm neonates: lessons learned*. *Respiratory Research*, 2021. **22**(1): p. 1-31.
172. Ari, A. and J.B. Fink, *Guidelines for aerosol devices in infants, children and adults: which to choose, why and how to achieve effective aerosol therapy*. *Expert review of respiratory medicine*, 2011. **5**(4): p. 561-572.
173. Borgstrom, L., B. Olsson, and L. Thorsson, *Degree of throat deposition can explain the variability in lung deposition of inhaled drugs*. *Journal of Aerosol Medicine*, 2006. **19**: p. 473-483.
174. Delvadia, R., et al., *In vitro tests for aerosol deposition II: IVIVCs for different dry powder inhalers in normal adults*. *Journal of Aerosol Medicine and Pulmonary Drug Delivery*, 2013. **26**(3): p. 138-144.
175. Delvadia, R., et al., *In vitro tests for aerosol deposition. IV: Simulating variations in human breath profiles for realistic DPI testing*. *Journal of Aerosol Medicine and Pulmonary Drug Delivery*, 2015. DOI: **10.1089/jamp.2015.1215**.
176. Manion, J.R., et al., *Inhalable antibiotics manufactured through use of near-critical or supercritical fluids*. *Aerosol Science and Technology*, 2012. **46**(4): p. 403-410.
177. Boc, S., et al., *Development and Characterization of Excipient Enhanced Growth (EEG) Surfactant Powder Formulations for Treating Neonatal Respiratory Distress Syndrome*. *AAPS PharmSciTech*, 2021. **22**(4): p. 1-12.
178. Hassan, A., et al., *Characterization of excipient enhanced growth (EEG) tobramycin dry powder aerosol formulations*. *International Journal of Pharmaceutics*, 2020. **591**: p. 120027.
179. Howe, C., et al., *Advancement of the Infant Air-Jet Dry Powder Inhaler (DPI): Evaluation of Different Positive-Pressure Air Sources and Flow Rates*. *Pharmaceutical Research*, 2021: p. 1-18.
180. Bass, K. and P.W. Longest, *Development of DPI patient interfaces for improved aerosol delivery to children*. *AAPS PharmSciTech*, 2020. **21**: p. 157.

181. Farkas, D., et al., *Advancement of a Positive-Pressure Dry Powder Inhaler for Children: Use of a Vertical Aerosolization Chamber and Three-Dimensional Rod Array Interface*. *Pharmaceutical Research*, 2020. **37**: p. 177.
182. Bass, K., et al., *High-efficiency dry powder aerosol delivery to children: Review and application of new technologies*. *Journal of Aerosol Science*, 2021. **153**: p. 105692.
183. Youngquist, T.M., C.P. Richardson, and R.M. DiBlasi, *Effects of condensate in the exhalation limb of neonatal circuits on airway pressure during bubble CPAP*. *Respiratory care*, 2013. **58**(11): p. 1840-1846.
184. Xi, J., P.W. Longest, and T.B. Martonen, *Effects of the laryngeal jet on nano- and microparticle transport and deposition in an approximate model of the upper tracheobronchial airways*. *Journal of Applied Physiology*, 2008. **104**(6): p. 1761-1777.
185. Vorperian, H.K., et al., *Development of vocal tract length during early childhood: A magnetic resonance imaging study*. *The Journal of the Acoustical Society of America*, 2005. **117**(1): p. 338-350.
186. Weers, J., *Inhaled antimicrobial therapy - Barriers to effective treatment*. *Advanced Drug Delivery Reviews*, 2015. **85**: p. 24-43.
187. Walsh, B.K., et al., *Characterization of ribavirin aerosol with small particle aerosol generator and vibrating mesh micropump aerosol technologies*. *Respiratory Care*, 2016. **61**(5): p. 577-585.
188. Wright, M., C.J. Mullett, and G. Piedimonte, *Pharmacological management of acute bronchiolitis*. *Therapeutics and Clinical Risk Management*, 2008. **4**(5): p. 895.
189. Farkas, D.R., M. Hindle, and P.W. Longest, *Characterization of a new high-dose dry powder inhaler (DPI) based on a fluidized bed design*. *Annals of Biomedical Engineering*, 2015. **43**(11): p. 2804-2815.
190. Young, P.M., et al., *Overcoming dose limitations using the Orbital multi-breath dry powder inhaler*. *Journal of Aerosol Medicine and Pulmonary Drug Delivery*, 2013. **DOI: 10.1089/jamp.2013.1080**.
191. Yeung, S., et al., *Assessing aerosol performance of a dry powder carrier formulation with increasing doses using a novel inhaler*. *AAPS PharmSciTech*, 2019. **20**(3): p. 1-12.
192. Bilton, D., et al., *Inhaled dry powder mannitol in cystic fibrosis: an efficacy and safety study*. *European Respiratory Journal*, 2011. **38**(5): p. 1071-1080.
193. Smith, I.J., et al., *Inhaler Devices: What Remains to be Done?* *Journal Of Aerosol Medicine And Pulmonary Drug Delivery*, 2010. **23**: p. S25-S37.
194. Li, D., et al., *Development and validation of an LC-MS/MS method for quantification of dipalmitoylphosphatidylcholine as a promising biomarker for renal failure in urine*. *Journal of Chinese Pharmaceutical Sciences*, 2015. **24**: p. 73-79.
195. Kolanjiyil, A.V., et al., *Validating CFD predictions of nasal spray deposition: Inclusion of cloud motion effects for two spray pump designs*. *Aerosol Science and Technology*, 2022. **56**(4): p. 305-322.
196. Kolanjiyil, A.V., et al., *Importance of cloud motion and two-way momentum coupling in the transport of pharmaceutical nasal sprays*. *Journal of Aerosol Science*, 2021. **156**: p. 105770.
197. Kamga Gninzeko, F.J., et al., *Excipient Enhanced Growth Aerosol Surfactant Replacement Therapy in an In Vivo Rat Lung Injury Model*. *Journal of Aerosol Medicine and Pulmonary Drug Delivery*, 2020. **33**(6): p. 314-322.
198. Walther, F.J., J.M. Hernández-Juviel, and A.J. Waring, *Aerosol delivery of synthetic lung surfactant*. *PeerJ*, 2014. **2**: p. e403.
199. Walther, F.J., et al., *Efficacy, dose-response, and aerosol delivery of dry powder synthetic lung surfactant treatment in surfactant-deficient rabbits and premature lambs*. *Respiratory Research*, 2022. **23**(1): p. 1-16.

200. Walther, F.J., et al., *Aerosol delivery of dry powder synthetic lung surfactant to surfactant-deficient rabbits and preterm lambs on non-invasive respiratory support*. Gates Open Research, 2019. **3**.
201. Ruppert, C., et al., *Dry powder aerosolization of a recombinant surfactant protein-C-based surfactant for inhalative treatment of the acutely inflamed lung*. Critical Care Medicine, 2010. **38**(7): p. 1584-1591.



# Vita

## Connor Matthew Howe

### Education

- Doctor of Philosophy, Mechanical and Nuclear Engineering (2022)  
Virginia Commonwealth University (VCU), Richmond, VA, USA
- Bachelor of Science, Physics (2005)  
Longwood University, Farmville, VA, USA

### Professional Experience

- NCI Information Systems, Inc. (2008-2014)  
Springfield, VA, USA
- Modern Technologies Corporation (2005-2008)  
Haymarket, VA, USA

### Journal Publications

Howe, C., Momin, M. A., Aladwani, G., Hindle, M., & Longest, P. (2022). Development of a High-Dose Infant Air-Jet Dry Powder Inhaler (DPI) with Passive Cyclic Loading of the Formulation. *Pharmaceutical Research*, 1-14.

Bass, K., Momin, M. A., Howe, C., Aladwani, G., Strickler, S., Kolanjiyil, A. V., ... & Longest, W. (2022). Characterizing the Effects of Nasal Prong Interfaces on Aerosol Deposition in a Preterm Infant Nasal Model. *AAPS PharmSciTech*, 23(5), 1-18.

Howe, C., Momin, M. A., Bass, K., Aladwani, G., Bonasera, S., Hindle, M., & Longest, P. W. (2022). In Vitro Analysis of Nasal Interface Options for High-Efficiency Aerosol Administration to Preterm Infants. *Journal of Aerosol Medicine and Pulmonary Drug Delivery*.

Howe, C., Momin, M. A., Farkas, D. R., Bonasera, S., Hindle, M., & Longest, P. (2021). Advancement of the Infant Air-Jet Dry Powder Inhaler (DPI): Evaluation of Different

Positive-Pressure Air Sources and Flow Rates. *Pharmaceutical Research*, 38(9), 1615-1632.

Howe, C., Hindle, M., Bonasera, S., Rani, V., & Longest, P. W. (2021). Initial development of an air-jet dry powder inhaler for rapid delivery of pharmaceutical aerosols to infants. *Journal of Aerosol Medicine and Pulmonary Drug Delivery*, 34(1), 57-70.

Howe, C., Mishra, S., Kim, Y. S., Chen, Y., Ye, S. H., Wagner, W. R., ... & Yeo, W. H. (2018). Stretchable, implantable, nanostructured flow-diverter system for quantification of intra-aneurysmal hemodynamics. *ACS nano*, 12(8), 8706-8716.

Chen, Y., Howe, C., Lee, Y., Cheon, S., Yeo, W. H., & Chun, Y. (2016). Microstructured thin film nitinol for a neurovascular flow-diverter. *Scientific Reports*, 6(1), 1-10.

### **Conference Proceedings (Presenting author marked with an asterisk)**

Longest\*, P. W., Farkas, D. R., Bass, K., Howe, C., Boc, S. T., Momin, M., ... & Hindle, M. (2020). Reviving positive pressure DPIs for efficient and reproducible aerosol delivery to infants and children. In *Respiratory Drug Delivery* (Vol. 1, pp. 71-80).

Lee\*, Y., Howe, C., Mishra, S., Lee, D. S., Mahmood, M., Piper, M., ... & Yeo, W. H. (2018). Wireless, intraoral hybrid electronics for real-time quantification of sodium intake toward hypertension management. *Proceedings of the National Academy of Sciences*, 115(21), 5377-5382.

Chen\*, Y., Howe, C., Emery, S., Greene, S., Shridhar, P., Yeo, W. H., & Chun, Y. (2017, May). A Low-Profile Flow Sensing System for Monitoring of Cerebrospinal Fluid with a New Ventriculoamniotic Shunt. In *2017 IEEE 67th Electronic Components and Technology Conference (ECTC)* (pp. 230-235). IEEE.

Fondjo, F., Lee\*, D. S., Howe, C., Yeo, W. H., & Kim, J. H. (2017, May). Synthesis of a soft nanocomposite for flexible, wearable bioelectronics. In *2017 IEEE 67th Electronic Components and Technology Conference (ECTC)* (pp. 780-785). IEEE.

Howe\*, C., Lee, Y., Chen, Y., Chun, Y., & Yeo, W. H. (2016, May). An implantable, stretchable microflow sensor integrated with a thin-film nitinol stent. In *2016 IEEE 66th Electronic Components and Technology Conference (ECTC)* (pp. 1638-1643). IEEE.